Electric vehicles in the Nordic countries: Control strategies for coordinated grid services

Zecchino, Antonio

Publication date:
2019

Document Version
Publisher's PDF, also known as Version of record

Technical University of Denmark

Antonio Zecchino

Electric vehicles in the Nordic countries: Control strategies for coordinated grid services

Ph.D. Thesis, December 2018
Risø, Roskilde, Denmark

DTU Electrical Engineering
Department of Electrical Engineering

DANMARKS TEKNISKE UNIVERSITET

Center for Electric Power and Energy
DTU Electrical Engineering

Electric vehicles in the Nordic countries: Control strategies for coordinated grid services

Elbiler i de nordiske lande: Styringsstrategier for koordinerede netydelser

Ph.D. Thesis, by Antonio Zecchino

Supervisors:

Associate Professor Mattia Marinelli, Technical University of Denmark

Associate Professor Chresten Træholt, Technical University of Denmark

Professor Magnus Korpås, Norwegian University of Science and Technology

DTU - Technical University of Denmark, Roskilde - December 2018

Electric vehicles in the Nordic countries: Control strategies for coordinated grid services

This thesis was prepared by:

Antonio Zecchino

Supervisors:

Associate Professor Mattia Marinelli, Technical University of Denmark

Associate Professor Chresten Træholt, Technical University of Denmark

Professor Magnus Korpås, Norwegian University of Science and Technology

Dissertation Examination Committee:

Associate Professor Nenad Mijatovic (Chairman)
Department of Electrical Engineering, Technical University of Denmark, Denmark

Professor Lina Bertling Tjernberg
Department of Electromagnetic Engineering, KTH Royal Institute of Technology, Sweden

Associate Professor Samuele Grillo
Department of Electronics, Information, and Bioengineering, Politecnico di Milano, Italy

Center for Electric Power and Energy
DTU Electrical Engineering
Frederiksborgvej 399, Building 776
DK-4000 Roskilde
Denmark
www.cee.elektro.dtu.dk
Tel: (+45) 45 25 35 00
Fax: (+45) 45 88 61 11
E-mail: cee@elektro.dtu.dk

Release date: December 2018

Class: Public

Field: Electrical Engineering

Remarks: The dissertation is presented to the Department of Electrical Engineering of Technical University of Denmark in partial fulfilment of the requirements for the degree of Doctor of Philosophy.

A mia Mamma.

Preface

This thesis was prepared at the department of Electrical Engineering at the Technical University of Denmark (DTU) in partial fulfillment of the requirements for acquiring the degree of Doctor of Philosophy in Engineering.

The Ph.D. studies were supported by the Technical University of Denmark as a Nordic 5 Tech (N5T) scholarship. The author contributed to the European project "Electra IRP" (grant no. 609687) and the Danish research projects "Nikola" (ForskEL contract no. 2013-1-12088), "Parker" (ForskEL contract no. 2016-1-12410), and "ACES – Across Continents Electric Vehicle Services" (EUDP grant no. EUDP17-I-12499).

The Ph.D. project started on the 15th of December 2015 and was completed on the 14th December 2018. During this period, the author was hired by Technical University of Denmark as a Ph.D. candidate at the Center for Electric Power and Energy (CEE), DTU Electrical Engineering.

The thesis consists of a summary report and 9 attached scientific papers, documenting the research conducted by the author during the Ph.D. project period. 5 of these papers appear in conference proceedings and 2 are published in international peer-reviewed journals, whereas the remaining 2 papers have been submitted to international peer-reviewed journals and are under review.

Antonio Zecchino

Roskilde, December 2018

Acknowledgements

I would like to thank my supervisors Mattia Marinelli, Chresten Træholt and Magnus Korpås for their support, guidance and critical opinions throughout the three years of my Ph.D. studies. I am particularly grateful to my main supervisor Mattia Marinelli for his unconditional help whenever necessary. Without him, it is hard to picture myself at this point of my career. In fact, he introduced me to the scientific research and step-by-step he wisely led me to achieve this prestigious goal with inspiring discussions and advices. I thank Mattia not only for his help on research-related matters, but also for his presence every time I was in need for advice and support in my private life. He has always been available for me when it came to face life difficulties, helping me growing both as a researcher and as a man. Really, thank you.

I would also like to thank all the colleagues from CEE, especially the close colleagues from 776 at Risø campus, who made me feel part of a big family. The working environment here is something unique: it made me coming to work with a smile on the face, and I believe this contributed to achieve a better overall work outcome as well as to grow by meeting brilliant people from all over the world. So, thank you 776-people, both the present ones and the ones that already left. I am also grateful to the colleagues I met during my external stay in Trondheim at NTNU, who welcomed me in the best possible way and made me live a very enjoyable, yet productive, period of my Ph.D..

This journey would have been much tougher, or even impossible, without the continuous support of my closest friends in Italy and in Denmark. Feeling their consistent presence gave me the strength to reach this goal, and I really have to thank them for this.

A special thank is dedicated to a special person that I unexpectedly met at the beginning of this journey and that I have hold tight onto me for its whole duration: Asja. She made me becoming a better person, and this, together with her and her family's continuous splendid support, was definitely fundamental. A, thank you for everything.

An immense thank you is finally reserved to every single member of my Family. I received extra energies and moral support from all of them, necessary for the completion of my Ph.D.. In particular, I am grateful to my Mum, to my Dad and to my Sister Francesca for their unconditional love: they have always believed in me and have always positively supported me in every decision of my life. A sincere thank You for Your love and Your support, which made this achievement possible.

Antonio

Abstract

Nowadays, power system operators face challenges in supporting a stable and economic future power system based on renewable energy production and new types of flexible demand, such as electric vehicles (EVs). One of the main challenges is to address the adverse effects that the EVs may have on local distribution grids (distribution system operator (DSO) perspective) and enhance their usage to optimize utilization of renewables on a national/regional scale (transmission system operator (TSO) perspective). The research emphasis of this thesis is on power and energy services that EVs can provide both locally and system-wide. Three main topics are addressed:

1. Identification of current policies and barriers for system-wide and local grid service provision from EVs, as well as possible conflicts between TSO and DSO when acquiring such services. This problem comes from the TSOs' need for grid stability services from small dispatched units, and the simultaneous interest of the DSO not to have power provision from distributed energy sources violating the local grid constraints. The acquisition of such flexibility services from one grid operator may cause undesired effects to another operator: technical and economical conflicts may arise, and a detection and categorization strategy is proposed.

2. Investigations on the suitability of standard-compliant commercial hardware (series-produced EVs and chargers) for the provision of uni- and bi-directional grid services, in order to detect the technical challenges related to EVs control for grid balancing purposes. This was the starting point for the development and implementation of standard-compliant control logics able to guarantee power system frequency stability both on a simulation and on a laboratory validation level. Possible smart EV control solutions are proposed, which aim at stabilizing frequency oscillations, at reducing reserve provision error, and at providing a trade-off between error and the overall efficiency of the fleet power converters. Further, system stability is studied both on a microgrid and on a full-scale power system level in order to outline requirements for the overall fleet output, to secure an aggregated response that does not harm the system stability.

3. Identification of the technical impacts on the distribution system due to massive EV penetration levels and investigation of the effectiveness of reactive power provision from EV chargers. In general, reactive power modulation allows a reduction of the self-induced under-voltage conditions caused by EVs charging at distribution grid levels, but how effective is this solution in practice? An

analytical study is conducted, which aims to assess reactive power provision from EVs in typical distribution grids.

In conclusion, the research at a whole investigates the broad topic of EV integration from different stakeholders' point of view, such as market operators, DSOs, TSOs and EV aggregators. The proposed solutions and control strategies are expected to significantly contribute to the real power system operation, in order to pave the way for a harmonic, economic and safe utilization of the increasing number of EVs.

Resumé

Operatørerne af transmissionssystemet (TSO) står overfor store udfordringer når det kommer til at skabe et stabilt og samfundsøkonomisk gunstigt elsystem der både er baseret på vedvarende energi og nye typer af fleksibelt forbrug, såsom elbiler. En af hovedproblematikkerne, set fra de lokale operatører af distributionsnettets (DSO'ernes) side, er de negative effekter som elbilerne har på distributionsnettet. Set fra TSO'ens perspektiv handler det nærmere om hvordan man nationalt kan øge forbruget af vedvarende energi. Denne afhandling fokuserer på hvordan elbilen både kan bruge sin ladeeffekt og totale ladeenergi til at levere serviceydelser til DSO'en og TSO'en.

Tre hovedområder er undersøgt:

1. Identificering af hvilke love og regulativer der forhindrer elbiler i at levere ydelser for DSO'en og TSO'en, og hvilke konflikter der kan opstå når de to parter køber ydelser på samme tid. Konflikten opstår på grund af at TSO'en ønsker balancerende ydelser fra små distribuerede enheder imens DSO'en samtidig kan ønske at de samme enheder ikke har et forbrug der overstiger den lokale kapacitet. En ydelse leveret til den ene operatør kan have en uønsket effekt for den anden. En strategi til at opdage og kategorisere disse tekniske og økonomiske konflikter, når de opstår, er foreslået.

2. Vurdering af standard kommerciel hardwares, såsom elbiler og ladestanderers, evne til at levere envejs og tovejsydelser til elnettet med henblik på at finde tekniske problematikker i samspillet.

Dette er udgangspunktet for udvikling og implementering af en standardiseret kontrol algoritme der garanterer stabiliteten af netfrekvensen i både simulering og i laboratoriet. For at stabilisere svingninger i frekvensen og reducere fejllevering af ydelserne er der foreslået mulige intelligente ladealgoritmer til elbiler der giver en afvejning mellem at minimere fejl og at maximere effektiviteten af elbilsflådens effektelektronik. Derudover er stabiliteten af både små isolerede systemer og store internationale systemer blevet analyseret for at finde ud af hvilke krav man skal stille til bilflådens reaktion for at sikre at den samlede respons ikke gør systemet ustabilt.

3. Identificering af hvilken betydning massiv udrulning af elbiler har på distributionsnettet og undersøgelse af hvor egnet levering af reaktiv effekt er til at løse problemerne. Reaktiv effekt kan bruges til at undgå at spændingen falder som følge af den øgede belastning, men hvor anvendeligt er

det i virkeligheden? Det er analyseret ved at modellere reaktiv effekt fra elbiler i et typisk distributionsnet.

Som konklusion kan det siges at forskningen undersøger hele paletten for integration af elbiler med elnettet, set fra de forskellige aktørers side, det er både DSO'en TSO'en og dem der styrer elbilerne. De foreslåede løsninger og styringsalgoritmer forventes at være et vigtigt redskab til at stabilisere hele elnettet og give en harmonisk, samfundsøkonomisk og sikker brug af det stigende antal elbiler.

List of publications

Papers included in the thesis

A. A. Zecchino, K. Knezović, M. Marinelli, "Identification of Conflicts between Transmission and Distribution System Operators when Acquiring Ancillary Services from Electric Vehicles," *7th IEEE PES Innovative Smart Grid Technologies Europe (ISGT Europe)*, 26-29 September 2017, Torino, Italy.

B. A. Zecchino, M. Rezkalla, M. Marinelli, "Grid Frequency Support by Single-Phase Electric Vehicles: Fast Primary Control Enhanced by a Stabilizer Algorithm," *2016 Universities Power Engineering Conference (UPEC)*, 6-9 September 2016, Coimbra, Portugal.

C. M. Rezkalla, A. Zecchino, S. Martinenas, A. M. Prostejovsky, M. Marinelli, "Comparison between Synthetic Inertia and Fast Frequency Containment Control Based on Single Phase EVs in a Microgrid," *Applied Energy*, vol. 210, pp. 764-775, 2018.

D. A. Zecchino, S. D'Arco, A. G. Endegnanew, M. Korpås, M. Marinelli, "Enhanced Primary Frequency Control from EVs: a Fleet Management Strategy to Mitigate Effects of Response Discreteness", *IET Smart Grid*, 2018, under review.

E. A. Zecchino, M. Marinelli, A. Thingvad, P. B. Andersen, "Suitability of Commercial V2G CHAdeMO Chargers for Grid Services", *EVS 31 & EVTeC 2018 The 31st International Electric Vehicles Symposium and Exhibition & International Electric Vehicle Technology Conference 2018*, Kobe, Japan, 30 September - 3 October 2018.

F. C. Ziras, A. Zecchino, M. Marinelli, "Response Accuracy and Tracking Errors with Decentralized Control of Commercial V2G Chargers", *20th Power Systems Computation Conference (PSCC 2018)*, 11-15 June 2018, Dublin, Ireland.

G. A. Zecchino, A. M. Prostejovsky, C. Ziras, M. Marinelli, "Large-scale Provision of Frequency Control via V2G: the Bornholm Power System Case", *Electric Power Systems Research*, 2018, under 2nd round of review.

H. A. Zecchino, M. Marinelli, M. Korpås, C. Træholt, "Guidelines for Distribution System Operators on Reactive Power Provision by Electric Vehicles in Low Voltage Grids," *CIRED - Open Access Proceedings Journal*, vol. 2017, no. 1, pp. 1787-1791, 2017, presented at *24th International Conference on Electricity Distribution (CIRED)*, 12-15 June 2017, Glasgow, Scotland.

I. A. Zecchino, M. Marinelli, "Analytical Assessment of Voltage Support via Reactive Power from new Electric Vehicles Supply Equipment in Radial Distribution Grids with Voltage-Dependent Loads", *International Journal of Electrical Power & Energy Systems*, vol. 97, April 2018, pp. 17-27.

Other publications not included in the thesis

J. K. Knezović, S. Martinenas, P. B. Andersen, A. Zecchino and M. Marinelli, "Enhancing the Role of Electric Vehicles in the Power Grid: Field Validation of Multiple Ancillary Services," *IEEE Transaction on Transportation Electrification*, vol. 3, no. 1, pp. 201-209, 2017.

K. M. Rezkalla, A. Zecchino, M. Pertl, M. Marinelli, "Grid Frequency Support by Single-Phase Electric Vehicles Employing an Innovative Virtual Inertia Controller," *2016 Universities Power Engineering Conference (UPEC)*, 6-9 September 2016, Coimbra, Portugal.

L. M. Rezkalla, S. Martinenas, A. Zecchino, E. Rikos, M. Marinelli, "Implementation and validation of synthetic inertia support employing series produced electric vehicles," CIRED - Open Access Proceedings Journal, vol. 2017, no. 1, pp. 1197-1201, 2017, presented at *24th International Conference on Electricity Distribution (CIRED)*, 12-15 June 2017, Glasgow, Scotland.

M. K. Knezović, M. Marinelli, A. Zecchino, P. B. Andersen. C. Træholt, "Supporting involvement of electric vehicles in distribution grids: Lowering the barriers for a proactive integration," in *Energy*, vol. 134, pp. 458-468, 2017.

N. V. T. Sæmundsson, M. Rezkalla, A. Zecchino, M. Marinelli, "Aggregation of Single-Phase Electric Vehicles for Frequency Control Provision Based on Unidirectional Charging," *2017 Universities Power Engineering Conference (UPEC)*, 29 August - 1 September 2017, Heraklion, Greece.

O. A. Gadea, M. Marinelli, A. Zecchino, "A Market Framework for Enabling Electric Vehicles Flexibility Procurement at the Distribution Level Considering Grid Constraints", *20th Power Systems Computation Conference (PSCC 2018)*, 11-15 June 2018, Dublin, Ireland.

P. M. Lillebo, S. Zaferanlouei, A. Zecchino, H. Farahmand, "Impact of Large-Scale EV Integration and Fast Chargers in a Norwegian LV Grid", *7th International Conference on Renewable Power Generation*, 26-27 September 2018, Lyngby, Copenhagen, Denmark.

List of acronyms

Notation		Description
AC	–	Alternating Current
BRP	–	Balance Responsible Party
BEV	–	Battery Electric Vehicle
CHP	–	Combined Heat and Power plant
DER	–	Distributed Energy Resources
CGU	–	Conventional Generation Unit
DSO	–	Distribution System Operator
DC	–	Direct Current
DG	–	Distributed Generation
ESS	–	Energy Storage Systems
EV	–	Electric Vehicle
EVSE	–	Electric Vehicles Supply Equipment
FCEV	–	Fuel-Cell Electric Vehicle
FDR	–	Frequency-controlled Disturbance reserve
FNR	–	Frequency-controlled Normal operation reserve
HuT	–	Hardware under Test
LV	–	Low Voltage
MV	–	Medium Voltage
P-HiL	–	Power Hardware-in-the-Loop
PCC	–	Point of Common Coupling

PFC	–	Primary Frequency Control
PHEV	–	Plug-in Hybrid Electric Vehicle
PV	–	Photovoltaic units
RES	–	Renewable Energy Sources
RG-N	–	Regional Group Nordic
RMS	–	Root Mean Square
SOC	–	State of Charge
TSO	–	Transmission System Operator
V2G	–	Vehicle-to-Grid
VRB	–	Vanadium Redox Battery
VUF	–	Voltage Unbalance Factor

Contents

Part I

Summary Report

CHAPTER 1

Introduction

1.1 Context and motivation

Global warming and increasing environmental pollution are undoubtedly happening with considerable negative impact on both the natural environment and the human society [1]. The main cause of this is the massive use of fossil fuels as a primary energy resource, which contribute to the current dramatic levels of CO_2 emissions, causing stronger greenhouse effect. The most developed countries recognize the issues and agree on common policies towards a sustainable development. The European level, the European Commission in 2008 published the "20-20-20" agreement, setting goals for 2020 in terms of reduction of CO_2 emissions and increasing of exploitation of renewable energy sources (RES) [2]. In 2012 and 2014, new policies were introduced, setting higher targets for 2050 (Energy Roadmap 2050 [3]) and 2030 (2030 Energy Strategy [4]), respectively. At Global level, the sustainability effort was extended to 195 countries in 2015 with the Paris climate conference (COP21) agreement [5]. This is the first-ever legally binding global climate deal, which will enter into force in 2020, with the goal to limit the global warming to below 2 °C. To achieve these European and Global goals, national governments set interim goals. For example, in Denmark the goal is to reduce the national CO_2 emissions by 40% in 2020 and to reach the 100% renewable energy target in 2050 [6], whereas for Norway the mission is to cut the CO_2 emissions registered in 1990 to 30% and 40%, by 2020 and 2030, respectively [7]. Since transport accounts for approximately 25% of global CO_2 emissions [8], the electrification of the transport sector is considered a crucial element in achieving both the national and the global objectives [9], [10]. A key step towards the achievement of the reduction of CO_2 emissions is then the electrification of the transport sector, which can rely more and more on green electricity generated from RES. In particular, in the recent years great success is achieved in the electrification of road transport, with massive rollout of electric vehicles (EVs). Despite that EVs may introduce technical challenges to power system operators given the high electricity demand when charging, a smart integration can make them play an active role to increase even more the green side of their employment. For instance, EVs could adapt their charging patterns to improve the grid conditions and help further integration of RES: the synergy between EVs and RES allows a simultaneous reduction of fossil-fuel dependency in both the electricity generation and the transportation sector [11].

Within this context, the following subsections present the emerging changes in the modern power system framework, the recent increase success of EVs and their charging infrastructure in the Nordic countries, and a possible classification of charging strategies. This general overview provides the background of this thesis.

1.1.1 The evolution of the power system

The traditional layout of the electric power system is shown in Figure 1.1. Electricity is generated centrally in bulk power plants through synchronous machines, and then is transmitted over high voltage transmission lines and distributed to the users over medium voltage (MV) and low voltage (LV) networks with uni-directional power flows. Between the 1980s and the 1990s in many countries the historical monopolistic organization of the electric power system changed due to the introduction of liberalization and state-owned companies operating in the generation and retail sectors were privatized [12]. The privatization process did not involve the transmission and distribution grid operation, which remained regulated monopolies due to the traditional system's centralized nature. Thus, the key entities in the contemporary system operation are the transmission system operator (TSO) and the distribution system operator (DSO).

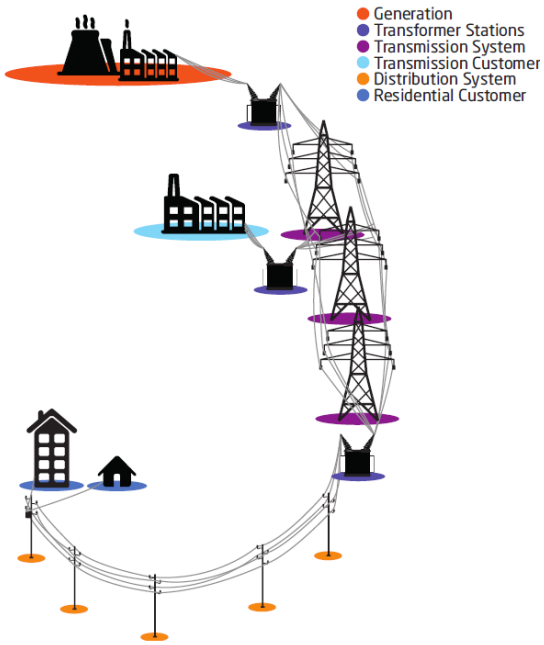

Figure 1.1 – The traditional electric power system. Source: [13].

The TSO is the entity responsible for keeping the balance between production and consumption at all times while ensuring the secure operation of the transmission system. Production-consumption imbalances are reflected in system frequency deviations from the operating nominal value, which is 50 Hz for both the Continental Europe Synchronous Area and the Regional Group Nordic (RG-N), i.e., the interconnected power systems of Norway, Sweden, Finland, and Eastern Denmark (DK2). In

order to cope with imbalances, the frequency need to be restored to the nominal value, and this is achieved by the TSO via procurement of ancillary services. Terminology and technical characteristics of frequency ancillary services vary from area to area and from country to country, but in general it can be divided into three categories: Primary frequency control, Secondary control and Tertiary control. A graphical representation of system frequency deviation and frequency control by different reserve types is shown in Figure 1.2.

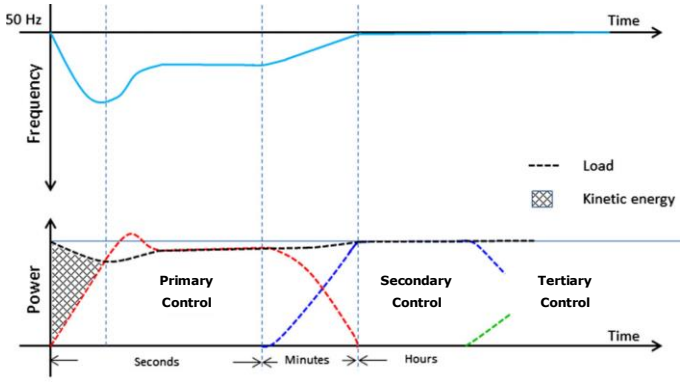

Figure 1.2 – Deployment of frequency control in the event of a grid contingency. Source: [14].

The primary frequency control stabilizes the system frequency within the first few seconds after a disturbance or an incident at an acceptable steady-state. The regulation is automatic and is usually achieved via droop controllers implemented in generator sets, which can change their power output proportionally to the frequency deviation. The overall primary frequency reserve is shared among all the control areas, with contributions proportional to the share of the annual energy production in that area over the annual energy production in the entire synchronous area. The secondary frequency control is a slower control and can be either automatic or manual. It restores the frequency back to its set-point value replacing the activated primary control reserve within a few minutes, typically up to 15 min after the contingency. Tertiary frequency control is achieved via the reserve replacement process, which replaces the activated reserve for secondary control. The reserve is activated manually and centrally at the TSO control center, typically within a timeframe from 15 min up to several hours. The European Network of Transmission System Operators for Electricity (ENTSO-E) defines the reserve for primary, secondary and tertiary frequency control respectively as frequency containment reserve (FCR), frequency restoration reserve (FRR), and replacement reserve (RR).

DSOs are mainly concerned about the efficient and reliable delivery of power to end users, meter management and reading, and voltage control and congestion management on their respective voltage levels [15]. DSOs' main tasks include maintaining the distribution network and ensuring the power quality in line with the international and national regulations. Typically, DSOs have historically operated their MV and LV grids with radial topology and unidirectional power flows. Consumption was not flexible but easily forecastable, thus, despite the limited grid observability and controllability, issues in the grid operation were prevented by planning and network development

[16]. In fact, DSO activities are mainly focused on long term planning and design rather than on real-time operation. DSOs' operational concerns are mainly on voltage regulation, congestion management and grid maintenance.

In the recent decades, electric power systems have been experiencing massive changes as part of the energy transition trends adopted in the developed countries. Large conventional generation units (CGUs) powered by fossil fuels are being replaced with distributed energy resources (DER) such as photovoltaic plants (PV), combined heat and power plants (CHP), and wind turbines. For instance, the global share of PV installations grew by almost 99 GW during the whole 2017, reaching the total amount of 400 GW [17]. Similar trends are observed also in the wind sector, with the global share at 540 GW at the end of 2017 [18]. New challenges arise with increasing DER penetration as the generation from renewable sources is less controllable due to uncertainty and variability of the primary energy source. Furthermore, unlike the large central CGUs, DERs are typically connected at distribution levels, thus possibly introducing bi-directional power flow conditions, which cannot be easily managed by the traditional system operators' means. In order to cope with the increasing operational challenges, grid operators needs to enhance the use of information and communication technology (ICT). This can lead to the exploitation of consumers' flexibility in terms of power consumption/generation modulation, making them an active player in the modern power system by providing different services to system operators. These concepts can be grouped within the so-called *smart grid paradigm* [19], which is depicted in Figure 1.3. Within this paradigm, new dynamics, stakeholders and rules need to be established for enabling an active involvement of small electricity users in the operation of modern power systems, e.g., via smart metering, aggregators and market frameworks.

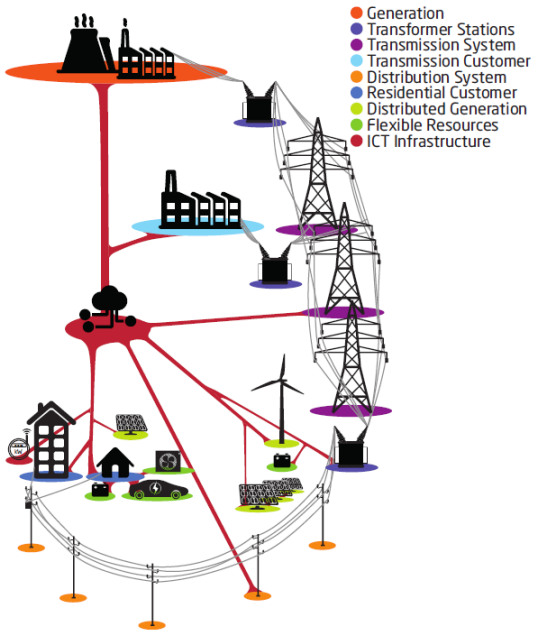

Figure 1.3 – The future smart grid paradigm. Source: [13].

1.1.2 Massive roll-out of EVs and charging infrastructure in the Nordics

In general, electric vehicles include battery electric vehicles (BEV), plug-in hybrid electric vehicles (PHEV) and fuel-cell electric vehicles (FCEV). As reported in the *Global EV Outlook 2018* [20], the global increasing success of EVs in the last years is indeed reflected in the sales numbers: sales of new EV worldwide surpassed 1 million units in 2017 – a record volume, growing by 54% compared with 2016. This made the global stock of EVs surpassing 3 million vehicles in 2017 after crossing the 1 million threshold in 2015 and the 2 million mark in 2016, meaning that in 2017 it expanded by 56% compared with 2016. Great success is present among the Nordic countries as well, with an overall fleet that crossed the threshold of 300.000 units by the second quarter of 2018 [21], almost one tenth of the global EV stock. An overview of the growth of the EV stock in the Nordics in 2010-2017 taken from the *Nordic EV Outlook 2018* [22] is shown in Figure 1.4.

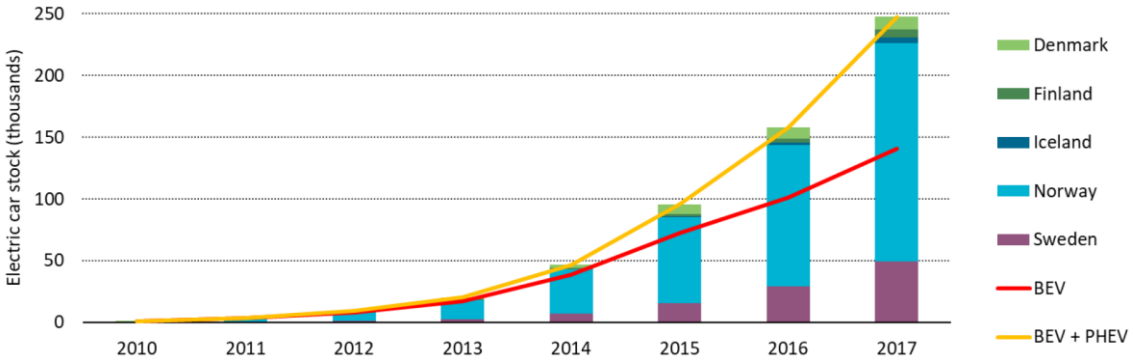

Figure 1.4 – Nordic EV stock for 2010-2017. Source: [22].

As for the sales, EVs accounted for 39% of new car sales in Norway in 2017 – the world's most advanced market of EVs in terms of sales share, i.e., the share of new EV registrations as a percentage of total new passenger light-duty cars registrations. Iceland and Sweden, the next two most successful markets, achieved 11.7% and 6.3% electric car sales share, in 2017 [20]. Figure 1.5 provides an overview of the EV sales, market share, and BEV-PHEV sales in the Nordics for 2012-2017. It can be noticed that BEVs prevail in Norway and Denmark (as their PHEV market shares in 2017 are below 50%), while Finland, Iceland and Sweden buy more PHEVs.

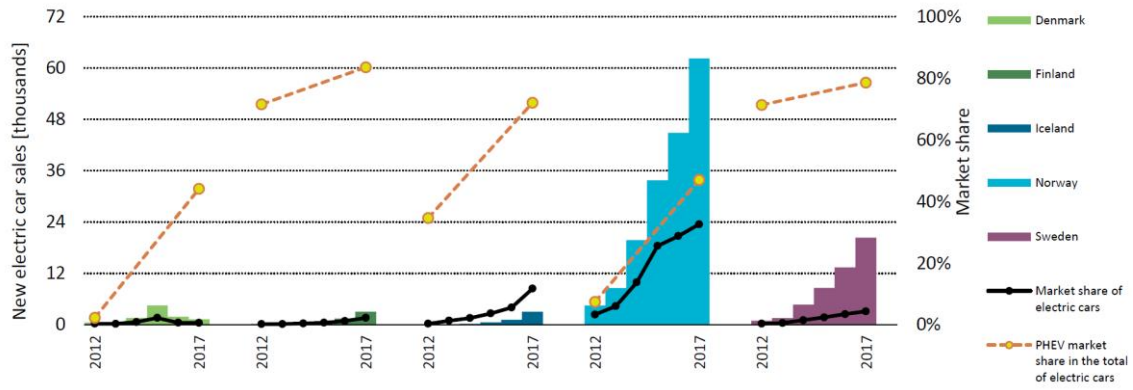

Figure 1.5 – EV sales, market share, and BEV/PHEV sales in the Nordics. Source: [22].

Another important aspect to analyze is the growth of the electric vehicle supply equipment (EVSE), i.e., chargers and charging infrastructure [20]. Chargers can be private or public chargers, and, along with the residential slow-rate chargers that use sockets in the households, they are crucial when it comes to the assessment of the grid impact of EV deployment. In general, EV chargers can be divided into slow and fast chargers according to the charging type and power level. EV charging is divided into 4 modes according to the IEC 62196 technical standard [23]. Mode 1 and 2 are slow charging modes with regular sockets, without and with some EV specific protection arrangements, respectively. Mode 3 can either be slow or fast charging, and requires a specific EV multi-pin socket, whereas Mode 4 is for fast charging, using DC charger technology e.g., CHAdeMO, CCS or the Tesla Supercharger. The total chargers in the Nordics by the end of 2017 amount to more than 260.000 with very large majority of private ones. Figure 1.6 shows the EVSE stock for 2010-2017 for private chargers and public fast or slow chargers, and their respective growth rates. One can note that EVSE deployment increased across all types of chargers in 2017, and publicly available slow and fast chargers grew less than the electric vehicle stock, as shown in Figure 1.5. Table 1.1 shows a detailed classification of the presence of different types of publicly available chargers in Denmark, Norway, Sweden and Finland, as of July 2018.

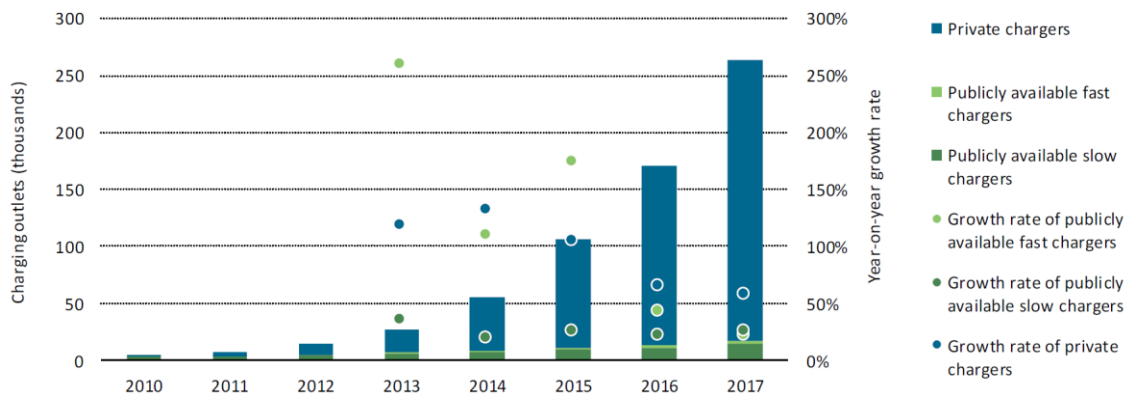

Figure 1.6 – EVSE deployment in the Nordics. Source: [22].

Table 1.1. Number of public chargers available in each country (July 2018), adapted from [21].

	Slow chargers	**Fast Chargers**		
		Tesla Supercharers	**CHAdeMO**	**CCS**
DK	2240	94	131	151
NO	8617	420	922	877
S	4431	200	306	299
FL	706	58	75	75

Another important aspect to mention is the high-level policies that each country implements to facilitate and incentivize massive EV roll-out. Norway is the country with the highest incentives for EV usage compared to the other Nordic countries, in line with the much higher EV penetration. The *Nordic EV Outlook 2018* [22] reports EV owners survey results showing that the most influencing

means of state incentives are VAT exemption and registration tax exemption. Exemptions on registration taxes are frequently available in Nordic countries, with no policy applied only in Iceland. Table 1.2 provides a more detailed outline of the current incentives implemented in Denmark, Norway, Sweden and Finland as of July 2018.

Table 1.2. Comparison of national incentives, adapted from [21].

	Tax Incentives	**Financial Incentives**	**Convenience Incentives**
DK	• 80% reduction in reg. tax (until end of 2018 or until 5.000 new EVs registered) • Tax exemption for FCEV • Reg. tax limit raised to 24800 €	• Tax reduction (0.13 €/kWh) for businesses • EV subsidies for business and municipalities	• Reserved parking spaces for EVs • Differential prices
NO	• Reg. tax exemption • VAT exemption • Road tax exemption • Reduced company car tax (50%) • Exemption from VAT (25%) on leasing	• Free parking spaces • Toll road exemption • Free public charging • Higher mileage allowance • No charges on ferries	• Bus lane driving • Reserved parking spaces • Fast charging station every 50 km on all main roads by 2017
S	• Bonus for cars with very low or zero emission (highest bonus is 5800 €) • Company tax benefits	• Super Green Car Rebate. • EV: Max 4500 € • PHEV: Max 2200 €	None
FL	• Reg. tax reduction (2.5% for BEVs) • Ownership tax benefits • Cash-for-clunkers – financial incentive worth up to 2500 € to exchange a vehicle for a modern, lower-emission model.	• Cheaper/free parking	None

1.1.3 EV charging strategies

Given the presented increasing EV penetration and the evolution of the power systems, to make EV integration successful, it is of interest to investigate the different charging strategies that may lower possible adverse effects on the electrical infrastructure. In case of uncontrolled charging, system operators would have to face technical issues such as components' overloading, under-voltages, voltage unbalances, peak load increase, and overall energy demand increase. In general, the traditional "fit-and-forget" approach would lead to the need for more grid reinforcements, resulting in an overall high cost for the society. This paves the way for the design and implementation of EV charging control for different purposes.

Controlled charging strategies can be divided in two categories, i.e., passive control and active control. Although the costumers are actively involved in both cases, the term 'passive' refers to the grid operator's perspective. Passive strategies usually encourage EV owners to shift the charging to off-peak time by using the so-called *Time-of-Use* tariffs. This kind of control is nowadays widely

used due to the simplicity of its implementation. However, such strategies may result in a sudden demand increase in the off-peak period when all EVs start charging almost simultaneously [24]. Using fixed hours for *Time-of-Use* tariffs is beneficial for the grid in case of traditional operating conditions, when load variations are the dominating variable in the power system. With increasing production from fluctuating renewable sources, the price variations will not be as predictable as before, possibly making this strategy counterproductive for the grid operation. The implementation of *Time-of-Use* tariffs is then seen as a feasible solution only for small EV penetration levels: with the increase of the EV market share, active charging strategies need to be adopted. Active smart charging strategies allow customers and grid operators to schedule the EV charging profiles in order to achieve different economic or technical objectives, which are presented in detail further on in this thesis. For achieving the chosen objectives, two EV operating modes can be utilized: uni-directional or bi-directional. For the first one EVs can only modulate the charging power, whereas for the second one EVs can also reverse the power flow, injecting power back to the grid via the so-called vehicle-to-grid (V2G) technology. Given the adopted charging strategies, EVs can be considered merely as passive electric loads or as distributed flexible resources, with high potentials for flexible grid operation. Table 1.3 reports the potential advantages and drawbacks of each possible charging strategy.

Table 1.3. Advantages and drawbacks of different strategies for EV charging.

Strategy		Advantages	Drawbacks
Uncontrolled charging		• Cheap and easy to implement • User friendly	• Peak power increase • Components' overloading • Voltage deviations • Power quality degradation • Additional grid reinforcement costs • Electricity cost increase
Passive control (Time-of-Use tariffs or Adaptive charging)		• Easy to implement • Consumption shifted to cheaper hours • Grid reinforcement deferred	• Unbalances due to fast load increase • Not always aligned with power price variations and grid constraints • Possible components' overloading • Possible power quality degradation such as voltage deviations • Customers active participation required
Active control	uni-directional	• Flexibility provision • Grid reinforcement deferred • Peak power reduction	• Complex implementation, yet easier than V2G • ICT required • Costumers active participation required
	bi-directional (V2G)	• Flexibility provision • Grid reinforcement deferred • Peak power reduction • Optimal RES integration	• Complex implementation • ICT required • Costumers active participation required • Possible battery degradation • Losses in grid-EV-grid transfers

1.2 Research objectives

This thesis deals with EV integration issues, in particular the challenges and opportunities for power system operators when exploiting EVs as flexible resources. The concept of flexibility is defined as the power adjustment sustained for a certain duration at a specific location, activated to meet a grid operator's need – a thorough definition is presented in Chapter 2. **EV flexibility is the key aspect of the work**: on the one hand it can reduce the self-induced adverse effects of EVs charging in weak distribution grids, on the other hand it can provide grid balancing services to transmission system operators. Issues arising in practical implementation are investigated, and recommendations for the different involved stakeholders are outlined.

In this thesis, the studies are performed on a number of electricity grids from low voltage distribution feeders to large-scale power system models. In particular, the analysis on radial Danish and Norwegian residential low-voltage grids can be a benchmark throughout the Nordic Region, making the results applicable to other Nordic countries as well. The thesis also reports stability studies on an islanded experimental micro grid within the SYSLAB-PowerLabDK infrastructure facility [25], in a power hardware-in-the-loop environment, and via simulations on the full-scale power system of the Danish Island of Bornholm.

The primary research question this thesis seeks to answer is: **What are the main challenges and opportunities when pro-actively integrating electric vehicles in the power system?** The overarching question can be split into the following sub-questions along with the corresponding research objectives:

Q1. *Focusing on both distribution and transmission level, what is the impact when integrating EVs, and what prerequisites are needed for supporting active EV involvement in the Nordic region?*

After analyzing the impact of uncontrolled EV charging on a system level and in representative residential LV grids, the need for flexibility is evident. The current policies and barriers against the roll-out of an active EV participation need to be identified in the different countries, and the need for defining appropriate requirements is highlighted both from the technical perspective as well as from the organizational and regulatory framework.

Q2. *What technical and economical conflicts may arise when acquiring flexibility products from EVs? How can they be detected and categorized?*

Different needs for flexibility services of each involved stakeholder can raise potential conflicts between two or more stakeholders with opposing needs. Given one possible market framework for DSOs, potential conflicts need to be identified and categorized, by using a respective conflict identification procedure.

Q3. *Are EVs able to provide reliable frequency regulation to the power system? What technical challenges can be identified when employing contemporary technology, standards and requirements?*

The identification of both the technical capabilities of series-produced EVs and controllability standard requirements enables the development and the implementation of control logics able to guarantee reliable power system frequency regulation.

Q4. *What operation strategies should be implemented by EV aggregators to enhance grid balancing service provision?*

Smart EV control solutions meant for EV aggregators are proposed. These are aimed at stabilizing potential frequency oscillations, at reducing reserve provision error, and at providing a trade-off between error and fleet efficiency.

Q5. *What guidelines are recommended for EV fleet operators for a safe replacement of conventional grid balancing units?*

A realistic EV fleet aggregation model is important for reliable power system studies when assessing the effect of EV fleets providing frequency regulation. The inclusion of appropriate requirements in the overall fleet output is necessary to assure an aggregated response similar to the to-be-replaced conventional grid balancing units.

Q6. *When integrating EVs in LV networks, to what extent can EV reactive power be considered as a tool to support voltages? What guidelines could DSOs require in terms of reactive power provision from off-board EV chargers?*

Similarly to the requirements for residential PV plants, it is of interest to assess the effectiveness of EV reactive power provision for voltage support when evaluating the installation of new off-board chargers in residential LV grids.

1.3 Thesis structure and research contributions

The thesis is structured as follows. Part I introduces and describes the main topics investigated in this thesis, while summarizing the main contributions of the scientific papers developed and published during the Ph.D. project. It is organized in six chapters: an introduction, four self-contained technical chapters, and conclusion. Part II includes the publications that contribute to this thesis. The description of each chapter in Part I is as follows.

Chapter 2 presents the consequences of massive EV penetration levels in the power system both for the transmission and the distribution grid level, including simulation studies in two representative Danish and Norwegian study cases. The need for flexibility is motivated, and its definition and attributes are outlined. Different needs for flexibility services of each involved stakeholder are then outlined, showing the rise of potential conflicts between two or more stakeholders with opposing

needs. Within a proposed market framework for the trading of EV flexibility on a distribution level, a number of technical and non-technical conflicts are identified and categorized, by using an innovative conflict identification procedure. The chapter addresses the research questions **Q1** and **Q2**, and includes content of **Paper A**.

Chapter 3 presents studies on the applicability of power system frequency control strategies employing EVs. A standard-compliant primary frequency controller is designed for uni-directional EV Mode 2 charging and is implemented to carry out investigations by means of both simulations and validations in an experimental microgrid with real EVs. Criticalities related to the implementation of EV controllers for frequency regulation considering the need for compliance with technical standards and commercial hardware limitations are identified, i.e., the control discreteness. Analytical formulations are proposed and the elasticity of an experimental power hardware-in-the-loop setup was used to implement different granularities of the EV response, complementing the investigation. The chapter addresses the research questions **Q3** and **Q4**, and includes content of **Paper B**, **Paper C** and **Paper D**.

Chapter 4 focuses on bi-directional EV operation. First, it reports results of hardware test with focus on the technical capabilities of commercial EV and off-board charger when performing V2G operations, assessing the suitability for the provision of grid services by testing the attributes of the flexibility product. Then, it investigates possible challenges that EV aggregators and transmission system operators may face when EV fleets provide frequency control. An EV fleet management strategy for aggregators is presented, which implements a stochastic logic to achieve a trade-off between the average error in the reserve provision during a V2G session and the overall fleet efficiency. Further, Realistic EV fleet models are utilized to perform full-scale power system stability simulation studies aimed at outlining guidelines for the TSOs for a safe frequency control via aggregated EVs performing V2G operations. The chapter addresses the research questions **Q4** and **Q5**, and includes content of **Paper E**, **Paper F** and **Paper G**.

In Chapter 5, the focus is moved to the distribution grid level. A generalized analytical investigation on reactive power control for voltage support is reported. The outcome is a tool for DSOs for evaluating the effectiveness of reactive power for voltage control in representative radial distribution feeders when evaluating new installations of off-board EV chargers. With the proposed formulation the DSO is able to assess the voltage drop compensation due to the application of a specific power factor by the EV charger as function of the LV feeder length, given as input the EV charger installed power and the voltage dependencies of loads in LV networks. The chapter addresses the research question **Q6**, and includes content of **Paper H** and **Paper I**.

Finally, Chapter 6 gathers the most important conclusions and suggestions for future research.

Short abstracts of each relevant publication included in Part II are listed as follows:

Paper A is a peer-reviewed article published in the Proceedings of the *7th IEEE PES Innovative Smart Grid Technologies Europe (ISGT Europe)* in 2017. This work concerns the prioritization problem of electric vehicles service provision among different system operators, from a technical point of view. The goal of this paper is to provide an identification procedure that is able to detect, identify and catalogue possible conflicts among the involved stakeholders that take place when requesting and/or acquiring ancillary services from flexible units connected at a distribution level.

Paper B is a peer-reviewed article published in the Proceedings of the *2016 Universities Power Engineering Conference (UPEC)* in 2016. This paper presents modeling and analysis of the benefits of primary frequency regulation by electric vehicles in a microgrid. Criticalities related to the implementation of standard-compliant EV controllers for frequency regulation are investigated, i.e., the control discreteness. Further, an innovative control logic algorithm is introduced, with the purpose of curtailing the number of current set-point variations that the battery needs to perform during the regulation process.

Paper C is a journal article published in *Applied Energy* in 2018. This paper investigates the technical feasibility of series-produced EVs to provide frequency support through a set of laboratory experiments in a microgrid. Moreover, this work assesses the technical barriers when controlling commercial EV hardware via smart controllers and investigates the EV responsiveness when it comes to the provision of time-critical flexibility services.

Paper D is a journal article submitted to *IET Smart Grid* (under review). This paper addresses the effects on power systems of control discreteness in aggregated EVs providing frequency regulation. The EV chargers are controlled according to the system frequency deviation by implementing a standard-compliant fast primary frequency controller. Challenges related to discrete EV responses are first identified by a theoretical analysis and then an EV fleet management solution relying on droop shift strategies for the individual EVs within a fleet is proposed. The controller is implemented in a microgrid with a power hardware-in-the-loop approach, to complement the investigation with an experimental validation.

Paper E is a peer-reviewed article published in the Proceedings of the *EVS 31 & EVTeC 2018 the 31st International Electric Vehicles Symposium and Exhibition & International Electric Vehicle Technology Conference* in 2018. This work presents results from V2G-ready equipment tests. The technical capabilities of an EV connected to a commercial V2G charger are investigated when controlled either locally or remotely. The charger is characterized in terms of efficiency characteristics, activation time, response granularity, ramping-up/down time, accuracy and precision. Results show the performance for different operating conditions, highlighting the importance of a good calibration and knowledge of the employed hardware when providing standard-compliant grid regulation services via V2G technology.

Paper F is a peer-reviewed article published in the Proceedings of the *20th Power Systems Computation Conference (PSCC 2018)* in 2018. This work investigates some possible challenges that EV aggregators may face when managing their fleets. A controller with tunable response granularity is designed, allowing the EV fleet operator to optimize the overall fleet operation. The paper shows that the proposed controller can significantly reduce reserve errors and increase efficiency for a given fleet size, while at the same time minimizing the switching actions.

Paper G is a journal article submitted to *Electric Power Systems Research* (under 2nd round of review). This paper assesses the impact of aggregated electric vehicles providing primary frequency regulation via vehicle-to-grid technology. The aim of the work is the definition of a set of recommendations to fulfil in order to guarantee a safe large-sale employment of EV fleets as primary reserve providers responding similarly to the replaced conventional rotating units.

Paper H is a journal article published in *CIRED - Open Access Proceedings Journal* in 2017, which was presented at the *24th International Conference on Electricity Distribution (CIRED).* It investigates the effectiveness of reactive power provided by electric vehicles in supporting the local voltage in distribution networks. Specifically, the work focused on the requirements of voltage regulation from the grid operator's point of view, when it comes to allow installations of new charging stations with fast charging capability.

Paper I is a journal article published in *International Journal of Electrical Power & Energy Systems* in 2018. This paper was written as a continuation of the work carried out in Paper H. The main difference is the completeness of the analytical formulation, now including the load voltage dependency. Furthermore the model has been validated also in typical radial distribution feeders on a simulation basis.

CHAPTER 2

EVs as a flexible resource: towards a proactive grid integration

In this chapter, the consequences of massive EV penetration levels in the power system are presented both for the transmission and the distribution grid level. For the transmission system, the increase of the total early energy and peak demand is presented, whereas simulation studies in LV feeders showed the negative effects of uncontrolled EV charging in terms of unacceptable congestion and under-voltages in two representative Danish and Norwegian study cases. The need for *flexibility* is so motivated, and its definition and attributes are outlined. Then, current policies and barriers against the roll-out of an active EV participation are identified with emphasis on the Nordics, and the need for defining appropriate requirements is highlighted both from the technical perspective as well as from the organizational and regulatory framework. The focus is so moved to the different needs for *flexibility* services of each involved stakeholder, showing the rise of potential conflicts between two or more stakeholders with opposing needs. A market framework for the trading of *flexibility* on a distribution level is finally proposed, and a number of technical and non-technical conflicts are identified and categorized, by using a conflict identification procedure.

The chapter includes results of the publication **Paper A**, attached in Part II. Furthermore, the two LV grid impact studies are taken from the co-authored works [26] and [27].

2.1 EV integration in the power system

Given the decommissioning of traditional large power plants in favor of generation from RES, the need for additional ancillary services is evident, especially for balancing purposes. In the modern power system, every user can become an active player within the context of the smart grid: traditional service providers are being replaced by aggregated units mostly connected to LV grids. This poses challenges to DSOs, who are in charge of maintaining their distribution networks within acceptable voltage and loading levels, while searching for solutions that defer investments in grid reinforcement. Since grid balancing is a responsibility of the TSO, whereas respecting the local grid constraints needs to be secured by the DSO, it is clear that greater cooperation between TSOs and DSOs is needed [28]–[30].

2.1.1 Integration on a system level

The main effects of an increasing penetration of EVs on a system level are the increase in terms of electricity consumption and peak load. As stated in the *Nordic EV Outlook 2018*, in 2017 the EVs' electricity consumption in the Nordic region was limited: about 500 GWh, which is less than 0.1% of the total demand in the Nordics. In the extreme case of all light-duty vehicles being electric, the additional consumption of EVs would be 6.1% in Norway and 20% in Denmark, given the overall lower total electricity demand compared to Norway. However, this is not seen as an insurmountable issue, as it is expected that the 100% penetration level will be reached via a gradual process until 2050 [31], and it can be seen as an opportunity of augmenting the penetration of RES in the generation mix in the Nordic countries, which can already claim a very heterogeneous, low-emission portfolio [22]. As for the peak demand, the main concerns are on the distribution grid infrastructure, i.e., charging EVs may cause transformer or lines over-loadings or power quality issues. As shown in the next subsection, this may happen in case of high penetration levels, although residential users in the Nordic region have higher available power at the connection point compared to the households in the rest of the European countries (9-15 kW for detached houses and 6 kW for apartments).

Furthermore, as presented in Chapter 1, the increasing share of RES in the generation mix brings along the need for more ancillary services to be delivered for counteracting the fluctuations in the generation from volatile resources. Since within the context of this thesis charging EVs are considered fast responsive units with potentials for grid regulations, it is of interest to outline the current conditions for participating in the trade of ancillary services within the framework of system frequency regulation in the RG-N, benchmarking the required performance of an EV fleet. In the RG-N synchronous area, primary frequency control consists of two separate services, namely frequency-controlled normal operation reserve (FNR), activated linearly for all system frequency deviations within ±100 mHz, and frequency-controlled disturbance reserve (FDR), activated only when the frequency drops below 49.9 Hz. In the current framework there is no automatic secondary frequency control in the RG-N power system, whereas tertiary reserve is in place [32]. FNR is a symmetrical service, which means that the provider must offer the same upwards and downwards reserve capacity. The reserve is provided linearly with no dead band and with full activation for deviations of ±100 mHz. According to the service requirements, the reserve has to be provided within 150 seconds [32]. The minimum size of total FNR reserve that has always to be procured in the RG-N is 600 MW, divided proportionally to each TSO in the synchronous area. FDR is a non-symmetrical service, as the involved units respond with only frequency up-regulation by linearly injecting power into the system when the measured frequency is below 49.9 Hz, with full reserve activation at 49.5 Hz. The 50% of the response has to take place within 5 s, whereas the remaining 50% within an additional 25 s. The minimum bid size for FNR and FDR is 0.3 MW, which can be achieved already with relatively small EV fleets: 30 EVs in case of off-board ±10 kW bi-directional chargers or 260 slow-charging uni-directional EVs controlled as presented in Chapter 3.

2.1.2 Integration on a distribution level

Charging EVs behave as large concentrated loads and, since mostly charging in residential areas at a LV level, one of the most challenging aspects is the impact on distribution networks [33], [34]. In fact, DSOs should be always able to operate their distribution networks seuring standard-compliant levels of power quality, according to the European technical standard EN 50160 [35]. DSOs' tasks include finding the most efficient and affordable way to deliver the electricity to consumers while ensuring the quality of service, which comprises continuity of supply and power quality. A number of different technical requirements have to be met, laid out in national and international laws, standards and grid codes [36]. To achieve a proper distribution grid operation, DSOs have to solve network contingencies, which are divided into congestion and voltage issues, as indicated in Figure 2.1.

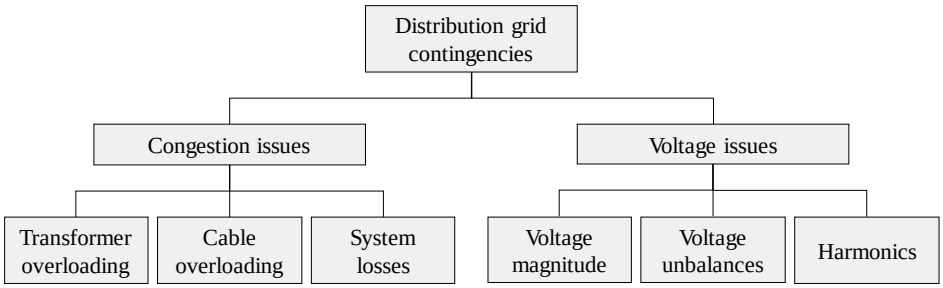

Figure 2.1 – Classification of distribution grid contingencies to be solved by DSO.

Nowadays, DSOs mainly perform voltage regulation by adding capacitor banks or installing transformers with on-load automatic tap changing capability [37]. If such strategies are not successful, the distribution feeders are usually reinforced. In addition to voltage regulation, DSOs are also concerned on overloading issues as grid components are manufactured to operate at a given rated power or current, so overloading will inevitably result in shorter life expectancy. In Denmark (and likely in the other Nordic countries as well), the capacity limit is typically kept at 70% as a "rule-of-thumb" in normal operation, since the remaining 30% is saved for supplying neighboring feeders in case of a contingency [38]. Hence, if components are often operating above their 70% capacity, the DSO needs to reinforce the grid by upgrading to components with a higher rated power.

Two grid impact studies in representative LV grid in Denmark and Norway are reported in the following. They show the negative impact of massive EV roll-out in distribution grids, highlighting the need for counter-actions by the grid operator. Within this context, great research effort is put on smart solutions as an alternative to the mentioned conventional grid reinforcement investments. This can be enabled via the exploitation of the controllability of inverter-interfaced DER units such as EVs, by means of grid services to DSOs. In this regard, the effectiveness of voltage regulation via reactive power modulation in representative distribution feeders will be investigated in Chapter 5, in order to assess to what extent this technology can effectively be beneficial for voltage regulation purposes.

2.1.2.1 Impact study on a Danish LV grid

To investigate the impact of uncontrolled EV charging on LV electrical infrastructure, simulations in DIgSILENT PowerFactory software environment are conducted for a representative Danish LV grid located in Borup, Zealand [26]. It is a 400 V radial distribution grid with 4 feeders connected to the 10 kV MV network through a 400 kVA distribution transformer. For one of the four feeders, consumption and PV production smart meter data was available for 43 individual households on hourly basis for one year, whereas the remaining three are represented as a single aggregated load connected to the LV transformer side. The grid layout Figure 2.2 shows also the buses where new installations of off-board chargers are evaluated within the analysis in Chapter 5. For a detailed description of the grid the reader is referred to Appendix A.

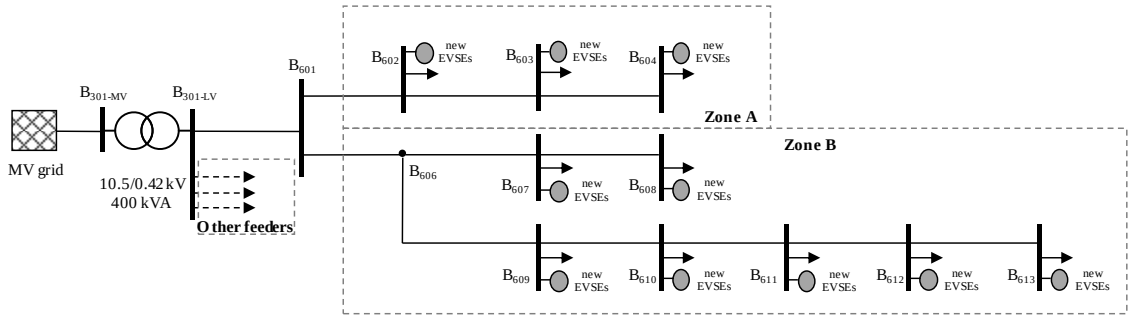

Figure 2.2 – Single-phase circuit diagram of the modelled Danish distribution grid.

The implemented individual real-metered consumption and production profiles provided by the DSO SEAS-NVE showed uneven distribution among the three phases, leading to neutral currents and consequent voltage unbalance conditions, as depicted for a representative time period in Figure 2.3.

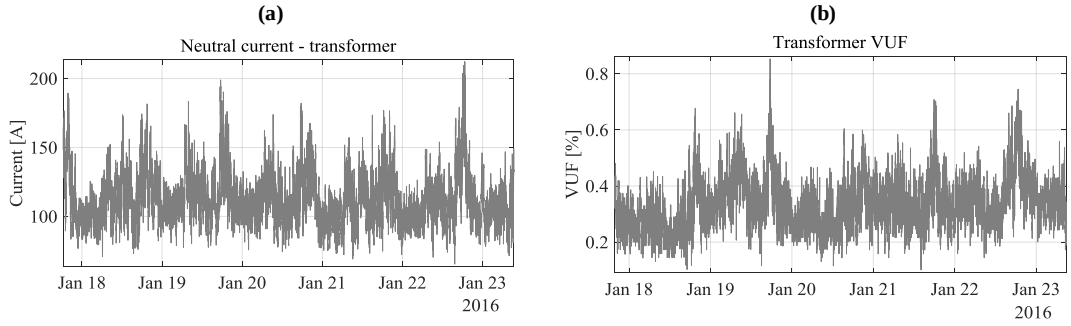

Figure 2.3 – Neutral current (a) and voltage unbalance factor (b) at the transformer. The voltage unbalance factor (VUF) is calculated as the ratio between the negative and the positive voltage sequence according to the *True Definition* [39].

For the simulation studies, an EV is added to each household in the observed feeder (43 EVs) resulting in a 100% local penetration rate, and the worst case of all EVs charging simultaneously is considered. As a side note, the penetration rate at the transformer level is 25% since all feeders have approximately the same amount of households and no EVs are added to the remaining three feeders. EVs are connected through a Mode 2 charging infrastructure with a single-phase 16 A plug, i.e., consuming 3.7 kW under nominal voltage V_n=230 V. The charging pattern is adapted from measured

real pattern within the *Test-an-EV program* [40] and corresponds to an average uncontrolled charging profile that lasts for 5 hours with starting time randomly distributed between 18:45 and 19:15. Figure 2.4-a shows the voltage magnitudes for all buses in the observed feeder in case of uncontrolled EV charging by means of box plots. The buses corresponding to Zone B are the most critical due to a extended use of heat pumps, especially the ones on the second branch due to the higher distance from the point of common connection. To evaluate the unbalanced conditions in which the studied grid operates, attention is given to the three individual phase-neutral voltages. In this regards, the voltage magnitudes for each phase for the selected most critical buses are shown in Figure 2.4-b, again by means of box plots. From there, phase *a* individually is identified as the only one that could be problematic. As completion of the graphical results in Figure 2.4, Table 2.1 reports under-voltage conditions along the year, in hours and percentage of the year, assuming $0.90V_n$ as lower voltage limit. The comparison with the no EV case is shown, and it can be noticed that the 100% EV penetration case leads to non-negligible under-voltages. The table also includes the VUF, for which the European standard EN 50160 requires values below 2% [35]. Since the EVs are integrated into the simulated grid trying to maintain a balanced distribution, no remarkable worsening on the voltage unbalance is expected for this 100% penetration scenario, with VUF values always below the upper acceptable limit of 2%.

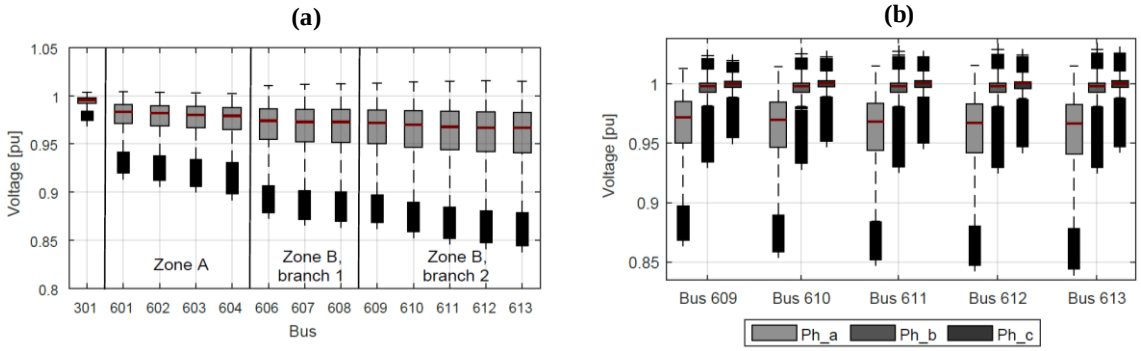

Figure 2.4 – 1 year simulation results: voltage magnitudes for different buses of the observed feeder (a), of each phase for selected buses (b). The boxes indicate 50% of the observations, whereas the median is in red. Upper and lower quartiles (25% of the data) are located within the vertical lines. The dark horizontal lines outside the boxes are overlying outliers.

Table 2.1. Under-voltage occurrences in hours and % of the year, and maximum VUF.

Scenario	**Under-voltage V<0.90V_n occurrences in one year**					**Max VUF [%]**
	Bus 609	**Bus 610**	**Bus 611**	**Bus 612**	**Bus 613**	
No EVs	0.17 h 0.002%	9.17 h 0.10%	14.00 h 0.16%	33.00 h 0.38%	38.50 h 0.44%	1.63
100% penetration on the feeder	170.33 h 1.94%	281.67 h 3.21%	375.50 h 4.29%	439.67 h 5.02%	477.33 h 5.45%	1.78

It is of interest also to assess the possible components' overloading issues. Table 2.2 shows the loading analysis for the whole simulated year of cable 301-601 (the most critical cable), as well as for the transformer. The maximum loading values and a quantification of the time that each component is overloaded are provided. Results confirm a considerable impact of adding the EVs as

passive loads in a distribution network concerning to components loading level. Values above the technical limits are reached several times over the year, for both the cable and the transformer.

To conclude, it is clear that such conditions are not acceptable for a safe and reliable grid operation. DSOs are then supposed to opt for grid reinforcement investments, unless looking into smart EV charging solutions such as active or reactive power control to reduce self-induced negative effects.

Table 2.2. Annual cable 301-601 and MV/LV transformer loading analysis.

Scenario	Cable 301-601		MV/LV transformer	
	Max. loading	Overloading time over a year	Max. loading	Overloading time over a year
No EVs	68.14%	0.00 h 0.00%	96.82%	0.00 h 0.00%
100% penetration on the feeder	124.65%	165.67 h 1.89%	129.53%	333.00 h 3.80%

2.1.2.2 Impact study on a Norwegian LV grid

Similarly to the analysis in the Danish LV context, results from a simulation study for a representative Norwegian LV grid located in Steinkjer, Trøndelag are now proposed [27]. Simulations are carried out with the power system simulation tool Matpower for Matlab. The modelled LV grid is connected to the 22 kV MV level through a 500 kVA distribution transformer, which supplies 20 distribution feeder lines (A1-M2) for a total of 54 end-user buses. The local DSO Nord-Trøndelag Elektrisitetsverk (NTE) provided real data in terms of hourly three-phase power consumptions for the whole year of 2012 for all end-users in the system. The grid layout is shown in Figure 2.5. For more insights on the grid, the reader is referred to Appendix A.

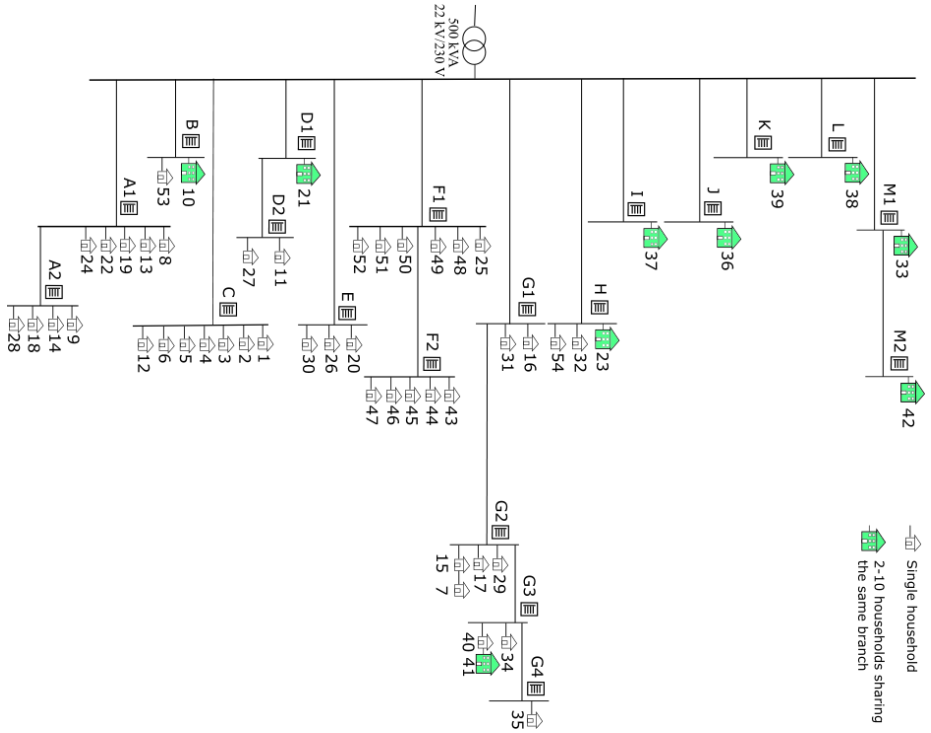

Figure 2.5 – Single line diagram of the Norwegian distribution grid.

Different levels of EV penetration have been studied to assess their impact on the distribution network. A realistic EV charging profile was derived by real measurements (provided by NTE) from a dedicated smart meter installed in one household owning an EV for the whole 2016. The charging energy was approximately 12 kWh, with power peak values between 3.7 and 7.3 kW (Mode 2). Such charging pattern was utilized for the study, considering balanced three-phase EV connections, thus not introducing any unbalances to the system. Figure 2.6 shows the lowest voltage magnitudes for all the buses in the observed feeders in case of uncontrolled EV charging for growing EV penetrations, where 100% means that all end-users have an EV and charge simultaneously, to analyze the worst possible scenario. As expected, the buses G3 and G4 are the most critical, as located with the higher distance from the secondary side of the transformer. For these buses, the lower threshold of $0.90V_n$ imposed by the EN 50160 technical standard is achieved already for an EV penetration rate of 60%. Also, for the 100% penetration case, it can be noticed that critical values of $0.85V_n$ are found, which are substantially below the limit of 0.90.

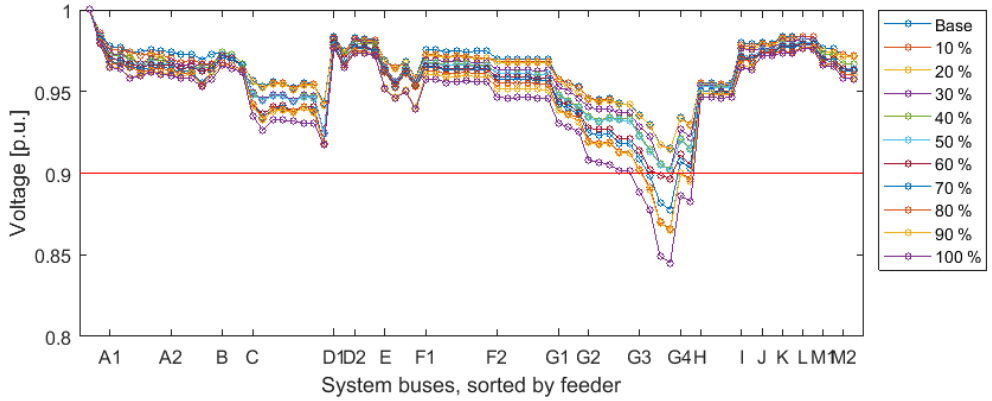

Figure 2.6 – Lowest voltage magnitudes for all buses in the system, for growing EV penetrations.

Table 2.3 reports the overall results of under-voltage conditions along the year, in hours and percentage of the year, assuming $0.90V_n$ as lower voltage limit. The table shows a summary of the end-consumer state under all EV penetrations, stating the number of hours where one or more end-users experienced under-voltages, for the whole year. Results for all EV penetration levels are shown, and it can be noticed that uncontrolled EV charging with 100% penetration rate leads to 75 hours of under-voltages, which is a non-negligible scenario.

Table 2.3. Under-voltage occurrences for at least one user in hours and % of the year.

EV penetration level	Under-voltage $V<0.90V_n$ occurrences in one year
0-50%	0 h 0.00%
60%	2 h 0.02%
70%	11 h 0.12%
80%	31 h 0.35%
90%	37 h 0.42%
100%	75 h 0.85%

Table 2.4 reports the loading analysis for the whole simulated year of cable G1-G2 (the most critical cable), as well as for the LV/MV transformer. Again, the maximum loading values and a quantification of the time that each component is overloaded are included. Results show that in general critical overloading do not appear for the 100% scenario, as a consequence to the fact that the components in this particular LV grid are heavily over-sized. However, overloading are found for the cables connecting the end-users to the respective buses: 511 h of overloading, meaning 5.81% of the time of the year. In general, it is shown that high EV penetration levels may lead to an increase of components' loading by almost 50% compared to the base case, confirming a considerable impact of adding the EVs as passive loads in a distribution network.

As concluded in the previous subsection, under-voltage and/or overloading conditions may be prevented only if DSOs opt for grid reinforcement investments, or implement smart solutions such as stationary batteries, load shedding/shifting, or charging EVs.

Table 2.4. Annual cable G1-G2 and LV/MV transformer loading analysis.

Scenario	Cable G1-G2		LV/MV transformer	
	Max. loading	**Overloading time over a year**	**Max. loading**	**Overloading time over a year**
No EVs	50%	0 h 0.00%	65%	0 h 0.00%
Uncontrolled Charging (100%)	95%	0 h 0.00%	105%	12.00 h 0.14%

2.1.3 EV as a flexible resource: the flexibility service

To limit the self-induced adverse effects on the power system, **EVs can be considered as promising flexible resources able to improve the system operation**, making them an attractive asset for both TSOs and DSOs. In fact, from a power system point of view, EVs are distributed energy storage systems with large potential for network regulation, being capable of adjusting the battery charging/discharging process in order to provide different ancillary services for supporting the power grid [41]–[44]. It is clear that many different control logics can be implemented according to specific control objectives. Typically, when providing a grid service the individual EV owner interfaces with the grid operators through an *EV aggregator* or *EV fleet operator*. This entity's main role is to aggregate a number of EVs and to manage their charging profiles, providing various flexibility services on their behalf. This role is crucial, as most of the ancillary services have a significant impact only if provided by a large EV fleet. The aggregator's main responsibility is the provision of flexibility services to the power system operators with optimal management and allocation of EV resources, while satisfying the user's driving needs.

The control infrastructure of an EV fleet providing grid services is shown in Figure 2.7. In this case the EV aggregator remotely controls the individual EVs in a centralized fashion, and bi-directional communication is continuously performed. Note that the EV battery power flow can be bi-directional (V2G) (in the example, EV 1 and EV 2) or uni-directional (EV n). In the first case, the controlled charger can either be located off board (DC current flows in/out the battery by-passing the on-board power electronics) or on board (AC current flows in/out the on-board charger before/after reaching the battery). Also in case of uni-directional AC charging, the on-board charger is in operation and controlled.

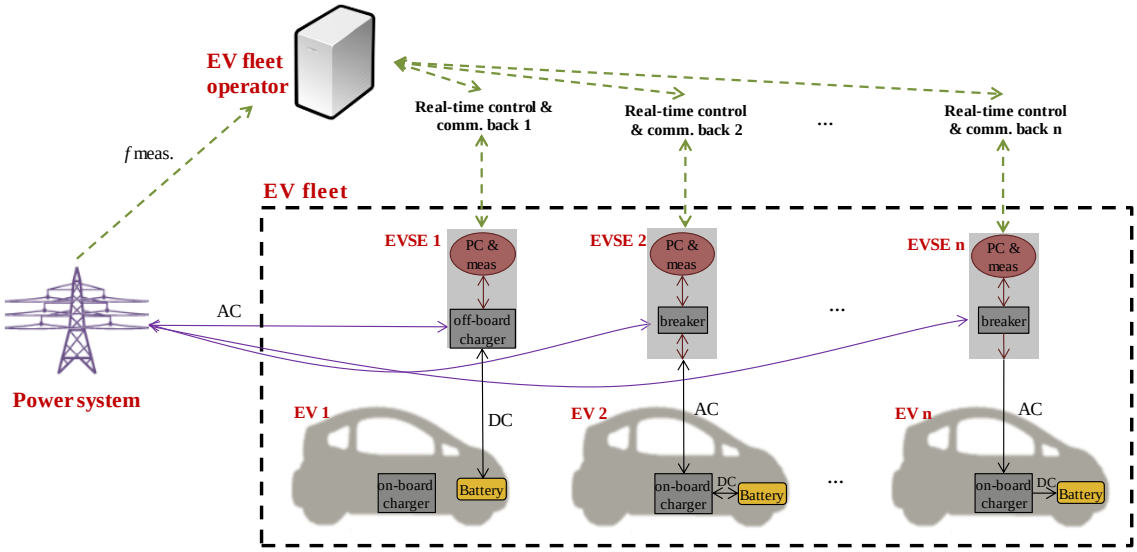

Figure 2.7 – Centralized control setup for grid service provision via EVs, with continuous bi-directional communication for real time operation.

Another possible setup is based on decentralized control logics. In this case each individual EV has an independent local controller embedded in the EVSE, which computes the charging/discharging set-point to achieve the desired service provision. With this setup, the aggregator has less observability of its fleet, but the operation would be faster and more reliable, as bad data or bad communication issues are now excluded in the real time operation. Bi-directional communication with the EV aggregator can be performed periodically (every 5-10-15 minutes) exchanging information, e.g., regarding battery state of charge (SOC) and target set-point around which the local control action takes place and the service is provided. Figure 2.8 shows an example of a decentralized control setup, again with bi-directional DC charging (EV 1), bi-directional AC charging (EV 2), and uni-directional AC charging (EV n).

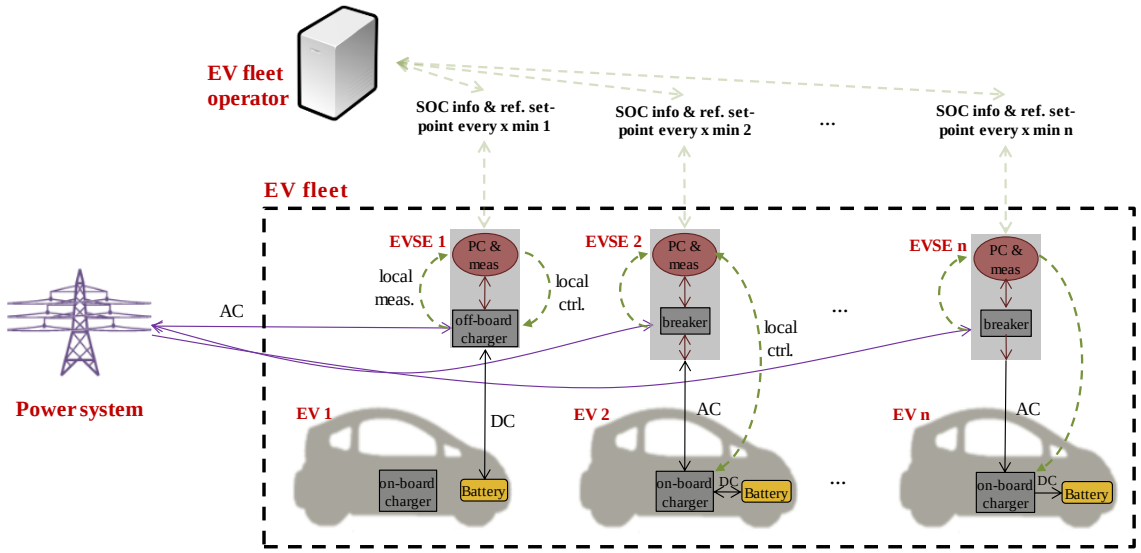

Figure 2.8 – Decentralized control setup, with periodical bi-directional communication.

On behalf of the individual EV owners belonging to the fleet, the EV aggregator interacts with the electricity markets, and trades the flexibility grid services. Among the main stakeholders involved in the trading of EV flexibility, the balance responsible party (BRP) is the entity financially responsible for the energy acquired from the power market, and interacts with the TSO. To summarize, Table 2.5 lists the main stakeholders and describes their role.

Table 2.5. Main stakeholders involved in the trading of EV flexibility.

Stakeholder	Role
TSO	Responsible for the transmission system operation stability. It needs services, among others, for frequency control (from primary to tertiary reserve) and voltage support for the transmission grid
DSO	Responsible for the distribution grid operation and thereby for ensuring power delivery to customers at all times, without disturbing the transmission system. It needs services, among others, for peak-shaving (MV/LV transformer or lines congestion management) and local voltage control
BRP	Financially responsible for the energy acquired from the power market. In case of deviations from the purchased energy, the BRP has to pay for imbalances to the TSO, since the TSO is forced to activate additional regulation in order to correct the imbalances
EV owner	Willing to offer flexibility to the EV aggregator within certain comfort and technical boundaries
EV aggregator	Collects all the flexibility offers from the EV owners of his fleet, makes correspondent contracts with them, and bids in the market. Based on individual EV capabilities, flexibility products are grouped and offered to the market

Now that the possible control setups for EV services procurement along with main involved stakeholders have been outlined, it is relevant to provide a definition of the concept of **EV flexibility product**, and what this means for TSOs and DSOs. This completes the overview of the EV flexibility trading, as introduction to the next analyses concerning the challenges on EV flexibility acquirement for DSOs and TSOs across the Nordic countries, and possible conflicts that may arise.

In order for the EV to correctly procure the amount of power needed for a given ancillary service, it is necessary to define the most important attributes that characterize the unit response. So, similarly to the ancillary services for the TSO, a definition for an EV flexibility product when providing services either to DSOs or TSO is presented. The flexibility product can be defined as the **power adjustment sustained from a particular moment for a certain duration at a specific location**, as defined in **Paper A** and in [45]. Based on the characterization of a given EV flexibility product, it may be classified as more suitable for a system-wide service rather than for solving a local problem, or vice versa. Thus, establishing standardized tests for evaluating the individual EV parameters is needed to categorize the supplied EV flexibility product. A flexibility product is characterized by four theoretical attributes, in Figure 2.9-a, as well as by six practical attributes which arise due to imperfections, as shown in Figure 2.9-b, taken from [45].

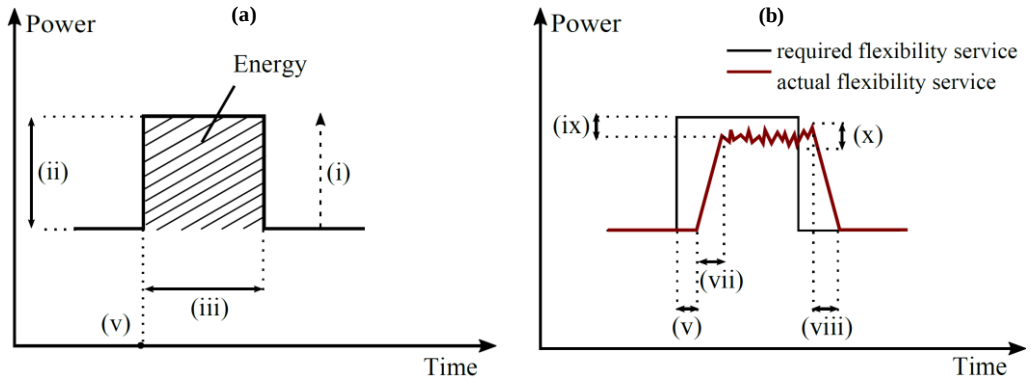

Figure 2.9 – Theoretical (a) and practical (b) attributes of a flexibility product.

Based on the individual EV capability, the flexibility can be grouped by the aggregator and offered to the interested stakeholder within a dedicated market framework. To make such management possible, generic requirements must be defined with respect to the described attributes, including:

(i) Direction: The information if an EV can provide uni-directional or bi-directional power flow.

(ii) Power capacity: The nominal rating of the charging/discharging equipment and the active/reactive power capability.

(iii) Duration: The period within which flexibility is acquired. The maximum energy which can be exchanged is implicitly contained through power capacity and duration.

(iv) Location: Either the node of coupling or the corresponding superior substation.

(v) Activation time: Period between receiving the set-point and activating the flexibility.

(vi) Set-point linearity: The discreteness of the charging/discharging power set-point. It is not shown in Figure 2.9, but will be thoroughly investigated in Chapter 4.

(vii-viii) Ramp-up/ramp-down time: The acceptable and/or desirable up/downwards rate-of-change duration between the activation time and full service provision, and vice versa.

(ix) Accuracy: The acceptable difference between the required and the delivered response.

(x) Precision: The acceptable variation of the delivered response, i.e., the amount of variation that exists in the delivered response for the same required value.

The procurement of ancillary services for TSOs in the electricity markets is addressed in different ways, depending on the market design and power system rules. Detailed surveys on current ancillary service markets in Europe and US are reported in Ref. [46] and [47], respectively. The principal ancillary services that TSO acquires to maintain stability and safe electricity transmission and procurement are commonly oriented towards the frequency control domain. They are divided into primary, secondary and tertiary frequency control, as described in Chapter 1. Moreover a new service is recently considered prominent: the synthetic inertia. It exploits the fast reacting properties of converter-connected resources to counteract the reduction of system inertia due to the replacement of conventional synchronous generators with RES. As for the distribution systems, the grid operation is currently achieved with independent actions of the operators, without any involvement in any market environment. Nonetheless, considering a future local electricity market framework, the tradable EV flexibility services for DSOs would aim at achieving technical objectives. They can be divided in two groups depending on the targeted grid constraint, namely services for solving loading issues and services for solving voltage issues [48].

Table 2.6. EV flexibility services.

Name	Description	Required Performance
System-wide Services		
Primary Frequency Control in RG-N, Normal (FNR)	Symmetrical, activated linearly with no deadband for freq. deviations <±100 mHz	Full activation < 150 s
Primary Frequency Control in RG-N, Disturbance (FDR)	Asymmetrical, activated linearly for freq. deviations within -100,-500 mHz	50% of response < 5 s, remaining 50% < 30 s
Primary Frequency Control in Continental Europe (FCR)	Symmetrical, ±20 mHz deadband, activated for freq. deviations <±200 mHz	50% of response < 15 s, remaining 50% < 30 s
Secondary Frequency Control in Continental Europe (FRR)	It restores the frequency to 50 Hz after deviations	Response time < 30 s
Tertiary Frequency Control in RG-N (Manual Reserve)	It replaces secondary regulation	Full activation < 15 min
Tertiary Frequency Control in Continental Europe (RR)	It replaces secondary regulation	Full activation < 15 min
Synthetic Inertia	It aims at emulating the mechanical inertia of the rotating generators	Response time < 1 s
Adaptive Charging	The charging is shifted in time	Charging controllability
Distribution grid Services		
Congestion management	It helps to mitigate over-loadings	Charging controllability
LV over-/under-voltages management	Massive penetration of DERs as well as EVs could lead to over- or under-voltages	Charging controllability
LV grid phase balancing	Single-phase EVs could help to mitigate the phase unbalances in LV networks	1-phase connection and charging controllability
Islanded microgrid and black start	EVs able to sustain a small power system could be a valuable resource	Power electronics able to set the system freq.

2.2 Provision of system-wide services: current policies/barriers

Ancillary service provision from EVs (both with uni- and bi-directional power flow) pertains to the domain of demand response, which in general is growing in popularity as an alternative to traditional grid service providers. Many studies and research projects analyzed the current state of the art in relationship to the electricity markets opening towards the inclusion of demand response resources [49]–[53]. A study carried out by the SEDC (Smart Energy Demand Coalition) consortium provides an overview of the actual status of the current regulatory framework in 18 countries of the EU zone, and proposes a demand response map in its *Explicit Demand Response in Europe - Mapping the Markets 2017* technical report [53]. The following criteria have been utilized to assess the market opening towards demand response: 1) Demand Response access to the markets, 2) Service providers' access, 3) Product requirements, and 4) Measurement and verification, payments and penalties. The classification is done by assigning a grade to each criteria (0 to 5, with 0 for markets closed to demand response, and 5 for more open cases), leading to an overall grade for the general status of demand response in the overall electricity market. The map in Figure 2.10 indicates the overall categorization of the different countries. The red color is for grade 0, orange is for 1, yellow for 3 and green for 5.

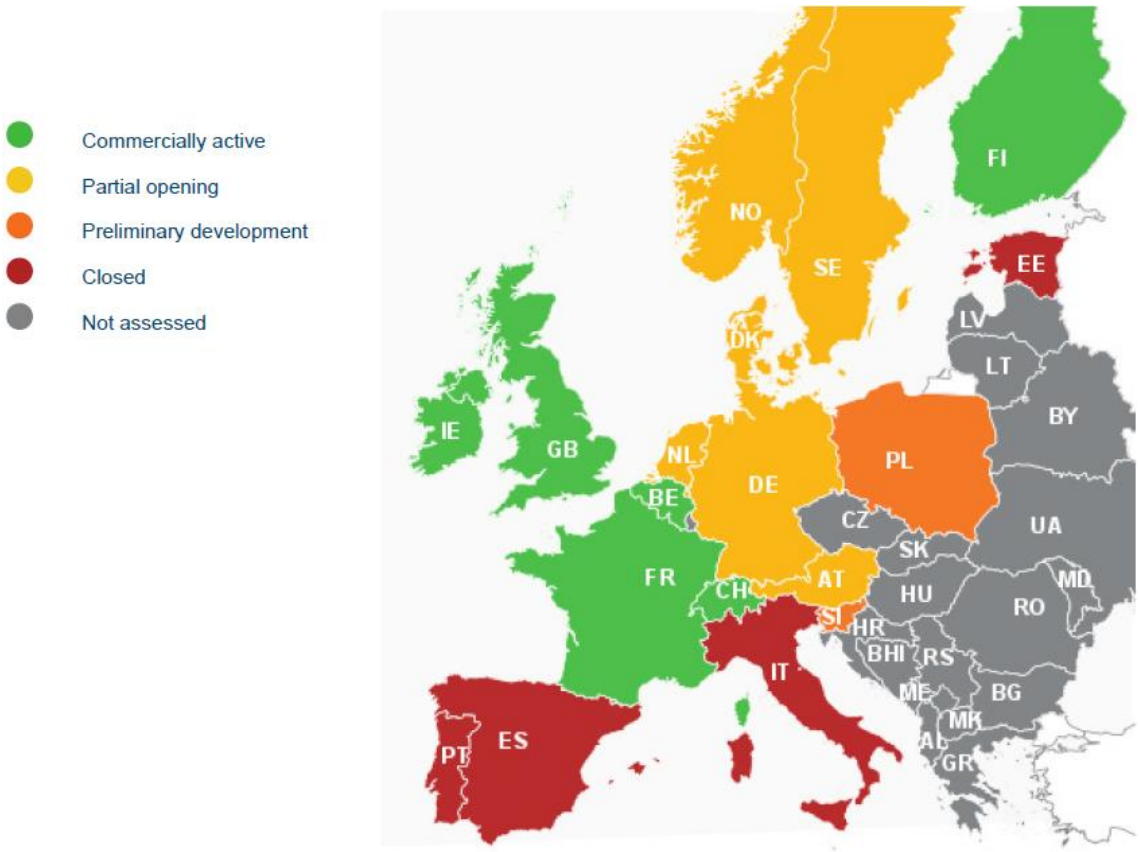

Figure 2.10 – Map of demand response development in Europe today. Source: [53].

As for the Nordic countries, one can note that Finland is marked green (it allows independent aggregation in at least one of the programs in the ancillary services), whereas Denmark, Norway, and Sweden are marked yellow, since regulatory barriers remain an issue and hinder market growth. Although several markets are open to demand response in principle, program requirements continue to exist which are not adjusted to enable demand-side participation. The study highlights that the issue of access by independent aggregators to the wholesale market is prevalent across the majority of the analyzed countries. In most cases, the framework allows only for BRPs or retailers to aggregate and sell flexibility on the wholesale market. However, relatively good progress has been made by most countries in providing access to demand-side resources to the balancing markets (ancillary service provision), and positive cooperation between stakeholders (new market entrants, regulators, TSOs, and retailers) is underlined. However, the Nordic countries have started processes to find a standard solution for the role of independent aggregation.

For example in Denmark possible new market models for aggregators are jointly proposed and studied by the national TSO and the Danish Energy Association [54]. Such models are characterized by increasing responsibilities for the aggregators, which in the future will be seen as a stakeholder (a player, not a mere role) independent from an existing BRP, as it is today. In the more advanced model (*market model 3*) the aggregator will be in fact capable of competing in the wholesale market and in all the electricity markets, acting at the same time as a BRP as well as an electricity supplier. This can be achieved via intermediate steps (*market models 1 and 2*), and further studies, pilot projects, and standardizations for the roll-out of smart metering are recommended. Figure 2.11 shows a conceptual summary of the gradual expansion of the aggregator market model. To further facilitate and incentivize the development of market participation of EV flexibility in the provision of ancillary services, some market, technical and regulatory recommendations are needed. They are presented in the next paragraph, extending the considerations also to the possibility of involving DSOs as an active player in the trading of flexibility products.

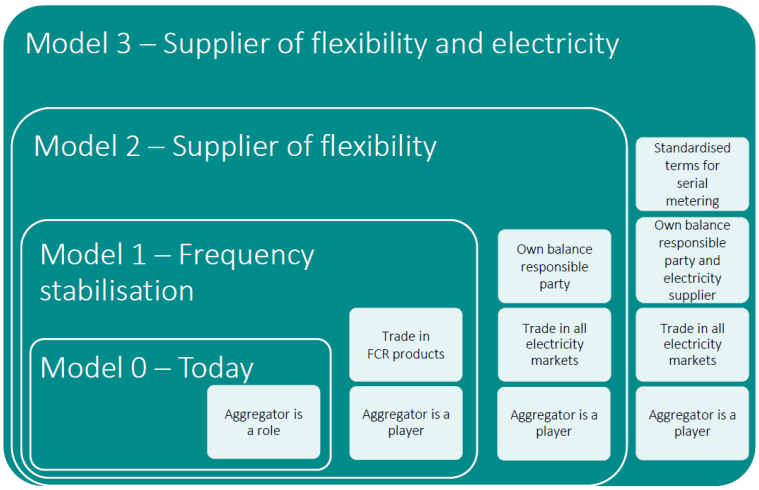

Figure 2.11 – Development of market models for aggregators. Source: [54].

2.3 Provision of distribution grid services: current policies/barriers

Trading and acquisition of ancillary services from distributed resources at the distribution level is currently nonexistent in all European countries, Nordic countries included. Many barriers can be identified from a technological/infrastructure and regulatory/market point of view. On the one hand, the EV flexibility product should be characterized (as seen previously), DSOs should enhance their grid observability through smart meters [55]–[58], and EV supply equipment (EVSE) should be safely controllable, in compliance with technical standards and communication protocols [59]–[65]. On the other hand, a dedicated flexibility platform to enable DSO markets does not exist yet, and this lack is seen as a major barrier [45], [53], [66]. In Ref. [45], a number of regulatory aspects are defined to enable the establishment of such platforms:

Flexibility platform administration and operation: The flexibility operator must manage and operate the flexibility platform by accumulating the bids and obtaining the optimal EV schedules. Possibly, it deals with flexibility both for DSO and TSO needs, as in the market framework presented in the following.

Independence and fair access: Regulations are required to ensure open and fair platform access for all interested participants as well as independency of any participant or EV owner in the flexibility trading operation.

Transparency: Participants must have access to financial information such as the cleared prices, whereas the bidding process, if existing, should be blind. Transparency in terms of data exchange among different parties, rules on the clearing process, operating costs and system operation procedures is recommended.

Flexibility products: Clear and generic flexibility products must be defined with clear conditions for procurement, as described in the beginning of this chapter.

Minimum bid: At a distribution level relatively low power exchanges can already represent a valuable assets for DSOs.

Settlement period: The settlement period should not be lower than the data sampling rate. From the DSO perspective, sampling rates on second basis are not a necessity, but such could be required if EVs were to provide TSO services as well.

Consumption baseline: If a common baseline is not accepted by all involved participants, many settlement disputes will arise.

Flexibility price: The price for each flexibility product should be determined and transparently communicated in advance. One possibility is to consider that settled price must be lower than the cost of grid reinforcement [26].

After identifying the major barriers for an active involvement of DSOs in EV flexibility trading, a series of recommendations is now provided, meant to facilitate the transition to a future flexible distribution system where EVs become proactive participants at the distribution level. Table 2.7 presents these recommendations divided in several categories depending on the targeted aspect [45].

Table 2.7. Main recommendations for supporting active EV involvement, adapted from [45].

	Recommendations
Smart metering	• Wide-scale deployment of smart meters with standardized functionalities to ensure interoperability. • Sampling frequency in line with flexibility trading settlement period (max 5-min). • Clear pre-qualification and validation protocols
EV/EVSE technology	• Define standards and regulation for deploying EVSEs with embedded intelligence. • Harmonize communication protocols between the EV aggregator and other participants. • Determine standardized tests for evaluating internal EV parameters (accuracy, response time, etc.).
DSO regulation	• Remove regulation which forbids aggregation and flexibility procurement. • Incentivize long-term innovation (longer regulatory period, incentives for new technologies, etc.). • Revise tariffs to include both the capacity and the energy charge. • Define new DSO tasks (active grid operation and data management). • Remunerate current DSO services to provide basis for comparing different solutions and estimating the flexibility price.
Flexibility trading	• Establish an open, transparent and fair flexibility trading platform. • Define clear and generic flexibility products. • Define technical requirements which must be included in flexibility requests/offers (power capacity, duration, direction, location, etc.). • Define the minimum bid in the kilowatt range and the settlement period of max. 5-min to encourage EV owner participation. • Define common EV baseline (uncontrolled charging) and the corresponding measurement methodology. • Introduce capacity and energy payments, and a premium for rewarding the more reliable resources.
TSO-DSO collaboration	• Define standards for the interface and data exchange between the TSO and DSOs. • Define clear priorities between TSO and DSOs for normal operation and emergencies. • Make local flexibility trading platform transparent to the TSO.
Consumer	• Define regulations to ensure data protection and allow sharing of sensitive data if EV user is willing. • Develop interface for providing insight into signed contracts and EV schedules. • Define standards for providing a unique ID for flexibility procurement & remuneration.

2.4 Conflicts when acquiring ancillary services from EVs

Flexibility provided by EVs at a distribution level can match different needs and could potentially create conflicts dependent on which stakeholder uses flexibility and for what purpose. Today, unlike TSOs, DSOs cannot acquire local services from the same DERs, as there is not yet a role for DSOs in the market [67]. To prevent issues at DSO level, as an alternative to the acquisition of flexibility products, the literature proposes distribution locational marginal pricing (DLMP) solutions [68]–[70]. These can be beneficial in case the load is forecasted in a traditional way, thus not considering power flow variations related to the provision of TSO services, e.g., following frequency variations. In the current market setup, the TSO/DSO conflicts that could take place mostly concern the constraints of the distribution system infrastructure. In fact, since connected at a distribution level, EVs' adaptive management aimed at providing a TSO service may lead to local grid constraints

violations. The induced technical issues that the DSO is supposed to face would mostly be congestions or under/over voltages. A possible mean to reduce these conflicts is the enhancement of TSO/DSO cooperation. This can be achieved via information and data exchange in the grid expansion planning phase (long term), for congestion management contracts (long/medium term), as well as for the real time operation (short term) [28]–[30]. In the following, a catalogue of possible TSO/DSO conflicts is proposed within a given active involvement of DSOs in the EV flexibility trading. Then, the logical assessment employed for the identifications of such conflicts is presented.

2.4.1 Proposed market framework

The work in **Paper A** assumes a possible future DSO role as an active market player. In [71], several key attributes essential for the successful operation of future flexible distribution systems are identified, along with the possible DSO designs. The considered future European DSO model is called *evolvDSO* [16] and is expected to take the following responsibilities: network planning and operation processes, contracting of flexibility services and market facilitation with cooperation between system operators. Within this framework, it is clear that – compared to the contemporary situation – new issues will arise: not only technical but also economical and political when considering remuneration schemes and potential conflicts of interests. Thus, in order to catalogue such conflicts between TSO and DSOs when acquiring flexibility products, the prominent flexibility market framework '*Common TSO-DSO Ancillary Service market model*' presented within the SmartNet project [67] is taken as a benchmark. It includes all the listed stakeholders and defines a new day-ahead market dynamics, as such a framework is analyzed with respect to the day-ahead trading of EV grid services. As a specific trait, it has a single flexibility platform that has to cope with all the flexibility requests presented by the system operators as well as the flexibility offers received from the aggregators. In this way, it is expected that grid constraints are implicitly taken into account, as the flexibility operator (*Flex Operator*) would manage both information about the location of flexible sources and the DSOs' needs for flexibility in different areas. The DSOs' flexibility requests are formulated according to the forecasted demand profiles that each DSO receives from the suppliers, which communicate directly with the users. Such a platform is supposed to allow flexibility procurement without jeopardizing the grid operation or creating extra costs [67]. A scheme of the designed framework is shown in Figure 2.12. It operates in several phases:

Phase 0 – Before the clearing process: the suppliers communicate to the DSOs the forecasted load profiles of their customers. EV aggregators contract flexibility with the EV owners in their fleets. The TSO trades flexibility through the BRP. (Figure 2.12-a).

Phase 1 – Before the clearing process: DSOs and BRP present flexibility requests to the *Flex Operator* according to the information received by suppliers and TSO, respectively. EV aggregators offer flexibility according to the contracted aggregated availability from their EV fleets. (Figure 2.12-a).

Phase 2 – The clearing process: the *Flex Operator* performs an evaluation based on optimization algorithms that aim at optimally allocating the available flexibility products from a technical and economical point of view (e.g., respecting the technical needs while minimizing the total costs). The evaluation considers that DSOs' local flexibility needs are linked to a particular localized congestion problem, whereas the TSO needs flexibility to maintain the system stability independently of the location of the resource. Eventual conflicts are identified and addressed at this stage.

Phase 3 – After the clearing process: the *Flex Operator* communicates the obtained optimal flexibility profiles to DSOs, BRP and EV aggregators, who will properly manage corresponding EV fleets. (Figure 2.12-b).

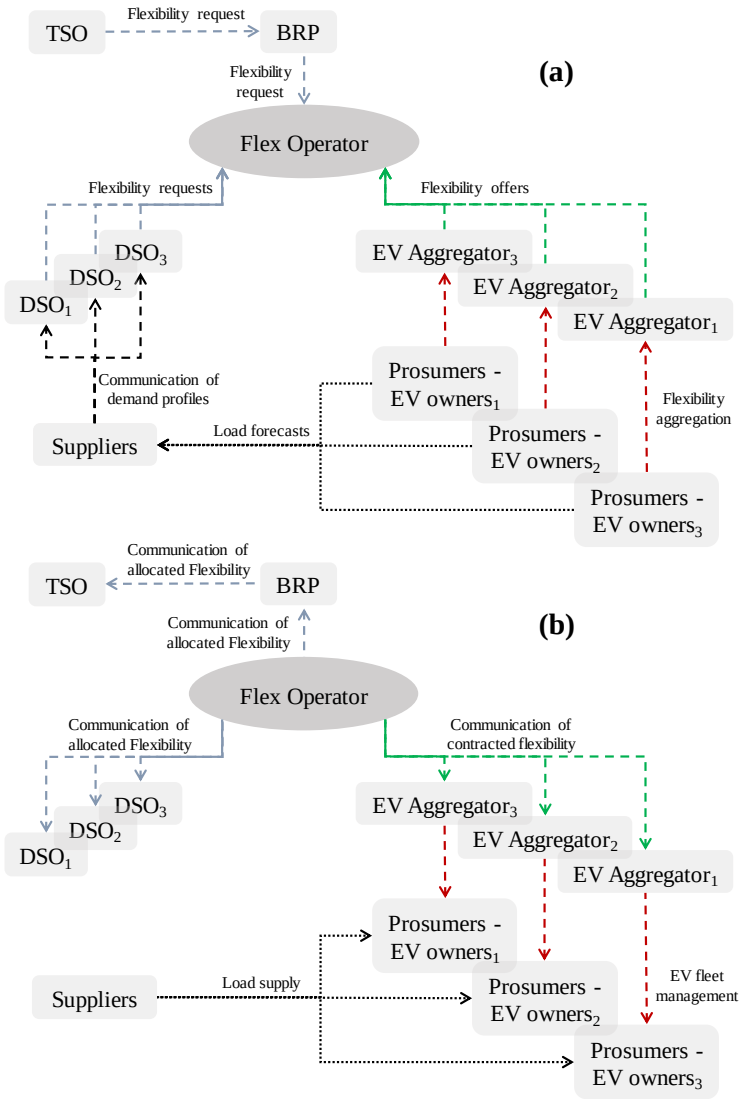

Figure 2.12 – Adopted flexibility market framework for the day-ahead trading of EV grid services. (a) and (b) show the interactions among the involved stakeholders before and after the clearing process, respectively.

2.4.2 TSO/DSO conflicts and proposed method for identification

Different needs for flexibility services of each involved stakeholder can raise potential conflicts between two or more stakeholders with opposing needs. Within the proposed market framework, this kind of conflicts are taken into consideration by the *Flex Operator* platform, which detects them and then address them accordingly. In the following, an identification procedure is provided, which is able to detect, identify and catalogue possible DSO/TSO conflicts that may take place when requesting and/or procuring flexibility products. Since the complexity of the problem brings enormous amount of different potential conflicts, the here-presented analysis focuses on conflicts coming from TSO and DSOs flexibility requests for acquiring two specific services, namely primary frequency regulation and transformer congestion management, respectively.

Within this context, four conflicts are identified:

Conflict (a): Need for compensating imbalances caused by activation of flexibility for solving a local distribution issue. The need for activating a service to solve a local DSO problem in a particular area may cause a problem at a system level in terms of balancing. In fact, considering a system in balanced operating conditions, a consumption decrease for preventing congestion at a distribution level would force the BRP to increase the consumption (or decrease the generation) elsewhere. In this way, the balance would be guaranteed and the local congestion would be prevented.

Conflict (b): To solve a TSO request, activating the only available flexibility product causes distribution overloading. It concerns the prioritization problem between DSOs and TSO. When activating the only available flexibility to satisfy a TSO request would cause distribution overloading.

Conflict (c): The available flexibility can satisfy either the DSO request or the TSO request. It concerns the prioritization problem between DSOs and TSO. The offered flexibility would not be enough to satisfy all the needs.

Conflict (d): One flexibility product can solve several problems. Rather than a technical conflict, *conflict (d)* presents an economical conflict that the Flex Operator may face mainly when remunerating aggregators. In fact, one offered asset could have all the necessary capabilities to concurrently satisfy both a TSO and a DSO need. Thus, it is important to define a fair way to remunerate the aggregator.

The flow-chart diagram in Figure 2.13 shows step by step the proposed procedure that the *Flex Operator* is supposed to follow when managing flexibility requests and offers. First, the *Flex Operator* receives flexibility requests from DSOs and TSO as well as the offers profiles from the aggregators. Then, a possible allocation of flexibility over time for each location is formulated to accommodate the DSOs' needs. So, the *Flex Operator* checks whether the new power profiles (original DSOs' demand profiles over time with the addition/subtraction of the activated flexibility) would introduce problems from a balancing point of view. In this case, *conflict (a)* would be

identified, and a new resource allocation would need to be obtained. Once a solution that does not introduce imbalances is found, the flexibility needs of the TSO are considered on top of the already allocated shares for the DSOs' needs. At this point, the methodology proposes to check whether with the same flexibility product both DSOs' and TSO's problems are solved. If yes, the best solution from a social point of view would be found, as it would involve the least possible amount of flexibility to satisfy all the needs. Though, the remuneration *conflict (d)* would be identified, which needs to be addressed while – in parallel – formulating the optimal solution. In case *conflict (d)* is not detected, the check on the presence of the other eventual technical *conflicts (b)* or *(c)* needs to be done. In particular, they concern the prioritization problem between DSOs and TSO when the offered flexibility is not enough to satisfy all the needs (*conflict (c)*), or in case the activation of the only available flexibility would cause distribution overloading (*conflict (b)*). Once one of these two conflicts is detected, an appropriate optimization algorithm with grid constraints would be necessary to find an optimal solution, which will finally be communicated to all the involved stakeholders.

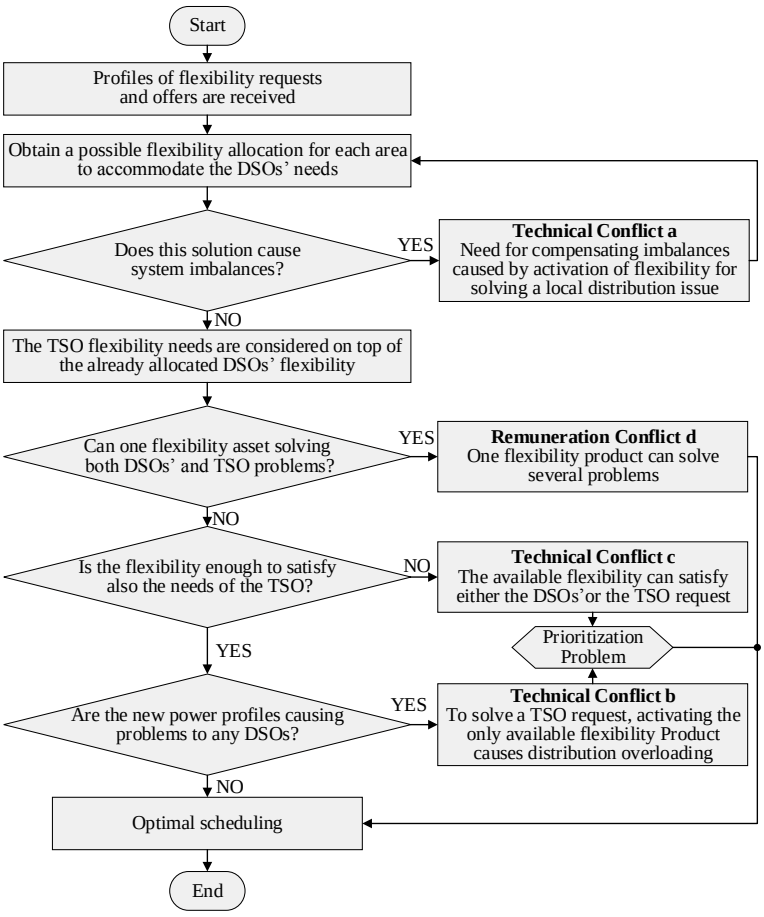

Figure 2.13 – Flow-chart of the DSO/TSO conflict detection methodology.

Within the contemporary market situation, it is clear that the proposed conflict detection methodology may change. In fact, the *Flex Operator* would have to manage requests for flexibility coming only from the TSO, so the only possible conflict would be *conflict (b)*. Thus, after receiving requests and offers, the *Flex Operator* would have to check whether problems are caused to DSO. If yes, then *conflict (b)* would be detected, and the optimal solution would be decided including technical grid constraints, and finally communicated to the involved stakeholders.

2.4.3 TSO/DSO conflict identification examples

The proposed analysis is based on the investigation of possible dynamics in which the listed conflicts could take place. The investigation is carried out considering the simplified 3-area power system shown in Figure 2.14. TSO's transmission lines link the DSOs' areas to each other through three transformers (T1, T2 and T3), whose points of common coupling (PCCs) are named PCC1, PCC2 and PCC3, respectively.

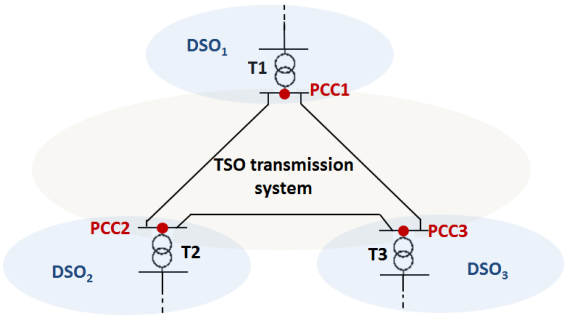

Figure 2.14 – 3-area power system.

For the sake of simplicity, the analysis considers only the need for preventing overloading of T1, T2 and T3, while all the others DSOs' technical needs (such as line congestion, under/over-voltages, or phase unbalances) are neglected. Regarding the TSO needs for ancillary services for primary regulation, a certain profile is assumed to be requested. On the one hand, the TSO needs reserve, i.e., availability of flexible units to solve a problem that could potentially take place. On the other hand, for the DSO flexibility represents a real need for power to solve a concrete forecasted congestion problem.

To allow a visualization of the involved forecasted/requested/available flexible power sets, a schematic representation is given. For each area, bar plots over the time represent the amount of flexibility (in this case positive or negative active power expressed in MW) that is requested by DSOs and TSO as well as the available flexibility offers, as in Figure 2.15. Such profiles are arbitrarily defined, as they are meant for conceptual example purposes. It is expected that similar situations may appear in the future, if an active DSO role within the ancillary service market will be established.

Figure 2.15-a shows the TSO request of flexibility over the time, here expressed in Time Units of 15 minutes. It can be seen that at Time Unit 2, there is a need for up-reserve, which can be achieved via power consumption curtailment, increase of generation or EV battery discharge. Whereas for Time Units 4 and 5 there is a need for down-reserve, which would mean total power consumption increase. In case of Time Units 1 and 3 no flexibility is requested, since the TSO forecasted an acceptable generation-consumption match for that Time Unit. Figure 2.15-b reports the power demand profiles at PCC1, PCC2 and PCC3 forecasted by the DSOs. Accordingly, each DSO will formulate correspondent flexibility requests to prevent transformer congestion, as shown in Figure 2.15-c. It can be seen that for T1 no congestion situations are forecasted, whereas for T2 and T3, congestions are forecasted for Time Unit 3 and 4, and Time Unit 2, respectively. Note that to face such congestions, DSOs in area 2 and 3 would request flexibility with negative sign, i.e., load reduction, increase of generation or EV battery discharge. An example of possible flexibility offers is reported in Figure 2.15-d which shows the available flexibility over time at the three points of common coupling.

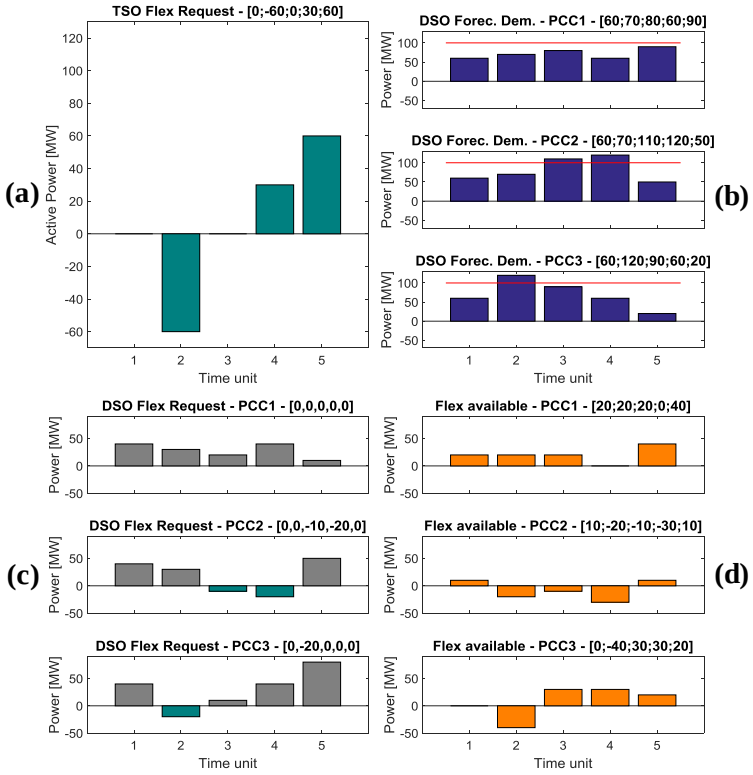

Figure 2.15 – TSO (a) and DSO (c) flexibility requests over the time, DSO forecasted demand (b), and flexibility available in each area (d).

Herein, examples of each one of the identified conflicts that the *Flex Operator* could face are presented. In particular, Figure 2.16 to Figure 2.19 report the new area-by-area power profiles that the *Flex Operator* obtained following the methodology proposed in Figure 2.13. Graphically, bar plots show the DSOs forecasted demand profiles over time at the three PCCs, with the activated flexibility, which is added (orange) or subtracted (dashed white) in order to satisfy the requests.

An example of system imbalances caused by flexibility activation for solving a local distribution issue (*conflict (a)*) is schematized in Figure 2.16. It can be seen that at Time Unit 3, congestion of T2 is solved. Nevertheless, as noticeable from Figure 2.15-a, the system was already balanced at that Time Unit. Therefore, the BRP would need to rely on other flexible products located in other areas (in this case in area 1) to maintain the system balance.

Figure 2.17 depicts one possible situation which could lead to *conflict (b)*, i.e., when solving a TSO request, the activation of the only available flexibility causes distribution overloading.

Furthermore, it can be seen that at PCC1 at Time Unit 5, an overloading condition is caused. As an example of a possible situation of *conflict (c)*, the need for prioritizing a DSO request over the TSO's and vice versa is presented. Figure 2.15 shows that at Time Unit 4, the TSO needs an increase of the power consumption, while the DSO in area 2 requests a power reduction to solve a forecasted congestion of T2. Figure 2.15-d shows that the available flexibility at Time Unit 4 allows to satisfy either the TSO or the DSO need. The two possible cases of prioritization to TSO or DSO are reported in Figure 2.18-a and -b, respectively.

As presented in the previous paragraph, *conflict (d)* represents an economical conflict that the *Flex Operator* may face mainly when remunerating aggregators. This conflict is shown in Figure 2.19, which shows that congestion of T3 is solved, while at the same time this power reduction can also satisfy the TSO need for frequency up-regulation at Time Unit 2, as deducible from Figure 2.15-a.

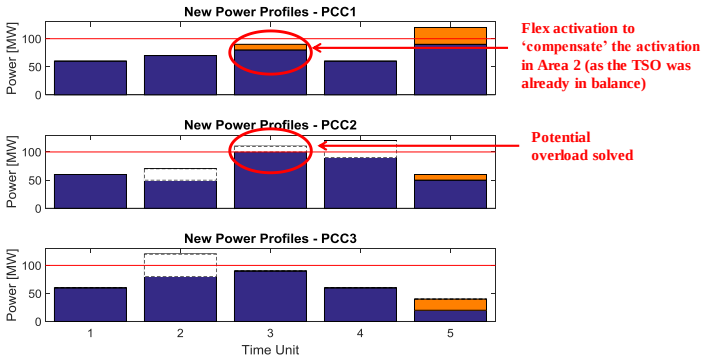

Figure 2.16 – New profiles for each area: original DSOs demand profiles over time with the addition/subtraction of the activated flexibility. Example of compensation of activated DSO flexibility, to keep the system balanced – *conflict (a)*.

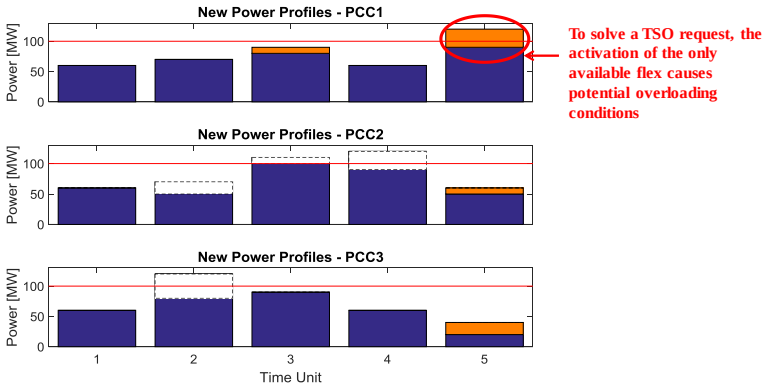

Figure 2.17 – Example of induced congestion problem to DSO, due to the activation of flexibility to provide a service for the TSO – *conflict (b)*.

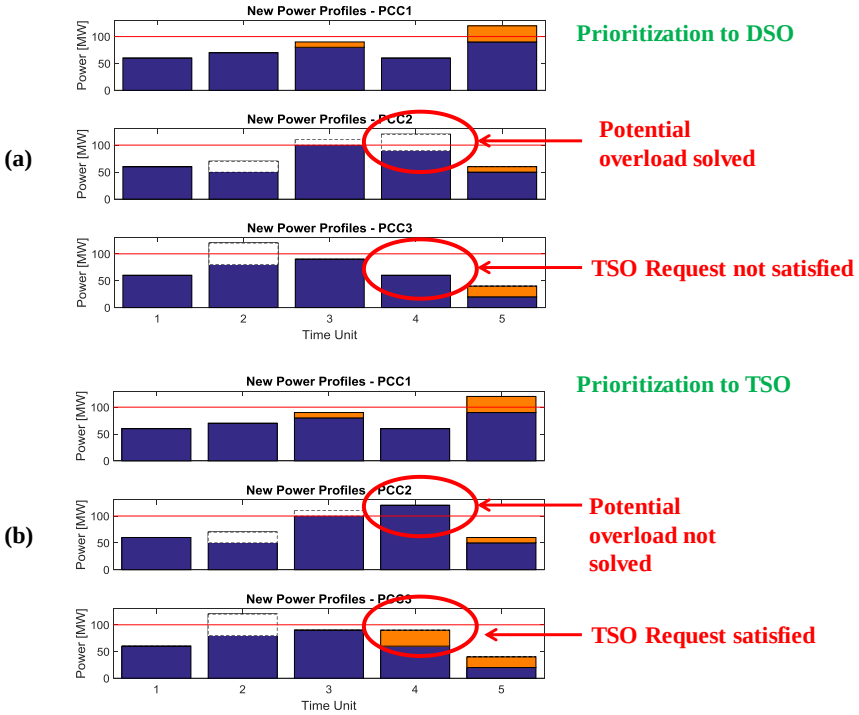

Figure 2.18 – Example of prioritization problem when acquiring the available flexibility: it is possible to solve either the DSO (a) or the TSO (b) – *conflict (c)*.

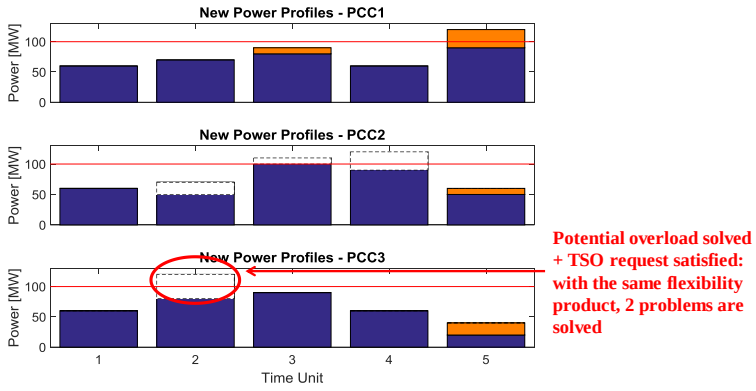

Figure 2.19 – Example of satisfaction of needs of both DSO and TSO, by exploiting the same flexibility product – *conflict (d)*.

It is important to point out that, within the considered example and time units of 15 minutes, the distribution grid needs would need to be prioritized over the TSO's. In fact, as a larger, more flexible and more controllable system, the transmission system may be able to rely on more traditional sources for reserve, possibly most of the time. This way, in case the activation of a flexibility product for a TSO service would potentially cause congestion problems to the DSO, the TSO would be invited to procure reserve relying on alternative sources. On the other hand, in case of frequency dynamics (i.e., within the intraday market) the TSO's needs may have to be prioritized over the DSOs' in order to support the system in case of emergency situations.

In conclusion, it is clear that each one of the identified conflicts raises debates, whose resolutions are out of the scope of **Paper A** and this thesis, but are expected to cover a broad interest within the scientific power engineering community. Thus, as a final remark, the following open questions are proposed for future works:

• When the activation of a DSO service causes system imbalance, the BRP needs to provide compensation in order to maintain the balance. Is the BRP compensated for this? If yes, by whom?

• When the activation of a flexibility product would cause problems to another stakeholder, or in case of limited availability of flexibility, how does the Flex Operator proceed? Who would be prioritized and why?

• In case one asset has the capabilities to satisfy at the same time both a TSO and a DSO need, will the aggregator be remunerated twice? If not, which service will it be remunerated for? Is it realistic to expect the same price although the required performances could be different?

2.5 Summary

This chapter started with the motivation of the need for flexibility in modern power systems, characterized by increasing EV penetration levels. In particular, the increase of the total early energy and peak demand has been presented, whereas simulation studies in LV feeders showed the negative effects of uncontrolled EV charging in terms of unacceptable congestion and under-voltages in two representative Danish and Norwegian study cases. The concept of flexibility product has then been introduced, with a set of practical and theoretical attributes, and current policies and barriers against the roll-out of an active EV participation have been identified with emphasis on the Nordics. The focus moved further to the different needs for flexibility services of each involved stakeholder, showing the rise of potential conflicts between two or more stakeholders with opposing needs. A newly proposed DSO model with an active market role in managing distribution grids by relying on flexible resources has been described, and a number of technical and non-technical TSO/DSO conflicts have been identified and categorized, by using a conflict identification procedure. Within the considered market framework, day-ahead trading process of ancillary services provided by EVs have been analyzed. The investigation showed the potential conflicts arising when acquiring services

for congestion management and primary frequency regulation. Considering a 3-area power system, each of the analyzed conflicts has been presented through case studies that allowed to visually appreciating the nature of the conflict.

After this high-level overview of EV charging strategies for ancillary services provision and the contemporary and future flexibility trading challenges, the thesis proceeds with mainly technical investigations within the broad topic of pro-active EV integration in the power system. Uni- and bi-directional charging/discharging capabilities are investigated by means of hardware tests, to characterize the models for subsequent analysis within the scope of frequency service provision. Possible challenges that EV aggregators and TSOs may face when EV fleets provide frequency control will then be investigated, and solutions will be proposed.

CHAPTER 3

Uni-directional EVs as frequency control providers

This chapter presents investigation studies on the applicability of power system frequency control strategies employing EVs. A standard-compliant primary frequency controller is designed for uni-directional EV Mode 2 charging and is implemented to carry out studies by means of both RMS simulations in DIgSILENT PowerFactory and validations in an experimental microgrid with real EVs. These studies allowed the identification of criticalities related to the implementation of EV controllers for power system frequency regulation, i.e., the control discreteness. This is then investigated in detail in the last sections of the chapter: analytical formulations are proposed and the elasticity of an experimental power hardware-in-the-loop setup enabled the implementation of different granularities of the EV response, complementing the investigation. The chapter includes partial results of the separate papers **Paper B**, **Paper C** and **Paper D**, attached in Part II.

3.1 On the provision of power system frequency control via EVs

As described in Chapter 1, modern power systems are experiencing the decommissioning of traditional conventional generating power plants in favor of power electronics-interfaced plants from RES. Among a number of related consequences, this leads also to the need of providing grid services relying more and more on small aggregated units connected to distribution grids, thus introducing new challenges on an operational level. Beside small generating units such as photovoltaics and wind turbines, demand-side management (e.g., EVs management) is seen as one of the most prospective sources of frequency regulation, such a primary frequency control (PFC) [72]–[76]. However, as the primary function of the mentioned DERs differs from the provision of grid services, many technical challenges arise when it comes to aggregate and control them. For example, the response time of both single EVs as well as aggregated EV fleets is one of the most challenging aspects in enabling EVs participation in the reserve provision. Furthermore, the compliance of each EV/EV charger with technical standard IEC 61851 for AC charging [59] and IEC 15118 for DC charging possibly with V2G [61], along with the limitations in commercial standard-compliant hardware for EV charging [77], [78], require a given granularity in the current set-point.

The aggregation of EVs as possible source of frequency regulation services with both uni- and bi-directional charging has been investigated in many works. A number of studies show the potential capability of EV fleets in performing power system services. In particular [79] shows that evident improvements in islanded power system dynamics can be achieved relying on EV droop controllers. Reference [80] demonstrates how large-scale EVs utilized as a demand response resource can promote the development of wind generation in the Great Britain power system, also including travelling behavior of EV users in the problem formulation. Similar results are found in other studies [81]–[86], which confirm the positive impact of EV charging control strategies at a system level with high penetration rate of generation from renewable energy resources, also on an environmental and economical level [86]–[88].

Certainly, possible EV aggregation models and control strategy approaches are also od interest. Most of EV control algorithms solve optimization problems aimed at meeting a number of objectives (e.g., maximize profit/renewable generation, or minimize operation costs/power losses), while respecting grid constraints (e.g., voltage/overloading limits) and users' needs (e.g., SOC limits and availability). For a comprehensive overview of the possible optimization strategies for V2G applications, the reader is referred to the review papers [89]–[91]. As an example of optimal dispatch of EVs performing V2G, in [92] a discretized regulation dispatch approach is utilized, which aims at meeting the desired calculated total power signal by turning certain EVs on or off according to a priority index. In this way the control architecture is merely centralized, since the aggregator sends on/off signals as results of its centralized dispatch algorithm. In general, this kind of centralized approach require bi-directional real-time communication capabilities, as signals from the charging stations are supposed to be sent back to aggregators. In [93]–[95] the communication complexity is drastically reduced by relying on a decentralized approach. In particular, in [95] the decision to change charging set-point is taken locally by the single EV, while a remote centralized frequency measurement is performed by the aggregator, who will dispatch the same correspondent signal to his EVs. Nevertheless, despite the potential positive effects, the aggregate response can induce problems to the power system when the share of EV providing regulation is high and all the units respond to the same frequency signals. In this regard, accurate aggregated EVs models need to be implemented, which include proper overall response behavior. Thus, [96] proposes a distributed frequency control that randomly assigns delays to each EV of the fleet. Additionally, [97] presents a novel methodology to design EV droop controller in a way to ensure the same stability margin with and without EVs during the frequency primary control.

The above-presented works within the domain of PFC provision via EVs mostly focus on simulation studies, whereas experimental validation is rarely carried out. In fact, technical limitations due to standard requirements are neglected, and ideal response in terms of EV power exchange is considered. Testing activities have been performed in [98], investigating the performance of a real charging EV at a charging post complying with the IEC 61851 technical standard. In [99] the authors

test a price signal-based charging algorithm on commercial EVs, although without providing any ancillary services. By contrast, experimental activities validating how series-produced EVs can provide a number of grid services have been carried out both on an experimental testbed [100] and in a real field test [42]. These practical validations deal, among others, with the issue of charging-related controllability limitation due to technical standards requirements and real commercially-available hardware, commonly neglected in most of the literature.

To extend the existing literature, this chapter outlines an EV standard-compliant controller for primary frequency regulation. Simulation and laboratory test studies when implementing the controller in a microgrid are presented (**Paper B** and **Paper C**). Such investigations are then complemented with analytical assessment of possible consequences of criticalities found in simulations and while testing real hardware, and a fleet management strategy based on droop shift is proposed (content included in **Paper D**).

In Chapter 4, experimental investigations of commercial V2G-ready hardware are presented, proposing an operational characterization aimed at investigating the suitability for critical and demanding grid services such as PFC (**Paper E**). The employed test cycles can be considered an important tool for the assessment of bi-directional hardware performance, and may represent the first step towards a classification of the technical eligibility for PFC of commercial EV controllable hardware. The investigations are then extended towards possible control strategies to overcome the previously-identified operational challenges, both from the EV aggregator's and the transmission system operator's perspective, including results from **Paper F** and **Paper G**, respectively.

3.2 A primary frequency controller for EVs

One aspect of interest that has been found in previous experimental activities involving standard-compliant commercial controllable hardware is the granularity in the response [42], [100]. It is expected that a discretization (in this case 1 A granularity) in the charging/discharging set-point may in fact introduce challenges when operating a relatively large fleet in a low-inertia power system. In this context, the thesis proceeds with investigations of probable effects of such a discrete response: a standard-compliant EV controller with the 1 A granularity is implemented first in a simulation and then in an experimental microgrid setup with three uni-directional real series-produced EVs.

Typically, primary frequency control is achieved by a joint action of PFC providing units within the whole synchronous area with respect to the frequency deviation. This is achieved via droop controllers, meaning that governors operating in parallel share the load variation according to their rated power [101]. The droop constant k_{droop} represents how much the machine is sensible to frequency changes, and quantifies its contribution to primary frequency/power regulation. The contribution in terms of active power variation ΔP referred to its available reserve power P_{res} is correlated to the frequency variation Δf referred to the nominal value f_n (50 Hz) by k_{droop}, as in (3.1).

$$\frac{\Delta f}{f_n} = k_{droop} \cdot \frac{\Delta P}{P_{res}} \tag{3.1}$$

In absolute terms, the droop constant K_{PFC_pow} in [W/Hz] represents the change in power output ΔP for a given frequency deviation Δf:

$$\Delta P = K_{PFC\_pow} \cdot \Delta f \tag{3.2}$$

In this investigation frequency regulation is achieved via EVs by modulating their battery power flow (uni-directional flow). As the technical standards IEC 61851 [59] and IEC 15118 [61] require the charging/discharging process to be modulated by setting the current, (3.1) and (3.2) can be re-written as in (3.3) and (3.4), where I_{res} is the available reserve in terms of current, ΔI_{PFC_id} is the ideal EV current variation in case of a given Δf, and K_{PFC} is the absolute f-i droop constant in [A/Hz].

$$\frac{\Delta f}{f_n} = k_{droop} \cdot \frac{\Delta I}{I_{res}} \tag{3.3}$$

$$\Delta I_{PFC\_id} = K_{PFC} \cdot \Delta f \tag{3.4}$$

In practice, the real current variation applied to the EV ΔI_{PFC} differs from ΔI_{PFC_id} mainly for three reasons. First, an upper limitation of the set-point is determined by the size of the breaker in the EV charger circuit, e.g., for the single-phase Mode 2 charging it is typically 16 A. Second, EV technical standards impose constraints in the set-point granularity, which is typically handled by aggregators and hardware manufactures with 1 A discreteness [77], [78] (same granularity found in the hardware test presented in the next chapter for bi-directional hardware). Third, lower current limits are imposed by the standards for some charging modes, e.g., IEC 61851 requires a minimum current set-point of 6 A for Mode 2 charging. The controller will then add the calculated current ΔI_{PFC} (>0 in case of over-frequency, <0 for under-frequencies) to the initial current value I_{init}, which corresponds to a stable system load condition at 50 Hz, obtaining the new current set-point I_{set} that the controllers will set on the EV charger.

$$I_{set} = I_{init} + \Delta I_{PFC} \tag{3.5}$$

The proposed controller can be implemented for both uni- and bi-directional EV control applications. In case of V2G, the initial current I_{set} is in general set to 0 A to have maximum symmetrical controllability, while appropriate up/down limits will be set according to the type of charger. For example, in occasion of the investigations on the IEC 15118-compliant V2G-capable hardware using the CHAdeMO protocol included in Chapter 4, the limit of ±25 A are used, being the charger's size ±10 kW. The characterization tests of such commercial hardware operating in field projects also confirms the presence of similar 1 A current discreteness when setting the EV current set-point.

In the following, the controller is tuned for uni-directional charging of single-phase EVs according to Mode 2. Given the mentioned 6-16 A regulating window for Mode 2 charging, the middle value of 11 A is chosen for the EV's initial current set-point I_{init}. This way, the available range of

regulating current, i.e., the EV's available reserve I_{res}, is ±5 A, which allows to have the desired symmetrical up/down regulation capability. The new current set-point I_{set} that the controllers will set on the EV charger is calculated as in (3.5). For these studies, four different proportional f-i droops have been considered: 1% (frequency limits of 49.5 – 50.5 Hz), 2% (49–51 Hz), and 3% (48.5–51.5 Hz), and 4% (48-52 Hz). If the frequency exceeds the limits, then the current limit value (6 or 16 A) is set, as ±5 A is added to the initial current I_{init} 11 A. Table 3.1 reports the absolute current and power droop constants for the four employed relative droops. Figure 3.1 shows the 1% and 4% droops: the dashed line represents the ideal current variation ΔI_{PFC_id} while the solid one shows the real current variation ΔI_{PFC} with 1 A granularity required by the technical standard IEC 61851 for uni-directional Mode 2 charging.

Table 3.1. Parameters for the four droop cases for the uni-directional PFC controller.

k_{droop}	K_{PFC}	K_{PFC_pow}	I_{res}	I_{init}
1%	10 A/Hz	2300 W/Hz	±5 A	11 A
2%	5 A/Hz	1150 W/Hz	±5 A	11 A
3%	3.3 A/Hz	766 W/Hz	±5 A	11 A
4%	2.5 A/Hz	575 W/Hz	±5 A	11 A

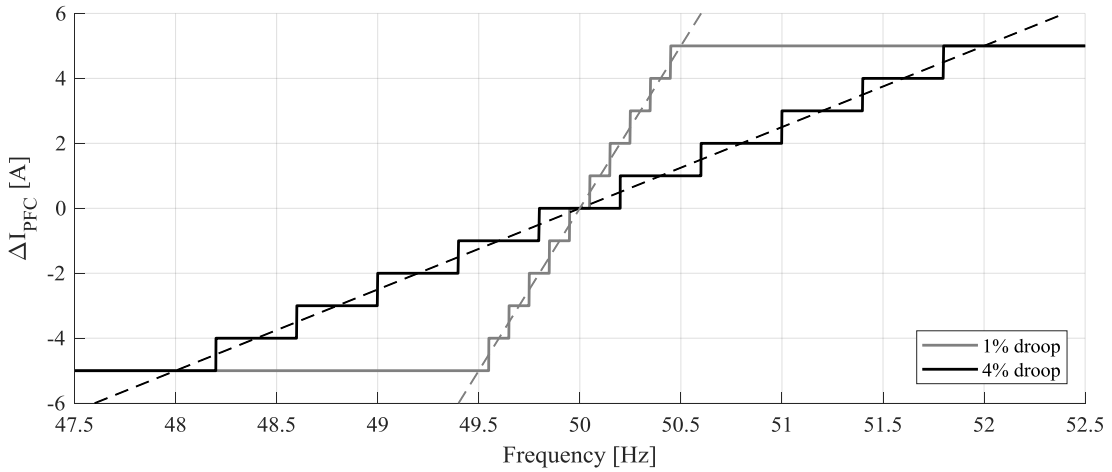

Figure 3.1 – PFC ideal and discrete regulation curves for 1% and 4% droop.

Figure 3.2 depicts the block diagram of the EV control loop, which can be divided into 2 sub-groups. The first one concerns the implementation of (3.4), which calculates the frequency deviation Δf and provides as output ΔI_{FPC_id}. This is the input of the second group, which serves at implementing the appropriate discreteness as well as setting up/down current limitations, as required by the technical standards. The output ΔI_{FPC} is then added to the initial current set-point I_{init} according to (3.5). In order to implement a proper granularity in the EV response, the index α indicates the size of the steps when controlling the EV charging; $\alpha = \{1, 2, 4, \infty\}$ corresponds to the cases of granularity of 1 A, 0.5 A, 0.25 A and 0 A (which is the ideal continuous case), respectively. Bearing in mind that

when controlling an EV charger the EV set-points represent the RMS limit values of the current waveform, and that in this implementation EVs are single-phase units charging in a uni-directional fashion according to charging Mode 2.

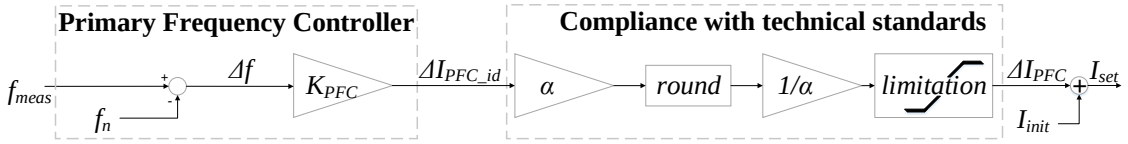

Figure 3.2 – Block scheme for the implementation of the standard-compliant PFC. The implemented logics along with adjustments for the compliance with standards and employed hardware give the reference current signal to be set on the EV charger I_{set}, given the measured frequency f_{meas} as input.

3.2.1 Implementation in a microgrid: simulation studies

A set of simulations are performed to assess the implications of providing primary frequency regulation by EVs in a microgrid, which are reported herein below. For more insights on an innovative control logic algorithm aimed at curtailing the number of current set-point variations during the regulation process, the reader is referred to **Paper B**.

The studies are carried out by means of RMS simulations in DIgSILENT PowerFactory software environment. The modelled grid is a reproduction of an islanded configuration of the experimental LV grid SYSLAB-PowerLabDK. SYSLAB is a research laboratory facility for development and test of control and communication technology for active and distributed power systems, located at the Technical University of Denmark, Risø campus. To enable a further practical experimental validation study, the modelled microgrid is built considering real power system components. Specifically, the following units are modelled, which are highlighted in the single line diagram representation of the whole experimental facility in Figure 3.3:

- 3 controllable EVs, each equipped with single-phase 16 A (230 V) charger and 24 kWh Lithium-ion battery. The chargers allow only uni-directional power flows.

- A 60 kVA diesel synchronous generator, with active power P_{gen} up to 48 kW. Since designed for operating in microgrid contexts, the inertia of the unit is rather high ($2H$ = 50 s). The automatic frequency control of the governor of the diesel generator is set with K_{gen} = 1.67 kW/Hz.

- A 45 kW (up to 15 kW per phase) resistive load with power adjustable independently on each phase.

- A 10 kW Aircon wind turbine (nominal wind speed 11 m/s) with full converter and active stall control.

A 725 m Aluminum cable line connects the two buses which the components are connected to (AC-Resistance at 20 °C and Reactance are respectively 0.313 and 0.077 Ω/km). Both the synchronous and the wind generators are connected to the same bus (*Generation bus* or *Busbar 1*), while the resistive load and the EVs are placed on the other terminal of the line (*Load/EVs bus* or *Busbar 2*).

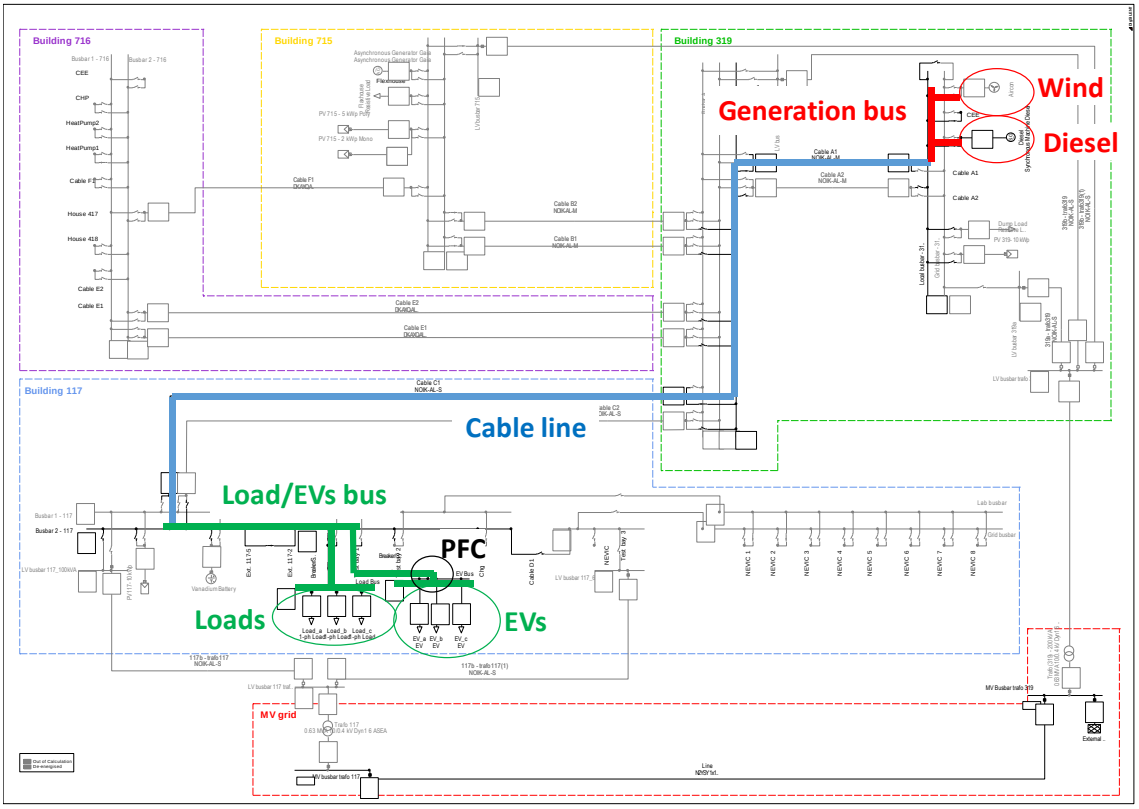

Figure 3.3 – Single line diagram of the whole SYSLAB-PowerLabDK LV grid. Highlighted are the components utilized to compose the microgrid and the PFC controller.

The overall PFC control chain for the EV chargers is implemented in DIgSILENT PowerFactory. It is composed by three main parts: the frequency measurement, the control algorithm and the EV model. As explained, the control algorithm in Figure 3.2 receives the frequency measurement and provides the EV current set-point. To represent the digital time delay due to measurement and communication, a time delay is considered before the control algorithm block (T_{mc} = 0.5 s). The rounded and limited current signal is sent to the EV model (Figure 3.4), which is composed by:

- A time constant block to imitate the EV battery dynamics (T_b = 1 s).

- A time delay block to represent the delay due to internal EV communication and activation of the EV charger power electronics (T_{EV} = 1.5 s).

- A block that converts the current signal to a power signal, as for RMS simulations in PowerFactory loads need power inputs (P_{EV} and Q_{EV}). For the sake of simplicity, in these studies the reactive power Q_{EV} is equal to 0 kVAr as the focus is on frequency control, achieved via active power modulation. EV reactive power will be included in Chapter 5, where its crucial role will be discussed and investigated in representative LV distribution grids.

- A load block, i.e., the EV unit in the modelled grid.

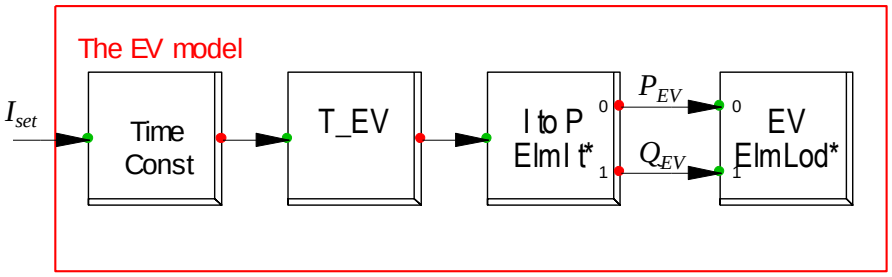

Figure 3.4 – EV model block diagram implemented in DIgSILENT PowerFactory.

The reported simulations are carried out with 1% and 3% droop. The main objective is to assess the performance of the employed PFC controller in a microgrid. In the initial situation, the diesel power generation amounts to 19.59 kW, which corresponds to 12 kW of the resistive load (4 kW per phase) plus 7.59 kW of the three single-phase EVs (2.53 kW each, which corresponds to the mentioned initial condition of I_{init} = 11 A and 230 V of nominal voltage V_n). Three-phase balanced events have been used to destabilize the microgrid frequency, whose deviations have been contained by the employed PFC. The event is a 3 kW load increase, which corresponds to 15.3% of the total generated power and to 6.3% of the generation capacity P_{gen} of the diesel generator, i.e., of the microgrid. One has to note that the total initial EVs absorbed power (7.59 kW) corresponds to 15.8% of P_{gen}. This percentage can appear as a very high share, but in reality is of roughly the same order of magnitude as a future scenario in the Nordic synchronous area. In fact, from the *Nordic EV Outlook 2018* report [22], the number of EVs in the Nordics is forecasted to be 4 million, whereas the Nordic generation capacity is 103 GW, as stated in the *Nordic Market Report* [102]. In the scenario of all the EVs charging simultaneously at 11 A, the correspondent initial absorbed power amounts to about 10 GW, which represents a share of about 10% of the installed Nordic generation capacity.

The simulation results reported in Figure 3.5 show notice that for both the two different steady-state frequencies (in cases of 1% and 3% droop from EVs) continuous undamped oscillations appear. This is due to the non-linearity in the EVs response: 1 A discreteness is implemented in the PFC controller, as discussed above. Such undesired current oscillations take place because the share of the discrete regulating PFC is high in relation to the size of the microgrid, leading in turn to induced oscillations on the system frequency.

For one possible case-specific (non-generalized) stabilizing algorithm to handle such 1 A oscillatory conditions, the reader is referred to **Paper B**. However, such strategy is not included in this chapter, as the thesis now proceeds with more in depth analysis of such oscillation conditions, before introducing in Chapter 4 generalized operational strategies to overcome the presented issues.

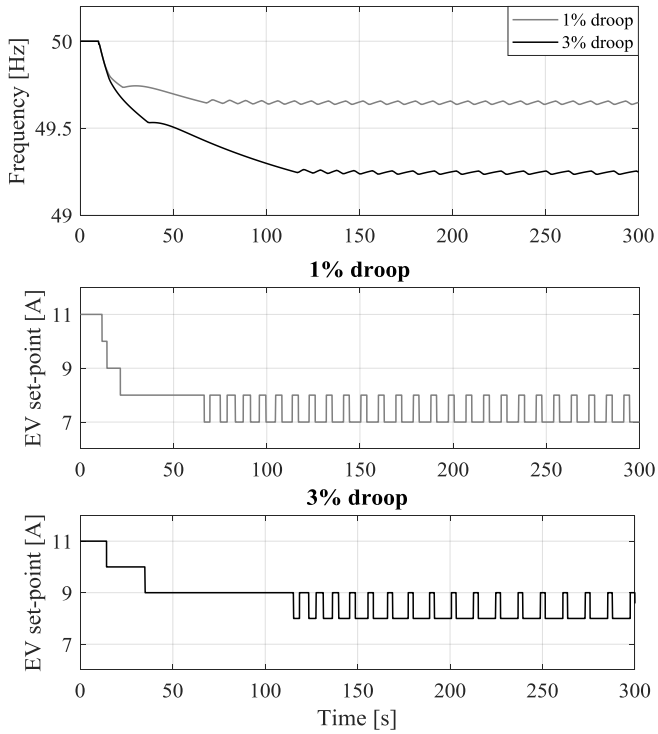

Figure 3.5 – Simulated frequency trends and EV set-point for the employed 1% and 3% droops.

3.2.2 Implementation in a microgrid: experimental tests

Experimental activities are performed to assess the capability of real series-produced EVs and commercial controllable hardware in providing grid regulation services in a microgrid. For more insights on a novel synthetic inertia controller aimed at decreasing the rate of change of the frequency after a contingency, the reader is referred to **Paper C**.

The microgrid is built as an islanded configuration of the experimental LV grid SYSLAB. The setup is similar to the one utilized for the simulation activities, and a schematic representation with the employed hardware is shown in Figure 3.6. Again, the Aircon wind turbine is present, yet not utilized for the operative scenarios included in this thesis. The only difference with the previously-simulated microgrid is that now a 120 kWh (±15 kW) vanadium redox battery (VRB) is connected to Busbar 2, which allows precise active power step events in the experimental validation, thus it is utilized as a passive load element. A resistive load and the EVs are connected with the diesel gen-set to Busbar 1. The total load excluding the EVs (each with I_{init} = 11 A) now amounts to 16 kW, i.e., 9 kW for the VRB and 7 kW for the dump-load. In this islanded microgrid the diesel gen-set acts as the grid forming unit and the only synchronous device. The 60 kVA (P_{gen} = 48 kW) diesel gen-set has an inertia constant $2H$ = 2 s, and is equipped with a governor acting with droop constant K_{gen} = 2 kW/Hz. This droop corresponds to 48% droop on system base, which represents a high value when compared to conventional power plants, however if seen from a system point of view it can represent a realistic case given the increasing penetration of uncontrolled small wind and solar plants that contribute to increase the total generation capacity without increasing the system absolute droop K_{gen}. High values mean that the conventional generator reacts smoothly, leaving space for regulation

to other non-conventional units, such as EV fleets. These conditions may appear in islanded power systems or microgrids, where frequency regulation from small DERs will be crucial when increasing the penetration of renewables.

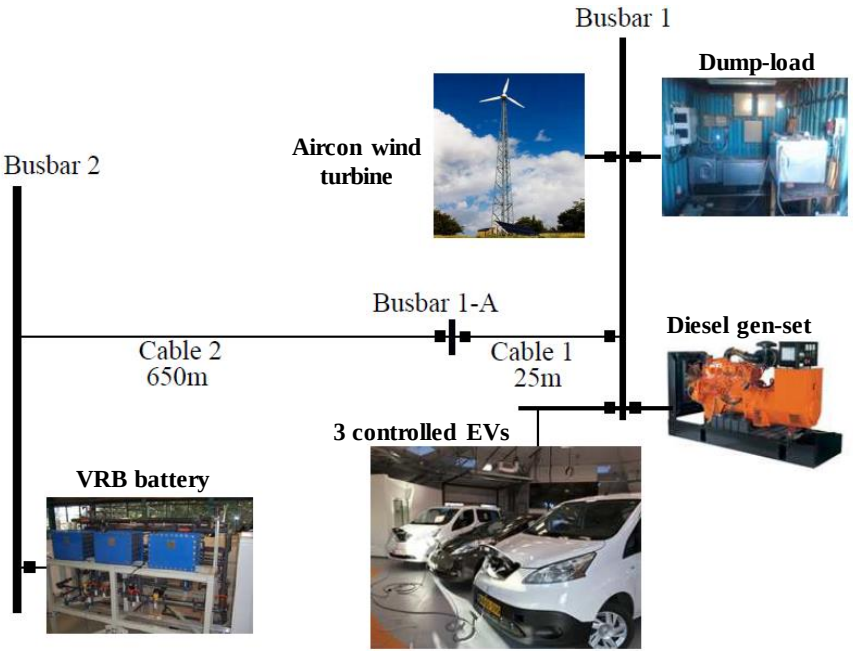

Figure 3.6 – Experimental layout.

The VRB and the dump-load are controlled through a Matlab/Java interface, while the EVs through a Python interface. Given that all of the components are 3-phase except the 3 EVs (single-phase Mode 2 charging up to 16 A), an intermediate phase splitter is utilized to connect each of the 3 EVs to a different phase of the grid by means of three EVSEs. In particular, three standard Mennekes plugs (IEC 62196 Type 2) are used, along with three commercial controllers by Phoenix [78], which are controlled separately by three different pieces of EVSE. Figure 3.7 shows a picture of the employed custom-made three-phase splitter for the connection of the 3 single-phase EVs to Busbar 1 in SYSLAB.

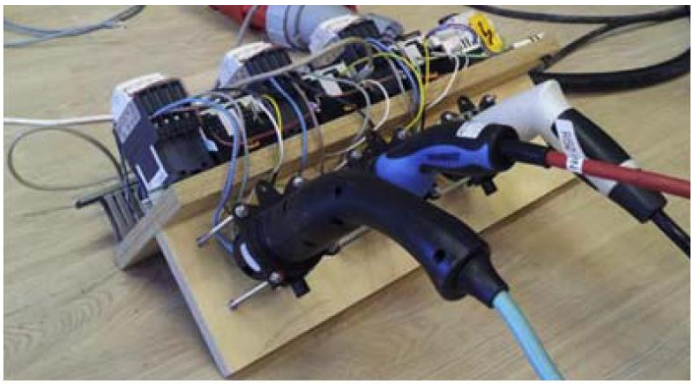

Figure 3.7 – Three-phase splitter: three Mennekes plugs connect each EV to a separate phase.

The control and communication setup is shown in Figure 3.8, and consists of the following components:

- *The smart charging controller* – receives the measurements from the multi-instrument, it calculates the response and it sends control signals to the EVSE;
- *DEIF MIC-2* – a multi-instrument measurement device for voltage, current and power measurements with 0.2, 0.2, and 0.5% accuracy, respectively which are polled every 200 ms. The device is only used for data logging;
- *DEIF MTR-3* – a multi-instrument measurement device that is used here for fast frequency measurements with accuracy of 10 mHz, which are polled every 200 ms;
- *EVs* – 3 EVs with Li-ion battery have been controlled: two 24 kWh Nissan e-NV200 (2014 and 2015) and one 30 kWh Nissan Leaf (2016);
- *EVSE* – rated for 16 A.

The smart charging controller consists of many subcomponents, as follows:

- *Controller logic* – reads the latest frequency measurements from the message bus and calculates the frequency deviation Δf. Calculated set-points are directly sent to the EVSE controller;
- *EVSE controller* – acts as an interface between the physical EVSE and the controller logic;
- *Frequency poller* – acts as an interface to the frequency measurement device. In this case DEIF MTR-3 instrument used for frequency sampling every 0.2 s;
- *MIC-2 poller* – multi instrument device interface;
- *Data logger* – monitors the data exchange on the message bus and logs it to the database;
- *ZMQ message bus* – is the message bus that is used to represent the data exchange between the previously mentioned controller components.

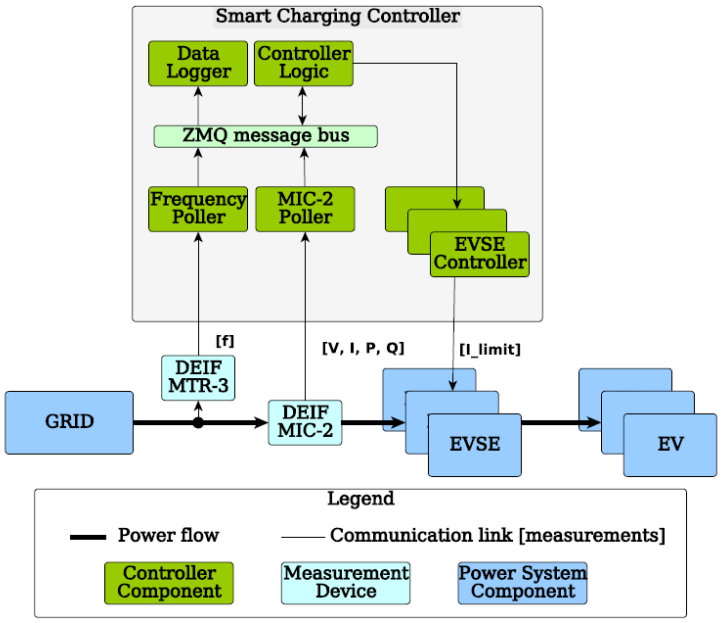

Figure 3.8 – The communication architecture for the implemented smart charging controller.

The VRB absorbed power is increased/decreased by ±2 kW for a user-settable time window, to obtain frequency dynamics that will be enhanced by the implemented EV controllers. The employed EV droop is 4%, i.e., the current of the three EVs was modulated proportionally to frequency deviations within 48-52 Hz, as shown in Figure 3.1. Figure 3.9 shows results from the uncontrolled EVs case and the PFC control case with 4% droop. After the load contingency due to the discrete EV response, the current absorbed by the EVs oscillates between two consecutive set-points, as none of them allows a steady-state frequency to be reached without passing the threshold that triggers the consecutive set-point. Such results confirm the expected oscillation conditions found on the simulation studies, leading to the conclusion that it is then of outmost importance tackling these aspects in the detail by means of analytical assessments and further experimental tests. This aims at identifying the conditions for such oscillations to start and at assessing the possible consequences in small and large size power systems.

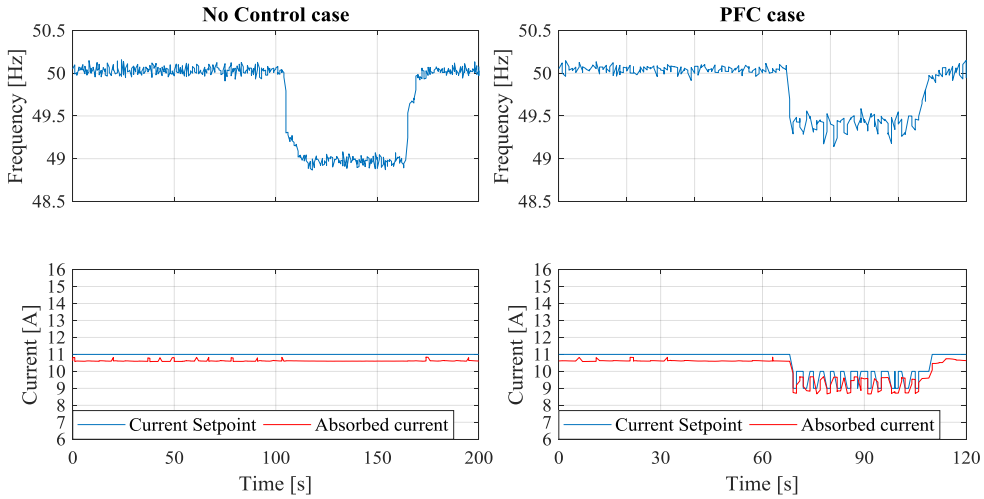

Figure 3.9 – Experimental results with 3 EVs performing PFC with a granularity of 1 A (α = 1) in an experimental microgrid. Frequencies and currents are measured with DEIF MTR-3 and MIC-2, respectively.

3.3 Effects of a discrete EV response

The EV set-point granularity is now investigated in order to assess potential implications on power systems of primary frequency control via aggregated EVs with discrete responses. As first step of the analysis, the case of ideal EV response is proposed, with no granularity when fixing the current set-point. So, to stabilize the frequency to a new steady-state value, a total power equal to the size of contingency ΔP_{load} that caused the imbalance will be provided by the conventional synchronous generators ΔP_{gen_id} and one EV ΔP_{EV_id}, with shares given by their droops as in (3.6). For the sake of simplicity, the following formulation considers only one synchronous unit, whose governor droop is K_{gen}.

$$\begin{cases} \Delta P_{gen\_id} = \Delta P_{load} \cdot \frac{K_{gen}}{K_{PFC\_pow}+K_{gen}} \\ \Delta P_{EV\_id} = \Delta P_{load} \cdot \frac{K_{PFC\_pow}}{K_{PFC\_pow}+K_{gen}} = V_n \Delta I_{PFC\_id} \end{cases} \tag{3.6}$$

The after-contingency ideal steady-state frequency value f_{eq_id} will be

$$f_{eq\_id} = \frac{\Delta P_{load}}{K_{PFC\_pow} + K_{gen}} + f_n \tag{3.7}$$

The EV contribution in terms of current ΔI_{PFC_id} is calculated using (3.4) and a linear droop, while the correspondent power is ΔP_{EV_id}, assuming nominal phase-to-neutral voltage conditions V_n. In the realistic case of a given discreteness in the current set-point, a correspondent step function as the solid one in Figure 3.1 is utilized. To do this, the index α is recalled to indicate the size of the steps when controlling the EV charging. So, for a given measured frequency the correspondent ideal current set-point would be rounded up/down to the closest *i*-th value of the step function, with *i* representing the *i*-th current set-point for a given granularity. The current ΔI_{PFCi} is then calculated as:

$$\Delta I_{PFC} = \Delta I_{PFCi}\,, if\ \ \Delta I_{PFC\_id} \in \{\Delta I_{PFCi\_min};\ \Delta I_{PFCi\_max}\}$$

$$with \begin{cases} \Delta I_{PFCi\_min} = \Delta I_{PFCi} - 0.5\alpha^{-1} \\ \Delta I_{PFCi\_max} = \Delta I_{PFCi} + 0.5\alpha^{-1} \end{cases} \tag{3.8}$$

Such condition determines which set-point is set on the EV, given the calculated ideal value and the implemented granularity α. It is now investigated which consequences this may induce to the operation, both on a large power system and on a small one, i.e., on a microgrid level.

3.3.1 Consequences in a microgrid

In low-inertia systems, e.g., in a microgrid, the discreteness in the response may cause different consequences related to the impossibility of reaching a stable steady-state frequency, f_{eq_id} in (3.7). This can lead to continuous oscillations between two consecutive current set-points, which will influence the frequency consequently. To better investigate the phenomena, the condition of setting a given set-point ΔI_{PFCi} reported in (3.8) can be re-written in terms of frequency limits, as in (3.9):

$$\Delta I_{PFC} = \Delta I_{PFCi}\,, \qquad if\ f_{meas} \in \{f_{i\_min};\ f_{i\_max}\}$$

$$with \begin{cases} f_{i\_min} = f_n - \frac{\Delta I_{PFCi\_min}}{K_{PFC}} \\ f_{i\_max} = f_n - \frac{\Delta I_{PFCi\_max}}{K_{PFC}} \end{cases} \tag{3.9}$$

Between two consecutive frequency intervals, a threshold value $f_{threshold(i;\, i-\alpha^{-1})}$ is defined, which is equal to the minimum frequency value of the *i*-th step's interval f_{i_min} and the maximum value of the previous step $f_{(i-\alpha^{-1})\_max}$. In case of current oscillations, two different steady-state values calculated for the two consecutive current set-points would be below and above the threshold $f_{threshold(i;\, i-\alpha^{-1})}$, meaning that:

$$f_{i\_eq} < f_{threshold(i;\, i-\alpha^{-1})} < f_{(i-\alpha^{-1})\_eq} \tag{3.10}$$

where

$$\begin{cases} f_{i\_eq} = f_n - \frac{\Delta P_{load} - V_n \Delta I_{PFCi}}{K_{gen}} \\ f_{threshold(i;\, i-\alpha^{-1})} = f_n - \frac{\Delta I_{PFCi} + 0.5\alpha^{-1}}{K_{PFC}} = f_n - \frac{V_n(\Delta I_{PFCi} + 0.5\alpha^{-1})}{K_{PFC\_pow}} \\ f_{(i-\alpha^{-1})\_eq} = f_n - \frac{\Delta P_{load} - V_n \Delta I_{PFC(i-\alpha^{-1})}}{K_{gen}} \end{cases} \quad (3.11)$$

The condition for current set-point oscillations between ΔI_{PFCi} and $\Delta I_{PFC(i-\alpha^{-1})}$ can be expressed as in (3.12):

$$f_{i\_eq} < f_{eq\_id} < f_{(i-\alpha^{-1})\_eq} \quad (3.12)$$

The condition in (3.12) is true whenever the steady-state frequency for any given current set-point differs from the ideal steady-state frequency value f_{eq_id} defined in (3.8). Thus, for any *i*-th set-point, the condition for two consecutive current set-point oscillations can be expressed as in (3.13) and in (3.14):

$$\forall\, i\,, f_{i\_eq} \neq f_{eq\_id} \quad (3.13)$$

Which means

$$V_n \alpha^{-1} \boldsymbol{round}(\alpha K_{PFC} \Delta f) \neq \Delta P_{load} \left(1 - \frac{K_{gen}}{K_{gen} + K_{PFC\_pow}}\right) \quad (3.14)$$

It can be noticed that the evaluation of these conditions depends on the tuning of the regulating units (K_{gen}, K_{PFC}, α), on the size of the contingency (ΔP_{load}), and on ΔI_{PFCi}, which in turn depends on α, K_{PFC} and the measured frequency variation Δf. Differently from all the other parameters, the measured system frequency cannot be known a priori, but an estimation can be carried out by relying on Eq. (3.21) introduced in the next section, which includes parameters of the overall power system such as the total system inertia as well as the total apparent power of the rotating machines.

3.3.2 Consequences in a large power system

The main consequence related to a discreteness in the response for primary frequency regulation is the inaccuracy in the primary reserve provision. This is identified as the difference between the requested (or expected) power to be exchanged with the grid P_{req} and the actual provided power P_{prov}, and is defined as ε_P:

$$\varepsilon_P = \left| P_{req} - P_{prov} \right| \quad (3.15)$$

The presence of such difference, thus of the error in the reserve provision, is due to the granularity of the set-points. In fact, the expected power is calculated with the ideal current set-point, derived by the linear ideal droop curve, whereas the actual delivered power is the result of the rounding. As the source of the error is merely the granularity in the current that is added to the initial current set-point, (3.15) can be re-written in terms of current error:

$$\varepsilon_I = \left| I_{req} - I_{prov} \right| \quad (3.16)$$

where I_{req} is the requested current calculated using the expected ideal change in the current ΔI_{PFC_id} in (3.5), whereas I_{prov} is the actual current exchanged with the grid, obtained using ΔI_{PFC} in (3.5). With reference to Equation (3.8), one can note that for each *i*-th set-point the maximum error is given by the extreme values ΔI_{PFCi_max} and ΔI_{PFCi_min}. This means that the maximum error ε_{I_max} is:

$$\varepsilon_{I\_max} = 0.5\alpha^{-1} \tag{3.17}$$

It is clear that higher discreteness (smaller α) in the response reflects to larger reserve provision errors when delivering PFC. A visual representation of the reserve provision error as function of the requested current, for a number of granularity cases, is shown in Figure 3.10. It may be noted that a granularity of 1 A (α = 1) implies a maximum error of 0.5 A, which represents the 10% of the available regulating window I_{reg} of ±5 A, i.e., the available reserve. For finer granularities the maximum error decreases proportionally: for α = 2 it is 0. 25 A (5% of I_{reg}), and for α = 4 it is 0. 125 A (2.5% of I_{reg}).

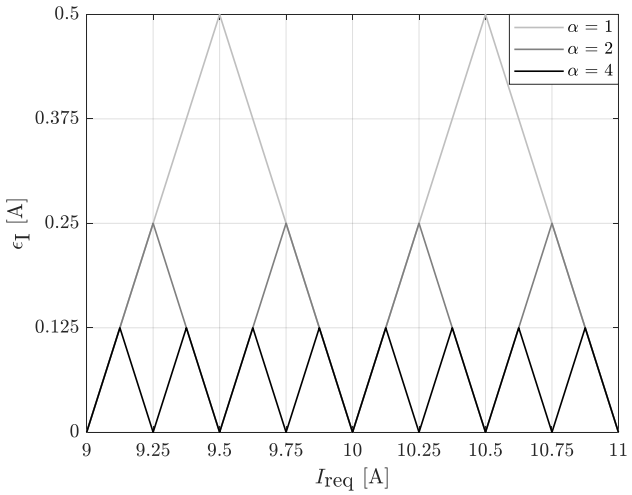

Figure 3.10 – Response error as a function of the requested current, for different granularities.

To counteract the presented negative consequences of discrete responses, a smart fleet management strategy is reported in the following.

3.3.3 An EV fleet management strategy to reduce the response granularity

As seen, a deterministic droop controller with a discrete response always leads to a response error, except for the cases where the requested response coincides with a discrete step of the charger's output. To overcome such problem, an EV fleet management strategy is proposed, which is meant for centralized EV fleet operation, as each individual EV would receive the set-point remotely calculated by the aggregator. The control is based on a droop shift logic, in order to achieve an overall response granularity that is smaller than the one implemented in the single EV. An aggregated smoother response can be achieved if the EV fleet is properly managed, albeit each EV would be controlled using larger discrete steps, in fact, the proposed EV fleet management logic

guarantees a more accurate fleet response, still relying on larger granularities for each individual EV. For a given individual EV granularity $\alpha_{individual}$ it is possible to obtain an aggregated granularity α_{aggr} for a certain number of EVs n_{EV}, calculated as:

$$n_{EV} = \frac{\alpha_{aggr}}{\alpha_{individual}} \tag{3.18}$$

With reference to the typical frequency-current step-wise droops presented in Figure 3.1, the shift f_{shift} is calculated as a translation along the x-axis in terms of frequency, and depends on the absolute current droop constant K_{PFC}. The shifts for each EV are calculated as in (3.19):

$$f_{shift} = (2n_i + 1) \cdot (\pm \frac{0.5}{\alpha_{aggr} \cdot K_{PFC}}) \tag{3.19}$$

where

$$n_i \in A, A = \{n \in N \mid n \leq (n_{EV}/2 - 1)\} \tag{3.20}$$

As an example, the case of EV charging Mode 2 compliant with IEC 61851 [59] with droop constant K_{PFC} = 2.5 A/Hz is studied, which corresponds to the PFC control conditions tested in occasion of the P-HiL tests presented above. In this case, in order to obtain an α_{aggr} = 4, employing EVs with $\alpha_{individual}$ = 1, the number of needed EVs n_{EV} is 4 and the frequency shifts are ±0.05 and ±0.15 Hz. Figure 3.11 shows the combination of the 4 shifted droops, along with the aggregated equivalent droop, which allows the EV aggregator to reduce the reserve provision error from 5% to 1.25%, which in terms of currents is from 0.5 to 0.125 A. For the sake of completeness, Table 3.2-Table 3.4 show the parameters for the implementation of the proposed smart fleet management strategy for the example cases of individual EV granularity of 1 A, 0.5 A and 0.25 A, respectively.

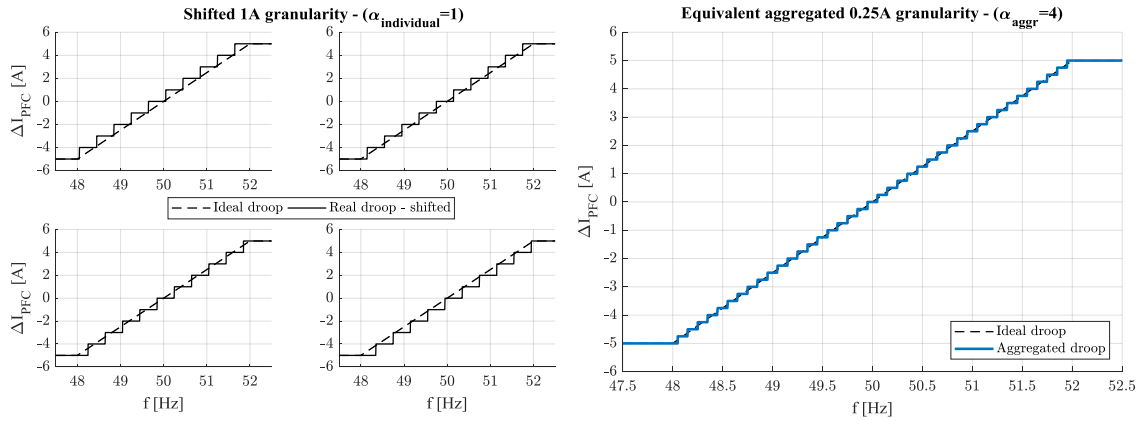

Figure 3.11 – With proper shifting of the droops of 4 EVs with $\alpha_{individual}$=1, the aggregated response is equivalent to the case α_{aggr}=4.

Table 3.2. EV fleet parameters in case of $\alpha_{individual} = 1$.

α_{aggr}	n_{EV}	n	f_{shift} [Hz]
2	2	0	±0.1
4	4	0; 1	±0.05; ±0.015
8	8	0; 1; 2; 3	±0.025; ±0.075; ±0.0125; ±0.175
16	16	0; 1; 2; 3; 4; 5; 6; 7	±0.0125; ±0.0375; ±0.0625; ±0.0875; ±0.1125; ±0.1375; ±0.1625; ±0.1875

Table 3.3. EV fleet parameters in case of $\alpha_{individual} = 2$.

α_{aggr}	n_{EV}	n	f_{shift} [Hz]
4	2	0	±0.05
8	4	0; 1	±0.025; ±0.075
16	8	0; 1; 2; 3	±0.0125; ±0.0375; ±0.0625; ±0.0875

Table 3.4. EV fleet parameters in case of $\alpha_{individual} = 4$.

α_{aggr}	n_{EV}	n	f_{shift} [Hz]
8	2	0	±0.025
16	4	0; 1	±0.0125; ±0.0375

In general, this EV fleet management strategy may not guarantee the prevention of induced oscillations in a microgrid, as it is not guaranteed that for a given frequency deviation the ideal current value ΔI_{PFC_id} would be reached. However, the advantages are clear: on the one hand, the size of oscillations can be drastically reduced, which can then be damped in a faster and easier way. On the other hand, in case of application in large-size power systems, the reserve provision error is reduced since the fleet operates as if each EV would have finer responses. It is relevant to point out that this strategy does not take into account one important aspect of the operation of the power converters, i.e., the charging/discharging efficiency for different set-points, which varies as shown in Chapter 4. With the knowledge of the technical properties of the employed hardware, the aggregator can enhance the fleet operation, as operating at power levels with higher efficiencies mean less energy losses during the V2G session.

3.4 Assessment of EV response granularity in a P-HiL environment

One more experimental investigation is now reported, whose main purpose is to assess the consequences on the system dynamics of a set of EVs performing frequency regulation with discrete responses. The SYSLAB microgrid in the same configuration as before is reproduced in a power hardware-in-the-loop (P-HiL) environment, and different granularities of the EV charging current set-point are implemented. The implementation of granularities < 1 is possible thanks to the flexibility of the P-HiL setup, so overcoming the limitations found during the experimental activities in the SYSLAB. Results are compared with the ones expected from the analytical investigations, completing the investigation on the consequences of a discrete EV response of large-scale PFC providing units in a system.

3.4.1 P-HiL experimental setup

P-HiL experimental activities are carried out at the Norwegian National Smart Grid Laboratory (NSGL), located in Trondheim at the campus of the Norwegian University of Science and Technology (NTNU) and jointly operated by SINTEF and NTNU [103]. The P-HiL hardware equipment utilized for the tests consists of the six-leg 200 kVA 5kHz Egston *power amplifier*, the real time simulator OPAL-RT OP5600 unit with I/O devices OP4520 (representing the *digital simulation system*), and two 60 kW two-level three-phase converters. In particular, either one or two of the converters (depending on the tested scenario) is the *hardware under test (HuT)*, i.e., the physical hardware under examination within a P-HiL test activity. In this case, each converter can reproduce the aggregated behavior of up to six single-phase EVs charging according to Mode 2 charging. The EV batteries are considered to be connected to the DC link, whose voltage is kept constant at 680 V by a third converter (identical to the ones described above) that is constantly operating as constant DC voltage source. The P-HiL experimental setup is depicted in Figure 3.12, where the three main parts of the typical P-HiL setup are highlighted, namely the *digital simulation system*, the interface with *power amplifier*, and the *HuT* [104]–[106].

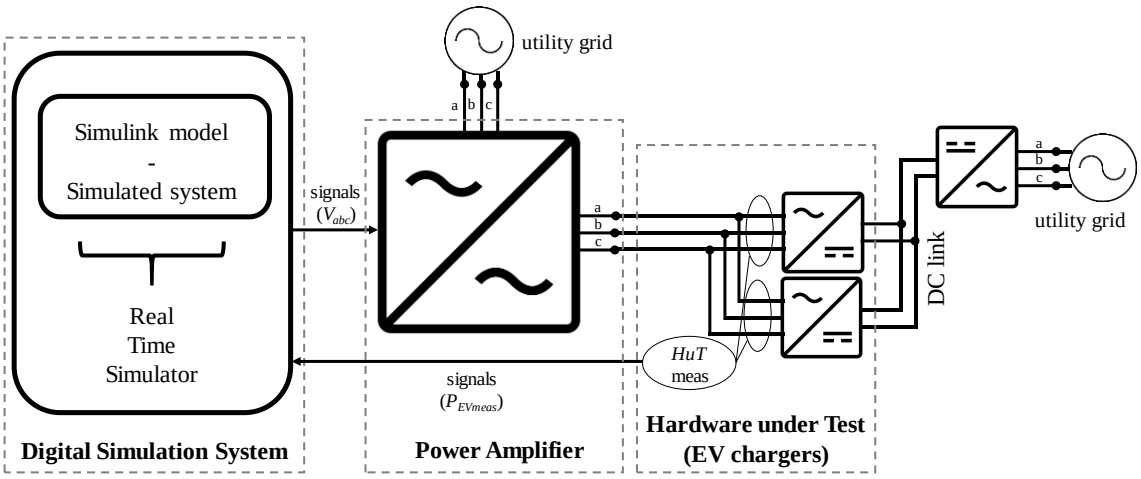

Figure 3.12 – P-HiL experimental setup.

As for the generation of the voltage signals V_{abc} that the *power amplifier* sets at its output channels to create the AC microgrid, the block diagram in Figure 3.13 is implemented in the *digital simulation system*, utilizing Simulink in Matlab 2013a with simulation time step equal to 0.2 ms. The RMS phase-to-neutral voltage reference value V_{ref} is manually set constantly equal to 230 V, while its reference angle θ is calculated as follows. The Simulink model for the calculation of V_{abc} employs the power system parameters (in this case the SYSLAB microgrid), given values for electrical load P_{load} (with eventual steps ΔP_{load}), and a physical input signal, i.e., the measured total active power absorbed by the two converters under study, namely P_{EVmeas} in Figure 3.13. P_{EVmeas} is measured with a DEIF MIC-2. The implementation of (3.21) enables the calculation of the rate of change of the angular velocity $d\omega/dt$ that, integrated twice, gives the reference angle θ for the generation of the

voltage signals to create the AC microgrid for the tests. S_{gen} is the diesel generator apparent power, whereas its inertia constant is *2H*. A change in the difference between mechanical power P_m and electrical power P_e would be reflected in a change in the system frequency as described by (3.21):

$$P_m - P_e = \frac{2H \cdot S_{gen} \cdot \frac{d\omega}{dt}}{\omega_n}, \qquad \text{with } \omega_n = \frac{2\pi \cdot f_n}{p} \tag{3.21}$$

where ω is the angular velocity of the rotor [rad/s], ω_n is its nominal value, and p the number of pole pairs of the rotating machine (= 2).

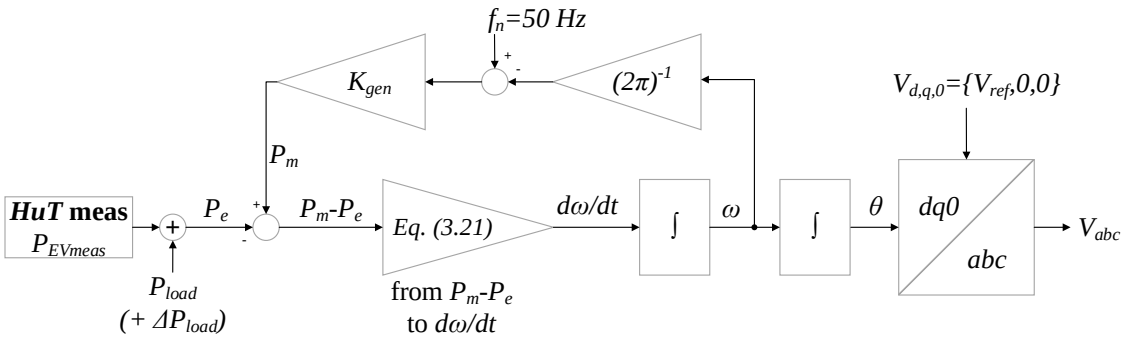

Figure 3.13 – The generation of the three-phase voltage reference signals that are set at the output of the *power amplifier* is implemented in Simulink in the *digital simulation system*.

The EV current set-points to be set on the physical converters are computed as described in Section 3.2 It is important to highlight that multiple set-points can be individually and independently computed per each EV, to emulate the case of a number of EVs with different time responses, droops or response discreteness. In fact, before aggregating the overall signal to be set on the converter under test, each EV control scheme can compute a different set-point for instance according to eventual droop shifts in case of implementation of the proposed droop shift-based fleet management strategy.

3.4.2 Test results

The modeled microgrid reflects the one utilized for the tests with real EVs in SYSLAB, and again the investigation is carried out by monitoring the system frequency dynamics after a contingency. Starting on a stable operating condition with f = 50 Hz, the grid contingency takes place, which is obtained with a load increment ΔP_{load} = 2 kW, causing under-frequency conditions. The PFC controller is implemented with a 4%, starting with I_{init} = 11 A. The first P-HiL test results are shown in Figure 3.14, which shows the uncontrolled EV case. It can be seen that the P-HiL tests match the ones measured in the real microgrid in SYSLAB (Figure 3.9), with an after-contingency steady-state frequency of 49 Hz. This value is motivated by the fact that the PFC controller is deactivated, and after the 2 kW contingency, frequency regulation is provided only by the diesel gen-set, whose governor acts with a droop K_{gen} of 2 kW/Hz. The frequency obtained via a PLL is filtered over observation windows of 100 ms, in order to emulate realistic measurements devices. The filtered

frequency (in red in the results plots) is then utilized for the calculation of the EV current set-points, to set on the converters.

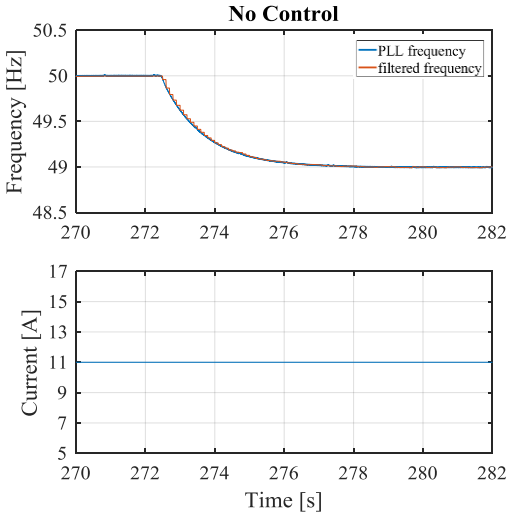

Figure 3.14 – P-HiL experimental results: measured frequency and EV current for the uncontrolled EV case.

To complement the analytical formulation proposed in Section 3.3, Figure 3.15 shows results from experimental P-HiL tests with PFC implemented for four different granularities: $\alpha = \{1, 2, 4, \infty\}$, which correspond to the cases of granularity of 1 A, 0.5 A, 0.25 A and 0 A, respectively. First, one can note that the controller and experimental microgrid in the P-HiL setup are tuned in a safe operation zone since system instabilities do not occur. Second, it can be noted that for $\alpha = 1$ the 1-A oscillations found in the previous simulation and experimental works are replicated. In fact, since the operating condition are the same as in Subsection 3.2.2, the same current oscillations are obtained, i.e., between 9 A and 10 A. Thanks to the elasticity of the employed P-HiL test setup, a deeper and more exhaustive investigation is now possible. In particular, the cases of finer granularities are studied, and the experimental results are evaluated against the analytical formulations described in Section 3.3. From Figure 3.15, one can note that oscillations take place even for the 0.5 A and 0.25 A discreteness cases, as none of the considered granularities lead to the ideal steady-state frequency value f_{eq_id} which is 49.463 Hz. Such value of f_{eq_id} is calculated using Equation (3.7) and confirmed from the P-HiL results in case of $\alpha = \infty$. The ideal case of $\alpha = \infty$ is achieved thanks to the flexibility of the P-HiL, and shows how the system would be smoothly stabilized in case of ideal EV response. However, as motivated in the beginning of the chapter, the compliance with technical standards and the limitations in commercial hardware for EV charging impose a discrete response of the EV when it comes to real implementations. For the three studied discrete responses ($\alpha = 1, 2, 4$), current set-point oscillations appear because the condition in Equation (3.12) is matched and the threshold $f_{threshold(i;\, i-\alpha^{-1})}$ between two consecutive set-points is crossed. However, the case $\alpha = 4$ shows very limited frequency oscillations, that can be achieved either via a very fine granularity or by smartly controlling the individual EV set-point as proposed smart EV fleet strategy. In fact, an

analogue response can be obtained if 4 EVs are controlled with shifted 1-A step functions. This is the case of applying horizontal shifts to the f-i step droop functions by f_{shift} of ±0.05 and ±0.15 Hz, obtaining α_{aggr} = 4 (0.25 A granularity) relying on implementation of 1-A step functions for each individual EV ($\alpha_{individual}$ = 1).

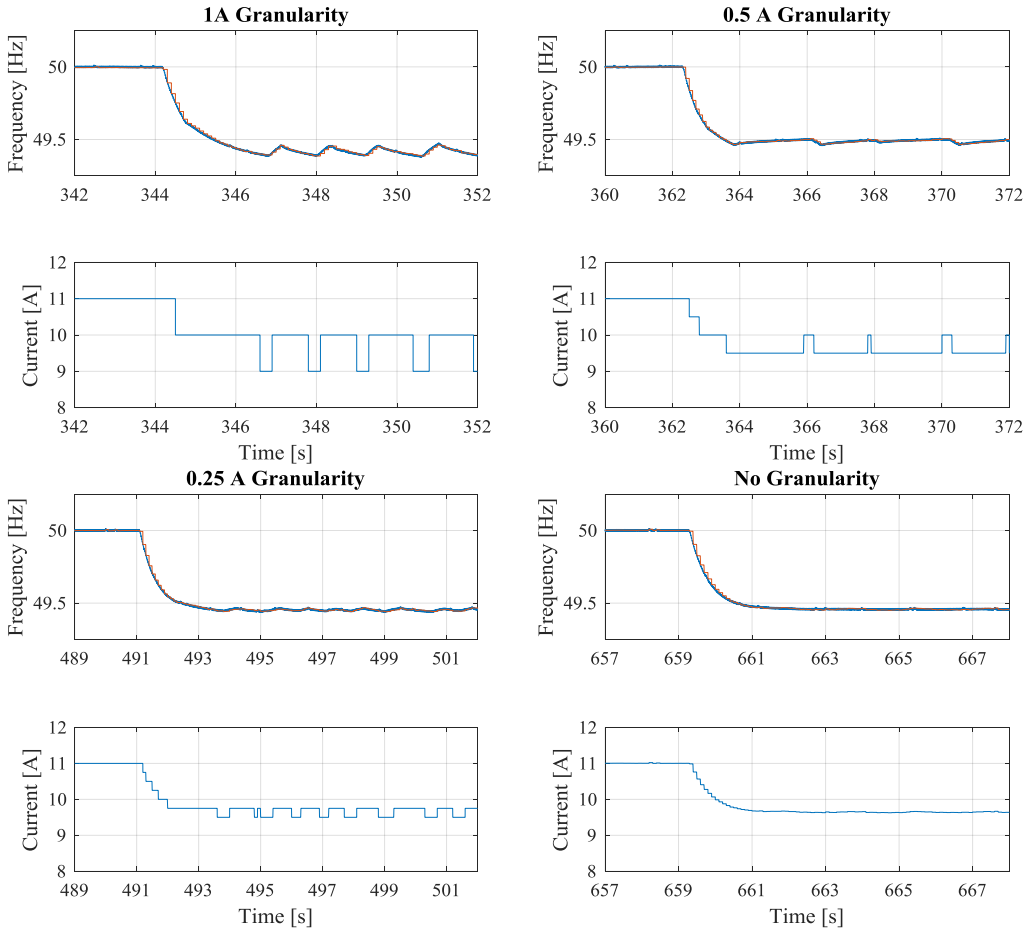

Figure 3.15 – P-HiL experimental results: Frequency and current set-points for the EV response granularity sensitivity analysis.

Table 3.5 reports steady-state frequency values for the consecutive set-points where the oscillations take place for different granularities, which easily allow us to verify that the above-presented oscillation conditions are respected. In fact, the numerical results calculated using the equations above match the P-HiL experimental results reported in Figure 3.15. For α = 1 the current set-point oscillates between 10 and 9 A, for α = 2 between 10 and 9.5 A, and for α = 4 between 9.75 and 9.5 A. In all the three α cases, it can be noticed that when the *i*-th EV set-point is set the frequency tries to reach its correspondent equilibrium value f_{i_eq}. By doing so, the threshold frequency value $f_{threshold(i;\, i-\alpha^{-1})}$ is crossed leading to a subsequent new change of the set-point. This happens because f_{i_eq} differs from the ideal steady-state value f_{eq_id}, causing repeated EV set-point changes between two consecutive values, experimentally confirming the condition for oscillations expressed in Equation (3.12).

Table 3.5. Results from experimental P-HiL activities.

	$\alpha = 1$	$\alpha = 2$	$\alpha = 4$
ΔI_{PFCi}	-1 A	-1 A	-1.25 A
$\Delta I_{PFC(i-\alpha^{-1})}$	-2 A	-1.5 A	-1.5 A
f_{i_eq}	49.345 Hz	49.345 Hz	49.431 Hz
$f_{(i-\alpha^{-1})\_eq}$	49.690 Hz	49.518 Hz	49.518 Hz
$f_{threshold(i;\, i-\alpha^{-1})}$	49.400 Hz	49.500 Hz	49.450 Hz
f_{eq_id} $(\alpha = \infty)$	49.463 Hz	49.463 Hz	49.463 Hz
ΔI_{PFC_id} $(\alpha = \infty)$	-1.3425 A	-1.3425 A	-1.3425 A

3.5 Summary

This chapter presented technical challenges that have to be taken into account when considering EVs as prospective sources of power system services. A primary frequency controller for EVs has been designed, which considered limitations related both to real hardware limitations and to EV technical standards. The proposed investigations covered both simulation and experimental studies in a microgrid, where the controller was tuned and implemented to control three single-phase EVs to support the system frequency after a destabilizing contingency. Results highlighted the effectiveness of the PFC controllers, as the frequency deviations were contained by the PFC actions of the EVs. Nevertheless, the discreteness of the EV response introduced frequency oscillations, as none of the discrete EV set-points could lead to a stable after-contingency steady-state frequency. So, the crucial role played by the EV current set-point granularity was analytically investigated assessing the consequences in applications in microgrids and large-scale power systems. The analysis was finally complemented with real time P-HiL experimental tests in a microgrid, where frequency oscillations have been decreased by gradually reducing the amplitude of the required EV charging rate granularity, matching the expected numerical results obtained via the proposed analytical formulation.

After this identification of challenges related to the control of uni-directional commercial standard-compliant hardware, the thesis proceeds with the test and control of V2G hardware. In particular, a possible EV fleet management strategy is designed in accordance with the outcome of the presented hardware tests. It aims at enhancing the operation of the EV aggregator, who is concerned about an efficient and accurate management of the fleet. Furthermore, realistic EV fleet models are utilized to perform full-scale power system stability simulation studies aimed at outlining guidelines for the TSOs to guarantee stable acquirement of large-scale frequency control via commercial V2G-capable EVs.

CHAPTER 4

Bi-directional EVs as frequency control providers

After the identification of the main challenges on an operational level of uni-directional control of EVs aimed at the provision of PFC, this chapter presents algorithms for EV aggregators to make their operation more performing as well as guidelines for TSOs to guarantee stable large-scale frequency control via V2G-capable EVs. First, hardware test results are reported, with focus on the technical capabilities of a series-produced EV and off-board charger when performing V2G operations. The attributes of the flexibility product outlined in Chapter 2 are tested, and the suitability of the hardware under test for the provision of system-wide services is assessed. Then, an EV fleet management strategy is presented, which implements a stochastic logic aimed at achieving a trade-off between the average error in the reserve provision during a V2G session and the overall fleet efficiency. The algorithm considers the technical capabilities of the commercial V2G off-board chargers, e.g., in terms of charging/discharging efficiency for all the possible set-points. In the second part of the chapter, realistic EV fleet models are utilized to perform full-scale power system stability simulation studies aimed at outlining guidelines for the TSOs when relying on large-scale frequency control via aggregated EVs performing V2G operations. The chapter includes results of the separate papers **Paper E**, **Paper F** and **Paper G**, attached in Part II.

4.1 Suitability of a commercial bi-directional EV charger for grid services

Today, bi-directional V2G is only accessible through DC chargers using the CHAdeMO protocol [62]. While DC chargers typically are associated with public fast-charging stations, reduction in size and price may ultimately allow for domestic use as well. A number of contemporary EV integration projects explore the use of early V2G-enabled DC chargers [107]–[109]. These chargers represent a key technology, enabling V2G across a broad number of EV models. It then becomes important to investigate the performance of these chargers with respect to the provision of V2G based services – going beyond traditional one-way charging. This is the focus of the following subsections, investigating the technical capabilities of V2G equipment when controlled either locally or remotely.

This section presents an operational characterization of a commercial ±10 kW V2G DC charger [77] aimed at investigating the extent to which DC chargers may be used to critical and demanding smart grid services such as FCR, which requires higher performances than FNR, as previously shown in Table 2.6. On the one hand, the knowledge of the EV charger efficiency for different charging/discharging set-points is needed to assess the accumulated losses during a V2G session. On the other hand, it is of utmost importance to assess the relevant characteristics of the EV flexibility product, in line with the definition presented in Chapter 2. This becomes a crucial step towards the certification and validation of the employed hardware with respect to the fulfilment of the required performance when providing a power system service as FCR.

4.1.1 Local and remote performance tests

The first tests aim at assessing the efficiency of the V2G charger for a number of set-points. This has been done in a local fashion, i.e., the set-points have been manually and locally set on the hardware, enabling the derivation of the activation time of only the employed hardware under test (HuT). To evaluate the influence on the total activation time of additional communication latencies, the second tests have been performed in a remote control fashion. The remote control test setup includes the communication and control infrastructure utilized by an actual EV aggregator, operating in on-field projects such as the Danish-funded ACES [107] and Parker [108]. Figure 4.1 shows the setup for both the remote and local control tests. The EVSE can receive a power set-point remotely computed and respond accordingly setting appropriate power flows in/out of the battery. In real operation, with this design the aggregator can calculate in a centralized way the appropriate V2G control signals to dispatch to its EVs, e.g., according to frequency measurements in case of FCR, as depicted in Figure 2.7. In case of the local control tests, the EV fleet operator platform for remote control is not utilized, as the set-points are directly set on the EVSE computer embedded in the charger.

Two different active power test patterns are sent to the V2G-capable EVSE/EV for testing the local and the remote control cases, respectively. The first one, outlined in Figure 4.2-a, presents a monotone charging power profile from -10 to +10 kW with steps of 400 W – a symmetrical monotone discharging profile is also tested, but not included in Figure 4.2-a. This test pattern allows the characterization of the V2G charger in terms of *efficiency mapping*, bi-directional power flow capability (*direction*), and hardware *activation time* in case of local control. The second one, shown in Figure 4.2-b, is characterized by continuous power ramps as well as instantaneous steps. Such design allows an evaluation of the six practical flexibility service attributes defined in Chapter 2. Specifically, it enables the assessment of the total response time (*activation time*) when controlling EVs in a remote fashion, thus including both communication latencies and charger and EV response time. This information is needed when assessing the capabilities on the provision of time-critical power system services from remotely aggregated small DERs. Further, the continuous part of the pattern allows the estimation of the *set-point granularity*, whereas the step-wise part allows the estimation of the *ramping times*, the *accuracy* and the *precision*. The remote test cycle is repeated 4

times, in order to have a larger dataset for a more exhaustive performance evaluation. It is worth mentioning that, although the charger's size is ±10 kW, the extreme power set-points are ±8.5 kW due to a limitation set on the internal charger software.

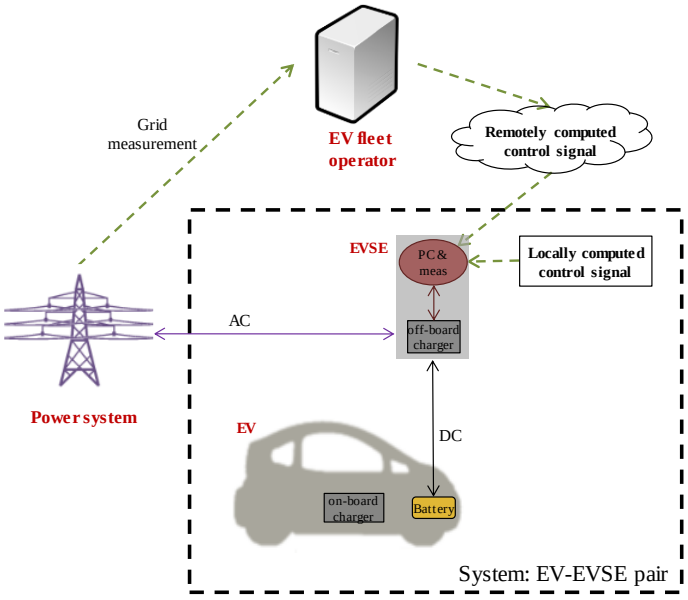

Figure 4.1 – Test configuration for the local and the remote control tests.

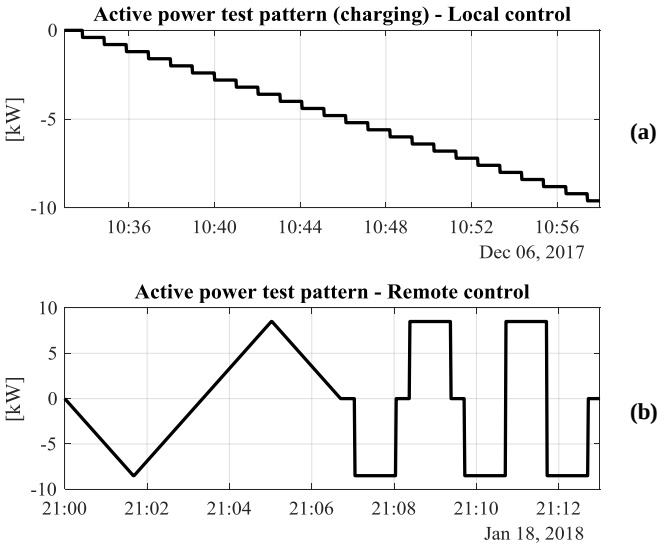

Figure 4.2 – Active power test patterns.

4.1.2 Outcome of local control tests

The local control test intends to quantify the charger efficiency at all possible charging and discharging levels at different SOC. The tests are performed with a 30 kWh Nissan Leaf (2016) parked in the SYSLAB laboratory with room temperature 20 °C. The measurements at the AC grid side are performed with a DEIF MIC-2 power meter with 0.2% accuracy and 1 s reporting time, while the DC side is measured with the internal DC voltage and current probe of the V2G charger, each with 1 s reporting time and 0.2% accuracy. The full charging/discharging power capability is studied by repeatedly stepping through current set-points with 1 A steps at the DC side, i.e., 400 W

in case of 400 V DC. For each power set-point, the efficiency is calculated by means of the procedure in Figure 4.3-a. In order to assess the influence of the SOC, the results reported in Figure 4.3-b show the efficiency as a function of the power, for a number of SOC.

4.1.2.1 Calculation of efficiency map

In a first set of tests, the efficiency was calculated during a FCR session, and it resulted in a large variance of efficiency values for each power set point due to the relatively large time constant of the charger, and the constantly changing set-point [110]. To avoid this issue, for the here-presented test the power set-point is changed only with 1 minute intervals, giving each charge/discharge cycle a 25 minute duration. The efficiency calculated for each DC power set-point value is the average during the whole minute, giving a granularity of 25 values for each SOC level. The efficiency during charging operation η_{ch} is defined as the ratio between the power flowing into the charger (AC power, P_{AC}) and the power flowing out (DC power P_{DC}). Similarly, the discharging efficiency η_{dis} is defined as P_{DC}/P_{AC}. They are calculated as in Figure 4.3-a. Results are reported in Figure 4.3-b, which shows that the large difference in the SOC has a negligible influence on the efficiency. The tests are performed only in the SOC range where the voltage changes linearly, so eventual difference in the results when operating in the extreme regions are not considered. However, it is not relevant considering the BMS limits in the useable range of the battery.

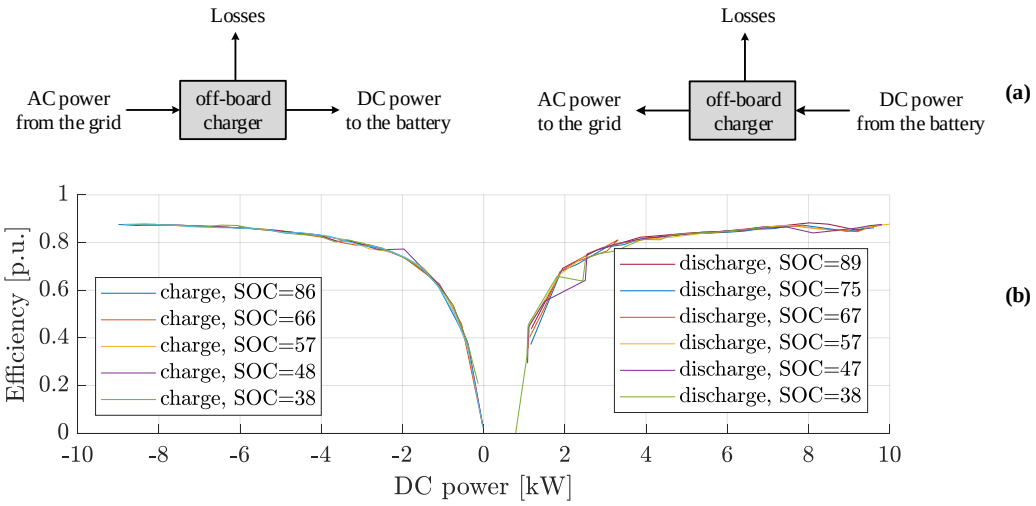

Figure 4.3 – V2G charger efficiency calculation (a), and efficiency map for charging/discharging DC set-points from -10kW to +10kW with steps of 400 W (b).

4.1.2.2 Calculation of activation time

The set-point control signal and the AC power provided on the grid side are shown in Figure 4.4-a, that is a zoom of a part of the AC power measured during the charging test of Figure 4.2-a. The time shift represents the activation time given the employed local control setup, thus it includes only the actual hardware response without any additional latencies due to control communications. Figure 4.4-b shows the correlation of the two signals when applying different time shifts to one of them for

the whole duration of the test. The maximum is found for a shift of 4 s, which is then considered as the activation time of the tested V2G equipment.

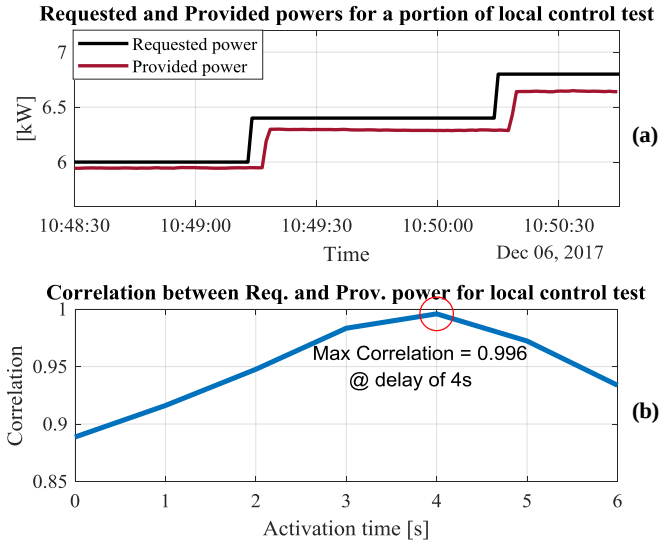

Figure 4.4 – Derivation of the hardware response time.

4.1.3 Outcome of remote control tests

The HuT and the laboratory environment conditions are the same as for the local control test. Figure 4.5 shows the requested and the provided power of one cycle of the active power test pattern. The time shift between the two signals represents the *total activation time* given the employed remote control setup. The non-perfect linearity in the response in the continuous portion is due to the *set-point granularity* imposed by protocols and the power electronics in the V2G charger. The time needed to reach the 0, ±8.5 kW set-points is utilized for the calculation of the *ramping rates*, while the measured power at the stable set-point levels allows the calculation of *accuracy* and *precision*. All these attributes are calculated in the following subsections.

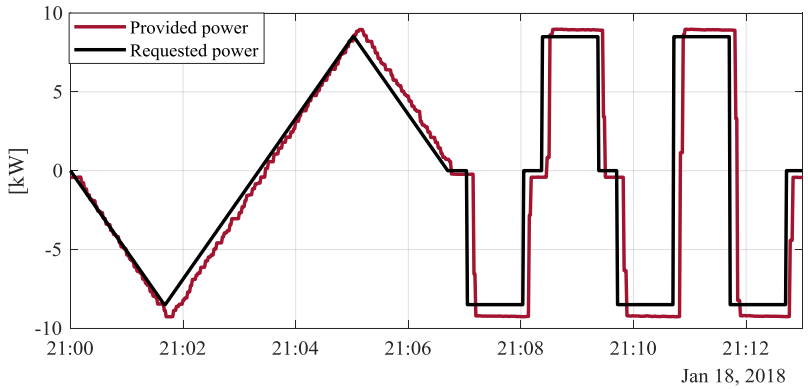

Figure 4.5 – 1 cycle of the performed remote performance assessment test.

4.1.3.1 Calculation of set-point linearity

The linearity in the response is studied in the continuous portion of the tested cycles, when a continuous linear signal is sent to the unit, i.e., from 21:00:00 to 21:06:30 in Figure 4.5. The

amplitude of the response is calculated as the difference of the measured provided power calculated at two consecutive time stamps. Hence a number of set-point granularities are calculated and then analyzed. Two sources of probable errors are neglected: the noise in the measurements, and the response precision when setting a given set-point value. The calculation of the response linearity is performed after applying a manual discreteness of 50 W on the measured data, given the average precision in the response calculated in Subsection 4.1.3.5. Results are reported in Figure 4.6. The bar plot shows the distribution of the observed granularities for different positive or negative sizes. A symmetrical distribution for charging (<0) and discharging (>0) can be noticed. The 2 bars with more observations (~50%) cover the range ±{300 400}W, whereas only in few cases (less than 5%) the absolute value of the granularity is > 400 W. The same results are reported in the boxplots, which show the median values -300 W and +350 W. In general, one can conclude that in very few cases the EV responds with a discreteness > 400 W when controlled with a linear signal. 400 W in AC can thus be considered as the finest response granularity for the HuT. In this case, neglecting conversion losses, 400 W in DC means a granularity of 1 A, being the DC link voltage equal to 400 V, according to the technical CHAdeMO protocol.

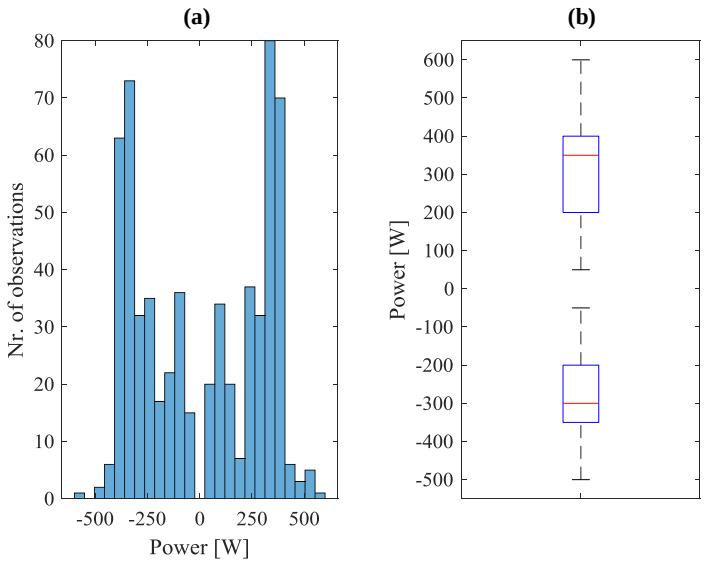

Figure 4.6 – Distribution of the observed granularities (a). In (b), the blue boxes indicate 50% of the observations, whereas the median is in red. Upper and lower quartiles (25% of the data) are located within the vertical black lines.

4.1.3.2 Calculation of total activation time

Figure 4.5 shows a time shift, which represents the total activation time given the employed remote control setup, including the 4 s delay of the actual hardware response time found in Subsection 4.1.2.2 and the additional latencies due to the remote control. Figure 4.7 shows the correlation of the two signals of Figure 4.5 when applying different time shifts to one of them. The maximum is found for a shift of 7 s, which is then considered as the total activation time when the tested V2G equipment is controlled via the centralized remote control setup. By comparing these results with the

ones for local control, the influence on the overall response time due only to remote control can be assessed.

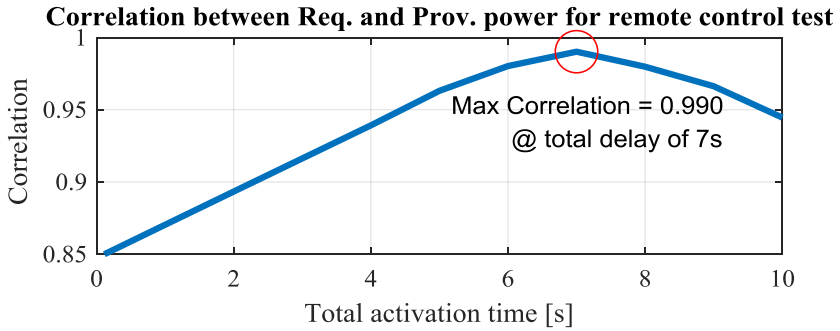

Figure 4.7 – Derivation of the total activation time.

4.1.3.3 Calculation of ramping up/down

The ramping capabilities are studied in the step-wise portion of the tested cycles, with 4 events up and 4 events down (Figure 4.8). The power flow is changed from the zero set-point to the minimum and maximum values, and back. Also the largest possible steps are analyzed, i.e., when setting the maximum power starting from the minimum set-point, and vice versa. Table 4.1 reports numerical results of the calculated up/down ramping rates. The average up/down rates almost coincide: about 3.3 kW/s when expressed in the general unit of measurement [kW/s], i.e., related to 1 s-time window. Nevertheless, the minimum calculated up and down rates are 1.8 kW/s (up2-cycle4) and 2.2 kW/s (down1-cycle2,3 and down3-cycle1) respectively, lower than the average, meaning that the unit on average responds with 3.3 kW/s, but may respond slower.

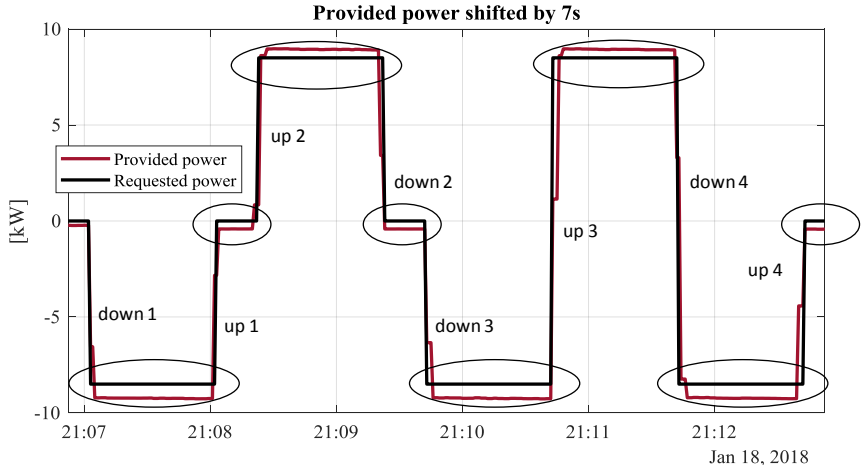

Figure 4.8 – Step events are performed to calculate the *ramping rate* capability, whereas for *accuracy* and *precision* the calculation is done during the constant set-point levels.

Table 4.1. Measured ramping rates up/down.

Event	Cycle 1	Cycle 2	Cycle 3	Cycle 4
up 1	8.84kW in 3s	8.84kW in 4s	8.82kW in 3s	8.84kW in 4s
up 2	9.03kW in 4s	9.04kW in 4s	9.03kW in 4s	9.04kW in 5s
up 3	17.87kW in 6s	17.85kW in 6s	17.88kW in 4s	17.86kW in 6s
up 4	8.84kW in 4s	8.84kW in 1s	8.83kW in 4s	8.84kW in 3s
Ramp-up avg.		**3.35 kW/s**		
down 1	8.99kW in 3s	8.79kW in 4s	8.79kW in 4s	8.99kW in 3s
down 2	9.33kW in 3s	9.16kW in 1s	9.17kW in 1s	9.16kW in 4s
down 3	8.79kW in 4s	8.98kW in 3s	8.97kW in 4s	8.99kW in 4s
down 4	18.12kW in 6s	18.14kW in 7s	18.13kW in 7s	18.14kW in7s
Ramp-down avg.		**3.31 kW/s**		

4.1.3.4 Calculation of set-point accuracy

The set-point accuracy is calculated during the constant set-point levels of the step-wise portion of the tested cycles, as highlighted in Figure 4.8. The accuracy is calculated as the difference between the requested and the provided power over the appropriate time windows. It is found that for charging operations (power<0) the power drawn from the grid is larger than the requested power. The same happens in case of zero set-point, where the power consumption is justified as the own consumption of the power electronics in stand-by mode. During the discharge operations, the power injected into the AC grid is higher than expected. This is probably due to a wrong calibration of the charger power electronics, which should be calibrated to avoid injection of power higher than the requested value, as it could compromise the safe operation. At zero set-point the charger draws from the grid on average 420 W, which can then be considered the unit's stand-by loss. In case of full charging operation, the calculated accuracy is 740 W, which represents the 8.7% of the maximum power set-point. Such difference in power is higher than in case of zero set-point, probably due to a non-optimal calibration of the unit. During the full discharging operation, the average power provided is higher than the requested by 440W, which is the 5.2% of the set-point.

4.1.3.5 Calculation of set-point precision

As done for the accuracy, the precision is calculated from the constant set-point levels of the step-wise portion of the test cycles, as the difference between the maximum and the minimum values of the provided power over the whole range of the time windows with stable extreme set-points. This means that the precision calculated with this test cycle can be considered as the worst case as for the extreme charging and discharging set-points. It is found that the precision is about 50 W for both extreme charging and discharging operation. This value justifies the choice of 50 W as manual discretization factor that is utilized in the analysis of the granularity in Subsection 4.1.3.1. In case of zero-setpoint the precision is much higher, since the difference between maximum and minimum of the measured power is about 6 W.

4.1.4 Overall outcome of performance tests

Table 4.2 shows the summary outcome of the performance tests for each identified flexibility product attribute, with the respective performance target defined by current technical standards. The requirements are adapted from the Danish technical standard for FCR provision in DK1 [32] and the newly-released Danish technical regulation for grid connected battery plants, which applies also for a number of aggregated EV chargers providing V2G services [111]. Such requirements are then considered as benchmarks when evaluating the eligibility of EVs in primary frequency control service provision. Going through the listed attributes, firstly it can be seen that the symmetric power bid requested by [32] applies to bi-directional power flow capability, which is available with the V2G technology. As for the set-point linearity, generally a linearity of 1% of the rated power is requested. It is found that the finest response has a granularity of 400 W, which represents the 4% of the rated power, thus not fulfilling the requirement. However, as 4% is the linearity for only one single unit, when managing an EV fleet the fleet operator should then apply smart logics to reach the requested 1% on an aggregated level, e.g., employing stochastic logics (**Paper F**). As for the activation time, the latencies due to remote control communication amount to about 3 s, while the mere hardware is characterized by an activation time of 4 s. Ref. [32] requires the activation of half of the full capacity within 15 s, which is then respected considering an instantaneous response. In reality, the response has an up-down ramping rate, which amounts to an average value of 3.3 kW/s. For the tested charger, this means that the total activation time for half of the reserve (5 kW) would be about 8.6 s, which is lower than the requested 15 s. Ref. [111] requires a ramping rate capability for the aggregated fleet within the range of 10-300 kW/s, which is out of the range of a single unit. This means that, considering again the average value of 3.3 kW/s, the minimum and maximum number of EVs to be employed for matching the required 10-300 kW/s ramping range will be 3 and 91, respectively. Finally for accuracy and precision, [111] requires a response within ±5% of the set-point and ±0.5% of the rated power. The requirement on the precision is respected, whereas for the accuracy the limits at the two maximum levels are overcome. This issue may be dealt by applying proper calibration of the internal power electronics to avoid such inaccuracies. Furthermore, as the requirements refer to the overall battery plant, smart fleet management solutions could be implemented, to reduce the reserve provision error via appropriate individual control of the single EVs (**Paper E**).

As motivated in Chapter 2, **a deep knowledge of the controllable hardware is needed to make the EV flexibility product a tradable asset**. On the one hand, insights into the charger's efficiency for different set-points allow the calculation of the accumulated losses during a V2G session, which is a crucial information for the estimation of the actual SOC of the controlled EV. On the other hand, the proposed investigation on the V2G flexibility provides valuable information for grid operators when performing grid studies, assessing the impacts of FCR provided by such units with realistic models to emulate their behavior. Furthermore, it can be useful also when defining new requirements for

grid connected V2G technologies, provided an indicative knowledge of the employed technology's capabilities (as investigated in **Paper G**). Ultimately, the investigation results provide insights also for the EV fleet operators in terms of actions needed for smart fleet management aimed at respecting the grid code restrictions (as investigated in **Paper F**).

Table 4.2. Evaluation of test results.

Attribute	Short description	Unit	Target for FCR [32], [111]	Test results
Direction	Support of bidirectional power flow	+/-/±	±	± i.e. V2G capable
Set-point linearity	Supported set-point throughout the power range	[W]	Linear at 1%	< 400 W (4%) (1 A @ 400V DC)
Activation time	Time between set-point request and change in power	[s]	< 15 s	Local control:4s Remote control:7s
Ramp-up time	Supported rate of change in power (increase)	[kW/s]	For the aggregate: 10-300 kW/s	AVG = 3.35 kW/s Max = 8.84 kW/s min = 1.81 kW/s
Ramp-down time	Supported rate of change in power (decrease)	[kW/s]	For the aggregate: 10-300 kW/s	AVG = 3.31 kW/s Max = 9.17 kW/s min = 1.98 kW/s
Accuracy	Difference between required and delivered response	[W]	±5% of set-point & ±0.5% of rated pow.	Neg. set-point:740W (+8.7% of set-point) (+7.4% of rated pow.) Pos. set-point: -440W (-5.2% of set-point) (-4.4% of rated pow.) 420W @zero set-point (4.2% of rated pow.)
Precision	Variation of the delivered response	[W]	±5% of set-point & ±0.5% of rated pow.	≈ 50 W (0.6% of set-point) (0.5% of rated pow.) 6 W @zero set-point (0.06% of rated pow.)

4.2 From the aggregator's perspective: a decentralized EV fleet control algorithm

Given the identified technical challenges of PFC provision and the characterization of commercial V2G hardware, a decentralized control algorithm is outlined in the following, which allows a trade-off between the average reserve provision error during a V2G session and the overall fleet efficiency. The controller is decentralized because, in general, decentralized control strategies are faster and (to a certain extent) less demanding from a communication point of view than centralized strategies, as discussed in Chapter 2. Despite microgrid applications where too steep droop characteristics may lead to continuous activation of the primary reserve or even to system instabilities, frequency deviations in large-size power systems are more limited in size, given, among others, the large synchronous inertia. For example, as presented in the first part of the thesis, FNR in

the RG-N area is a symmetrical service, and reserve is provided linearly, with full activation for deviations of ±100 mHz. The realistic frequency-current PFC droop curve in Figure 4.9 is implemented with ±25 A as current limits, with reference to the commercial off-board EV chargers tested in the previous chapter. With respect to the formulation in Equations (3.3) and (3.4), the employed absolute droop K_{PFC} is 250 A/Hz, whereas the relative droop k_{droop} is 0.2% given the available regulating reserve of ±25 A. The typical case of α = 1 (1 A steps) for the EV set-point is shown in Figure 4.9, along with the ideal case of linearity.

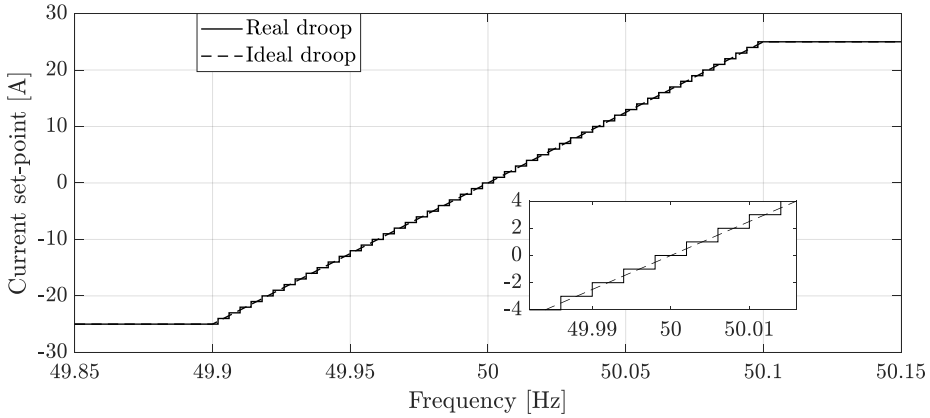

Figure 4.9 – Real and ideal droop curves with 1 A granularity for PFC control.

The system frequency is typically changing in the proximity of the 50 Hz with a normal distribution, as shown in Figure 4.10, which reports a histogram of 10 days of frequency values for 2016, measured in the RG-N area from the Norwegian TSO [112]. Approximately 85% of the samples are between 49.95 Hz and 50.05 Hz, confirming that a droop curve like the one in Figure 4.9 would result in relatively small current values for most of the time, with consequently low average efficiencies, according to the efficiency results of the V2G hardware tests in Figure 4.3. Therefore it is important to highlight that **the main drawback of standard droop methods is that they result in very low efficiencies, since the EVs operate at low loadings most of the time**.

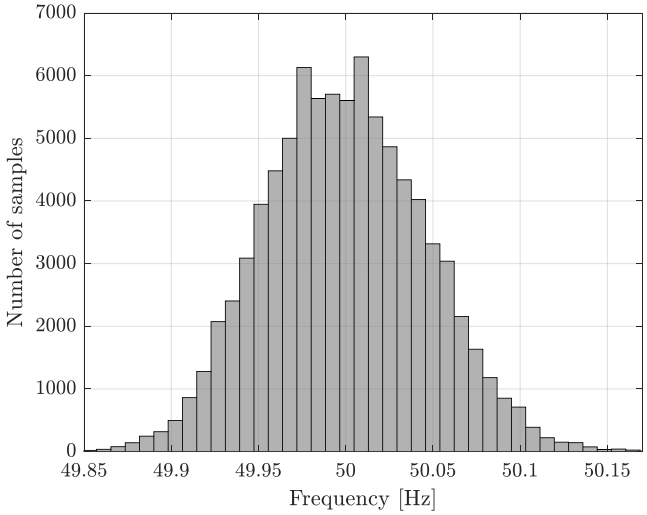

Figure 4.10 – Histogram of frequency values for 10 days in the RG-N area.

If the normal distribution of the frequency is discretized in 25 steps, the resulting probability distributions for each possible current set-point can be very well approximated by uniform distributions. Considering a uniform distribution of the frequency within each discrete current value, given the 1 A granularity case, the distribution of the response errors will retain the triangular shape shown by the light gray line in Figure 3.10. This means that the average error is 0.25 A (0.1 kW for DC voltage equal to 400 V), which for a reserve capacity of ±25 A (±10 kW) is equivalent to a *MAPE* of 1%. In this case, this error is independent of the number of EVs and is relatively small; however, it can be drastically reduced by employing the stochastic strategy explained herein below. The reserve *MAPE* is the mean average percentage error of the overall fleet of n_{EV} EVs during a V2G session period t_{tot}. It is defined as in (4.1), where $P^i_{req,t}$ and $P^i_{prov,t}$ are the requested and the actual exchanged power by the EV *i* at step time *t*.

$$MAPE[\%] = \frac{\sum_{i=1}^{n_{EV}} \sum_{t=1}^{t_{tot}} |P^i_{prov,t} - P^i_{req,t}|}{n_{EV} \cdot t_{tot}} \cdot 100\% \tag{4.1}$$

4.2.1 Stochastic switching algorithm

The objective of the proposed decentralized stochastic controller is a trade-off between efficiency and reserve errors, taking into account the size of the EVs fleet. This approach differs from other stochastic controllers that force loads to operate either at full capacity or to be idle ([74], [92]), because it employs an arbitrary discretization of the response to address efficiency and aggregation size. On the one hand, a very fine discretization results in small errors but poor efficiencies. On the other hand, 3 states (idle, fully charging or discharging) result in high efficiencies but high errors, unless the aggregation is large (500+ EVs would be needed for a *MAPE* of 1%, as shown later).

The algorithm operates as follows. First, the response of each EV is discretized in bins (corresponding to the employed granularity) represented by a vector $\boldsymbol{v}$ in ascending order and normalized per reserve capacity. The mapping $\boldsymbol{g} : \mathbb{R} \rightarrow \mathbb{R}^2$ is defined, which maps a value $P_{req,t}$ (calculated with the measured frequency deviation at time *t* and the employed droop constant for PFC) to bins $\boldsymbol{i}$ and $\boldsymbol{j}$ of the vector $\boldsymbol{v}$ so that $\boldsymbol{v(i)} \leq P_{req,t} \leq \boldsymbol{v(j)}$. Depending on the calculated $P_{req,t}$, the controller identifies the 2 bins its response must lie within, i.e., two consecutive set-points. Then, it calculates a switching probability *p* and draws a random number. This Bernoulli trial is denoted by *h(p)* and its outcome *b*, will determine the state *s* of the EV. The stochastic switching control algorithm is illustrated in detail in **Paper F**.

To better understand the working principles of the implemented control algorithm, an example is reported herein below. If the measured frequency is 50.043 Hz then the current set-point will be 10.75 A if the droop curve in Figure 4.9 is considered. Ideally, the fleet operator would wish 75% of the EVs to set 11 A, and 25% at 10 A, to have an equivalent average response of 10.75 A. To achieve this, the controller calculates the switching probability *p* as *p* = (10.75-10)/(11-10)=0.75, and then performs a *Bernoulli trial* with a random number $n \in$ [0-1] for each EV. If $n < p$ then the EV

sets 11 A, whereas if $n > p$ it sets 10 A. So, since there is the 75% of probability for n to be < 0.75, for an infinitely large number of trials, 75% of the EVs will set 11 A, and 25% 10 A, which corresponds to the ideal case. It is intuitive that the larger is the number of employed EVs, the more performing will be the overall EV response.

A potential disadvantage of using a stochastic decentralized controller is the frequent switching of the EV chargers' set-points. Typically power electronics converters are designed to handle frequent changes in their output but the impact on the inverters and EV batteries should also be considered when designing the controller. Recognizing the potential wear on the equipment, a modification of the controller to minimize the switching actions is now proposed.

The minimization logic is enabled when the requested power lies within the same 2 bins in two consecutive time steps. As continuation from the previous example, in time t_1 the calculated current set-point is 10.75 A, and at the next time step t_2 it is 10.66 A. Ideally, in t_2 the fleet operator would wish 66% of the EVs to set 11 A, and 33% at 10 A, to have an equivalent average response of 10.66 A. The controller will apply the stochastic logic only to some of the EVs, specifically to the ones that are already at 11 A, while the ones at 10 A will keep the set-point. So, the switching probability will be $p = (10.66\text{-}10)/[(11\text{-}10)\cdot 0.75] = 0.88$. As before, the *Bernoulli trial* is performed, which compares a random number n to the calculated p. There will be 88% of probability for n to be < 0.88, meaning that (for infinitely large EV fleets) 88% of the EVs that are already set at 11 A, keep 11 A, while the remaining 12% will switch to 10 A. This will lead the overall fleet to result to 66% of EVs set at 11 A, and 33% at 10 A, which is the ideal situation for the fleet operator. This enhancement of the algorithm can drastically reduce the number of switching actions without noticeably increasing the reserve *MAPE*s, as shown in the following subsection.

4.2.2 Simulation results

Simulation studies are carried out in Matlab environment, and a real 4-hour frequency sample with time steps of 1 s from the 10-day data provided by the Norwegian TSO is used to assess the performance of the different control strategies. This EV fleet management study for primary reserve assumes that all EVs in the fleet are available for reserve provision with the maximum reserve capacity of ±10 kW, as for the commercial V2G chargers tested in the previous chapter. The 4-hour frequency sample satisfies two conditions: (a) there is no significant bias in the frequency trend, so that charging and discharging operations are almost equally represented, and (b) it presents a relatively large variance around 50 Hz so that small frequency deviations are not over-represented. The latter condition serves at considering one of the worst cases, as frequency samples with small variance are expected to yield lower efficiencies when using a droop curve than in the case of the proposed controller. The normalized requested power corresponding to the utilized frequency sample is shown in Figure 4.11.

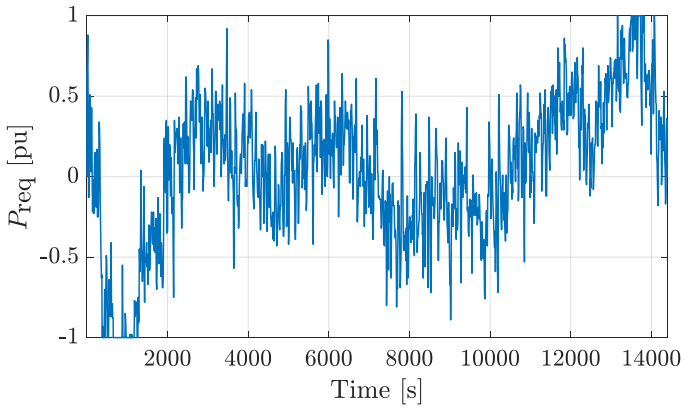

Figure 4.11 – Normalized requested power for a 4-hour frequency sample.

First, the performance of a deterministic controller with 1 A steps (corresponding to α = 1) is analyzed, which resulted in a reserve *MAPE* equal to 1%, as theoretically calculated above. As expected, it is also found that the error does not depend on the aggregation size, due to the deterministic nature of the controller.

The effect of the discretization step on the average reserve error is now examined. The modified controller including the switching rate minimization is used. As already explained, the finer the discretization, the smaller the expected reserve errors, since any inaccurate number draws have a small impact on the error. By contrast, larger steps are expected to result in larger *MAPE*s because inaccurate number draws produce larger errors. However, if the EV fleet size increases, the results of the overall EV fleet provided response is closer to the expected values and the errors decrease. Figure 4.12 shows the reserve *MAPE*s as a function of the EVs number for 6 different discretization cases: {1; 2.5; 5; 6.25; 12.5; 25} A, i.e., α = {1; 0.4; 0.2; 0.16; 0.02; 0.04}.

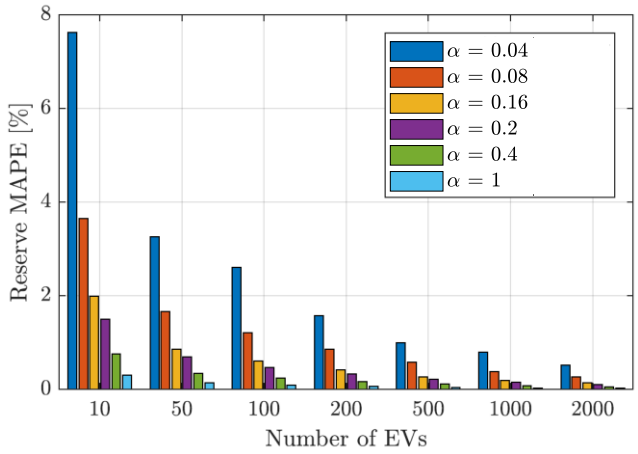

Figure 4.12 – Reserve *MAPE*s as a function of the EVs number for different response granularities.

One can note that, as anticipated, for small fleet sizes a large granularity results in significant *MAPE*s. The use of the stochastic controller even for the case of 1 A granularity brings evident advantages: the reserve *MAPE* decreases from 1% for the deterministic case to 0.4% for 10 EVs and 0.17% for 50 EVs. To guarantee a *MAPE* of 1% in case of larger granularities, more than 500 EVs

are needed for a granularity of 25 A (α = 0.04) and 50 EVs if a granularity of 6.25 A (α = 0.16) is implemented. For the sake of completeness, the *MAPEs* is calculated also for the case without switching minimization logic. Simulations show that the exclusion of the switching minimization logic in the controller results in very small differences in the *MAPE* and for fleet sizes larger than 100 EVs, the errors are almost the same. For 10 EVs and the largest possible granularity (α = 0.04), the modification increases the *MAPE* only from 7.6% to 7.9% and for 50 EVs from 3.36% to 3.4%.

Given the minimal effect on the *MAPE*s of the switching minimization logic, it is used for the calculation of the effect of the response granularity on the average efficiency. The average charging and discharging efficiencies for the entire session of V2G reserve provision is calculated for the six analyzed granularity cases, and results are reported in Figure 4.13. The size of the EV fleet does not influence the overall efficiencies, because the stochastic process itself is the same for all loads and on average it has no impact on the fleet efficiency. As most frequency samples are distributed close to 50 Hz, EVs would operate on low charging/discharging rates if small granularities are employed. In this regard, simulation results show that the average efficiencies increase significantly as the steps become larger: when large steps are used, e.g. α = 0.04, the EVs will be either idle or charging/discharging at much higher rates even for small requested powers.

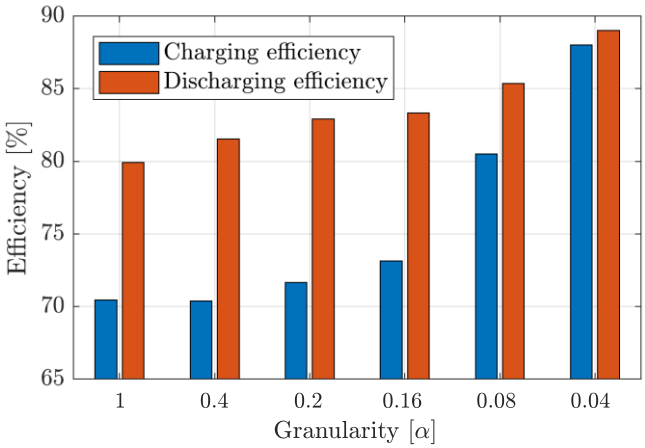

Figure 4.13 – Average EV fleet efficiencies for different response granularities.

One crucial aspect that the EV fleet operator should always bear in mind is the evolution of the SOC of the EV batteries. On the one hand, it depends on the overall frequency trend during the regulation period, e.g., if it is biased towards over-frequencies, the final SOC will be smaller than the starting value, and vice versa in case of predominance of under-frequencies. On the other hand, it will be strongly influenced also by the conversion losses of the chargers, which will dramatically influence the actual energy drawn or injected by the EV battery (as schematically depicted in Figure 4.3-a). The latter effect is assessed in Figure 4.14, where four different granularity cases are compared to the ideal case of no conversion losses. In this study, the average SOC is expressed in pu of P_{res}, i.e. for P_{res} = 10 kW a SOC = 1 corresponds to 10 kWh. The change of SOC during the V2G primary frequency regulation session is denoted by ΔSOC. In the ideal case of no conversion losses, the

average SOC at the end of the period is equal to 0.15 pu, i.e., 1.5 kWh. This means that a low-frequency bias is present, which makes the controller charge more the EV battery. If a 1 A granularity is implemented, the accumulated losses would lead to an overall discharge of 2 kWh, whereas with other discrete responses other average ΔSOC have been found. Regarding the variance in the evolution of the SOC: the larger it is throughout the reserve provision period, the harder it is for the EV aggregator to offer reserve. Specifically, the aggregator needs to be more conservative in the amount of offered reserve capacity despite the size of his chargers, in order not to reach the upper or lower limits of the EV battery while providing reserves.

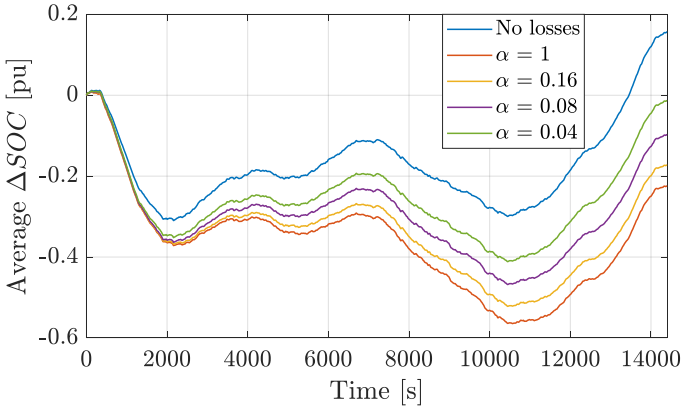

Figure 4.14 – Evolution of the average ΔSOC during a 4-hour control session for different response granularities, compared to lossless operation.

As last step, both control approaches (with and without switching minimization logic) are simulated, and the average switching rates for each granularity are presented in Figure 4.15. The average switching rate is calculated as a percentage of the time steps, i.e., a rate of 1% means that an inverter will change state 144 times over 4 hours. It can be noticed that without switching minimization the average switching rate is almost constant and very high (>30%), meaning that (for the control time step of 1 s) on average each EV inverter switches every 3 s, which is a very high rate. If the minimization logic is included, the switching rates are reduced dramatically, reaching an average value of 1.4% (or less than 1 switching per minute) if only 3 modes are used (α = 0.04).

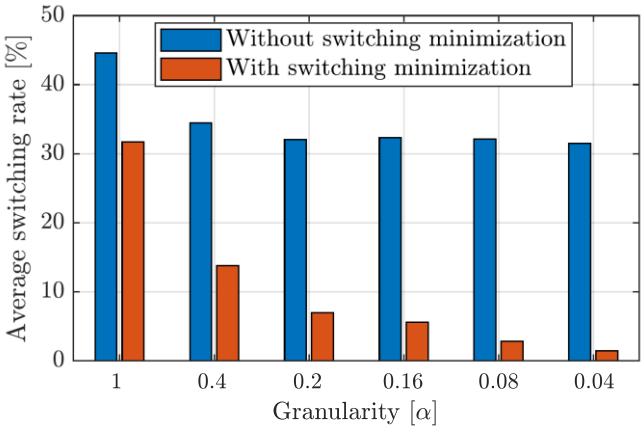

Figure 4.15 – Real and ideal droop curves with 1 A granularity for PFC control.

The proposed stochastic, decentralized controller relies on local frequency measurements and its discretized response can be optimized according to a set of criteria. In particular, it provides a trade-off among efficiency, average switching rates and reserve errors for a given EV fleet size. The most efficient operations would be guaranteed only for the operation with three states (charging, idle or fully discharging), but the reserve provision error would be limited by the size of the fleet. In case the EV fleet is sufficiently large, the aggregator is able to optimize the discretization based on an efficiency, reserve error and average switching rate trade off. To conclude, it is worth highlighting that since the chargers' efficiency is highly non-linear, the definition of the best response discretization maximizing efficiency and minimizing reserve errors is not straightforward. In particular, this study demonstrated that **(i) the chargers' efficiency curves, (ii) the allowed reserve errors based on the service requirements, (iii) the allowed switching rates, and (iv) the fleet size must be all taken into account when designing an EV fleet controller for primary frequency control provision**. However, the purpose of the proposed investigation was not to present the best discretization for the employed efficiency values, but to show that there could be various trade-offs when designing the controllers.

The thesis now proceeds with assessments of the grid impact of large-scale reserve provision via V2G technology. The focus is in fact moved from the EV aggregator's to the grid operator's perspective, aiming at defining technical guidelines to guarantee a safe operation on a system level.

4.3 From the TSO's perspective: need for overall fleet requirements

As discussed, many technological barriers need to be overcome when EVs are aggregated and controlled for power system regulation purposes. Critical response times of the aggregated EV fleet, as well as the need for each EV to comply with the IEC 15118 technical standard requirement of charging/discharging rate granularity, play an important role when dynamically assessing the response characteristics. In fact, relatively large discrete step responses may trigger frequency stability problems, as presented in the literature within the domain of demand response [96], [113]–[116], and also experienced in the previously-presented simulation and experimental works in a microgrid. The stability of the power system may be jeopardized by V2G EV fleets in case of simultaneous and high ramping-rate responses, especially under large response delays. Within this context, the thesis proceeds with investigations on the potential impact of aggregated ±10 kW off-board EV chargers performing PFC in a real power system. The employed EV fleet model is characterized with the realistic parameters obtained from the presented commercial V2G hardware tests. Then, the stability margin of the model is investigated, and the need for dedicated recommendations for grid operators is presented in terms of PFC from EVs replacing PFC provided by conventional generation units (CGUs). As outcome of the investigation in the real power system of the Danish island of Bornholm, two recommendations that EV fleet operators performing PFC need to fulfill in order to participate in the regulating market will be defined. The findings of this

investigation will support system operators facing the future challenges due to frequency service procurement by EVs.

4.3.1 A real study case: the Bornholm power system

Bornholm is a Danish island in the Baltic Sea, located in the east of Denmark and south of Sweden. The Bornholm electric power system is composed of distribution networks at three voltage levels: 60 kV, 10 kV and 0.4 kV [117], [118]. A 43.5 km long sea cable at 60 kV with 60 MW capacity connects the island to the Swedish system, which means that the Bornholm system is electrically coupled with the Nordic power system [119]. As from an electricity market and regulatory framework point of view the system belongs to the RG-N, frequency control is performed as indicated Chapter 2. Occasionally, the sea cable connection to Sweden is disrupted due to maintenance or incidents, forcing the Bornholm power system to operate in islanding mode. During these periods, system frequency control is performed by the local DSO Bornholm Energi & Forsyning (BEOF) [120] relying on a set of units that provide conventional reserve, while at the same time shutting down most of the wind generators. As the goal of the proposed investigation is to replace CGUs employed for reserve with EV fleets providing PFC via V2G, the islanded operation mode is studied.

The grid is modelled at the 60 kV MV level with real models of all the 60 kV lines along with the 60/10 kV substations. Aggregated loads, conventional generation units, renewable energy plants (wind turbines and PVs) and EV fleet models are connected at the 10 kV buses, and the detailed 10 kV lines are not modelled since the 10 kV system is not presenting any potential overloading issues. Since the aim of the analysis is the assessment of large-scale V2G employment on a system level, the complete 60 kV grid is considered sufficient. The 60 kV grid is shown in Figure 4.16, with names and locations of the nodes with 60/10 kV substations. The 60 kV network has 16 60/10 kV substations, 23 60/10 kV transformers with On-Load Tap Changers, and 22 cables and overhead lines of a total length of 131 km. The peak load in Bornholm is 63 MW, whereas the minimum load is 13 MW. The complete generation portfolio updated in May 2018 includes:

- 16 MW biomass CHP with steam turbine, named **Blok 6**. It has an inertia time constant $2H$ = 6.4 s and apparent power S = 46.8 MVA. It is equipped with primary frequency droop control at 2%, and automatic voltage regulator. The unit responds with a ramping rate of 0.2 MW/min (1.25% P_{nom}/min). As a side note, if it runs with coal/oil it can be boosted to 24/36 MW, respectively.
- 2·1 MW biogas CHP gas turbine, each with inertia $2H$ = 5.6 s and apparent power S = 1 MVA. These units are not equipped with primary frequency droop control.
- 37 MW wind (24 units < 100 kW; 16 units between 100 and 1000 kW; 17 units > 1000 kW).
- 22 MW PV (8 MW distributed on rooftops at 0.4 kV; 2 newly-installed 7.5 MW plants at 10 kV).

On top of the above listed generating units, there are other conventional units utilized only during islanded operation, for a total amount of 58 MW of reserve. The total reserve includes:

– 25 MW oil-powered steam turbine, named **Blok 5**. It has an inertia *2H* = 8.6 s and an apparent power *S* = 29.4 MVA. It is equipped with primary frequency droop control at 2%, and an automatic voltage regulator. The unit responds with a ramping rate of 0.25 MW/min (=1% P_{nom}/min). It is important to note that the droop control of Blok 5 is generally not used in conjunction with **Blok 6** due to hunting issues.
– 4·4.5 MW diesel generators, each equipped with 2% frequency droop control and voltage control. Each unit has inertia *2H* = 8 s. 2 units have *S* = 5.8 MVA and the others *S* = 6.3 MVA.
– 10·1.5 MW diesel generators, named **Blok 7**. Each unit has an inertia *2H*=1.1 s and an apparent power *S* = 2 MVA. They are not equipped with primary frequency droop nor voltage control. Each unit responds with a ramping rate of 1 MW/min (66% P_{nom}/min).

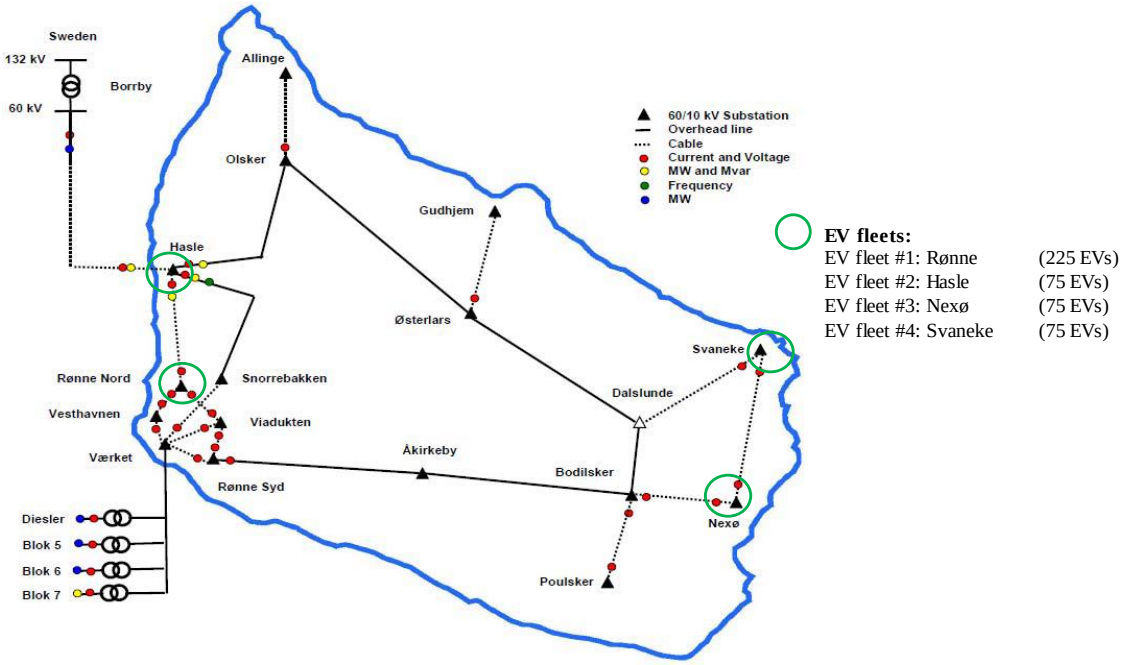

Figure 4.16 – Bornholm Island 60 kV grid with the locations of the major CGUs, the nodes with 60/10 kV substations, and the 4 EV fleets that will be modelled for DIgSILENT PowerFactory validations within Subsection 4.3.4.

Today on the island of Bornholm there are more than 17000 internal combustion engine cars. The share of EVs will increase dramatically in the coming years, according to the *Nordic EV Outlook 2018* report [22]. As it is expected that a number of EVs will constantly be available for V2G services, realistic models of controlled EV fleets need to be developed when assessing the major impacts on the power system. Already today, 21 ±10 kW chargers with bi-directional capability (of the same type as the ones tested in the beginning of the chapter) are employed to provide primary frequency regulation, as part of the activities of the Danish founded ACES project. Some of these V2G chargers with a number of EVs controlled for frequency regulation are shown in the picture in Figure 4.17.

Figure 4.17 – Already today, V2G-ready off-board chargers and EVs are present in Bornholm Island, and provide frequency regulation within the Danish founded ACES project.

4.3.2 EV fleet model

An EV aggregation model is commonly utilized for power system studies [96], [97], [121]. The fleet model is then characterized with some of the results of the real V2G hardware tests. Given a population of n_{EV} EV chargers indexed by i, the most common representation of their response to a change in their power output is via a transfer function of the following form:

$$H_i(s) = \frac{K_{PFC\_pow,i}}{1+T_{b,i}s} e^{-T_{EV,i}s} \tag{4.2}$$

where $K_{PFC\_pow,\,i}$ is the EV controller's gain, $T_{b,\,i}$ the first-order time constant of EV batteries, and $T_{EV,\,i}$ the response delay. The adopted aggregation model is a model where average values for the three sets of parameters are used, along with a gain n_{EV}, representing the fleet size. A good approximation of the actual response of n_{EV} EV chargers is given by the transfer function $R_{EV}(s)$:

$$R_{EV}(s) = \frac{N\overline{K_{PFC\_pow}}}{s+\overline{T_b}s^2} e^{-\overline{T_{EV,i}}s} \tag{4.3}$$

The symbol $\overline{(\cdot)}$ denotes the average value of the three parameters in (4.2) (gains, first-order time constants and response delays) for the n_{EV} considered EVs. From here onwards this model is named *average model*. The presented *average model* has been characterized with parameters derived from test results, and is adopted for the stability investigation when large-scale provision of frequency control is achieved via V2G technology. The response times of the ±10 kW V2G chargers responding to charging/discharging control signals and controlled in a local and in a remote fashion have been implemented. This allows the characterization of the models in case of local or remote control of the hardware, thus assessing the implications of the additional communication latencies on the total activation time when an aggregator acts remotely. It is worth reminding that the remote control test setup includes the communication and control infrastructure utilized by an actual EV aggregator, operating in field projects such as the Danish-funded ACES [107] and Parker [108].

The employed response delay is derived by the test results shown in Figure 4.4-b and Figure 4.7, which report the correlation between the requested and provided power when applying different time shifts to one of them for the whole duration of the test. The most probable response time resulted in

7.0 s and 4.0 s for the remote and local control, respectively. These values were obtained for one type of V2G chargers and control/communication infrastructure, meaning that slightly different results can be obtained in case of faster or slower hardware and/or communications. However, these results provide a valuable asset for the characterization of the proposed fleet model, within the analysis of power system stability aspects related to PFC provision.

4.3.3 Effects of PFC via EVs replacing conventional generation units

The purpose of this investigation is to provide general insights on the effects of large-scale PFC provision via aggregated EVs, and to outline safety recommendations to prevent system instability. Firstly, the dynamic performance of the aggregation model is evaluated by assessing the frequency response of the model's transfer functions by their own as well as in a simulated simplified power system. Secondly, a set of simulations is carried out with increasing EV penetration, for different activation times. The analysis proposes a method for defining critical activation times and V2G primary frequency regulation shares over the total primary reserve from conventional units. However, the numeric outcome of this investigation is not meant to be safely applicable in the real operation of any possible power system, but it should rather be considered as a benchmark for further grid analysis in more complete and complex simulation environments. In this context, the outlined recommendations will then be implemented in the detailed model of the Bornholm power system to evaluate their effectiveness in a real low-inertia system.

4.3.3.1 Simplified power system layout and modelling

The first analysis is carried out by implementing the simplified power system in Figure 4.18, with the single-bus layout proposed by [122] extended with the EV fleet models. CGUs are modelled with the transfer functions representation proposed in the literature, equipped with a proportional droop for primary regulation. The system parameters are chosen in accordance with one possible islanded configuration of the Bornholm power system, and are listed in Table 4.3.

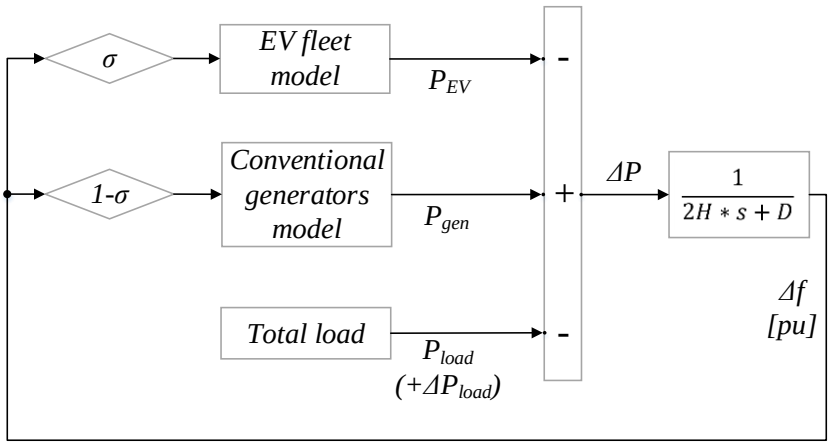

Figure 4.18 – Simplified power system with the classical single-bus layout.

Table 4.3. System parameters.

Parameter	Symbol	Value	Unit
Base frequency	ω_n	314	rad/s
Inertia constant	H	3.6	s
Rated power	S_{rated}	108.2	MVA
Damping factor	D	0	%
Total load	P_{load}	60	MW
Load step	ΔP_{load}	2	MW
Primary reserve	$P_{reserve}$	10	MW
Primary frequency control normalized droop gain	k_{droop}	2	%

The EV fleet is modelled as described above, acting with the same relative droop of the replaced CGUs and with different participation factor σ and activation times, which for the first set of simulation are considered to have an average value of 7 s. The combined response of 100 individually simulated EVs with normally distributed delays around 7 s and standard deviation of 0.1 s serves as the reference. Frequency dynamics are modelled using the linearized swing equation $J\omega_n\dot{\omega} + D\omega = \Delta P_{load}$ and the inertia constant $H = \frac{J{\omega_s}^2}{2S_{rated}}$, where J is the combined moment of inertia of generators and turbines [kg·m^2] [122]. No damping (D = 0) is considered as conservative assumption for the stability analysis. The Laplace-transformed representation of the grid is therefore

$$G_{grid}(s) = \frac{f_n}{2HS_{rated}s} \tag{4.4}$$

Despite the typical variety of types of rotating CGUs within the portfolio of an operating power system, in this preliminary study we consider only one type of CGU, i.e., diesel generator sets. In fact at this stage the aim is not a detailed power system analysis, but rather the provision of general insights on technical barriers of EV fleets management on a system level. The detailed power system with complete generation portfolio, real line and load models and voltage dependencies will be implemented later on, in order to validate the outcome of this first part of the study. The standard diesel model given in [123], equipped with an electric control box (with the correspondent time constants T_1-T_4 equal to 0.1, 0.3, 0.05, 1 s, respectively) is implemented, where T_g is the governor time constant equal to 0.2 s and K_{CGU} is the absolute primary droop gain for the CGUs:

$$R_{CGU}(s) = \frac{1}{1+T_g s}\frac{1+T_3 s}{1+T_1 s+T_1 T_2 s^2}\frac{K_{CGU}}{1+T_4 s} \tag{4.5}$$

The implemented EV aggregation model is the *average model*, which guarantees a fine representation of a large-scale EV fleet. The resulting dynamic system in open- and closed-looped form is so described by *L(s)* and *T(s)*

$$L(s) = G_{grid}(s)(R_{CGU}(s) + R_{EV}(s)), \quad T(s) = \frac{G_{grid}(s)}{1+L(s)} \tag{4.6}$$

where $R_{EV}(s)$ is the average EV aggregation model defined in (4.3). The share of EVs and conventional resources is expressed over the factor σ as in

$$K_{PFC\_pow} = \sigma K_{tot}\,,\quad K_{CGU} = (1-\sigma)K_{tot}\,,\qquad K_{tot} = \frac{P_{res\_tot}}{f_n}\frac{1}{k_{droop}} \tag{4.7}$$

K_{tot} is the absolute primary droop gain, and P_{res_tot} the total power allocated for primary reserve.

4.3.3.2 Model dynamics

Figure 4.19-a shows the Bode magnitude plot of the real EV fleet (used as reference) and the *average model*, where the input is the frequency deviation $\Delta f = f - f_0$ and the output is the power delivered by the EVs. As can be observed, magnitude and phase of the *average model* match well with the real EV fleet in the frequency range below 1 Hz. At 1 Hz the deviation amounts to about 1 dB, whereas a deviation of 3 dB is found for a frequency of 1.5 Hz.

Within the given Bornholm power system context, we expect similar behavior of the models due to the smoothing effect of the grid's inertia and the 50 % conventional resources, being $\sigma = 0.5$ for this first simulation. This is confirmed in Figure 4.19-b on the open-loop $L(s)$ of (4.6), where the characteristic system behaviors happen in frequency ranges a full magnitude below those seen in Figure 4.19-a. Here, load power is the input signal and requested EV power the output. The results of the full EV fleet and the aggregation model are furthermore compared to the response of ideal conventional primary resources with no dynamics of their own, shown by the dotted line in Figure 4.19-b. The *average model* performs almost identical to the simulated fleet, rendering it valid for subsequent investigations.

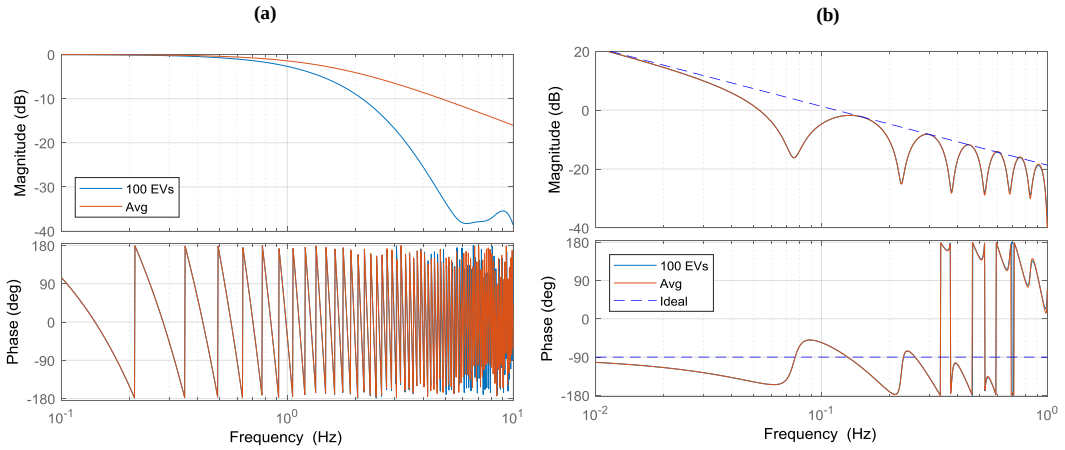

Figure 4.19 – Bode plot of the EV fleet and the corresponding aggregated *average model* in its open-loop form (a) and within a simulated one-bus system (b). Input is the frequency deviation Δf, output the delivered EV power normalized to their nominal droop gain. The phase is wrapped between ±180 degrees.

4.3.3.3 Stability investigation

In order to make more generalized statements on stability of primary support using EVs, the impact of the EV share σ to the total primary reserve is now investigated. The linearized dynamic system can be written as

$$\dot{x}(t) = A_0 x(t) + A_1 x(t-\tau)\,, \;\; \tau \geq 0 \tag{4.8}$$

with the n states $x \in \mathbb{R}^{n\times 1}$, the system matrices A_0, $A_1 \in \mathbb{R}^{n\times n}$ on which the normal and delayed states act, and the delay time τ (T_{EV} in (4.3)). Rearranging the strictly proper transfer functions (4.3)-(4.5) into the monic form $G(s) = \frac{b_0+b_1 s+\cdots+b_{n-1}s^{n-1}+b_n s^n}{a_0+a_1 s+\cdots+a_{n-1}s^{n-1}+a_n s^n}$ allows their transformation into the canonical state-space observer representation $A_{grid} = 0$, $\boldsymbol{b}_{grid} = b_{grid}$, $A_{CGU} \in \mathbb{R}^{4\times 4}$, $\boldsymbol{b}_{CGU} \in \mathbb{R}^{4\times 1}$ and $A_{EV} = a_{EV}$, $\boldsymbol{b}_{EV} = b_{EV}$. By choosing the state vector $x = \left[\Delta f\ \Delta\dddot{P}_{CGU}\ \Delta\ddot{P}_{CGU}\ \Delta\dot{P}_{CGU}\ \Delta P_{CGU}\ \Delta P_{EV}\right]^T$, the system matrices of (4.8) result in

$$A_0 = \begin{bmatrix} 0 & \left[\mathbf{0}\ \mathbf{0}\ \mathbf{0}\ -b_{grid}\right] & -b_{grid} \\ \boldsymbol{b}_{CGU} & A_{CGU} & \mathbf{0} \\ \mathbf{0} & \mathbf{0} & -a_{EV} \end{bmatrix},\; A_1 = \begin{bmatrix} \mathbf{0} & \mathbf{0} \\ -b_{EV} & \mathbf{0} \end{bmatrix} \tag{4.9}$$

Using these system matrices of the instantaneous and delayed states, a frequency sweeping test as described by Theorem 2.1 in [124] is utilized, which allows to find the maximum share of EVs for which the system remains stable independently of the delay. Independence of delay is imperative, as the response of real EVs is non-deterministic and subject to various uncertainty factors (battery management, communication systems, charging station electronics, etc.). The three necessary and sufficient conditions of the test are:

1) A_0 is stable (for $\tau \to \infty$);

2) $A_0 + A_1$ is stable (for $\tau \to 0$);

3) $\rho((j\omega I - A_0)^{-1}A_1) < 1,\ \forall\omega > 0$, with $\rho(\cdot)$ as the spectral radius of a matrix.

Conditions 1 and 2 are fulfilled for the given system because the corresponding eigenvalues are in the left half of the complex plane. Condition 3 is evaluated in Figure 4.20-a, where valid solutions are found for $\sigma < 0.5$. The system is stable independently of the delayed EV response for EV shares < 50%. It is noted that the results mark the fundamental stability limit of the linearized system. Non-linearities inherent to real systems as well as voltage-related dynamics will generally decrease the available margin. For practical applications with the given EV/Diesel primary reserve mix**, it is therefore recommended that the share of EVs stays below 50% (*Recommendation 1*) in order to guarantee stable, EV delay-independent grid operation**. For the sake of completeness, Figure 4.20-b confirms that only for $\sigma > 0.5$ the stable operation is limited by the critical time delays, which are inversely proportional to the EV share.

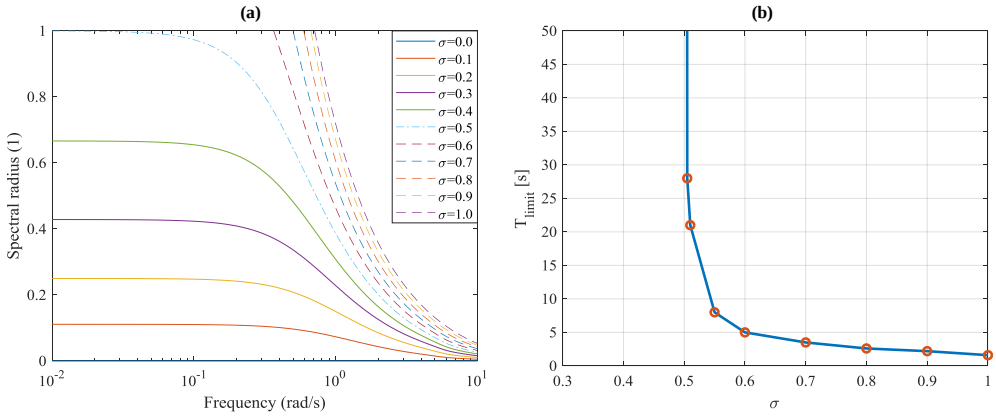

Figure 4.20 – (a) Frequency sweep of the spectral radius as part of the frequency sweep test. (b) Limit delay T_{limit} for σ>0.5. A delay-independency of the stability is graphically confirmed for σ<0.5.

In order to take into account the probable reduction of the σ limit in case of non-linearities and voltage-dependencies related to more complex systems, a recommendation in terms of maximum time delay is also introduced. In this respect, results from a sensitivity study allows the definition of a set of first-order equations that enables the calculation of the maximum acceptable EV delay. It is important to note that the time limits are calculated for a share that is larger than the limit (σ = 0.55), in order to have delay-dependency of the stability margin. The analysis is performed for different system parameters that can influence the results: the system inertia *2H*, the primary reserve k_{droop}, and the index ξ, which gives an idea of the amount of total primary reserve over the rotating energy $E_{rotating}$ for the *n* rotating CGUs with installed capacity $P_{n,i}$:

$$\xi = \frac{P_{reserve}}{E_{rotating}} \quad , \quad E_{rotating} = \sum_{i=1}^{n} P_{n,i} 2H_i \tag{4.10}$$

A set of values of three parameters are utilized to assess the influence on the critical EV delay: *2H* = {2.4, 3.6, **7.2**, 14.4}, k_{droop} = {**0.02**, 0.03, 0.04, 0.05, 0.06}, ξ = {0.01, 0.02, **0.03**, 0.04}. Note that the bold values correspond to the reference case of the Bornholm system in the considered islanded configuration; the same is valid for Table 4.4-Table 4.6. The dependency of the time limits T_{limit} on the three parameters is considered almost linear, as deducible by the example in Figure 4.21. The figure shows the dependency on the three parameters and the linear interpolation, performed to derive the three first order equations. This parametric study allows the identification of the coefficients a_i and b_i for the calculation of T_{limit}, given the considered system parameters.

$$T_{limit} = \begin{cases} a_k \cdot droop + b_k & with\ a_k, b_k\ function\ of\ (2H, \xi) \\ a_{iner} \cdot 2H + b_{iner} & with\ a_{iner}, b_{iner}\ function\ of\ (droop, \xi) \\ a_\xi \cdot \xi + b_\xi & with\ a_\xi, b_\xi\ function\ of\ (droop, 2H) \end{cases} \tag{4.11}$$

The resulting coefficients are reported in Table 4.4-Table 4.6, which allow the calculation of the maximum EV response time in order to prevent system instability. Note that the bold values both in the text and in the tables relate to the realistic islanded operation mode of the Bornholm power system, which gives a delay limit of 8 s. It is so deducted the second recommendation (***Recommendation 2***) for a safe and stable primary reserve provision from a fleet of EVs: $\boldsymbol{\tau < T_{limit}/2}$,

i.e., **operate with a delay smaller than the half of the calculated T_{limit}.** 2 is a safety factor, introduced to prevent operating too close to the limit and to take into account possible imperfections in the calculation of T_{limit} given the extrapolation of the coefficients.

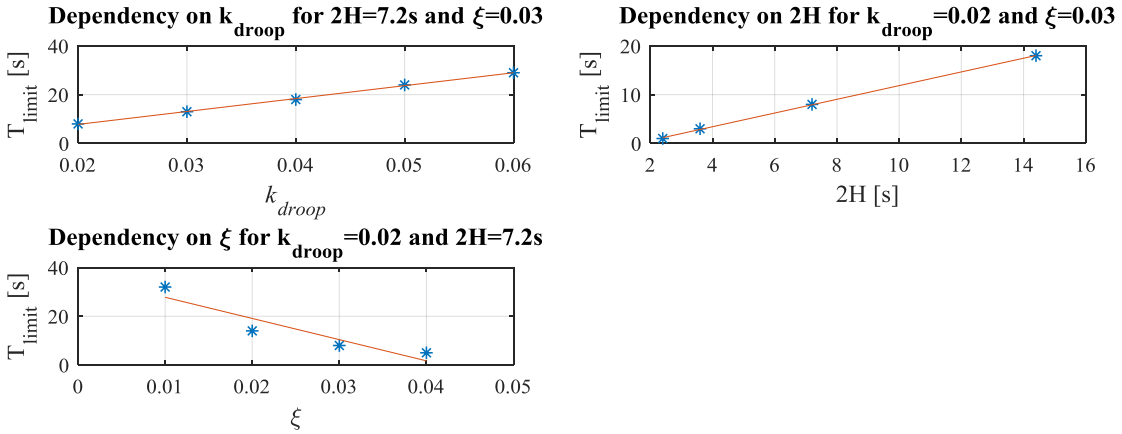

Figure 4.21 – Dependency of the limit time T_{limit} for different system parameters. It can be noticed that the approximation to a first-order equation for the dependency of the three parameters causes a relatively small error in the calculation of T_{limit}.

Table 4.4. Coefficients to calculate T_{limit} as a function of k_{droop}.

		***2H* [s]**			
		2.4	3.6	7.2	14.4
ξ [s^{-1}]	0.01	a = 570 ; b = -2.2	a = 860 ; b = -2.2	a = 1720 ; b = -3	a = 3360 ; b = -2.4
	0.02	a = 270 ; b = -2.4	a = 400 ; b = -2	a = 800 ; b = -2	a = 1710 ; b = -5.4
	0.03	a = 170 ; b = -2.4	a = 250 ; b = -2.2	**a = 530 ; b = -2.8**	a = 1000 ; b = -2
	0.04	a = 111 ; b = -2.12	a = 164 ; b = -1.9	a = 360 ; b = -2.4	a = 720 ; b = -2.8

Table 4.5. Coefficients to calculate T_{limit} as a function of *2H*.

		k_{droop}				
		0.02	0.03	0.04	0.05	0.06
ξ [s^{-1}]	0.01	a=4.74;b=-2.20	a=6.89;b=-1.29	a=9.08;b=-0.66	a=11.67;b=-1.55	a=13.96;b=-0.81
	0.02	a=2.24;b=-2.20	a=3.25;b=-1.66	a=4.48;b=-2.40	a=5.74;b=-2.88	a=7.01;b=-3.37
	0.03	**a=1.41;b=-2.20**	a=2.10;b=-2.26	a=2.81;b=-2.40	a=3.31;b=-2.23	a=4.17;b=-1.77
	0.04	a=0.98;b=-2.12	a=1.39;b=-2.02	a=1.98;b=-2.40	a=2.59;b=-3.12	a=2.94;b=-2.26

Table 4.6. Coefficients to calculate T_{limit} as a function of ξ.

		k_{droop}				
		0.02	0.03	0.04	0.05	0.06
***2H* [s]**	0.01	a=-281;b=10.35	a=-441;b=17.35	a=-610;b=24	a=-740;b=30	a=870;b=36.5
	0.02	a=-441;b=17.35	a=-680;b=27.5	a=-870;b=36.5	a=-1100;b=46	a=-1350;b=57
	0.03	**a=-870;b=36.5**	a=-1290;b=55	a=-1710;b=74	a=-2180;b=95	a=-2600;b=113.5
	0.04	a=-1740;b=75	a=-2570;b=111.5	a=-3360;b=148	a=-4280;b=189	a=-5200;b=229

4.3.4 Validation on the Bornholm power system

The validation study carried out in DIgSILENT PowerFactory simulation environment replicating the Bornholm system completes the study, assessing the applicability of the recommendations on a real and complex power system of the recommendations. The investigation is performed on an islanded configuration of the Bornholm power system, in a probable 2040 scenario with 50% EV penetration, meaning that out of the total 17000 cars on the island, 8500 will be EVs [125]. An evening hour is considered (e.g., between 18:00 and 19:00) when it can be realistically assumed that 40% of the EVs are charging at home on the 3.7 kW slow charging mode (Mode 2), leading to about 12 MW of total extra load. This is added to the rather high evening load condition assumed to be 48 MW, leading to a total load of 60 MW. A portion of the remaining EVs not charging at home are assumed connected to V2G chargers and available for grid frequency regulation. Specifically, the V2G-ready EVs could be 5% of the total EVs, i.e., 450 EVs: considering each vehicle interfaced with a ±10 kW bi-directional charger, the total regulation capacity is equal to ±4.5 MW. To make the analysis more realistic the fleet is not considered connected to a single bus of the grid, instead the 450 EVs are connected to the four largest urban areas in the island with the following criteria: 225 EVs are in the capital city of Rønne (*EV fleet #1*), whereas the remaining 225 EVs are equally split over the cities of Hasle, Nexø, and Svaneke, leading to 75 EVs per city (*EV fleet #2, #3, #4*). In line with the simulations in Subsection 3.2.1, no EV reactive power is considered: its crucial role will be discussed and investigated in Chapter 5. As for the generation portfolio, a very high share of renewables is considered, i.e., half of the generation (30 MW) coming from wind turbines, whereas no PV production was included given the evening hour. The other half of the generation is coming from the two biogas plants (1 MW each), the CHP plant **Blok 6** (operating at 8 MW - 50% of full power), and the oil-powered steam turbine **Blok 5** (operating at 20 MW - 80% of full power). Furthermore one 4.5 MW diesel unit is considered connected but operating at zero set-point, ready to react in case of frequency disturbances as primary frequency regulator. In this configuration the system has a primary frequency control reserve capacity of 5 MW over 200 mHz from the **Blok 5**, and additional 4.5 MW which are available either by a dedicated 4.5 MW diesel unit (operating at zero set-point but connected as mere frequency regulation unit upwards), or alternatively by the V2G-capable EV fleet. This means that for the proposed study case the share of EVs participating in the reserve is $\sigma = 0.45$, fulfilling ***Recommendation 1***. Both the CGUs and the V2G EV fleet operate with a relative droop of 2%. In this islanded configuration the system inertia H will be 3.63 s if the diesel is connected, and 3.60 s in case it is not connected. The destabilizing contingency is the loss of a 2 MW wind turbine.

Figure 4.22 shows the effects of EVs replacing the diesel generator with $\sigma = 0.45$ (fulfilling ***Recommendation 1***) in case of different EV delays, with delays normally distributed around 1, 4, 7 and 10 s with standard deviation equal 0.1. In the previous subsection it was found that for this setup a response equal to or faster than 4 s is needed to fulfill ***Recommendation 2***. This is guaranteed in

the cases of 1 s and 4 s delay. The 7 s case would fulfill the recommendation only if the safety factor 2 is not be included, whereas the 10 s case is above the requirement.

With a very fast EV response (e.g., 1 s) the fleet can perform well, as the frequency settles to the steady-state value $f_{steady\text{-}state}$ = 49.65 Hz even faster than in the case of the diesel. In case of larger delays, frequency stability is compromised: with the EVs responding in 4 s and 7 s, damped oscillations appear, with settling time that increases dramatically in the case of 7 s, which is very close to the limit of 8 s found previously. It can be noticed that the fulfilment of ***Recommendation 2*** including the safety factor 2 guarantees the frequency to settle much faster than in the case of 7 s, justifying the need for the inclusion of the safety factor for safer operations. In case of 10 s delay, the frequency is not damped and stability is lost. At this point it is relevant to highlight the fact that, despite in a simplified system the share σ = 0.5 would allow any possible EV delay without incurring instabilities, here the complex dynamics that describe the real power system model's behavior are reducing the stability limits as instability conditions are found for σ = 0.45 for a 10 s delay. This is due to the fact the implemented Bornholm power system now includes the different dynamics of the CGUs of the complete generation portfolio along with the models of lines, transformers and loads. This brings along corresponding non-linearities and voltage dependencies that could not be included in the preliminary analysis, where a simplified single-bus power system was modelled. This shows the need for the additional requirement in terms of maximum EV time delay (***Recommendation 2***), as the limit of σ = 0.5 may not be sufficient to guarantee an EV delay-independent system stability in such large and complex systems. This confirms the previous considerations, when it comes to cautionary recommendations, and the inclusion of ***Recommendation 2***, which in addition to ***Recommendation 1*** allows the definition of safe operation conditions with large-scale frequency control via EV fleets replacing CGUs.

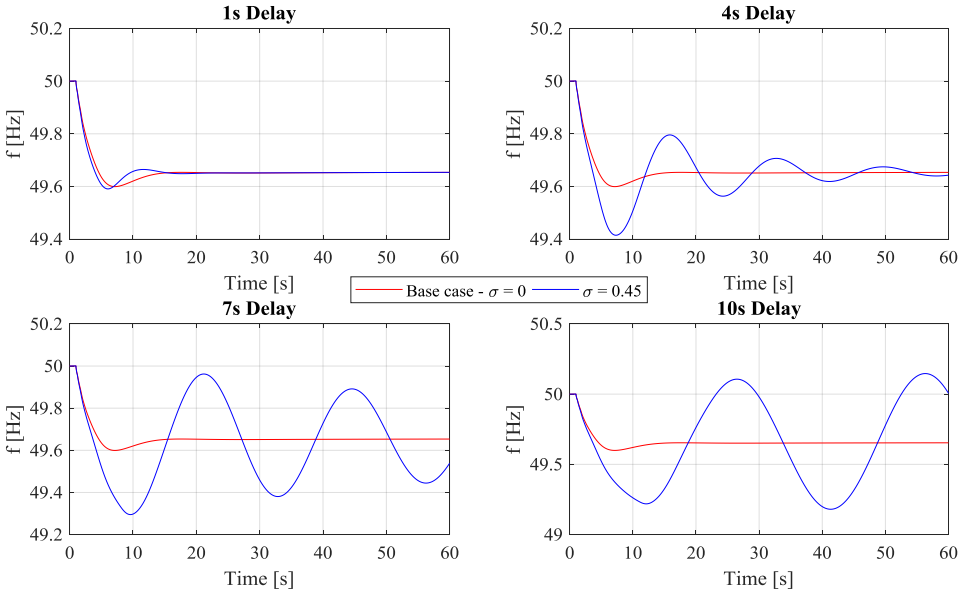

Figure 4.22 – Power system frequency for σ = 0 and σ = 0.45 with increasing EV response times.

The voltage profiles at the connection buses for the different study cases and the power exchanges from EV fleets and diesel are reported in Figure 4.23 and Figure 4.24, respectively. Acceptable voltage levels are found at the 4 EV fleets connection buses, as the RMS values of the line-to-ground bus voltages do not exceed the 10% of deviation from the nominal value, as required by the European grid standard EN 50160. As for the provided power, when σ = 0.45 at steady-state the sum of the powers from the EV fleets corresponds to the reserve that is provided by the diesel unit in the base case scenario with σ = 0. The power provided from the EV fleets has negative sign, since they are modelled with the load convention. Finally, as expected, it can be noticed that *fleet #1* provides triple the power of *fleets #2*, *#3* and *#4*, being the fleet sizes 225, 75, 75 and 75 EVs, respectively.

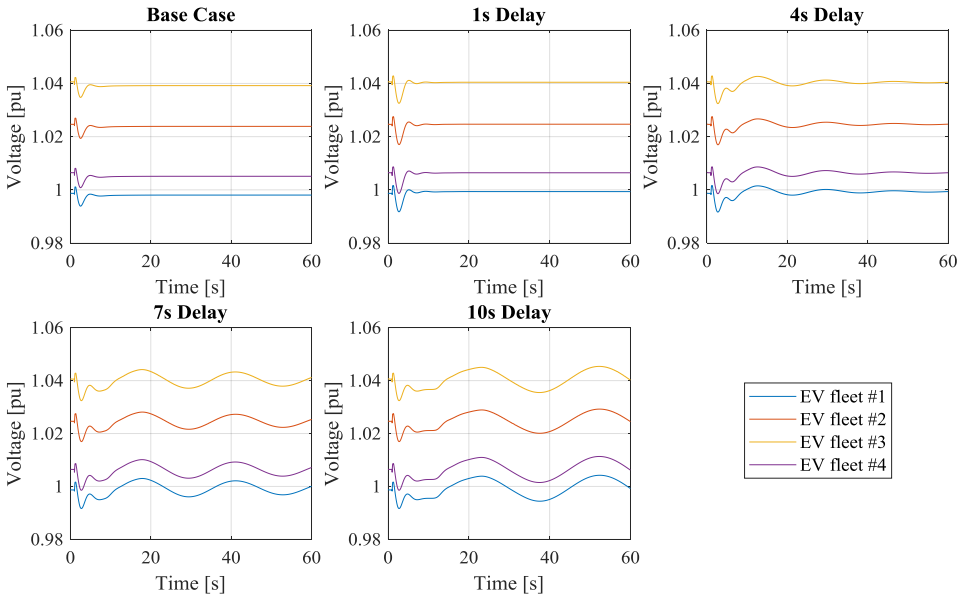

Figure 4.23 – Line-to-ground voltages at the EV fleet buses.

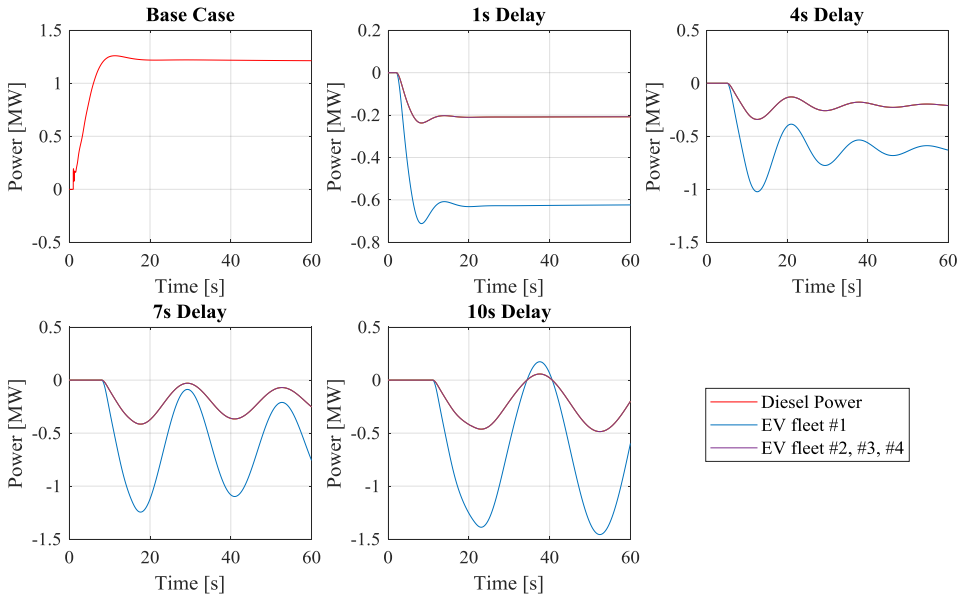

Figure 4.24 – Power profiles of the diesel generator when σ = 0, and of the 4 EV fleets with σ = 0.45.

4.4 Summary

This chapter concludes the analysis on frequency control service provision via aggregated EVs, with studies on V2G-capable EVs. Hardware tests, an EV aggregation strategy and a system stability study when large-scale provision of frequency control is achieved via V2G have been proposed. The first part of the chapter presented a complete characterization method of V2G-capable commercial hardware. A ±10 kW V2G off-board CHAdeMO charger was tested, with the aim of benchmarking its performance with respects to the attributes of the flexibility product, and to the efficiency performance for all possible operating set-points. This allowed an assessment of its suitability for the provision of power system services. This set the basis for further analysis aimed at enhancing the quality of frequency regulation services provided by bi-directional EVs. An EV fleet management strategy was then presented, which implemented a stochastic logic aimed at achieving a trade-off between the average error in the reserve provision during a V2G session and the overall fleet efficiency. Such analysis confirmed the importance of a deep knowledge of the controlled hardware performance in order to enable an optimal management of the EV fleet. Furthermore, realistic EV fleet models have been utilized to perform full-scale power system stability simulation studies aimed at outlining guidelines for the TSOs when relying on large-scale frequency control via aggregated EVs performing V2G operations. The studies have been carried out in an islanded configuration of the Bornholm power system with high penetration level of RES (50%). Two recommendations with conservativeness considerations have been derived to guarantee safe and stable operation: ***Recommendation 1*** requires to operate with a share of primary reserve from EVs that would not exceed the reserve from CGUs ($\sigma < 0.5$); ***Recommendation 2*** requires response times below the half of a limit value T_{limit} that can be calculated as function of the system inertia, of the total primary reserve over the rotating generation capacity, and of the employed droop gain. To conclude, the chapter highlighted the importance of benchmarking the controllable hardware performance with respect to the required capabilities for a quality flexibility service provision. This is crucial not only for the EV fleet operators, who can implement strategic management logics to enhance the fleet's operation, but also for TSOs, who can rely on the derived recommendations, considering them as a tool for power system studies to be utilized as a benchmark for grid analysis simulation environments.

After these analyses on uni- and bi-directional EV provision of system frequency control, the thesis proceeds with studies on EV integration on a distribution level. In particular, the issue of induced under-voltages is assessed and the possibility of voltage control via reactive power support is investigated in a generalized way. A formulation will be presented, whose application is meant for distribution system operators when evaluating new installations of fast chargers on the receiving end terminal of a low voltage feeder.

CHAPTER 5

Integration on a distribution level: need for connection requirements

As discussed in in Chapter 2, a massive penetration of electric vehicles charging at the distribution level may likely introduce severe challenges to distribution grid operators. In this chapter, the issue of under-voltage is assessed and the EV charging modulation for voltage control via reactive power support is investigated in a generalized way, with the aim of evaluating the effectiveness of such technology and its limits on all kinds of radial distribution feeders. A formulation is proposed, which allows the estimation of the voltage at the EV charger terminal, given the sending terminal voltage and the charger size with a given power factor. The application is meant for distribution system operators when evaluating installations of new fast chargers on the receiving end terminal of a low voltage feeder, given its length and the voltage dependencies of loads in LV networks. In the last section of the chapter, simulation studies in DIgSILENT PowerFactory software environment are included to validate the effectiveness of the proposed formulation.

The chapter includes results of the separate papers **Paper H** and **Paper I**, attached in Part II.

5.1 Voltage support via reactive power from EVs in distribution grids

Large-scale EV charging on the LV level may cause technical issues on the electrical infrastructure, leading to the conclusion that, **unless opting for grid reinforcement solutions, a massive EV penetration in distribution networks may force DSOs to rely on smart EV charging**. In general, reactive power provision can – to a certain extent – mitigate local voltage issues in distribution networks [126]. In case of small distributed generation plants connected at low voltage levels such as PVs, grid codes require reactive power capability to the inverter-interfaced units [127]–[129]. Many studies have proved the effectiveness of such capabilities in voltage support in active distribution networks [130]–[132]. Similarly, it is expected that there might by a need for DSOs to require voltage support capability also to the new EVSEs.

Under a technical feasibility point of view, many studies propose new on-board chargers design and investigate the barriers within the power electronics in applying reactive power solutions [133]–[135]. Among others, [135] shows how reactive power exchange could be achieved without any considerable changes in the converter type and size of the on-board charger. Furthermore, many other studies deal with the development of off-board chargers capable of reactive power operation, showing possible designs and layouts of such technologies [136], [137]. The EV charger typically presents a two-stage topology with a cascaded AC/DC converter, which rectifies the AC current drawn from the grid, and a DC/DC converter, which connects the DC bus to the battery pack. Figure 5.1 shows the schematic of EV grid connection through an on- or off-board charger controlled by a charging controller, and the 4-quadrant AC/DC converter operating scheme with the load convention.

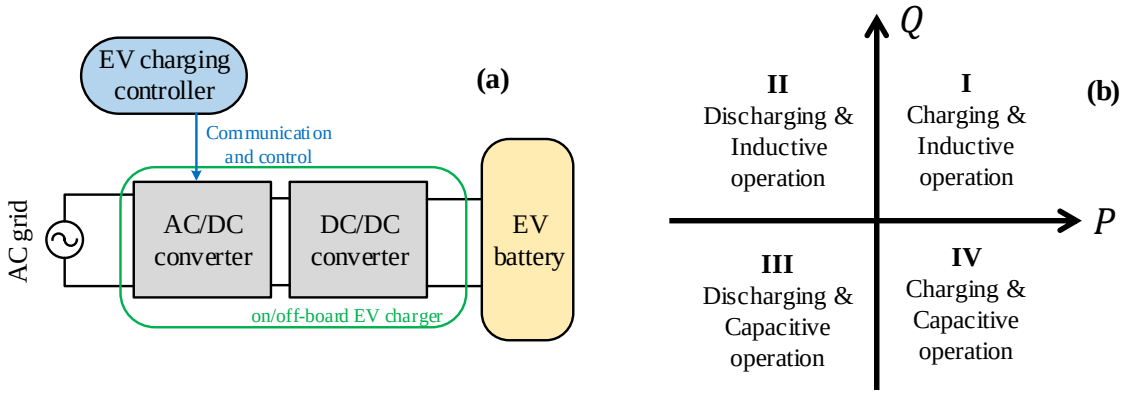

Figure 5.1 – Schematic of EV grid connection through on/off-board charger (a) and 4-quadrant EV converter operating scheme with load convention (b).

Given the mentioned technical feasibility of reactive power modulation strategies, it is of interest to perform assessment studies upon the effective contribution on voltage control. Among other possible control techniques, many control strategies based on solution of optimization problems are proposed in the literature, both with centralized and decentralized control structure. In general, centralized control approaches for this kind of voltage regulation at LV distribution level [138]–[141] may result in huge amount of data that need to be transported from smart meters to a centralized control room for the elaboration of the proper control signal to be dispatched back to the units. Thus, many volt-VAR optimization works prefer relying on decentralized logics, avoiding the need for complex data management [142]–[145]. Independently on the control logic applied, many other studies have been conducted with the aim to demonstrate the potentials of distributed EV chargers control to solve local voltage issues and allowing high EV penetration to be technically acceptable, deferring the need for grid reinforcement [43], [44], [146]–[148]. In [43] and [146] the positive effects of reactive power support by EVs applying voltage-dependent reactive power strategies is analyzed. An implementation of a bi-directional EVSE controller is developed in [147], which proposes a control logic able to regulate the bus voltage by exchanging reactive power, while maintaining a given DC-link voltage for the designed charging station. In [148] an example of the grid impact is evaluated by

implementing different reactive power control logics such as fixed power factor, power factor as function of either active power or local voltage, and hysteresis control. A reactive power capability curve as function of both active power and local voltage is proposed in [44], where the effects of single-phase EVs on the local voltage unbalances are also considered.

The above-listed works do present the positive effects on local voltage by reactive power provision from EVs; however, all these study cases are validated in single distribution grids. As the effectiveness of such controllers depends on the electrical characteristics of the power system, it is of interest to evaluate their influence in different grid cases. In this respect, in [149] the effectiveness of reactive power control from PV inverters is evaluated with respect to different *R/X* grid characteristic, and it is shown how, depending on the grid characteristics, over-voltages can be reduced. Similarly, it is expected that for installations of new commercial EVSEs with fast charging capability in existing LV distribution feeders, the reactive power needed to prevent undesired under-voltages depends on the grid characteristic. Within this context, the studies in **Paper H** and **Paper I** investigate the influence of the single distribution grid components on the reactive power effect. The reactive power effects on the local voltage are evaluated in case of different load models in terms of inductive power factor as well as voltage-dependent behavior. The works provide guidelines for DSOs, applicable to different types of customers, e.g., residential, commercial, and industrial. The proposed method is to be seen as an assessment criterion when DSOs have to evaluate requests for installation of new EV fast chargers in LV networks. The following section presents the analytical formulation for assessing reactive power effects in distribution grids and outlines the methodology to evaluate the contribution of the single power system components. Then, a detailed sensitivity study including load models is presented, along with a validation study of the proposed methodology.

5.2 Voltage drop assessment in distribution grids

Although reactive power management for voltage support has major effects at HV/MV levels due to low *R/X* ratios (0.1-0.2), it is also seen as a feasible mean in LV distribution networks (average *R/X* ratio of 0.5-5) to maintain voltages within the allowed limits of ±10% of the nominal value [35]. In fact, in most of the European countries for residential PV installations connected to LV distribution grids, voltage regulation by reactive power provision is already required [127]–[129]. Similarly, the EV charging process could be performed by utilizing a capacitive power factor, i.e., injecting reactive power, to avoid under-voltages.

In distribution grids the transversal parameters conductance and susceptance are negligible for LV levels. All the grids with negligible transversal parameters can be represented by an R-L circuit as the one in Figure 5.2, which shows the single-phase equivalent circuit of a balanced three-phase line, where R_l and X_l are the longitudinal parameters of the distribution line, $\overline{E_1}$ and $\overline{E_2}$ the phase-neutral voltages at the two terminals, and $\overline{\Delta E}$ the voltage drop along the line. The assumption of a balanced three-phase system is motivated by the fact that the new fast-charger has a three-phase connection,

thus not introducing significant additional unbalance components, such as the one utilized in the field trial above-mentioned [77] and tested in **Paper E**.

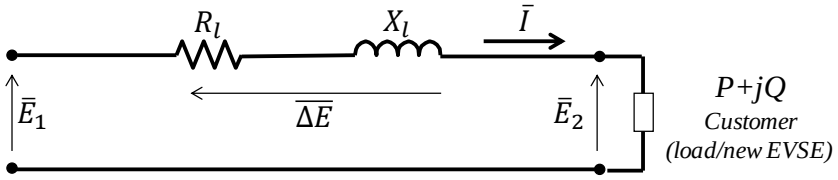

Figure 5.2 – Single-phase equivalent circuit of a three-phase LV line.

The apparent power absorbed by the customer at the end of the line $\bar{S}$, can be expressed as in Equation (5.1), where $\bar{I}^*$ is the conjugate of the drawn complex current $\bar{I}$.

$$\bar{S} = 3\overline{E_2} \cdot \bar{I}^* = P + jQ \tag{5.1}$$

From (5.1) it is possible to obtain $\bar{I}$ as function of the voltage $\overline{E_2}$ (taken as reference), and of the real and imaginary components of $\bar{S}$, i.e., P and Q, respectively:

$$\bar{I} = \left(\frac{\bar{S}}{3\overline{E_2}}\right)^* = \frac{\bar{S}^*}{3\overline{E_2}^*} = \frac{(P+jQ)^*}{3E_2} = \frac{P-jQ}{3E_2} \tag{5.2}$$

Equation (5.3) defines the complex phasor $\bar{I}$ and its real I_r and imaginary I_i components.

$$\bar{I} = I_r + jI_i, \begin{cases} I_r = \frac{P}{3E_2} \\ I_i = \frac{-Q}{3E_2} \end{cases} \tag{5.3}$$

Note that the sign of the real component of the current I_r indicates whether the customer is absorbing or injecting power. In case of an EV, this means it is charging or discharging, corresponding to the I/IV or II/III quadrants of the P-Q 4-quadrant EVSE converter operating scheme of Figure 5.1-b. The phase angle φ and therefore the imaginary component I_i, shows if the customer is exchanging inductive (positive) or capacitive (negative) reactive power, which corresponds to the I/II or the III/IV quadrant, respectively. As it can be seen in the phasor diagram in Figure 5.3, $\overline{E_2}$ is considered as reference, and therefore $\overline{E_1}$ and $\bar{I}$ are shifted by ε and φ, respectively.

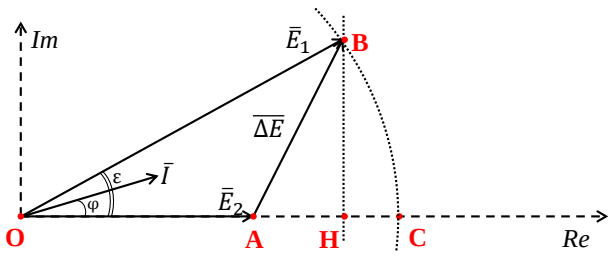

Figure 5.3 – Vector diagram.

The complex voltage at the starting terminal of the line $\overline{E_1}$ is equal to $\overline{E_2}$ with the addition of the complex voltage drop along the line $\overline{\Delta E}$, as in Equation (5.4). $\overline{\Delta E}$ is the complex product of current $\overline{I}$, which can be written as in (5.2), and the line impedance $\overline{Z_l}$, which can be written as (R_l+jX_l).

$$\overline{E_1} = \overline{E_2} + \overline{\Delta E} = \overline{E_2} + \overline{I} \cdot \overline{Z_l} = E_2 + \frac{P - jQ}{3E_2} \cdot (R_l + jX_l) = \left(E_2 + \frac{PR_l + QX_l}{3E_2}\right) + j\left(\frac{PX_l - QR_l}{3E_2}\right) \quad (5.4)$$

From Equation (5.4), the voltage magnitude E_1 and angle ε at the starting bus can be derived [150]:

$$\left|\overline{E_1}\right| = E_1 = \sqrt{\left(Re\left(\overline{E_1}\right)\right)^2 + \left(Im\left(\overline{E_1}\right)\right)^2} = \sqrt{{E_2}^2 + \frac{2}{3}(PR_l + QX_l) + \frac{(P^2+Q^2)\left({R_l}^2+{X_l}^2\right)}{9{E_2}^2}} \quad (5.5)$$

$$\varepsilon = \tan^{-1}\left[\frac{Im\left(\overline{E_1}\right)}{Re\left(\overline{E_1}\right)}\right] \quad (5.6)$$

In the proposed analytical assessment the module of E_1 (i.e., the length *OB* of Figure 5.3) is set to a particular value independently of its angle ε, which is thus not included in the final formulation. In fact, the proposed formulation enables us to estimate the actual magnitude of the voltage E_2 independently from its shift over E_1. In comparison to the traditional way of simplifying the formulation by neglecting the imaginary part of (5.4) (thus considering only the projection of E_1 on the real axis, i.e., *OH*), this formulation takes into account the entire magnitude of the vector E_1, i.e., *OB*=*OC*. Although it differs from the traditional exact complex estimation of the line voltage drop, crucial when assessing grid losses, still it represents a precise way for estimating the impact on the local voltage of new EVSEs installations.

By combining Equations (5.2) and (5.5), and with reference to the phasor diagram in Figure 5.3, the magnitude of E_2 ca be expressed as function of E_1, the real and imaginary components of the current (I_r and I_i), and the line impedance (R_l+jX_l):

$$E_2 = \sqrt{{E_1}^2 - (I_i R_l + I_r X_l)^2} - I_r R_l + I_i X_l \quad (5.7)$$

In case of capacitive reactive power (negative Q, which means positive I_i) the voltage drop due to active current absorption $+I_rR_l$ is partially compensated by the voltage rise due to the reactive current $+I_iX_l$. Thus, in order to support the grid during EV charging, instead of reducing the active charging power and thereby impacting the user comfort, injecting capacitive reactive power can be seen as an attractive alternative, thus operating in the IV quadrant of the EV converter charging capabilities in Figure 5.1-b.

The main purpose of the proposed analysis is to provide guidelines for DSOs in terms of reactive power provision requirement for new EVSEs installation. Therefore, the determination of the effect of reactive power on the voltage at the end of the line as function of the installed apparent power is important. For this reason, Equation (5.7) is combined with (5.3), in order to highlight separately the active power P and the reactive power Q, giving as result the formulation in Equation (5.8). Note

that (5.8) can be derived also directly from Equation (5.5), without making explicit the real and imaginary current components I_r and I_i.

$$E_2 = \frac{1}{\sqrt{2}}\sqrt{{E_1}^2 - \frac{2}{3}(PR_l + QX_l) + \sqrt{{E_1}^4 - \frac{4}{3}{E_1}^2(PR_l + QX_l) - \frac{4}{9}(PX_l + QR_l)^2}} \tag{5.8}$$

With (5.8) it is possible to calculate the voltage magnitude at the line ending terminal E_2, given the line parameters, the voltage at the source terminal, and the EV charging power in terms of P and Q. Equation (5.8) provides the expected phase-neutral voltage for fixed values of P and Q, thus considering that the actual absorbed power does not depend in any way on the local voltage. The assumption of considering no voltage-dependency, i.e., constant-power units, for new electrical installation is a common practice for grid operators when evaluating the grid impact of new eventual units (e.g., large loads, PVs, EVSEs). In fact, DSOs commonly consider the size of the new unit in terms of capacity, i.e., amount of power is going to be exchanged at the point of common coupling. For this reason, in this work the constant-power load model has been utilized for the new EV fast charger, whose size is indicated in terms of maximum charging power capacity.

By contrast, passive loads in power systems are typically characterized by different voltage-dependency behaviors. According to the ZIP theory [151], each load can be modelled with reference to its nature: it can simply be a 'constant-power', a 'constant-voltage' or a 'constant-impedance' load, or it could be represented as a mix of the previous characteristics. A typical load representation is given by the polynomial model in Equation (5.9), which shows voltage dependency of the actual absorbed active and reactive power P_{load} and Q_{load} according to the expected power values (P_{load_0} and Q_{load_0}) in case of nominal local voltage E_{2_0} of 230 V.

$$\begin{cases} P_{load} = P_{load\_0}\left[a_0 + a_1\frac{E_2}{E_{2\_0}} + a_2\left(\frac{E_2}{E_{2\_0}}\right)^2\right] \\ Q_{load} = Q_{Load\_0}\left[b_0 + b_1\frac{E_2}{E_{2\_0}} + b_2\left(\frac{E_2}{E_{2\_0}}\right)^2\right] \end{cases} \tag{5.9}$$

Coefficients a_0, a_1 and a_2 represent the shares of the constant-power, constant-current and constant-impedance contributions, respectively, and their sum is always equal to 1. The extreme cases of totally constant-power/current/impedance units are obtained by setting $a_i = 1$. Similar considerations are valid for coefficients b_0, b_1 and b_2, for the voltage-dependency of the reactive power. Typical ZIP coefficients for residential, industrial and commercial loads are reported further on in Table 5.4 [152].

The level of the investigation is now enhanced by considering the customer at the ending bus as a combination of certain load and the new EVSE. So, P and Q can be split in the two components relative to the EV (P_{EV} and Q_{EV}) and the load (P_{load} and Q_{load}):

$$\begin{cases} P = P_{EV} + P_{load} \\ Q = Q_{EV} + Q_{load} \end{cases}. \tag{5.10}$$

One can note that the definition of *P* and *Q* can be extended by including other types of units, such as inverter-driven DERs. In this case, with reference to the ZIP modelling, the new *P* and *Q* power exchanged would be modelled as constant-power units.

If the voltage rises, on the one hand it is expected that a constant-power load would draw less current, thus enhancing the voltage regulation effect determined by reactive power provision. On the other hand, a constant-impedance load would consume more, thus reducing the effectiveness. Note that for the load the absorbed *Q* is typically inductive ($Q_{load} > 0$), while for the charging EV it is generally capacitive ($Q_{EV} < 0$).

At this point, by combining Equation (5.8) with (5.9) and (5.10), it is possible to derive the fourth order equation, shown in Equation (5.11).

$$E_2{}^4 \cdot \beta_4 + E_2{}^3 \cdot \beta_3 + E_2{}^2 \cdot \beta_2 + E_2 \cdot \beta_1 + \beta_0 = 0 \tag{5.11}$$

The coefficients $\{\beta_4, \beta_3, \beta_2, \beta_1, \beta_0\}$ are calculated as in Equations (5.12)-(5.16):

$$\beta_4 = 1 + \frac{2(R_l P_{load\_0} a_2 + X_l Q_{load\_0} b_2)}{3E_{2\_0}{}^2} + \frac{(R_l{}^2 + X_l{}^2)\left[(P_{load\_0} a_2)^2 + (Q_{load\_0} b_2)^2\right]}{9E_{2\_0}{}^4} \tag{5.12}$$

$$\beta_3 = \frac{2(R_l P_{load\_0} a_1 + X_l Q_{load\_0} b_1)}{3E_{2\_0}} + \frac{(R_l{}^2 + X_l{}^2)(2P_{load\_0}{}^2 a_1 a_2 + 2Q_{load\_0}{}^2 b_1 b_2)}{9E_{2\_0}{}^3} \tag{5.13}$$

$$\beta_2 = -E_1{}^2 + \frac{2}{3}\left[R_l(P_{EV} + P_{load\_0} a_0) - X_l(Q_{EV} + Q_{load\_0} b_0)\right] + \frac{1}{9E_{2\_0}{}^2}\left\{(R_l{}^2 + X_l{}^2)\left[(P_{load\_0} a_1)^2 + 2P_{load\_0}{}^2 a_0 a_2 + 2P_{EV} P_{load\_0} a_2 + (Q_{load\_0} b_1)^2 + 2Q_{load\_0}{}^2 b_0 b_2 + 2Q_{EV} Q_{load\_0} b_2\right]\right\} \tag{5.14}$$

$$\beta_1 = \frac{(R_l{}^2 + X_l{}^2)}{9E_{2\_0}}\left(2P_{load\_0}{}^2 a_0 a_1 + 2P_{EV} P_{load\_0} a_1 + 2Q_{load\_0}{}^2 b_0 b_1 + 2Q_{EV} Q_{load\_0} b_1\right) \tag{5.15}$$

$$\beta_0 = \frac{1}{9}(R_l{}^2 + X_l{}^2)\left[P_{EV}{}^2 + (P_{load\_0} a_0)^2 + Q_{EV}{}^2 + (Q_{load\_0} b_0)^2 + 2P_{EV} P_{load\_0} a_0 + 2Q_{EV} Q_{load\_0} b_0\right] \tag{5.16}$$

With (5.11), E_2 is calculated as function of the source voltage E_1, the line impedance, and the total active and reactive power, given a certain voltage-dependency of the load. With this formulation, the effect of the capacitive reactive power can be evaluated given a certain active power charging capacity P_{EV} of the new EVSE installation, by applying different Q_{EV}. In the proposed assessment analysis, the amount of reactive power Q_{EV} provided by the EVSE is determined by the power factor $\cos\varphi_{EV}$ set for the charging process, resulting in a fixed power factor operation mode, as commonly applied in small PV inverters. Reactive power is provided only when the car is charging, i.e., when

there is a need for a certain active power flow for the analyzed voltage support control. So, for a given charging behavior influenced by stochastic factors, the reactive power is to be seen as a mean to reduce the potential self-induced voltage issues, by constantly raising the bus voltage via a fixed $\cos\varphi$ logic. The control is completely decentralized and based merely on the implemented constant power factor logic, thus not including any centralized remote grid monitoring. The logic of the proposed methodology can be therefore summarized with the block diagram reported in Figure 5.4.

The proposed formulation is a possible explicit formulation analytically derived by fundamental electrotechnical laws that gives the exact direct calculation of the voltage magnitude at the considered bus, with no need for iterative calculations as for the case of power flows calculation. The solution of Equation (5.11) can be seen as a computationally simple and fast method able to provide a precise estimation of the voltage magnitude at the EVSE bus, with no need for iterative calculations.

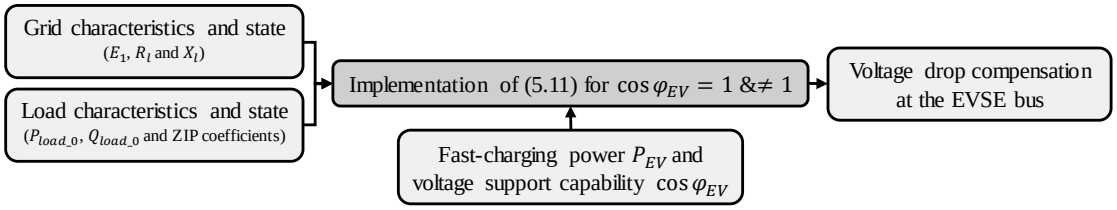

Figure 5.4 – Block diagram of the logic of the proposed method.

5.3 Grid and components equivalent models

The first part of the investigation aims at evaluating the influence of the different power components (MV grid, MV/LV transformer, and LV cable) on the effectiveness of reactive power for voltage support, highlighting how much each component contributes to the total voltage drop. The single-line equivalent circuit in Figure 5.5-a is considered. The representation seen from the LV side is illustrated by the equivalent single-phase circuit with all the parameters referred to the 0.4 kV level V_{n_LV}. At this stage, no other loads are considered, thus only the impact of charging EVs with/without reactive power support is investigated. Figure 5.5-b shows the resistive and inductive components referred to the LV level of MV grid (R_{grid} and X_{grid}), transformer (R_{trafo} and X_{trafo}), and line ($R_{LVfeeder}$ and $X_{LVfeeder}$). With regard to the analysis in the previous section, the series of the three resistive and inductive components correspond to R_l and X_l of Figure 5.2.

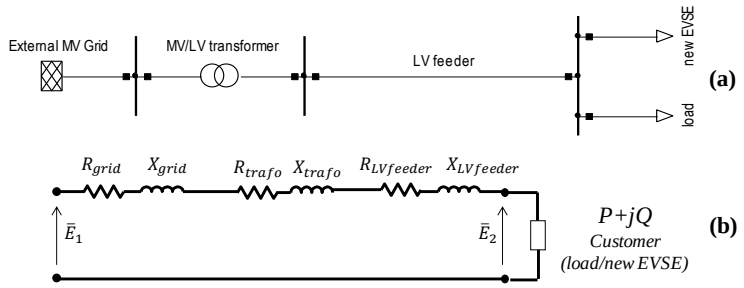

Figure 5.5 – Single-line (a) and single-phase equivalent circuit referred to the LV level (b) of a three-phase power system.

Typically, the V_{n_MV} 10 kV MV grid's characteristics can be represented by the short-circuit power S_{sc_grid} and the R/X_{grid} ratio: common values are 10 MVA and 0.5, respectively [153]. Through the calculation of the short-circuit impedance X_{grid_MV} and its components R_{grid_MV} and X_{grid_MV} the resistive and inductive components referred to the LV level R_{grid} and X_{grid} amount to 0.00716 Ω and 0.01431 Ω, respectively. The calculation is done using Equations (5.17) and (5.18).

$$Z_{grid\_MV} = \frac{{V_{n\_MV}}^2}{S_{sc\_grid}} = \sqrt{{R_{grid\_MV}}^2 + {X_{grid\_MV}}^2} \tag{5.17}$$

$$\begin{cases} R_{grid} = R_{grid\_MV} \left(\frac{V_{n\_MV}}{V_{n\_LV}}\right)^{-2} \\ X_{grid} = X_{grid\_MV} \left(\frac{V_{n\_MV}}{V_{n\_LV}}\right)^{-2} \end{cases} \tag{5.18}$$

A typical MV/LV distribution power transformer is modelled in [44]. It is characterized by nominal apparent power S_{n_trafo} = 0.4 MVA, short-circuit voltage $v_{sc\%\_trafo}$ = 4%, and R/X_{trafo} ratio = 0.1. Via calculation of short-circuit power S_{sc_trafo} and impedance Z_{sc_trafo} – Equations (5.19) and (5.20) – the resistive and inductive components referred to the LV level R_{trafo} and X_{trafo} amount respectively to 0.00159 Ω and 0.0159 Ω.

$$S_{sc\_trafo} = \frac{100 * S_{n\_trafo}}{v_{sc\%\_trafo}} \tag{5.19}$$

$$Z_{sc\_trafo} = \frac{{V_{n\_LV}}^2}{S_{sc\_trafo}} = \sqrt{{R_{trafo}}^2 + {X_{trafo}}^2} \tag{5.20}$$

This formulation does not include no-load current and no-load losses, which was found do not significantly impact the results. In particular, they only cause a minor off-set on the total voltage drop estimation of less than 0.1% of the nominal voltage. Typical values of cable resistance and reactance per km are 0.163 and 0.136 Ω/km, respectively ($R/X_{LVfeeder}$ = 1.2, i.e., $X/R_{LVfeeder}$ = 0.8) [153]. The length of 1 km is chosen, as it can be considered as an upper limit of LV feeders length [154]. So, absolute $R_{LVfeeder}$ and $X_{LVfeeder}$ amount to 0.163 and 0.136 Ω, respectively. Table 5.1 reports the typical values of power system components for LV distribution grids. It also includes the equivalent resistance and reactance referred to the LV level, with reference to the simplified single-phase equivalent circuit in Figure 5.5-b.

Table 5.1. Standard parameters for distribution grids, adapted from [26], [153].

	S_{sc_grid} [MVA]	S_{n_trafo} [MVA]	$v_{sc\%\_trafo}$ [%]	R/X	R referred to LV level [Ω]	X referred to LV level [Ω]
MV grid	10	-	-	0.5	0.00716	0.01431
MV/LV trafo	-	0.4	4	0.1	0.00159	0.0159
LV feeder	-	-	-	1.2	0.163	0.136

Equation (5.8) is implemented with E_1 set to 1 p.u. as for an ideal voltage source and P and Q equal to P_{EV} and Q_{EV}, respectively – only EVs as customer. Anyway, the aim of the study is assessing the

voltage difference, thus the findings are still applicable also in other situations (i.e., higher voltages such as 1.05 because of reverse flow, or lower voltages such as 0.95 because of loaded feeders). One should also note that Equation (5.8) could be implemented considering that the starting terminal of the line does not necessarily need to be at the MV grid or transformer level. Instead, it could be at any node of the distribution network. In this case, the ending terminal could be at the end of one of the branches derived from that very node. Considering installation at the ending terminal of new EVSEs with charging capability up to 10 kW, it has been decided to assume a total EV active power demand of 50 kW, which represents a realistic case of 5 new EVSEs. Equation (5.8) is implemented twice: with power factor $\cos\varphi_{EV}$ equal to 1 and then repeated with capacitive $\cos\varphi_{EV}$ equal to 0.9 leading, and the difference ΔE_2 was evaluated as in Equation (5.21).

$$\Delta E_2 = E_{2\_\cos\varphi_{EV}\neq 1} - E_{2\_\cos\varphi_{EV}=1} \tag{5.21}$$

The choice of the limit value of $\cos\varphi_{EV}$ of 0.9, is motivated by the fact that also in case of reactive power provision by PV inverters, the maximum reactive power exchange is limited by a power factor of 0.9 [127]–[129]. This value is identified as the maximum power factor that can be applied to the converter without excessive over-sizing. For this reason, the same value is set for the EVSE inverters under analysis. Considering the calculated constant values of the series resistive and inductive components of the circuit in Figure 5.4-b, a preliminary analysis of the influence of the three single components on the effects of reactive power is now presented. E_2 resulted in 0.9415 and 0.9673 p.u. for $\cos\varphi_{EV}$ equal to 1 and 0.9, respectively. It is clear that ΔE_2 (0.0258 p.u.) represents the voltage rise due to the reactive power injected by the EVs at the ending terminal of the line. The resulting ΔE_2 is obtained as effect of the three components. Specifically, the MV grid contributed 8.5%, the transformer 9.4%, while the LV feeder contributed 82.1%, as illustrated schematically in Figure 5.6.

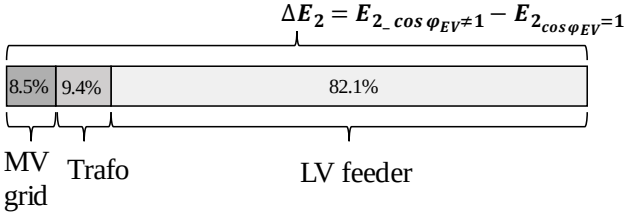

Figure 5.6 – Contribution of each component to the reactive power effect on the voltage at the ending terminal.

It is therefore found that the effect of the reactive power on the local voltage depends mainly on the characteristics of the LV feeder. This result was obtained considering one possible combination of typical distribution network components. Thus, it is of interest to see how different values of these components may impact the results. In this regards, the next part of the investigation aims at evaluating the single influence of the MV grid, the MV/LV transformer, and the LV feeder parameters.

5.4 Sensitivity analysis

5.4.1 Influence of MV grid

The influence of the external MV grid is evaluated by calculating ΔE_2 first for different S_{sc_grid} (1-10 MVA) and then for different R/X_{grid} (0.05-0.5), keeping constant the typical parameters of transformer and LV feeder of Table 5.1. Figure 5.7-a shows that the trend of ΔE_2 is influenced by the stiffness of the external MV grid, keeping R/X_{grid} = 0.5 [153]. In particular, for very weak grids results differ from the case of strong ones. Thus, hereafter all the studies consider two kinds of MV grid: weak and strong grid (S_{sc_grid} = 2 and 10 MVA, respectively). Figure 5.7-b shows that in both the cases the effect of reactive power on the ending terminal voltage is constant for all the considered R/X_{grid} ratios. Thus, hereafter the constant value R/X_{grid} = 0.5 is used.

5.4.2 Influence of MV/LV transformer

The influence of the distribution transformer is evaluated by calculating ΔE_2 for different S_{n_trafo} (0.1-1 MVA), keeping constant the typical values of $v_{sc\%\_trafo}$, R/X_{trafo} and LV feeder, as in Table 5.1. The analysis is carried out for weak and strong MV grid. Figure 5.7-c shows that the influence of the transformer on the effect of reactive power is marginal for $S_{n\_trafo} \geq 0.2$ MVA, while for smaller sizes, the contribution becomes noticeable. As the grid model considers a LV feeder at the secondary side of the transformer, it is to be expected that in addition to the new EVSEs at the line end, distributed loads are connected along the feeder. As this study considers a realistic case of new EVSEs installation for a total of 50 kW, a minimum size of 0.2 MVA has to be expected for the transformer (the examples for the Danish and Norwegian distribution grids in Chapter 2 show that typical sizes are 0.4-0.5 MVA). For this reason, hereafter the typical values of the MV/LV transformer reported in Table 5.1 are considered and kept constant, as its influence on the effect of the reactive power is considered marginal.

5.4.3 Influence of the LV feeder

The influence of the LV feeder is evaluated by calculating ΔE_2 first for different $R/X_{LVfeeder}$ and then for different lengths, considering both weak and strong MV grid, and the transformer from Table 5.1. Since it is known that the reactance per km is usually constant for different kinds of cables, for the first case different $R/X_{LVfeeder}$ are obtained by varying the value of the resistive component (0.07-0.7 Ω/km), i.e., by considering different sections of the cable conductors, keeping the length equal to 1 km [154]. For the case of different lengths (0-1 km), the values per km in Table 5.1 are used and kept constant. Figure 5.7-d shows that ΔE_2 is rather constant for different $R/X_{LVfeeder}$, while from Figure 5.7-e one can deduce that the main influence is given by the absolute values of $R_{LVfeeder}$ and $X_{LVfeeder}$, so by the length. To conclude, **the main influence of reactive power on the voltage support is determined** by the absolute values, i.e., **by the feeder impedance length**, rather than by the $R/X_{LVfeeder}$ ratio.

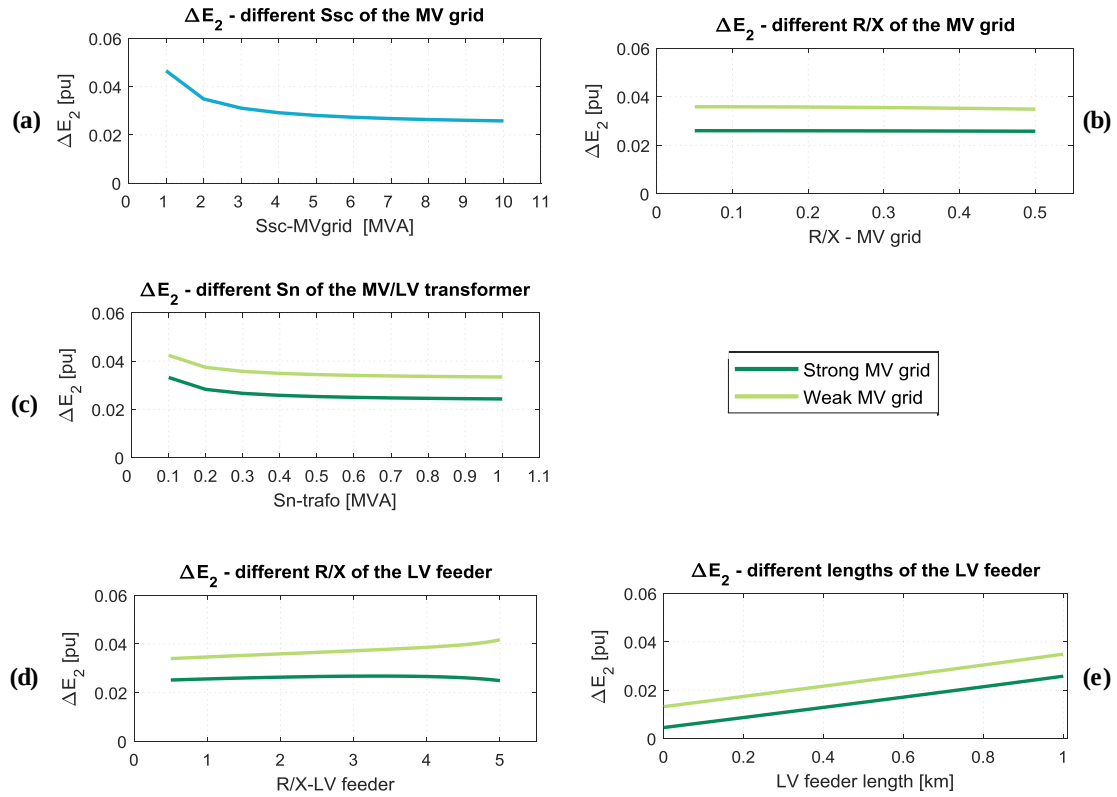

Figure 5.7 – Influence of the LV feeder for $\cos \varphi_{EV \neq 1} = 0.9$.

5.4.4 Voltage rise as function of $cos(\varphi_{EV})$ and length

It is clear that ΔE_2 depends on the amount of the capacitive reactive power provided by the EV, i.e., on the power factor $\cos \varphi_{EV}$ set by the EVSE. Therefore, the following formulation considers ΔE_2 as function of the LV feeder length and $\cos \varphi_{EV}$, varied between leading 0.9 and 1. Table 5.2 presents numerical results for the case of the strong MV grid, i.e., the most common one. As expected, the effectiveness of the reactive power on voltage support is increasing with decreasing power factor, up to the maximum value of 0.0258 p.u. for standard LV feeder length of 1 km, for strong MV grid. Moreover, it is noticeable that for any given $\cos \varphi_{EV}$, the effects are linearly dependent on the absolute value of the LV feeder impedance (thus the length), as previously demonstrated.

Table 5.2. ΔE_2 for different $\cos \varphi_{EV}$ – length combinations.

		ΔE_2 [p.u.]					
		$\cos \varphi_{EV} = 1$	$\cos \varphi_{EV} = 0.98$	$\cos \varphi_{EV} = 0.96$	$\cos \varphi_{EV} = 0.94$	$\cos \varphi_{EV} = 0.92$	$\cos \varphi_{EV} = 0.9$
Length [km]	**0.2**	0	0.0037	0.0053	0.0066	0.0077	0.0087
	0.4	0	0.0055	0.0078	0.0097	0.0114	0.0129
	0.6	0	0.0073	0.0104	0.0129	0.0151	0.0171
	0.8	0	0.0092	0.0131	0.0162	0.0189	0.0214
	1.0	0	0.0111	0.0158	0.0195	0.0228	0.0258

5.4.5 Inclusion of voltage dependent loads

The analysis presented so far has not considered any loading except for the new EVSE itself, in fact Equation (5.8) is implemented considering only EVs as customer. Now the investigation is enhanced through the implementation of (5.11), for different voltage-dependent loads in addition to the EVs. The nominal active power P_{load_0} is kept constantly equal to 50 kW, while different load types and different amount of inductive reactive power active power Q_{load_0} (i.e., different values of $\cos\varphi_{load}$) are considered. Figure 5.8 shows the effect of capacitive reactive power provided from EVs on the voltage E_2 at the ending terminal of the feeder for different load types (constant P, I or Z). The comparison is done for $\cos\varphi_{EV\neq1}$ = 0.9, considering constant $\cos\varphi_{load}$ = 0.9. It can be noticed that the load type influences the results for lines longer than 0.4 km, with more evident effects in case of no voltage-dependency (constant-P load) rather than for voltage-dependent load. Specifically, for a 1 km line, ΔE_2 amounts to 0.0319, 0.0277 and 0.0253 p.u. for constant-P, constant-I and constant-Z loads, respectively. Although an exhaustive sensitivity analysis would require load models with mixed coefficients, the results of the three analyzed load types represent the extreme cases. In fact, by using mixes of the coefficients, intermediate results would be obtained.

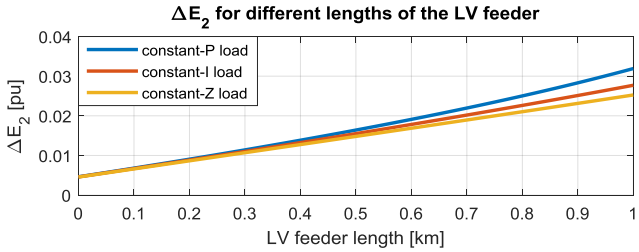

Figure 5.8 – Voltage rise effect of EV reactive power for $\cos\varphi_{EV\neq1}$ = 0.9, for different load types.

Similarly to the previous analysis, ΔE_2 is evaluated as function of LV feeder length and load types, varying $\cos\varphi_{EV}$ between 0.9 and 1. Figure 5.9 shows 3D bar plots of ΔE_2 for the different load types and $\cos\varphi_{load}$ equal 0.85, 0.9, 0.95 and 1, in subfigures (a), (b), (c) and (d), respectively. The three different widths of the bars indicate the load type: the widest one is for constant-Z loads, the middle one for constant-I loads, while the tightest one for constant-P loads. As expected, it is shown that the more the load is voltage dependent, the smaller is the contribution of the capacitive reactive power in rising the voltage. In fact, as shown in Figure 5.8 in case of constant-P load, ΔE_2 is higher than in the case of constant-I load, which is higher than in the case of constant-Z load. Furthermore, as seen above, ΔE_2 is higher with decreasing amount of EV reactive power (decreasing $\cos\varphi_{EV}$) for all load types. Table 5.3 presents numerical results of the cases of highest reactive power contribution from EVs ($\cos\varphi_{EV\neq1}$ = 0.9). Results confirm the linear trend with the LV feeder length, and show less voltage support effects in case of higher load power factors $\cos\varphi_{load}$.

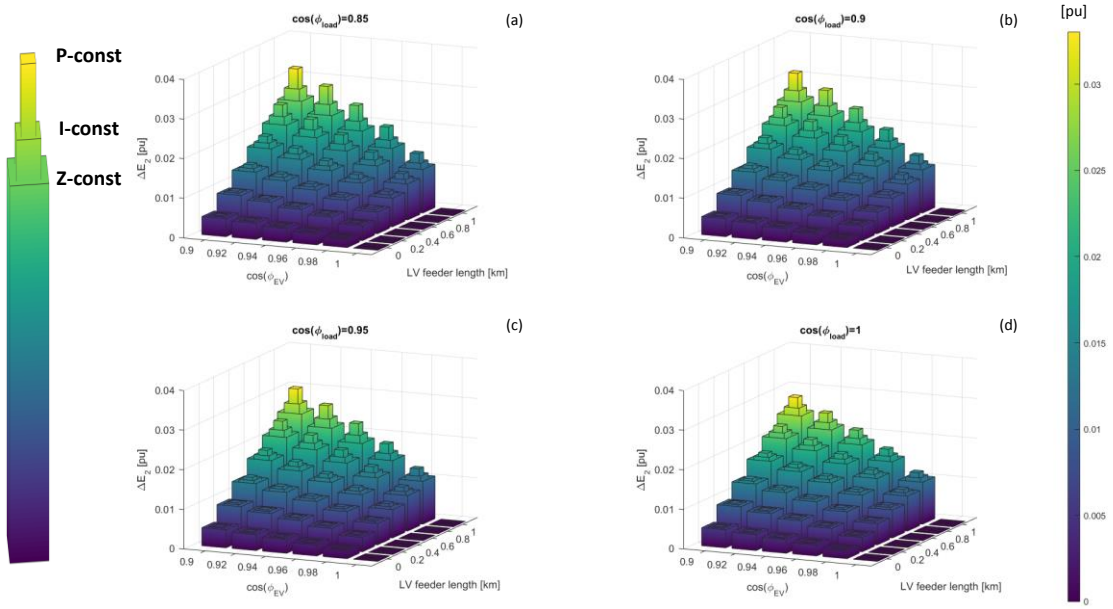

Figure 5.9 – Voltage rise effect of EV reactive power as function of the LV feeder length and $\cos\varphi_{EV}$, for different load types for $\cos\varphi_{load}$=0.85, 09, 0.95, 1 in (a), (b), (c) and (d), respectively.

Table 5.3. ΔE_2 for different lengths – load model combinations with $\cos\varphi_{EV\neq1}$ = 0.9.

			ΔE_2 [p.u.]			
			$\cos\varphi_{load}$ = 0.85	$\cos\varphi_{load}$ = 0.9	$\cos\varphi_{load}$ = 0.95	$\cos\varphi_{load}$ = 1
Length [km]	**0.2**	**Constant-P load**	0.0091	0.0091	0.0090	0.0089
	0.4		0.0140	0.0138	0.0137	0.0133
	0.6		0.0194	0.0191	0.0187	0.0180
	0.8		0.0256	0.0250	0.0243	0.0231
	1.0		0.0330	0.0319	0.0308	0.0286
Length [km]	**0.2**	**Constant-I load**	0.0089	0.0088	0.0088	0.0087
	0.4		0.0133	0.0132	0.0131	0.0129
	0.6		0.0180	0.0178	0.0176	0.0172
	0.8		0.0229	0.0226	0.0223	0.0216
	1.0		0.0282	0.0277	0.0272	0.0262
Length [km]	**0.2**	**Constant-Z load**	0.0087	0.0086	0.0086	0.0086
	0.4		0.0128	0.0127	0.0127	0.0126
	0.6		0.0169	0.0169	0.0168	0.0166
	0.8		0.0212	0.0210	0.0209	0.0206
	1.0		0.0254	0.0253	0.0250	0.0246

5.5 Implementation on representative LV distribution grids

This section reports a validation of the proposed method on the reference Cigrè European LV distribution feeder [153] as well as on the above-presented real Danish LV distribution network [26]. Simulations are carried out both applying the proposed formulation and by means of DIgSILENT PowerFactory load flows. For the calculation of P_{load} and Q_{load}, Equation (5.9) is implemented with

the typical ZIP coefficients for residential load class, which are reported in Table 5.4 along with industrial and commercial load classes [152].

Table 5.4. Typical values of coefficients for loads in distribution grids.

Load class	a_0	a_1	a_2	b_0	b_1	b_2
Residential	1.27	-1.12	0.85	8.77	-18.73	10.96
Industrial	1	0	0	1	0	0
Large commercial	1.06	-0.53	0.47	4.43	-8.73	5.30
Small commercial	0.63	-0.06	0.43	3.59	-6.65	4.06

5.5.1 Validation on Cigrè European LV reference grid

The residential reference Cigrè European LV distribution feeder has a radial topology and consists of 6 buses at the LV level, 5 of which are the point of common coupling of residential loads. The grid is schematized in Figure 5.10. Installation of five new 10 kW EVSEs (for a total of 50 kW) is considered at buses 2-6, which are, case by case, the ending terminal bus with respect to the formulation proposed in Section 5.3. The loading and the single-feeder characteristics (transformer-bus) are in Table 5.5.

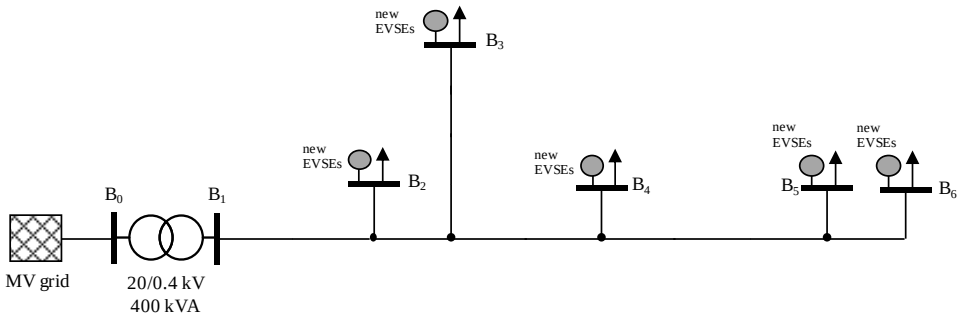

Figure 5.10 – Single-phase circuit of the modelled Cigrè distribution grid under study.

Table 5.5. Properties of the Cigrè transformer-bus feeder and loading at each bus.

Bus	Total Length [m]	$R/X_{LVfeeder}$	P_{load_0} [kW]	$\cos\varphi_{load}$
B2	95	3.67	5.13	0.9
B3	240	2.08	51.3	0.9
B4	205	1.57	22.5	0.9
B5	310	2.08	5.13	0.9
B6	345	1.74	22.5	0.9

Due to the limited length of the line, results are not expected to be dramatically influenced by the voltage dependency of the loads type. However, the typical ZIP coefficients for residential load class indicated in Table 5.4 are utilized. Results are reported in Table 5.6, which shows voltage E_2 for unitary $\cos\varphi_{EV}$, for $\cos\varphi_{EV}$ = 0.9, and the difference ΔE_2 in case of 50 kW of EVs charging at buses 2-6. As deducible from Table 5.6, the results from the implementation of the proposed method respect very accurately the ones obtained carrying out iterative power flow simulations in

DIgSILENT PowerFactory. This is true given a sufficiently small tolerance (equal to 0.1 kVA) when solving Newton-Rapson calculations. In this case the difference between the results from the two methods is smaller than 0.01%. In case of larger tolerance the convergence might still be obtained, though with minor differences in the results, as less iterations would be needed due to the less tight tolerance. Moreover, the expected trend of growing ΔE_2 with the line length independently from the $R/X_{LVfeeder}$ ratio demonstrated in Section 5.4 is confirmed.

Table 5.6. Results from validation analyses on the Cigrè grid for 50 kW EVSEs.

Bus	Proposed Method			Power Flow in PowerFactory		
	E_2 [p.u.]		ΔE_2 [p.u.]	E_2 [p.u.]		ΔE_2 [p.u.]
	$\cos\varphi_{EV}$ =1	$\cos\varphi_{EV}$ =0.9		$\cos\varphi_{EV}$ =1	$\cos\varphi_{EV}$ =0.9	
B2	0.9760	0.9825	0.0065	0.9760	0.9825	0.0065
B3	0.9491	0.9587	0.0096	0.9491	0.9587	0.0096
B4	0.9711	0.9796	0.0085	0.9711	0.9796	0.0085
B5	0.9629	0.9738	0.0109	0.9629	0.9738	0.0109
B6	0.9508	0.9626	0.0118	0.9508	0.9626	0.0118

5.5.2 Validation on a real Danish LV distribution grid

For the validation on the real Danish LV grid (Subsection 2.1.2.1 and Appendix A), the installation of five new 10 kW EVSEs is considered cyclically at each bus from 602 to 613. The voltage values of the EVSE bus is E_2 in the proposed formulation (Equation (5.11)), which corresponds to the ending terminal bus with reference to the diagram on Figure 5.5. It is important to highlight that the loading conditions described in Appendix A correspond to the worst case of maximum loading of a winter week is simulated, when high load demand is present due to heat pumps heating systems, while there is no PV production due to weather conditions. Again, the typical ZIP coefficients for residential load class in Table 5.4 are utilized. Results are reported in Table 5.7, which shows the voltage E_2 for unitary $\cos\varphi_{EV}$, for $\cos\varphi_{EV}$ = 0.9, and the difference ΔE_2 in case of 50 kW of EVs charging at all the buses. The results obtained from the implementation of the proposed formulation respect very accurately the ones obtained carrying out power flow simulations in DIgSILENT PowerFactory. Again, the sufficiently small tolerance (equal to 0.1 kVA) utilized when solving power flow calculations enables the results to look identical, as difference smaller than 0.01% are obtained. As in this case the cable lines of the modelled network are all of the same type, they have the same $R/X_{LVfeeder}$ ratio. Nonetheless, the expected trend of growing ΔE_2 with the line length is confirmed.

Table 5.7. Results from validation on the real Danish grid for 50 kW EVSEs.

Bus	Proposed Method			Power Flow in PowerFactory		
	E_2 [p.u.]		ΔE_2 [p.u.]	E_2 [p.u.]		ΔE_2 [p.u.]
	$\cos\varphi_{EV}$ =1	$\cos\varphi_{EV}$ =0.9		$\cos\varphi_{EV}$ =1	$\cos\varphi_{EV}$ =0.9	
B602	0.9866	0.9908	0.0042	0.9866	0.9908	0.0042
B603	0.9826	0.9875	0.0049	0.9826	0.9875	0.0049
B604	0.9728	0.9787	0.0059	0.9728	0.9787	0.0059
B607	0.9751	0.9805	0.0054	0.9751	0.9805	0.0054
B608	0.9741	0.9799	0.0058	0.9742	0.9800	0.0058
B609	0.9783	0.9836	0.0053	0.9783	0.9836	0.0053
B610	0.9736	0.9793	0.0057	0.9736	0.9793	0.0057
B611	0.9704	0.9765	0.0061	0.9704	0.9765	0.0062
B612	0.9670	0.9736	0.0066	0.9670	0.9735	0.0065
B613	0.9649	0.9718	0.0069	0.9649	0.9718	0.0069

5.6 Summary

In this chapter, the solution to under-voltages via EV reactive power provision has been investigated in a generalized way, with the aim of evaluating effectiveness and limitations of such technology on all kinds of radial distribution feeders. An analytical expression has been proposed, which allows the calculation of the voltage at the receiving terminal, given the sending terminal voltage and the EV charging rate with a given power factor. The application is meant for DSOs when evaluating new installations of fast chargers on the receiving end terminal of a low voltage feeder, as an alternative to more time consuming power flow calculations.

Results showed that the effect of the capacitive reactive power is influenced mostly by the absolute values of the LV feeder impedance. Specifically, the *R/X* ratio of the LV feeder did not significantly influence the results, while its absolute impedance (the length, in particular) was crucial. Therefore, **with the proposed formulation the DSO is able to assess the voltage drop compensation due to the application of a specific power factor by the EV charger as function of the LV feeder length, given as input the EVSE installed power and the load condition**. In this way, DSOs can clearly evaluate the effect of the reactive power for any of their LV feeders when the power absorbed by EVs chargers would cause unacceptable under-voltages. The validation analysis on realistic LV feeders for the case of a fixed capacitive power factor of 0.9 proved that the voltage rise would amount to 0.012 p.u., in comparison to the case of EV charging with unitary power factor. Such voltage drop reductions can potentially avoid the violation of voltage thresholds, thus assuring compliance with grid technical standards on voltage levels. At any rate, this precaution may not be sufficient for massive penetration of EVs, since a combination with other smart charging strategies such as charging modulation and/or charging shifting may be essential for prevention of unacceptable under-voltage conditions. In conclusion, reactive power control has to be seen as a

possible connection capability requirement, able to mitigate the self-induced negative effects of fast charging EVs in LV distribution grids, similarly to the current requirements for new PV system installation in many European countries. In this regard, reactive power capabilities are required by the newly released Danish technical standard for stationary storage systems including vehicle-to-grid EV charging stations [111].

CHAPTER 6

Conclusions and future research

The overarching question investigated in this dissertation focused on the main challenges and opportunities when pro-actively integrating electric vehicles in the power system. Around this major thread, in Section 1.2, six research questions have been outlined for the Ph.D. project. In the following, the results are concluded:

Q1. *Focusing on both distribution and transmission level, what is the impact when integrating EVs, and what prerequisites are needed for supporting active EV involvement in the Nordic region?*

Grid impact analyses on both system and distribution grid level showed the effects of uncontrolled EV charging in terms of increase of electricity demand and peak power, with consequences on the production-consumption equilibrium and on the distribution grids' electrical infrastructure, respectively. In this context, the need for flexibility was evident: the concept of *EV flexibility product* has been introduced, highlighting theoretical and practical attributes necessary for classification and subsequent trade. The different needs for flexibility of different stakeholders have been outlined, and the current policies and barriers against the roll-out of an active EV participation have been identified in different European countries with emphasis on the Nordics. Finally, the need for defining appropriate requirements has been highlighted both from the technical perspective as well as from the organizational and regulatory framework. This contribution can pave the way towards a classification and an active involvement also within prospective local electricity market frameworks of the *EV flexibility product* as a pro-active asset for grid regulation purposes.

Q2. *What technical and economical conflicts may arise when acquiring flexibility products from EVs? How can they be detected and categorized?*

Different needs for flexibility services of each involved stakeholder can raise potential conflicts between two or more stakeholders with opposing needs. A DSO model with an active market role in managing distribution grids by relying on flexible resources has been described. A number of technical and non-technical TSO/DSO conflicts have been identified and categorized, by using a conflict identification procedure. In particular, within the

considered market framework, day-ahead trading process of ancillary services provided by EVs has been analyzed, focusing on the potential conflicts arising when acquiring services for congestion management (DSO's perspective) and primary frequency regulation (TSO's perspective). Considering a 3-area power system, each conflict has been presented through appropriate case studies that allowed to quantify and identify the nature of the conflicts. The four identified conflicts are: *Conflict (a)*: Need for compensating imbalances caused by activation of flexibility for solving a local distribution issue; *Conflict (b)*: To solve a TSO request, activating the only available flexibility product causes distribution overloading; *Conflict (c)*: The available flexibility can satisfy either the DSO request or the TSO request; and *Conflict (d)*: One flexibility product can solve several problems.

Q3. *Are EVs able to provide reliable frequency regulation to the power system? What technical challenges can be identified when employing contemporary technology, standards and requirements?*

The importance in the identification of both technical capabilities of series-produced EVs and controllability standard requirements has been emphasized as the key enabler for the development and the implementation of control logics able to guarantee reliable power system frequency regulation. Within this context, contemporary standard-compliant commercial hardware has been tested, in order to characterize the performance with respect to the flexibility product attributes, which can make the EV a tradable asset. Criticalities on the response time and linearity in the response have been found when implementing EV controllers for primary frequency regulation in a number of simulated and experimental power systems. Such criticalities can cause an inefficient fleet operation, primary frequency provision reserve error, and even power system instabilities. Therefore, it was necessary to investigate control strategies and recommendations to achieve a reliable, safe and quality service.

Q4. *What operation strategies should be implemented by EV aggregators to enhance grid balancing service provision?*

Given the identified technological barriers related to the implementation of reliable EV primary frequency controllers, the need for smart EV control solutions for fleet operators has been highlighted. It has been shown how the issues related to the EV response discreteness could be mitigated via the implementation of a frequency-current droop shift to achieve an overall aggregated response smaller than the one of the individual EV. Another relevant aspect when managing a number of EVs has to be taken into consideration by fleet operators: the varying charging/discharging efficiency for different set-points found when testing commercial EV chargers. In fact it has been shown that with the knowledge of the technical performance of the employed hardware, the fleet operation can be enhanced, e.g., operating at

power levels with higher efficiencies, leading to less overall accumulated energy losses during the V2G session. In this respect, a decentralized controller has been proposed, which implements a stochastic logic aimed at achieving a trade-off between the average error in the reserve provision during a V2G session and the overall fleet efficiency.

Q5. *What guidelines should are recommended for EV fleet operators for a safe replacement of conventional grid balancing units?*

A realistic EV fleet aggregation model is important for reliable power system studies when assessing the effect of EV fleets providing frequency regulation. The complete power system of the Danish Island of Bornholm has been modelled in an islanded configuration with high share of renewable generation, and the contribution of EVs in frequency control provision has been investigated. Results outlined two recommendations with conservativeness considerations to guarantee safe and stable operation: ***Recommendation 1*** requires to operate with a share of primary reserve from EVs that would not exceed the reserve from the conventional generation units; ***Recommendation 2*** requires response times below the half of a limit value that can be calculated as function of the power system's parameters, such as system inertia, total primary reserve over the rotating generation capacity, and employed droop gain. The derived recommendations can be considered as a tool for TSOs when performing power system studies, to be utilized as a benchmark for grid analysis simulations. For the specific simulated case of the Bornholm power system with high share of wind power generation and almost 50% of the available reserve provided by EVs, results showed that for EV response times of 1 s and 4 s the stability was assured, whereas for 7 s slowly damped oscillations appeared before settling to the steady-state frequency value, and for slower responses (e.g., 10 s) the system stability could not be maintained.

Q6. *When integrating EVs in LV networks, to what extent can EV reactive power be considered as a tool to support voltages? What guidelines could DSOs require in terms of reactive power provision from off-board EV chargers?*

Large-scale EV charging in distribution grids may cause technical issues on the LV electrical infrastructure, leading to the conclusion that, unless opting for grid reinforcement solutions, a massive EV penetration may force DSOs to rely on smart EV charging. One of the main consequences is the power quality worsening, specifically in terms of under-voltages, which can be mitigated via solutions based on charging shift, EV load shedding, or reactive power modulation. The latter has been investigated in this thesis, with respect to the effectiveness of EV reactive power provision when evaluating the installation of new off-board chargers in residential LV grids. A generalized formulation has been proposed, with the aim of evaluating effectiveness and limitations of such technology on all kinds of radial distribution feeders. The application is meant for DSOs when evaluating new installations of fast chargers in LV

feeders, as an alternative to more computationally expensive power flow calculations. Results showed that the effect of the capacitive reactive power is influenced mostly by the absolute values of the LV feeder impedance, specifically by the length. The validation analysis on realistic LV feeders for the case of a fixed capacitive power factor of 0.9 proved that the voltage rise would amount to 0.012 p.u., in comparison to the case of EV charging with unitary power factor. Such voltage drop reductions can potentially avoid the violation of voltage thresholds, thus assuring compliance with grid technical standards on voltage levels. However, this precaution may not be sufficient for massive penetration of EVs, since a combination with other smart charging strategies such as charging modulation and/or charging shifting may be essential for the prevention of unacceptable under-voltage conditions. In conclusion, reactive power control has to be seen as a possible connection capability requirement, able to mitigate the self-induced negative effects of fast charging EVs in LV distribution grids. In this regard, the newly released Danish technical standard for stationary storage systems (which explicitly includes V2G charging stations) has included reactive power capabilities similarly to the requirements for new PV plants.

6.1 Future research

The results obtained in this Ph.D. project have also uncovered possible topics for further research. These topics are elaborated in the following:

- Within the broad topic of the acquisition of EV flexibility services, some aspects have not been touched upon in this thesis, and should then be investigated in future works. Among others, the development of market models for aggregators as well as for DSOs is of interest, along with the definition of a price for the flexibility service on the distribution level. Furthermore, within the domain of the proposed analysis on the arising conflicts when acquiring EV flexibility, the issue of double remuneration still needs to be investigated, i.e., when the activation of the same flexibility product can jointly satisfy the needs of different stakeholders.
- As extension of the contribution on the EV aggregation strategy that employs a stochastic logic, in a future work the controller has to be generalized by considering arbitrary target set-points and non-symmetrical assigned reserve capacities. Furthermore, an experimental validation on real V2G chargers performing FNR under realistic conditions has to be carried out.
- With respect to the proposed recommendations for TSOs on EV fleet requirements when providing primary frequency regulation, it is worth mentioning that possible additional precautions could be deployed and included with the aim at assuring safe and reliable operation also for larger EV shares and/or delays. In fact, in some cases a smooth overall response could be needed, achievable for instance by introducing additional requirements on

the whole aggregated EV fleet response. These aspects could be investigated within future works.

- System stability studies with heterogeneous mix of EV aggregation in terms of both uni- and bi-directional EVs and different response times are also of interest, in order to take into account more aspects of the realistic complexity of the portfolio of EV aggregators. Furthermore, the heterogeneity can also include the control of private EVs connected to slow-rate chargers in households, thus going beyond the investigation with EVs and chargers within commercial fleets carried out within this thesis.
- The proposed analyses of EV reactive power provision for voltage support in LV grids was meant for new three-phase off-board EV chargers, not assessing the issue of unbalanced conditions, typical of distribution networks. Future research should cover similar investigations in unbalanced grids. In this case, the approach to the problem would be slightly different, as the DSO analysis would not be aiming at evaluating permission for installation of new off-board fast chargers, instead the focus would be on the effects of unbalanced voltage support by capacitive reactive power provision by single-phase EVs.
- Last but not least, the impact on the battery degradation due to the provision of a grid service is of paramount importance. In fact, the knowledge of the added degradation is crucial when assessing the applicability and the economic viability of such technology. It is clear that only in case of limited loss of battery capacity, successful business models can be deployed. In this respect, detailed EV battery models should be developed and tests on EVs that have already been controlled for a sufficiently long period of time should be performed, in order to assess the life length reduction due the calendar losses, the driving, and the grid service provision.

APPENDIX A

Representative Danish and Norwegian LV distribution grids

The modelled Danish LV distribution feeder is operated by the local DSO SEAS-NVE, and has been extensively utilized for research activities within the framework of the NIKOLA project. The network is a semi-urban LV grid located in southern Zealand, Denmark. It is radially run and connected to the 10 kV MV network through a 400 kVA 10/0.4 kV distribution transformer.

Although in realty 4 distribution feeders branch out from the transformer, only one is modelled in detail as depicted in the singe line diagram in Figure 2.2. All LV network is supplied by underground cables composed of 13 segments, and a total of 43 households are connected within the observed area. They are three-phase connected with a common neutral conductor grounded only at the transformer station. However, when performing unbalanced load-flow studies, an uneven load distribution among the phases is considered (50%:25%:25% among phases a, b, and c, according to the DSO experience).

For the studies reported in Subsection 5.5.2, the 3-phase balanced loading and the single-feeder characteristics (transformer-bus) are in Table App.1. It has been decided to simulate the worst case of maximum loading condition of a winter week, when high load demand is present due to heat pumps heating systems, while there is no PV production due to weather conditions. Given the house location and specific characteristics, the feeder can be divided into two zones:

- zone A where houses have implemented district heating and no PVs, and
- zone B where each house is equipped with a heat pump and a PV installation.

Table App.1. Properties of the real Danish LV grid transformer-bus feeder and loading at each bus.

Receiving Bus	Total length from the transformer [m]	Cable type	R [Ω/km]	X [Ω /km]	$R/X_{LVfeeder}$	P_{load_0} [kW]	$\cos \varphi_{load}$
B601	112	4 x 150 mm^2 Al PEX	0.207	0.078	2.8	0	-
B602	161	4 x 150 mm^2 Al PEX	0.207	0.078	2.8	8.21	0.95
B603	225	4 x 150 mm^2 Al PEX	0.207	0.078	2.8	5.48	0.95
B604	312	4 x 150 mm^2 Al PEX	0.207	0.078	2.8	11.88	0.95
B606	217	4 x 150 mm^2 Al PEX	0.207	0.078	2.8	0	-
B607	263	4 x 150 mm^2 Al PEX	0.207	0.078	2.8	16.14	0.95
B608	300	4 x 150 mm^2 Al PEX	0.207	0.078	2.8	11.19	0.95
B609	257	4 x 150 mm^2 Al PEX	0.207	0.078	2.8	9.98	0.95
B610	292	4 x 150 mm^2 Al PEX	0.207	0.078	2.8	13.71	0.95
B611	328	4 x 150 mm^2 Al PEX	0.207	0.078	2.8	13.85	0.95
B612	363	4 x 150 mm^2 Al PEX	0.207	0.078	2.8	14.18	0.95
B613	398	4 x 150 mm^2 Al PEX	0.207	0.078	2.8	12.59	0.95

The analyzed Norwegian LV distribution grid is provided by the local DSO Nord-Trøndelag Elektrisitetsverk Holding AS (NTE). It is located in Steinkjer, in the county of Nord-Trøndelag.

A single-line diagram has been presented in Figure 2.5. It consists of the following main parts:

- A 500 kVA distribution transformer;
- 20 distribution feeder lines, A1-M2, branching out from the transformer;
- 54 end-user buses.

In reality, there are 95 end-users present in the system, but some of these live in various forms of shared housing, such as row houses or apartment blocks, thus sharing the same connection line. These larger nodes have been aggregated into single loads, and are marked with a larger, green-colored symbol in the single-line diagram in Figure 2.5. After this aggregation, the total number of end-users is 54. The numbering of the end-users is the same as in the data delivered from NTE. Note that three buses, no. 10, 32 and 53, are identified as an elderly care home, a grocery store and a school, respectively. 48 end-users have been anonymized by the DSO, but display load profiles and a total energy consumption indicative to common households, and the remaining buses is marked as households.

Table App.2 reports the line properties of the modelled Norwegian distribution grid.

Table App.2. Properties of the real Norwegian LV grid.

Sending Bus	Receiving Bus	Line length [m]	Cable type	*R* [Ω/km]	*X* [Ω /km]
Trafo	**A1**	89	3 x 240 mm^2 Al PEX	0.124	0.072
A1	**A2**	48	3 x 150 mm^2 Al PEX	0.209	0.069
Trafo	**B**	66	3 x 240 mm^2 Al PEX	0.124	0.072
Trafo	**C**	249	3 x 240 mm^2 Al PEX	0.124	0.072
Trafo	**D1**	45	3 x 240 mm^2 Al PEX	0.124	0.072
D1	**D2**	15	3 x 50 mm^2 Al PVC	0.641	0.079
Trafo	**E**	180	3 x 150 mm^2 Al PEX	0.209	0.069
Trafo	**F1**	85	3 x 150 mm^2 Al PEX	0.209	0.069
F1	**F2**	53	4 x 95 mm^2 Al PEX	0.320	0.075
Trafo	**G1**	190	3 x 240 mm^2 Al PEX	0.124	0.072
G1	**G2**	62	3 x 150 mm^2 Al PEX	0.209	0.069
G2	**G3**	47	3 x 95 mm^2 Al PEX	0.320	0.076
G3	**G4**	22	3 x 50 mm^2 Al PVC	0.641	0.079
Trafo	**H**	127	3 x 150 mm^2 Al PEX	0.209	0.069
Trafo	**I**	90	3 x 150 mm^2 Al PEX	0.209	0.069
Trafo	**J**	95	3 x 150 mm^2 Al PEX	0.209	0.069
Trafo	**K**	25	3 x 95 mm^2 Al PEX	0.320	0.076
Trafo	**L**	15	3 x 95 mm^2 Al PEX	0.320	0.076
Trafo	**M1**	50	4 x 95 mm^2 Al PEX	0.320	0.075
M1	**M2**	32	4 x 95 mm^2 Al PEX	0.320	0.075

Bibliography

[1] N. Stern, “The Economics of Climate Change,” 2006.

[2] European Commission, “EU action against climate change Leading global action to 2020 and beyond,” 2008.

[3] European Commission, “Energy Roadmap 2050,” 2012.

[4] European Commision, “A policy framework for climate and energy in the period from 2020 to 2030,” 2014.

[5] U. N., “The Paris agreement on climate change.” 2015.

[6] The Danish Government, “The Danish Climate Policy Plan,” 2013.

[7] IEA International Energy Agency, “Energy policies of IEA countries - Norway,” 2017.

[8] IEA International Energy Agency, “Transport Energy and CO2 : Moving towards Sustainability,” 2009.

[9] EPRI, “Environmental assessment of plug-in hybrid electric vehicles,” *Technical Report 1015325, Electric Power Research Institute*, vol. 1, pp. 1–38, 2007.

[10] L. D. D. Harvey, “Global climate-oriented building energy use scenarios,” *Energy Policy*, vol. 67, pp. 473–487, 2014.

[11] W. Kempton and J. Tomić, “Vehicle-to-grid power implementation: From stabilizing the grid to supporting large-scale renewable energy,” *Journal of Power Sources*, vol. 144, no. 1, pp. 280–294, 2005.

[12] “Internation Energy Agency. Lessons from liberalised electricity markets,” 2006.

[13] D. E. M. Bondy, “Demand Response for a Secure Power System Operation,” Technical University of Denmark, 2016.

[14] V. Lakshmanan, M. Marinelli, J. Hu, and H. W. Bindner, “Provision of secondary frequency control via demand response activation on thermostatically controlled loads: Solutions and experiences from Denmark,” *Applied Energy*, vol. 173, pp. 470–480, 2016.

[15] S. Ruester, S. Schwenen, C. Batlle, and I. Pérez-Arriaga, “From distribution networks to smart distribution systems: Rethinking the regulation of European electricity DSOs,” *Utilities Policy*, vol. 31, pp. 229–237, Dec. 2014.

[16] EvolvDSO, “D1.2 – Evaluation of current market architectures and regulatory frameworks and the role of DSOs,” 2014.

[17] “European Photovoltaic Industry Association. Global Market Outlook For Solar Power 2018-2022,” 2018.

[18] “Global Wind Energy Council. Global wind statistics.” [Online]. Available: http://gwec.net/global-figures/graphs/.

[19] “Institute of Electrical and Electronics Engineers (IEEE). IEEE Smart Grid.” [Online]. Available: http://smartgrid.ieee.org. [Accessed: 02-Dec-2018].

[20] IEA International Energy Agency, “Global EV Outlook 2018,” 2018.

[21] Insero, “Insero quarterly 2018 q2,” 2018.

[22] IEA International Energy Agency, “Nordic EV Outlook 2018,” 2018.

[23] International Electrotechnical Comission, “International Standard: Plugs, socket-outlets, vehicle couplers and vehicle inlets. Conductive charging of electric vehicles.,” 2003.

[24] S. Schey, D. Scoffield, and J. Smart, “A first look at the impact of electric vehicle charging on the electric grid in the EV project,” in *World Electric Vehicle Journal*, 2012, vol. 5, no. 3, pp. 667–678.

[25] “SYSLAB-PowerLabDK.” [Online]. Available: http://www.powerlab.dk/facilities/syslab.aspx.

[26] A. Gadea, M. Marinelli, and A. Zecchino, “A Market Framework for Enabling Electric Vehicles Flexibility Procurement at the Distribution Level Considering Grid Constraints,” in *20th Power Systems Computation Conference (PSCC 2018)*, 2018, pp. 1–7.

[27] M. Lillebo, S. Zaferanlouei, A. Zecchino, and H. Farahmand, “Impact of Large-Scale EV Integration and Fast Chargers in a Norwegian LV Grid,” in *7th International Conference on Renewable Power Generation*, 2018.

[28] A. Zegers and H. Brunner, “TSO-DSO interaction: An Overview of current interaction between transmission and distribution system operators and an assessment of their cooperation in Smart Grids,” 2014.

[29] ENTSO-E, CEDEC, GEODE, EURELECTRIC, and E. for S. Grids, “TSO–DSO Data Management Report,” 2016.

[30] Eurelectric, ENTSO-E, GEODE, E. for smart Grids, and CEDEC, “General Guidelines for Reinforcing the Cooperation between TSOs and DSOs,” 2015.

[31] Z. Liu, Q. Wu, A. H. Nielsen, and Y. Wang, “Day-ahead energy planning with 100% electric vehicle

penetration in the nordic region by 2050," *Energies*, vol. 7, no. 3, pp. 1733–1749, 2014.
[32] Energinet.dk, "Danish Technical Standard: ancillary services to be delivered in Denmark - tender conditions," *https://en.energinet.dk/-/media/Energinet/El-RGD/Dokumenter/Ancillary-services-to-be-delivered-in-Denmark.pdf*, 2017. .
[33] K. Clement-Nyns, E. Haesen, and J. Driesen, "The impact of vehicle-to-grid on the distribution grid," *Electric Power Systems Research*, vol. 81, no. 1, pp. 185–192, 2011.
[34] A. Rodriguez-Calvo, R. Cossent, and P. Frías, "Integration of PV and EVs in unbalanced residential LV networks and implications for the smart grid and advanced metering infrastructure deployment," *International Journal of Electrical Power and Energy Systems*, vol. 91, pp. 121–134, 2017.
[35] "European Technical Standard EN 50160," 2011.
[36] Eurelectric Union of the Electricity Industry, "Power Distribution in Europe: Facts & Figures," 2013.
[37] T. A. Short, "Voltage Regulation," in *Electric Power Distribution Handbook*, CRC Press, 2004.
[38] iPower consortium, "[iPower] Development of a Dso - Market on Flexibility Services," pp. 1–78, 2013.
[39] S. Chattopadhyay, M. Mitra, and S. Sengupta, *Electric power quality*. Springer, 2011.
[40] Test-an-EV consortium, "Test-an-EV project: Electric vehicle (EV) data." [Online]. Available: http://mclabprojects.di.uniroma1.it/smarthgnew/Test-an-EV/?EV-code=. [Accessed: 24-Sep-2018].
[41] P. Bach, O. Jan, C. Amtrup, P. B. Andersen, O. J. Olesen, and B. Christensen, "The Nikola Project Intelligent Electric Vehicle Integration," in *5th IEEE PES Innovative Smart Grid Technologies European Conference (ISGT)*, 2014, pp. 1–6.
[42] K. Knezović, S. Martinenas, P. B. Andersen, A. Zecchino, and M. Marinelli, "Enhancing the Role of Electric Vehicles in the Power Grid : Field Validation of Multiple Ancillary Services," *IEEE Transactions on Transportation Electrification*, vol. 3, no. 1, pp. 201–209, 2016.
[43] N. Leemput, F. Geth, J. Van Roy, J. Büscher, and J. Driesen, "Reactive power support in residential LV distribution grids through electric vehicle charging," *Sustainable Energy, Grids and Networks*, vol. 3, pp. 24–35, 2015.
[44] K. Knezović and M. Marinelli, "Phase-wise enhanced voltage support from electric vehicles in a Danish low-voltage distribution grid," vol. 140, pp. 274–283, 2016.
[45] K. Knezović, M. Marinelli, A. Zecchino, P. B. Andersen, and C. Træholt, "Supporting involvement of electric vehicles in distribution grids: Lowering the barriers for a proactive integration," *Energy*, 2017.
[46] ENTSO-E, "Survey on ancillary services procurement , balancing market design 2015," 2016.
[47] Z. Zhou, T. Levin, and G. Conzelmann, "Survey of U. S. ancillary services markets," 2016.
[48] K. Knezović, "Active integration of electric vehicles in the distribution network – theory, modelling and practice," Technical University of Denmark, 2017.
[49] C. Bergaentzlé, L. Boscán, K. Skytte, E. Rosenlund Soysal, and O. J. Olsen, "Framework Conditions for Flexibility in the Electricity Sector," 2016.
[50] O. Borne, K. Korte, Y. Perez, M. Petit, and A. Purkus, "Barriers to entry in frequency-regulation services markets: Review of the status quo and options for improvements," *Renewable and Sustainable Energy Reviews*, vol. 81, no. July 2016, pp. 605–614, 2018.
[51] J. Kester, L. Noel, G. Zarazua de Rubens, and B. K. Sovacool, "Promoting Vehicle to Grid (V2G) in the Nordic region: Expert advice on policy mechanisms for accelerated diffusion," *Energy Policy*, vol. 116, no. October 2017, pp. 422–432, 2018.
[52] J. MacDonald, P. Cappers, D. Callaway, and S. Kiliccote, "Demand response providing ancillary services - A Comparison Of Opportunities And Challenges In The US Wholesale Markets," in *Grid-Interop Forum 2012*, 2012.
[53] SEDC Smart Energy Demand Coalition, "Explicit Demand Response in Europe: Mapping the Markets 2017," 2017.
[54] M. G. Arentsen, H. Juhler-Verdoner, J. Møller Jørgensen, U. Stougaard Kiil, and M. Holst, "Market models for aggregators - activation of flexibility," 2017.
[55] Y. Arafat, L. Bertling Tjernberg, and P.-A. Gustafsson, "Possibilities of demand side management with Smart Meters," in *International Conference on Electricity Distribution, CIRED 2015*, 2015, pp. 1–5.
[56] P. Siano, "Demand response and smart grids - A survey," *Renewable and Sustainable Energy Reviews*, vol. 30, pp. 461–478, 2014.
[57] European Commission, "Commission recommendation on preparations for the roll-out of smart metering systems," *Official Journal of the European Union*, no. 2011, pp. 9–22, 2012.
[58] European Commission, "Directive of 2009/72/EC of the European Parliament and of the Council of 13 July 2009 Concerning Common Rules for the Internal Market in Electricity and Repealing Directive 2003/54/EC," *Official Journal of the European Union*, vol. L211, no. August, p. L 211/55-L 211/93, 2009.
[59] IEC 61851-1:2010, "Electric vehicle conductive charging system – Part 1: General requirements." 2010.
[60] SAE J1772:2010, "Electric vehicle and plug in hybrid electric vehicle conductive charge coupler." 2010.
[61] IEC/ISO 15118-1:2013, "Road vehicles — Vehicle to grid communication interface — Part 1: General information and use-case definition." 2013.
[62] "CHAdeMO protocol." [Online]. Available: https://www.chademo.com/. [Accessed: 08-Dec-2018].
[63] Open Charge Alliance, "Open charge point protocol (OCPP) 1.6." .
[64] e-Laad and Smartlab and Blue Corner, "Open clearing house protocol (OCHP) 1.3." .
[65] Open Charge Alliance, "Open smart charging protocol (OSCP) 1.0." .
[66] Eurelectric, "Flexibility and aggregation - requirements for their interaction in the market," 2015.

[67] H. Gerard, E. Rivero, and D. Six, “Basic schemes for TSO-DSO coordination and ancillary services provision,” 2016.
[68] R. Li, Q. Wu, and S. Oren, “Distribution Locational Marginal Pricing for Optimal Electric Vehicle Charging Management,” *IEEE Transactions on Smart Grid*, vol. 29, no. 1, pp. 203–211, 2014.
[69] L. Bai, J. Wang, C. Wang, C. Chen, and F. Li, “Distribution Locational Marginal Pricing (DLMP) for Congestion Management and Voltage Support,” *IEEE Transactions on Power Systems*, vol. 33, no. 4, pp. 4061–4073, 2018.
[70] Z. Liu, Q. Wu, S. S. Oren, S. Huang, R. Li, and L. Cheng, “Distribution locational marginal pricing for optimal electric vehicle charging through chance constrained mixed-integer programming,” *IEEE Transactions on Smart Grid*, vol. 9, no. 2, pp. 644–654, 2018.
[71] J. Lin and K. Knezović, “Comparative Analysis of Possible Designs for Flexible Distribution System Operation,” in *2016 13th International Conference on the European Energy Market (EEM)*, 2016, pp. 1–5.
[72] F. Baccino, S. Grillo, S. Massucco, G. Mauri, P. Mora, and F. Silvestro, “An aggregator for demand side management at domestic level including PEVs,” *2014 IEEE International Electric Vehicle Conference, IEVC 2014*, 2014.
[73] D. S. Callaway and I. A. Hiskens, “Achieving Controllability of Electric Loads,” *Proceedings of the IEEE*, vol. 99, no. 1, pp. 184–199, Jan. 2011.
[74] E. Vrettos, C. Ziras, and G. Andersson, “Fast and Reliable Primary Frequency Reserves from Refrigerators with Decentralized Stochastic Control,” *IEEE Transactions on Power Systems*, vol. 32, no. 4, pp. 2924–2941, 2017.
[75] C. Gouveia, C. L. Moreira, J. Abel, P. Lopes, and D. Varajão, “Microgrid Service Restoration,” *IEEE Industrial Electronics Magazine*, vol. 7, no. 4, pp. 26–41, 2013.
[76] F. Baccino, F. Conte, S. Grillo, S. Massucco, and F. Silvestro, “An Optimal Model-Based Control Technique to Improve Wind Farm Participation to Frequency Regulation,” *IEEE Transactions on Sustainable Energy*, vol. 6, no. 3, pp. 993–1003, 2015.
[77] “Nissan, enel and nuvve operate world’s first fully commercial vehicle-to-grid hub in denmark,” 2016. [Online]. Available: http://www.nissan-helsingor.dk/index.php/om-os/nyheder/show/news/id/4. [Accessed: 19-Oct-2018].
[78] Phoenix Contact, “EV Charge Control: Standard-compliant control of the Control Pilot and Proximity Plug interfaces between the electric vehicle and charging station. (User manual).” 2015.
[79] P. M. R. Almeida, F. J. Soares, and J. A. P. Lopes, “Electric vehicles contribution for frequency control with inertial emulation,” *Electric Power Systems Research*, vol. 127, pp. 141–150, 2015.
[80] J. Meng, Y. Mu, H. Jia, J. Wu, X. Yu, and B. Qu, “Dynamic frequency response from electric vehicles considering travelling behavior in the Great Britain power system,” *Applied Energy*, vol. 162, pp. 966–979, 2016.
[81] X. Luo, S. Xia, and K. W. Chan, “A decentralized charging control strategy for plug-in electric vehicles to mitigate wind farm intermittency and enhance frequency regulation,” *Journal of Power Sources*, vol. 248, pp. 604–614, Feb. 2014.
[82] S. Izadkhast, P. Garcia-Gonzalez, and P. Frías, “An Aggregate Model of Plug-In Electric Vehicles for Primary Frequency Control,” *IEEE Transactions on Power Systems*, vol. 30, no. 3, pp. 1475–1482, 2015.
[83] H. Liu, Z. Hu, Y. Song, and J. Lin, “Decentralized Vehicle-to-Grid Control for Primary Frequency Regulation Considering Charging Demands,” *IEEE Transactions on Power Systems*, vol. 28, no. 3, pp. 3480–3489, Aug. 2013.
[84] H. N. T. Nguyen, C. Zhang, and J. Zhang, “Dynamic Demand Control of Electric Vehicles to Support Power Grid With High Penetration Level of Renewable Energy,” *IEEE Transactions on Transportation Electrification*, vol. 2, no. 1, pp. 66–75, 2016.
[85] P. Hanemann, M. Behnert, and T. Bruckner, “Effects of electric vehicle charging strategies on the German power system,” *Applied Energy*, vol. 203, pp. 608–622, 2017.
[86] H. Shareef, M. M. Islam, and A. Mohamed, “A review of the stage-of-the-art charging technologies, placement methodologies, and impacts of electric vehicles,” *Renewable and Sustainable Energy Reviews*, vol. 64, pp. 403–420, 2016.
[87] Y. Zhao, M. Noori, and O. Tatari, “Vehicle to Grid regulation services of electric delivery trucks: Economic and environmental benefit analysis,” *Applied Energy*, vol. 170, pp. 161–175, 2016.
[88] F. Yang, C. Bai, H. Huang, B. He, and B. Hu, “Evaluation of the impact of large-scale electric vehicle on power grid economy,” *Proceedings - 2015 International Conference on Smart Grid and Clean Energy Technologies, ICSGCE 2015*, pp. 164–169, 2016.
[89] K. M. Tan, V. K. Ramachandaramurthy, and J. Y. Yong, “Integration of electric vehicles in smart grid: A review on vehicle to grid technologies and optimization techniques,” *Renewable and Sustainable Energy Reviews*, vol. 53, pp. 720–732, 2016.
[90] I. Rahman, P. M. Vasant, B. S. M. Singh, M. Abdullah-Al-Wadud, and N. Adnan, “Review of recent trends in optimization techniques for plug-in hybrid, and electric vehicle charging infrastructures,” *Renewable and Sustainable Energy Reviews*, vol. 58, pp. 1039–1047, 2016.
[91] J. Hu, H. Morais, T. Sousa, and M. Lind, “Electric vehicle fleet management in smart grids: A review of services, optimization and control aspects,” *Renewable and Sustainable Energy Reviews*, vol. 56, pp. 1207–1226, 2016.
[92] E. Sortomme and K. W. Cheung, “Intelligent Dispatch of Electric Vehicles Performing Vehicle-to-Grid

Regulation," in *2012 IEEE International Electric Vehicle Conference*, 2012, pp. 1–6.
[93] A. Molina-garcía, F. Bouffard, and D. S. Kirschen, "Decentralized Demand-Side Contribution to Primary Frequency Control," *IEEE Transactions on Power Systems*, vol. 26, no. 1, pp. 411–419, 2011.
[94] S. Koch, J. L. Mathieu, and D. S. Callaway, "Modeling and Control of Aggregated Heterogeneous Thermostatically Controlled Loads for Ancillary Services," in *17th Power Systems Computation Conference*, 2011, pp. 1–8.
[95] M. González Vayá and G. Andersson, "Combined Smart-Charging and Frequency Regulation for Fleets of Plug-in Electric Vehicles," in *2013 IEEE Power & Energy Society General Meeting*, 2013, pp. 1–5.
[96] M. R. V. Moghadam, R. Zhang, and R. T. B. Ma, "Distributed Frequency Control via Randomized Response of Electric Vehicles in Power Grid," *IEEE Transactions on Sustainable Energy*, vol. 7, no. 1, pp. 312–324, 2016.
[97] S. Izadkhast, P. Garcia-Gonzalez, P. Frìas, L. Ramìrez-Elizondo, and P. Bauer, "An Aggregate Model of Plug-in Electric Vehicles Including Distribution Network Characteristics for Primary Frequency Control," *IEEE Transactions on Power Systems*, vol. 31, no. 4, pp. 2987–2998, 2016.
[98] F. Lehfuss, M. Nöhrer, M. Faschang, S. Ledinger, and F. Kupzog, "Comprehensive Infrastrusture for Electric Vehicle Charging Interoperability and Grid Compliance Testing," *International Journal of Distributed Energy Resources and Smart Grids*, pp. 29–42, 2015.
[99] R. Abousleiman and R. Scholer, "Smart charging: System design and implementation for interaction between plug-in electric vehicles and the power grid," *IEEE Transactions on Transportation Electrification*, vol. 1, no. 1, pp. 18–25, 2015.
[100] M. Marinelli, S. Martinenas, K. Knezović, and P. B. Andersen, "Validating a centralized approach to primary frequency control with series-produced electric vehicles," *Journal of Energy Storage*, vol. 7, pp. 63–73, 2016.
[101] ENTSO-E, "Frequency Stability Evaluation Criteria for the Synchronous Zone of Continental Europe - Requirements and impacting factors," Brussels, Belgium, 2016.
[102] Nordic Energy Regulators NordREG, "Nordic Market Report," 2014.
[103] "National Smart Grid Laboratory." [Online]. Available: https://www.sintef.no/en/all-laboratories/smartgridlaboratory/. [Accessed: 31-Jul-2017].
[104] E. De Jong, R. De Graff, P. Vaessen, P. Crolla, A. Roscoe, F. Lehfuss, G. Lauss, P. Kotsampopoulos, and F. Gafaro, "European White Book on Real-Time Powerhardware-in-the-Loop testing," Arnhem, Netherlands, 2011.
[105] C. Seitl, J. Kathan, G. Lauss, and F. Lehfuss, "Power hardware-in-The-loop implementation and verification of a real time capable battery model," in *IEEE International Symposium on Industrial Electronics*, 2014, pp. 2285–2290.
[106] Q. Hong, I. Abdulhadi, A. Roscoe, and C. Booth, "Application of a MW-Scale Motor-Generator Set to Establish Power-Hardware-in-the-Loop Capability," in *presented at IEEE International Conference on Innovative Smart Grid Technologies IEEE ISGT Europe 2017*, 2017, pp. 1–6.
[107] "ACES project - across continents electric vehicle services," *http://aces-bornholm.eu*, 2017. .
[108] "The Parker project," *http://parker-project.com*, 2016. .
[109] "INVENT project - Intelligent Electric Vehicle Integration," *https://rmp.ucsd.edu/_files/sei/INVENT-Flyer.pdf*, 2017. .
[110] A. Thingvad, S. Martinenas, P. B. Andersen, M. Marinelli, C. Bjørn E, and O. J. Olesen, "Economic Comparison of Electric Vehicles Performing Unidirectional and Bidirectional Frequency Control in Denmark with Practical Validation," in *2016 Proceedings of the 51st International Universities Power Engineering Conference*, 2016, pp. 1–6.
[111] "Danish Technical regulation 3.3.1 for battery plants." Energinet.dk, 2017.
[112] "Statnett." [Online]. Available: http://www.statnett.no/. [Accessed: 31-Oct-2018].
[113] J. A. Short, D. G. Infield, and L. L. Freris, "Stabilization of grid frequency through dynamic demand control," *IEEE Transactions on Power Systems*, vol. 22, no. 3, pp. 1284–1293, 2007.
[114] C. Ziras, E. Vrettos, and S. You, "Controllability and stability of primary frequency control from thermostatic loads with delays," *Journal of Modern Power Systems and Clean Energy*, vol. 5, no. 1, pp. 43–54, 2017.
[115] M. R. Vedady Moghadam, R. T. B. Ma, and R. Zhang, "Distributed Frequency Control in Smart Grids via Randomized Demand Response," *IEEE Transactions on Smart Grid*, vol. 5, no. 6, pp. 2798–2809, 2014.
[116] S. Izadkhast, S. Member, P. Garcia-gonzalez, and P. Fr, "Design of Plug-In Electric Vehicle ' s Frequency-Droop Controller for Primary Frequency Control and Performance Assessment," vol. 32, no. 6, pp. 4241–4254, 2017.
[117] J. Østergaard and J. Nielsen, "The Bornholm Power System An Overview," 2008.
[118] Y. Chen, Z. Xu, and J. Østergaard, "Frequency Analysis for Planned Islanding Operation in the Danish Distribution System - Bornholm," *Proceedings of the Universities Power Engineering Conference*, pp. 9–13, 2008.
[119] E. James-Smith and M. Togeby, "Security of Supply of Bornholm - Demand Side Options for System Reserves," 2007.
[120] "Bornholm Energi & Forsyning (BEOF)." [Online]. Available: https://beof.dk/el/. [Accessed: 06-Nov-2018].
[121] Y. MU, J. WU, J. Ekanayake, N. Jenkis, and H. JIA, "Primary Frequency Response From Electric Vehicles in the Great Britain Power System," *IEEE Transactions on Smart Grid*, vol. 4, no. 2, pp. 1142–1150, 2015.

[122] P. Kundur, *Power system stability and control*. 1994.
[123] S. R. P. Malik and G. S. Hope, "An adaptive control scheme for speed control of diesel driven power-plants," *IEEE Transactions on Energy Conversion*, vol. 6, no. 4, pp. 605–611, 1991.
[124] K. Gu, J. Chen, and V. Kharitonov, *Stability of Time- Delay Systems*. Secaucus, NJ, USA: Birkhauser Boston, Inc., 2003.
[125] C. Hjalmar, "Danish National Travel Survey," 2017.
[126] A. Kechroud, P. F. Ribeiro, and W. L. Kling, "Distributed generation support for voltage regulation: An adaptive approach," *Electric Power Systems Research*, vol. 107, no. 0, pp. 213–220, Feb. 2014.
[127] "Italian Technical Standard CEI 0-21 Rules for the connection to the LV electrical utilities." Norma Italiana CEI, 2012.
[128] "German Technical Standard VDE-AR-N 4105 Power generation systems connected to the low-voltage distribution network." FNN - Forum Netztechnik / Netzbetrieb im VDE, 2011.
[129] "Danish Technical Regulation 3.2.2 for PV power plants with a power output above 11 kW." Energinet.dk, 2015.
[130] R. Caldon, M. Coppo, and R. Turri, "Distributed voltage control strategy for LV networks with inverter-interfaced generators," *Electric Power Systems Research*, vol. 107, no. 0, pp. 85–92, Feb. 2014.
[131] J. Hu, M. Marinelli, M. Coppo, A. Zecchino, and H. W. Bindner, "Coordinated voltage control of a decoupled three-phase on-load tap changer transformer and photovoltaic inverters for managing unbalanced networks," *Electric Power Systems Research*, vol. 131, pp. 264–274, 2016.
[132] C. Heinrich, P. Fortenbacher, A. Fuchs, and G. Andersson, "PV-integration strategies for low voltage networks," *2016 IEEE International Energy Conference, ENERGYCON 2016*, vol. 2, no. 1, 2016.
[133] M. C. Kisacikoglu, M. Kesler, and L. M. Tolbert, "Single-Phase On-Board Bidirectional PEV Charger for V2G Reactive Power Operation," *IEEE Transactions on Smart Grid*, vol. 6, no. 2, pp. 767–775, 2015.
[134] R. J. Ferreira, L. M. Miranda, and R. E. Ara, "A New Bi-Directional Charger for Vehicle-to-Grid Integration," in *Innovative Smart Grid Technologies (ISGT Europe), 2011 2nd IEEE PES International Conference and Exhibition o*, 2011.
[135] M. C. Kisacikoglu, B. Ozpineci, and L. M. Tolbert, "Reactive Power Operation Analysis of a Single-Phase EV/PHEV Bidirectional Battery Charger," in *8th international conference on power electronics (ECCE)*, 2011, pp. 585–592.
[136] M. C. Kisacikoglu, B. Ozpineci, and L. M. Tolbert, "Examination of a PHEV Bidirectional Charger System for V2G Reactive Power Compensation," in *Proc. IEEE APEC Exposition*, 2010, pp. 458–465.
[137] M. Kesler, M. C. Kisacikoglu, and L. M. Tolbert, "Vehicle-to-Grid Reactive Power Operation Using Plug-In Electric Vehicle Bidirectional Offboard Charger," *IEEE TRANSACTIONS ON INDUSTRIAL ELECTRONICS*, vol. 61, no. 12, pp. 6778–6784, 2014.
[138] D. Steen, L. A. Tuan, O. Carlson, and L. Bertling, "Assessment of electric vehicle charging scenarios based on demographical data," *IEEE Transactions on Smart Grid*, vol. 3, no. 3, pp. 1457–1468, 2012.
[139] S. X. Chen, Y. S. F. Eddy, H. B. Gooi, M. Q. Wang, and S. F. Lu, "A centralized reactive power compensation system for LV distribution networks," *IEEE Transactions on Power Systems*, vol. 30, no. 1, pp. 274–284, 2015.
[140] B. A. De Souza, A. Márcio, and F. De Almeida, "Multiobjective Optimization and Fuzzy Logic Applied to Planning of the Volt / Var Problem in Distributions Systems," *IEEE Transactions on Power Systems*, vol. 25, no. 3, pp. 1274–1281, 2010.
[141] W. Huang, D. Gan, X. Xia, N. Kobayashi, and X. Xu, "Distributed Generation on Distribution System Voltage Regulation : An Optimization-based Approach," in *Power and Energy Society General Meeting, 2010 IEEE*, 2010, pp. 1–7.
[142] M. Manbachi, H. Farhangi, A. Palizban, and S. Arzanpour, "A novel Volt-VAR Optimization engine for smart distribution networks utilizing Vehicle to Grid dispatch," *International Journal of Electrical Power and Energy Systems*, vol. 74, pp. 238–251, 2016.
[143] H. Fakham, A. Ahmidi, F. Colas, and X. Guillaud, "Multi-Agent System for Distributed Voltage Regulation of Wind Generators Connected to Distribution Network," in *Proc innovative smart grid technologies conference Europe (ISGT Europe), IEEE PES*, 2010, pp. 1–6.
[144] B. Morvaj, K. Knezović, R. Evins, and M. Marinelli, "Integrating multi-domain distributed energy systems with electric vehicle PQ flexibility : Optimal design and operation scheduling for sustainable low-voltage distribution grids," *Sustainable Energy, Grids and Networks*, vol. 8, pp. 51–61, 2016.
[145] J. García-Villalobos, I. Zamora, K. Knezović, and M. Marinelli, "Multi-objective optimization control of plug-in electric vehicles in low voltage distribution networks," *Applied Energy*, vol. 180, pp. 155–168, 2016.
[146] R. Kohrs, K. Dallmer-Zerbe, M. Mierau, and C. Wittwer, "Autonomous Reactive Power Control by Electric Vehicles," in *Innovative Smart Grid Technologies Conference Europe (ISGT-Europe), 2014 IEEE PES*, 2014, pp. 1–6.
[147] J. Ying, V. K. Ramachandaramurthy, K. Miao, and N. Mithulananthan, "Bi-directional electric vehicle fast charging station with novel reactive power compensation for voltage regulation," *International Journal of Electrical Power and Energy Systems*, vol. 64, pp. 300–310, 2015.
[148] P. Krasselt, M. R. Suriyah, and T. Leibfried, "Reactive Power Support for Optimal Grid Integration of Fast-Charging Infrastructure in German Low-Voltage Networks," in *23rd International Conference on Electricity Distribution (CIRED)*, 2015, pp. 1–5.
[149] C. Winter, R. Schwalbe, M. Heidl, and W. Prüggler, "Harnessing PV inverter controls for increased hosting

capacities of smart low voltage grids Recent results from Austrian research and demonstration projects," in *4th Interntaional Workshop on Integration of Solar Power into Power Systems*, 2014, pp. 1–6.

[150] M. H. Haque, "Load flow solution of distribution systems with voltage dependent load models," *Electric Power System Research*, vol. 36, no. 3, pp. 151–156, 1996.

[151] W. W. Price, "IEEE Task Force on Load Representation for Dynamic Performance, Load representation for dynamic performance analysis," *IEEE Transactions on Power Systems*, vol. 8, no. 2, pp. 472–482, 1993.

[152] M. Diaz-Aguiló, J. Sandraz, R. Macwan, F. de León, S. Member, D. Czarkowski, C. Comack, D. Wang, and S. Member, "Field-Validated Load Model for the Analysis of CVR in Distribution Secondary Networks : Energy Conservation," *IEEE Transactions on Power Delivery*, vol. 28, no. 4, pp. 2428–2436, 2013.

[153] K. Strunz, "CIGRE Task Force C6.04.02 - Benchmark Systems for Network Integration of Renewable and Distributed Energy Resources," 2009.

[154] L. Felix, K. Serdar, and R. S. Raul, "COTEVOS - Specification of reference electricity networks," 2014.

Part II

Collection of Papers

Paper A

Title:

Identification of Conflicts between Transmission and Distribution System Operators when Acquiring Ancillary Services from Electric Vehicles

Authors:

Antonio Zecchino, Katarina Knezović and Mattia Marinelli

Published in:

7th IEEE PES Innovative Smart Grid Technologies Europe (ISGT Europe - 2017)

DOI: 10.1109/ISGTEurope.2017.8260127

Identification of Conflicts between Transmission and Distribution System Operators when Acquiring Ancillary Services from Electric Vehicles

Antonio Zecchino, Katarina Knezović, Mattia Marinelli
Center for Electric Power and Energy, Department of Electrical Engineering
Technical University of Denmark (DTU)
Risø Campus, Roskilde, Denmark
antozec@elektro.dtu.dk

***Abstract*—Distributed energy resources are able to provide services to grid operators, possibly with competing objectives. With the development of active distribution grid management, various market designs arise. Here, a reference market framework is considered, which allocates the available flexibility products according to requests coming from both distribution and transmission system operators. The goal of this paper is to provide an identification procedure that is able to detect, identify and catalogue possible conflicts among the involved stakeholders that take place when requesting and/or acquiring ancillary services from flexible units. The investigation is carried out considering a 3-area power system which allows to take into account local constraints as well as system-wide needs. As outcome, this paper identifies the conflicts from both a theoretical and a practical point of view, by means of descriptions/identification procedure and by visual examples, respectively.**

***Index Terms*—Ancillary services, Distribution system operator, Electric vehicles, Transmission system operator.**

I. Introduction

With the increasing penetration of intermittent distributed energy resources (DERs) in modern power systems, the need for additional ancillary services is evident, especially for balancing purposes. Furthermore, the displacement of traditional large power plants due to increased decentralization of generation poses challenges to transmission system operators (TSOs). In fact, they need to control the power system without access to conventional ancillary services from a few large power plants. This calls for replacing the traditional service providers with aggregated units mostly connected to low voltage (LV) grids.

By contrast, distribution system operators (DSOs) are facing technical challenges in accommodating the increasing amount of new electrical loads, e.g., electric vehicles (EVs), while searching for solutions that defer investment in grid reinforcement.

Since grid balancing is a responsibility of the TSO, whereas respecting the local grid constraints needs to be assured by the DSO, it is clear that greater cooperation between TSOs and DSOs is needed [1], [2].

Within this context, if managed properly, EVs become flexible resources that can improve the system operation, making them an attractive asset for both transmission and distribution system operators. In fact, EVs can be considered as distributed energy storage systems with large potential for network regulation [3], [4]. EVs can be capable of adjusting the battery charging process in order to provide different ancillary services for supporting the power grid, such as primary frequency control or voltage control [5]–[7].

It is clear that flexibility provided by EVs can match different needs and could potentially create conflicts dependent on which stakeholder uses flexibility and for what purpose. Flexibility products should be allocated based on technical and economic optimization, i.e., flexibility should be used where its potential is the highest [8]. Many possible market frameworks are proposed in the literature [9]–[13], defining roles and responsibilities of the involved stakeholders in different situations. In this work, a framework similar to the '*Common TSO-DSO Ancillary Service market model*' presented within the SmartNet project [13] is introduced. As a specific trait, it has a single flexibility platform, which has to cope with all the flexibility requests presented by the system operators, as well as the flexibility offers received by the aggregators.

The goal of the paper is to propose a catalogue of possible TSO/DSO conflicts that can take place when it comes to acquiring flexibility products. Furthermore, the work presents the logical assessment employed for the identifications of such conflicts, with highlighted research questions for future investigations. A simplified 3-area power system is taken as a reference for the investigation in order to consider both the local constraints and the system-wide needs. It is worth mentioning that the definition of an internal multi-objective

optimization algorithm that would be implemented by the flexibility platform operator is out of the scope of this work.

II. EV Flexibility Characteristics and Involved Stakeholders

Distributed energy resources are potential providers of flexibility services. This Section aims at defining a "flexibility product" when providing services either to DSOs or TSO, similar to the ancillary services for the TSO. The flexibility product can be defined as *the power adjustment sustained from a particular moment for a certain duration at a specific location* [10]. Among the various types of DERs, EVs are alleged to have special potentials that make them one of the most prominent sources of flexibility. Indeed, EVs are relatively large loads which are expected to be grid-connected and available for long periods of time (high degree of flexibility), and claim quick-response (even lower than 0.5 s [4]) potentially with bi-directional power flow capabilities (V2G) [3]. In this respect, the grid services that they can provide are presented in Table I [3].

TABLE I. EV Grid Services Adapted from [3]

System-wide services	
Name	***Description***
Primary Frequency Regulation	It keeps the frequency in an interval around 50 Hz
Secondary Frequency Regulation	It restores the frequency to 50 Hz after deviations
Tertiary Frequency Regulation	It replaces secondary regulation
Synthetic Inertia	It aims at emulating the mechanical inertia of the traditional rotating synchronous generators
Adaptive Charging	The charging is delayed or advanced in time based on, e.g., energy cost or renewable contents
Distribution grid services	
Name	***Description***
MV/LV Transformer and lines congestion management	It helps to mitigate over-loading of distribution transformers and cables
LV over-/under-voltages management	Massive penetration of small RES units as well as EVs could lead to over- or under-voltages
LV grid phase balancing	Single-phase EVs could help to mitigate the phase unbalances in LV distribution networks
Islanded microgrid and black start	One or a set of EVs able to sustain a small power system could be a valuable resource

The main stakeholders involved in the trading of EV flexibility products are listed below [11]:

TSO - responsible for the transmission system operation stability. It needs services, among others, for frequency control (from primary to tertiary reserve) and voltage support for the transmission grid.

DSO - responsible for the distribution grid operation and thereby for ensuring power delivery to customers at all times, without disturbing the transmission system. It needs services, among others, for peak-shaving (MV/LV transformer or lines congestion management) and local voltage control.

Balance Responsible Party (BRP) - financially responsible for the energy acquired from the power market. In case of deviations from the purchased energy, the BRP has to pay for imbalances to the TSO, since the TSO is forced to activate additional regulation in order to correct the imbalances.

EV owner - willing to offer flexibility to the EV aggregator within certain comfort and technical boundaries.

EV aggregator - collects all the flexibility offers from the EV owners of his fleet, makes correspondent contracts with them, and bids in the market. Based on individual EV capabilities, flexibility products are grouped and offered to the market.

III. Today DSO's role and Proposed Market Framework

Nowadays, in many European countries the TSO ancillary service provision from flexible DER units connected at LV levels is already possible. On the other hand, DSOs cannot acquire local services from the same DERs, since there is not yet a role for DSOs in the market [13]. Therefore, in the current market setup, the TSO/DSO conflicts that could take place mostly concern the local technical constraints of the distribution system infrastructure. In fact, since connected at a distribution level, DERs' adaptive management aimed at providing a TSO service may lead to local grid constraints violations. In particular, the induced technical issues that the DSO is supposed to face would mostly be congestions or under/over voltages. A possible mean to reduce these conflicts as much as possible is the enhancement of TSO/DSO cooperation. This can be achieved by information and data exchange in the grid expansion planning phase (long term), for congestion management contracts (long/medium term), as well as for the real time operation (short term) [8].

This work assumes a possible future DSO role as an active market player. In [14], several key attributes essential for the successful operation of future flexible distribution systems are identified, along with the possible DSO designs. The considered future European DSO model is called *evolvDSO* [15] and is expected to take the following responsibilities: network planning and operation processes, contracting of flexibility services and market facilitation with cooperation between system operators. Within this framework, it is clear that – compared to the contemporary situation – new issues will arise: not only technical but also economical and political when considering remuneration schemes and potential conflicts of interests. Thus, in order to catalogue such conflicts between TSO and DSOs when acquiring flexibility products, the prominent flexibility market framework is taken as a benchmark [13]. It includes all the listed stakeholders and defines a new day-ahead market dynamics in fact such a framework is analyzed with respect to the day-ahead trading of EV grid services. As a specific trait, it has a single flexibility platform that has to cope with all the flexibility requests presented by the system operators as well as the flexibility offers received by the aggregators. In this way, it is expected that grid constraints are implicitly taken into account, since the flexibility operator would manage both information about the location of flexible sources and the DSOs' needs for flexibility in different areas. The DSOs' flexibility requests are formulated according to the forecasted demand profiles that each DSO receives from the suppliers. Moreover, such a platform is supposed to allow flexibility procurement without jeopardizing the grid operation or creating extra costs [13]. A scheme of the

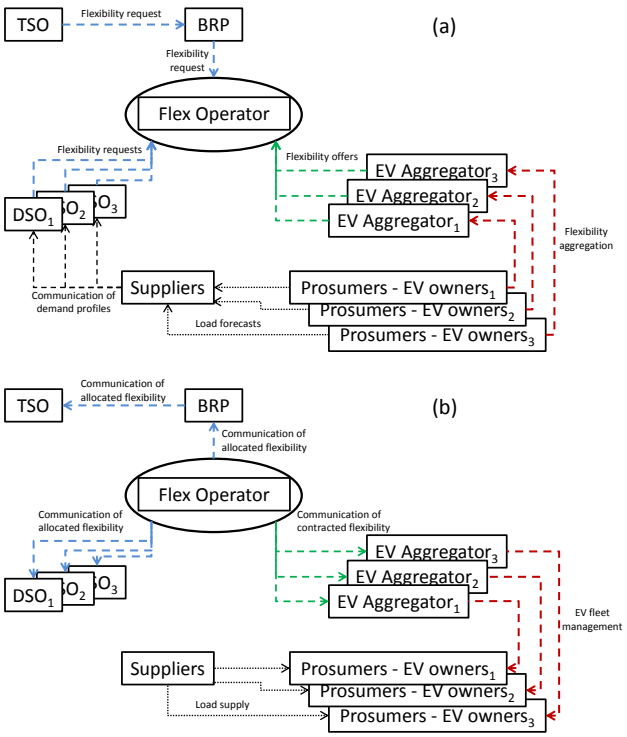

Figure 1. Proposed flexibility market framework for the day-ahead trading of EV grid services. (a) and (b) show the interactions among the involved stakeholders before and after the clearing process, respectively.

considered market framework is depicted in Fig. 1. It operates in several phases:

Phase 0 – Before the clearing process: the suppliers communicate to the DSOs the forecasted load profiles of their customers. EV aggregators contract flexibility with the EV owners in their fleets. The TSO trades flexibility through the BRP. (Fig. 1-a).

Phase 1 – Before the clearing process: DSOs and BRP present flexibility requests to the Flex Operator according to the information received by the suppliers and the TSO, respectively. EV aggregators offer flexibility according to the contracted aggregated availability from their EV fleets. (Fig. 1-a).

Phase 2 – The clearing process: the Flex Operator performs an evaluation based on multi-objective optimization algorithms that aim at optimally allocating the available flexibility products from a technical and economical point of view (e.g., respecting the technical needs while minimizing the total costs). The evaluation naturally considers that DSOs' local flexibility needs are linked to a particular localized congestion problem, whereas the TSO needs flexibility to maintain the system stability independently on the location of the resource. Eventual conflicts are identified and addressed according to the methodology proposed in Section IV.

Phase 3 – After the clearing process: the Flex Operator communicates the obtained optimal flexibility profiles to DSOs, BRP and EV aggregators, who will properly manage corresponding EV fleets. (Fig. 1-b).

IV. TSO/DSO Conflicts and Proposed Method for Identification

Different needs for flexibility services of each involved stakeholder can raise potential conflicts between two or more stakeholders with opposing needs. In fact, the activation of a given service could have a negative influence on other stakeholders or there could be a limited availability of flexibility, thus, only one stakeholder could acquire it. Within the market framework proposed in Section II, this kind of conflicts will be taken into consideration by the Flex Operator platform, which will detect them and then address them accordingly.

The goal of this Section is to provide an identification procedure, which is able to detect, identify and catalogue possible DSO/TSO conflicts that take place when requesting and/or acquiring flexibility products.

Since the complexity of the problem brings enormous amount of different potential conflicts, the here-presented analysis focuses on conflicts coming from TSO and DSOs flexibility requests for acquiring two specific services, namely primary frequency regulation and transformer congestion management, respectively.

Within this context, four conflicts have been identified:

Conflict (a): Need for compensating imbalances caused by activation of flexibility for solving a local distribution issue. The need for activating a service to solve a local DSO problem in a particular area may cause a problem at a system level in terms of balancing. In fact, considering a system in balanced operating conditions, a consumption decrease for preventing congestion at a distribution level would force the BRP to increase the consumption elsewhere. In this way, the balance would be guaranteed and the local congestion would be prevented.

Conflict (b): To solve a TSO request, activating the only available flexibility product causes distribution overloading. It concerns the prioritization problem between DSOs and TSO. When activating the only available flexibility to satisfy a TSO request would cause distribution overloading.

Conflict (c): The available flexibility can satisfy either the DSO request or the TSO request. It concerns the prioritization problem between DSOs and TSO. The offered flexibility would not be enough to satisfy all the needs.

Conflict (d): One flexibility product can solve several problems. Rather than a technical conflict, c*onflict (d)* presents an economical conflict that the Flex Operator may face mainly when remunerating aggregators. In fact, one offered asset could have all the necessary capabilities to concurrently satisfy both a TSO and a DSO need. Thus, it is important to define a fair way to remunerate the aggregator.

The flow-chart diagram in Fig. 2 shows step by step the proposed procedure that the Flex Operator is supposed to follow when managing flexibility requests and offers.

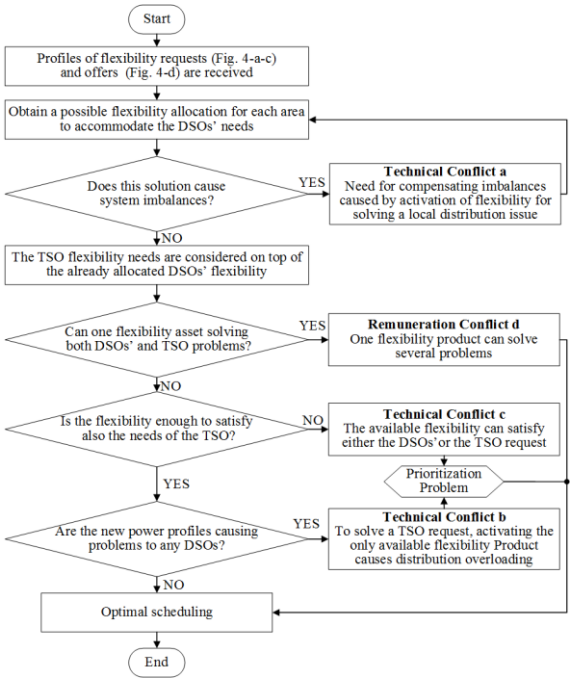

Figure 2. Flow-chart of the DSO/TSO conflict detection methodology.

First, the Flex Operator receives flexibility requests from DSOs and TSO as well as the offers profiles from the aggregators. Then, a possible allocation of flexibility over time for each location is formulated to accommodate the DSOs' needs. So, the Flex Operator checks whether the new power profiles (original DSOs' demand profiles over time with the addition/subtraction of the activated flexibility) would introduce problems from a balancing point of view. In this case, *conflict (a)* would be identified, and a new resource allocation would need to be obtained. Once a solution that does not introduce imbalances is found, the flexibility needs of the TSO are considered on top of the already allocated shares for the DSOs' needs. At this point, the methodology proposes to check whether with the same flexibility product both DSOs' and TSO's problems are solved. If yes, the best solution from a social point of view would be found, as it would involve the least possible amount of flexibility to satisfy all the needs. Though, the remuneration *conflict (d)* would be identified, which needs to be addressed while – in parallel – formulating the optimal solution. In case *conflict (d)* is not detected, the check on the presence of the other eventual technical *conflicts (b)* or *(c)* needs to be done. In particular, they concern the prioritization problem between DSOs and TSO when the offered flexibility is not enough to satisfy all the needs (*conflict (c)*), or in case the activation of the only available flexibility would cause distribution overloading (*conflict (b)*). Once one of these two conflicts is detected, an appropriate multi-objective optimization algorithm would be necessary to find an optimal solution, which will finally be communicated to all the involved stakeholders.

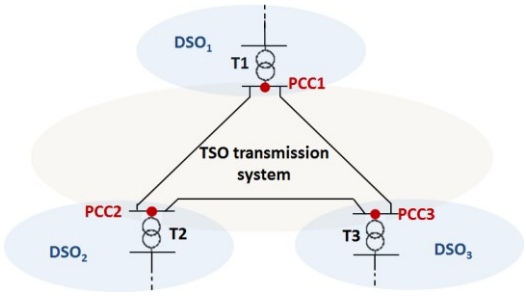

Figure 3. 3-area power system.

Within the contemporary market situation, it is clear that the proposed conflict detection methodology may change. In fact, the Flexibility Operator would have to manage requests for flexibility coming only from the TSO, so the only possible conflict would be *conflict (b)*. Thus, after receiving requests and offers, the Flexibility Operator would have to check whether problems are caused to DSO. If yes, then *conflict (b)* would be detected, and the optimal solution would be decided by the prioritization agreement and finally communicated to the involved stakeholders.

V. TSO/DSO Conflict Identification Examples

The proposed analysis is based on the investigation of possible dynamics in which the listed conflicts could take place. The investigation is carried out considering the simplified 3-area power system shown in Fig. 3. TSO's transmission lines link the DSOs' areas to each other through three transformers (T1, T2 and T3), whose points of common coupling are named PCC1, PCC2 and PCC3, respectively.

As aforementioned, for the sake of simplicity, the analysis considers only the need of preventing overloading of T1, T2 and T3, while all the others DSOs' technical needs (such as line congestion, under/over-voltages, or phase unbalances) are neglected. Regarding the TSO needs for ancillary services for primary regulation, a certain profile is assumed to be requested. Note that the TSO needs reserve, i.e., availability of flexible units to solve a problem that could potentially take place. On the other hand, for the DSO the flexibility product represents a real need for power to solve a concrete forecasted congestion problem.

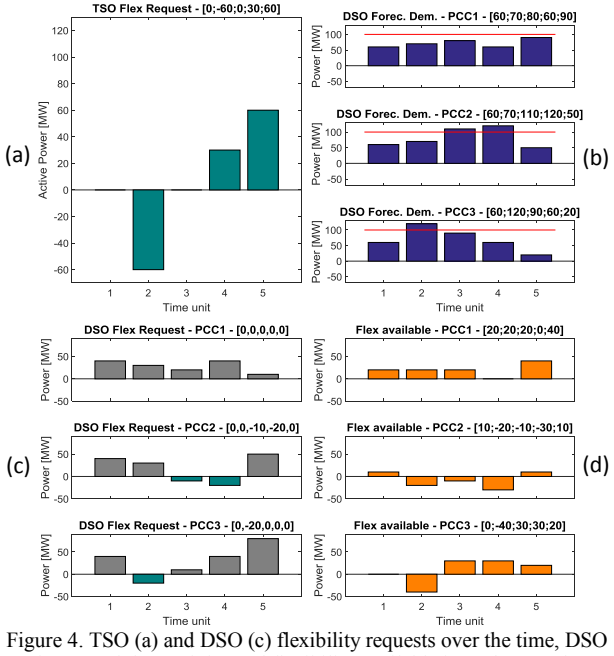

Figure 4. TSO (a) and DSO (c) flexibility requests over the time, DSO forecasted demand (b), and flexibility available in each area (d).

In order to allow a visualization of the involved forecasted/requested/available flexible power sets, a schematic representation is given. For each area, bar plots over the time represent the amount of flexibility (in this case positive or negative active power) that is requested by DSOs and TSO as well as the available flexibility offers, as in Fig. 4.

Fig. 4-a shows the TSO request of flexibility over the time, here expressed in Time Units of 15 minutes. It can be seen that at Time Unit 2, there is a need for up-reserve, which would mean power consumption curtailment due to a possible excess of generation. Whereas for Time Units 4 and 5 there is a need for down-reserve, which would mean total power consumption increase. In case of Time Units 1 and 3 no flexibility is requested. Fig. 4-b reports the power demand profiles at PCC1, PCC2 and PCC3 forecasted by the DSOs. Accordingly, each DSO will formulate correspondent flexibility requests to prevent transformer congestion, as shown in Fig. 4-c. It can be seen that for T1 no congestion situations are forecasted, whereas for T2 and T3, congestions are forecasted for Time Unit 3 and 4, and Time Unit 2, respectively. An example of possible flexibility offers is reported in Fig. 4-d which shows the available flexibility over time at the three points of common coupling.

Herein, examples of each one of the identified conflicts that the Flex Operator could face are presented. In particular, Fig. 5 to Fig. 8 report the new area-by-area power profiles that the Flex Operator obtained following the methodology proposed in Section III. Graphically, bar plots show the DSOs forecasted demand profiles over time at the three PCCs, with the activated flexibility, which is added (orange) or subtracted (dashed white) in order to satisfy the requests.

An example of system imbalances caused by flexibility

Figure 5. New profiles for each area: original DSOs demand profiles over time with the addition/subtraction of the activated flexibility. Example of compensation of activated DSO flexibility, to keep the system balanced.

Figure 6. Example of induced congestion problem to DSO, due to the activation of flexibility to provide a service for the TSO.

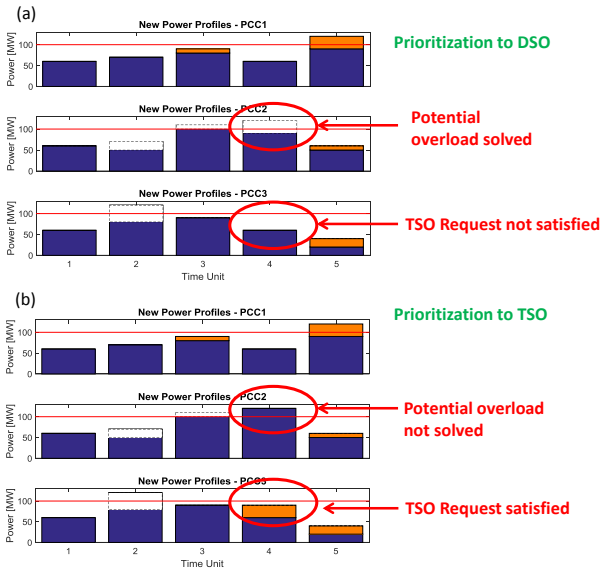

Figure 7. Example of prioritization problem when acquiring the available flexibility: it is possible to solve either the DSO (a) or the TSO (b).

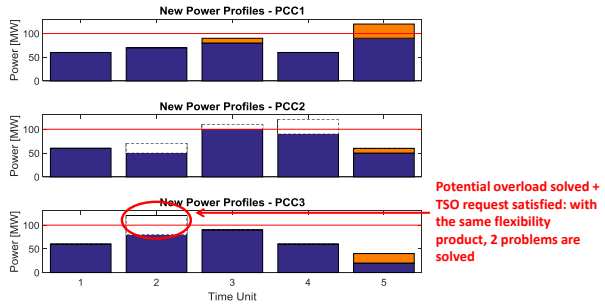

Figure 8. Example of satisfaction of needs of both DSO and TSO, by exploiting the same flexibility product.

activation for solving a local distribution issue (*conflict (a)*) is schematized in Fig. 5. It can be seen that at Time Unit 3, congestion of T2 is solved. Nevertheless, as noticeable from Fig. 4-a, the system was already balanced. Therefore, the BRP would need to rely on other flexible products located in other areas (in this case in area 1), to maintain the system balance.

Fig. 6 depicts one possible situation which could lead to *conflict (b)*, i.e., when solving a TSO request, the activation of the only available flexibility causes distribution overloading. It can be seen that at PCC1 at Time Unit 5, an overloading condition is caused.

As an example of a possible situation of *conflict (c)*, the need for prioritizing a DSO request over the TSO's and vice versa is presented. Fig. 4 shows that at Time Unit 4, the TSO needs an increase of the power consumption, while the DSO in area 2 requests a power reduction to solve a forecasted congestion of T2. Fig. 4-d shows that the available flexibility at Time Unit 4 allows to satisfy either the TSO or the DSO need. The two possible cases of prioritization to TSO or DSO are reported in Fig. 7-a and Fig. 7-b, respectively.

As said, *conflict (d)* represents an economical conflict that the Flex Operator may face mainly when remunerating aggregators. The example reported in Fig. 8 shows that

congestion of T3 is solved, while at the same time this power reduction can also satisfy the TSO need for frequency up-regulation at Time Unit 2, as deducible from Fig. 4-a.

VI. Conclusions and Future Works

This paper identified the TSO/DSO conflicts when acquiring flexibility from EVs both in the case of the actual typical European DSO design and in case of the newly proposed European DSO model *evolvDSO*. Assuming an active DSO market role in managing distribution grids by relying on flexible resources, it is clear that new technical and economical conflicts may appear. Here, the potential conflicts have been defined, described and visually presented from both a theoretical and a practical point of view with a proposal of respective conflict identification procedure.

Within the considered market framework, day-ahead trading process of ancillary services provided by EVs is analyzed. The investigation focused on the potential conflicts arising when acquiring services for component (e.g., transformer) congestion management and primary frequency regulation. The following conflicts have been identified:

(a) Need for compensating imbalances caused by activation of flexibility for solving a local distribution issue

(b) To solve a TSO request, activating the only available flexibility product causes distribution overloading

(c) The available flexibility can satisfy either the DSO request or the TSO request

(d) One flexibility product can solve several problems.

Considering a 3-area power system, each of the analyzed conflicts was presented through appropriate case studies that allowed to visually appreciating the nature of the conflict.

The authors point out that, within the considered example and time units of 15 minutes, the distribution grid needs would need to be prioritized over the TSO's. In fact, as a larger, more flexible and more controllable system, the transmission system would be able to rely on more traditional sources for reserve, possibly most of the time. In this way, in case the acquirement of a flexibility product for a TSO service would potentially cause congestion problems to the DSO, the TSO would be invited to procure reserve relying on alternative sources. On the other hand, in case of frequency dynamics (i.e., within the intraday market) the TSO's needs may have to be prioritized over the DSOs'.

In conclusion, the authors recognize that each one of the identified conflicts raises debates, whose resolutions are out of the scope of this work, but are expected to cover a broad interest within the scientific power engineering community. Thus, as a final remark, the following open questions are proposed for future works:

- When the activation of a DSO service causes system imbalance, the BRP needs to provide compensation in order to maintain the balance. Is the BRP compensated for this? If yes, by whom?
- When the activation of a flexibility product would cause problems to another stakeholder, or in case of limited availability of flexibility, how does the Flex Operator proceed? Who would be prioritized and why?
- In case one asset has the capabilities to satisfy at the same time both a TSO and a DSO need, will the aggregator be remunerated twice? If not, which service will it be remunerated for? Is it realistic to expect the same price although the required performances could be different?

Acknowledgment

The authors would like to acknowledge the support of the EUDP project ACES – Across Continent Electric Vehicle Services (grant EUDP17-I 12499). www.aces-bornholm.eu

References

[1] A. Zegers and H. Brunner, "TSO-DSO interaction: An Overview of current interaction between transmission and distribution system operators and an assessment of their cooperation in Smart Grids," Tech. Rep., 2014.

[2] ENTSO-E, CEDEC, GEODE, EURELECTRIC, and E. for S. Grids, "TSO–DSO Data Management Report," Tech. Rep., 2016.

[3] P. B. Andersen, M. Marinelli, O. J. Olesen, G. Poilasne, B. Christensen, C. Amtrup, and O. Alm, "The Nikola Project Intelligent Electric Vehicle Integration," in *5th IEEE PES Innovative Smart Grid Technologies European Conference (ISGT)*, 2014, pp. 1–6.

[4] S. Martinenas, M. Marinelli, P. B. Andersen, and C. Træholt, "Evaluation of Electric Vehicle Charging Controllability for Provision of Time Critical Grid Services," in *Proceedings of the 51st International Universities Power Engineering Conference Publication (UPEC)*, 2016, in press.

[5] K. Knezović, S. Martinenas, P. B. Andersen, A. Zecchino, and M. Marinelli, "Enhancing the Role of Electric Vehicles in the Power Grid : Field Validation of Multiple Ancillary Services," *IEEE Transactions on Transportation Electrification*, vol. 3, no. 1, pp. 201–209, 2016.

[6] N. Leemput, F. Geth, J. Van Roy, J. Büscher, and J. Driesen, "Reactive power support in residential LV distribution grids through electric vehicle charging," *Sustainable Energy, Grids and Networks*, vol. 3, pp. 24–35, 2015.

[7] A. Zecchino, M. Marinelli, M. Korpås, and C. Træholt, "Guidelines for Distribution System Operators on Reactive Power Provision by Electric Vehicles in Low Voltage Grids," in *24th International Conference on electricity Distribution (CIRED)*, 2017.

[8] Eurelectric, ENTSO-E, GEODE, E. for smart Grids, and CEDEC, "General Guidelines for Reinforcing the Cooperation between TSOs and DSOs," Tech. Rep., 2015.

[9] S. S. Torbaghan, N. Blaauwbroek, P. Nguyen, and M. Gibescu, "Local Market Framework for Exploiting Flexibility from the End Users," in *13th International Conference on the European Energy Market (EEM)*, 2016, pp. 1–6.

[10] K. Knezović, M. Marinelli, A. Zecchino, P. B. Andersen, and C. Træholt, "Supporting involvement of electric vehicles in distribution grids: Lowering the barriers for a proactive integration," *Energy*, vol. 137, pp. 458-468, 2017.

[11] H. Hansen, L. H. Hansen, H. Jóhannsson, and H. W. Bindner, "Coordination of System Needs and Provision of Services," in *22nd International Conference on electricity Distribution (CIRED)*, 2013, pp. 1–5.

[12] K. Heussen, D. Esteban, M. Bondy, J. Hu, O. Gehrke, and L. H. Hansen, "A Clearinghouse Concept for Distribution-Level Flexibility Services," in *4th IEEE PES Innovative Smart Grid Technologies Europe (ISGT Europe)*, 2013, pp. 1–5.

[13] H. Gerard, E. Rivero, and D. Six, "Basic schemes for TSO-DSO coordination and ancillary services provision," 2016.

[14] J. Lin and K. Knezović, "Comparative Analysis of Possible Designs for Flexible Distribution System Operation," in *2016 13th International Conference on the European Energy Market (EEM)*, 2016, pp. 1–5.

[15] A. Ramos, E. Rivero, and D. Six, "Evaluation of current market architectures and regulatory frameworks and the role of DSOs," Tech. Rep., 2014 [Online]. Available: http://www.evolvdso.eu/Home/Results

Paper B

Title:

Grid Frequency Support by Single-Phase Electric Vehicles : Fast Primary Control Enhanced by a Stabilizer Algorithm

Authors:

Antonio Zecchino, Michel Rezkalla and Mattia Marinelli

Published in:

51st International Universities Power Engineering Conference (UPEC - 2016)

DOI: 10.1109/UPEC.2016.8114063

Grid Frequency Support by Single-Phase Electric Vehicles: Fast Primary Control Enhanced by a Stabilizer Algorithm

Antonio Zecchino, Michel Rezkalla, Mattia Marinelli

Center for Electric Power and Energy, Department of Electrical Engineering, DTU – Technical University of Denmark
Contact person: Antonio Zecchino (antozec@elektro.dtu.dk)

***Abstract*—Electric vehicles are growing in popularity as a zero emission and efficient mode of transport against traditional internal combustion engine-based vehicles. Considerable as flexible distributed energy storage systems, by adjusting the battery charging process they can potentially provide different ancillary services for supporting the power grid. This paper presents modeling and analysis of the benefits of primary frequency regulation by electric vehicles in a microgrid. An innovative control logic algorithm is introduced, with the purpose of curtailing the number of current set-point variations that the battery needs to perform during the regulation process. It is shown that, compared to traditional droop-control approaches, the proposed solution assures same effects in terms of frequency containment, by employing a considerably lower number of variations of battery current set-point. The modeled low voltage microgrid is built to reproduce a real configuration of the experimental facility SYSLAB-PowerLabDK. Root-mean-square simulation studies have been carried out in DIgSILENT PowerFactory environment for the validation of the controller.**

***Index Terms*-- Distributed Energy Resources, Electric Vehicle, Fast Primary Control, Frequency Support.**

I. INTRODUCTION

Traditionally, frequency stability is assured relying on ancillary services provided by conventional large power plants, which nowadays are being replaced by renewable energy sources. This leads to the need of providing such services relying more and more on small aggregated units mostly connected to LV grids. Therefore, aiming at deferring grid reinforcement investments, system-wide ancillary services from distributed energy resources (DERs) need to be provided without violating distribution grids constraints.

Electric vehicles (EVs) can represent a reliable source of such services, since they can boast technical properties suitable for offering flexibility to the grid operators. In fact, they can be considered as distributed energy storage systems with large potential for network regulation [1], [2], and are almost continuously plugged into a LV charging post [3]. Furthermore, they are capable of adjusting the battery charging process according to pre-defined algorithms [4]–[8].

In [9]–[11] it is shown that EVs with or without vehicle-to-grid (V2G) capability can be effective in primary frequency regulation, both in isolated microgrids and larger systems. However, an ideal EV response to the control signals was assumed, in terms of response time and power, while communication and control latencies were neglected. These simplifications may greatly impact the results.

To fill this gap, in the here-presented paper both the EVs and the control/communication procedure are modelled considering appropriate response times and latencies for all the operational steps. EV response characteristics are based on the experimental finding described in [12]. Modeling and analysis of the effects of primary frequency regulation by single-phase EVs without V2G capability in an islanded LV microgrid are presented. Specifically, the work proposes an original controller to reduce the number of EV current set-point variations. The controller prevents undesired unstable situations due to frequency oscillations caused by the 1-Amp granularity for the setting of the charging current, foreseen by IEC61851 [13] and J1772 [14] standards.

For the characterization of the proposed controller, different droop functions are set, and, with the purpose of reproducing the real different behaviors that EVs may have, different response times are considered. In this way, situations of load unbalance among the three phases are introduced. These considerations allowed a further validation of the proposed controller. The implemented control algorithm complies with contemporary standards for limiting the EV charging rate. This means that it can be applied with all currently available EVs complying with [13] and [14]. For the validation of the controller, root-mean-square (RMS) simulations are carried out in DIgSILENT PowerFactory software environment. Both load events to destabilize the system frequency, and a realistic wind generation profile to create continuous frequency deviations are considered. To allow a future practical experimental validation study, the modelled microgrid, is built to reproduce a real configuration of the experimental facility SYSLAB-PowerLabDK.

The paper is structured as follows. Section II presents the modelled microgrid. Primary frequency regulation control by EVs is reported in Section III, together with a detailed description of the proposed innovative controller. Section IV presents the simulation studies: three scenarios are defined, and results are presented and discussed. Conclusions are reported in Section V.

II. MICROGRID LAYOUT

The study has been carried out by means of RMS simulation activities in DIgSILENT PowerFactory software environment. The modelled grid is a reproduction of an islanded configuration of the experimental LV grid SYSLAB-PowerLabDK. SYSLAB-PowerLabDK is a research laboratory facility for development and test of control and communication technology for active and distributed power systems, located at the DTU Risø campus.

In order to allow a future practical experimental validation study, the modelled microgrid, was built considering real available power system components. Specifically, the following units were considered for the proposed simulation studies:

- 3 controllable EVs, each equipped with single-phase 16 A (230 V) charger and 24 kWh Lithium-ion battery. The chargers allow only unidirectional power flows, i.e., not any V2G capability is utilized. The charging current can, however, be modulated between 6 and 16 A with granularity of 1 A [13], [14].
- A 60 kVA diesel synchronous generator, with active power provision up to 48 kW. Since designed for operating in microgrid contexts, the inertia of the unit is rather high (2H = 50 s). To allow the analysis of primary frequency regulation by EVs, the automatic frequency control of the governor of the diesel generator has been disabled.
- A 45 kW (up to 15 kW per phase) resistive load unit with active power independently settable on each phase.
- A 10 kW Aircon wind turbine (nominal wind speed: 11 m/s) with full converter and active stall power control.

As deducible from the highlights in the single line diagram representation of the whole mentioned experimental facility in Fig. 1, a 725 m Aluminum cable line is utilized to connect the two buses which the components are connected to (AC-Resistance at 20 °C and Reactance are respectively 0.313 and 0.077 Ohm/km). Both the synchronous and the wind generators are connected to the same bus, while the resistive load and the EVs are placed on the other terminal of the line.

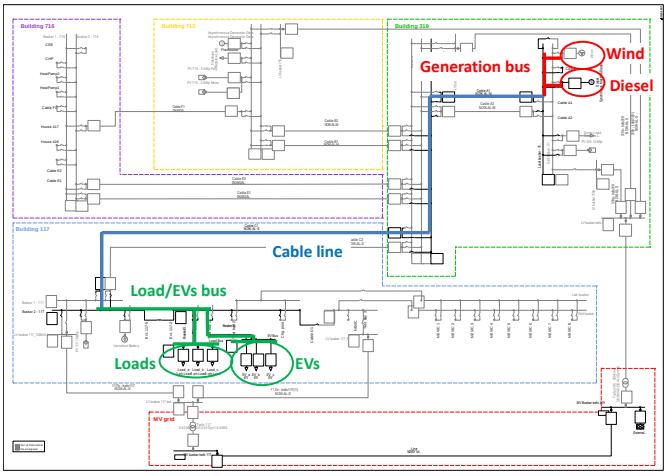

Fig. 1. Single line diagram representation of the whole SYSLAB-PowerLabDK experimental LV grid. Highlighted are the components utilized to compose the microgrid.

III. CONTROLLERS

This Section introduces a first possible approach for primary frequency regulation by EVs. Secondly, it describes the problem of undesired current oscillations. Finally, it presents the innovative logic algorithm to enhance the performances of the controller by preventing the oscillations.

A. FPC controller

By exploiting the high ramping times and precision that EVs can assure for primary frequency regulation [12], the regulation service here presented will be called Fast Primary Control (FPC).

Commonly, primary frequency control is provided by droop controllers, which modulate the synchronous machines' generation according to the power rating. The droop constant k_{droop} represents how much the machine is sensible to frequency changes, and quantifies its contribution to primary frequency/power regulation. The contribution in terms of active power variation ΔP [kW] referred to its nominal power P_n [kW] is correlated to the frequency variation Δf [Hz] referred to the nominal value f_n (50 Hz) by k_{droop}, as in (1).

$$\Delta f/f_n = k_{droop} \cdot \Delta P/P_n \quad (1)$$

In our application, the regulation is provided by EVs (loads), by modulating their power consumption. According to [13] and [14], the charging process is modulated by setting the charging current. Therefore, Equation (1) can be rewritten as in (2), where, for a defined droop, ΔI [A] is the current variation that the EV will assure in case of a certain Δf.

$$\Delta f/f_n = k_{droop} \cdot \Delta I/I_n \quad (2)$$

It is clear that, in order to define the droop value, the nominal current I_n – the correspondent of P_n in (1) – needs to be set. So, as the technical requirements delimit EV's charging current between 6 and 16 A, this available range of regulating current of 10 A has been assumed as the EV's I_n.

For this study, three different proportional f-I droops have been considered: 2% (frequency limits of 49.5 – 50.5 Hz), 4% (49–51 Hz), and 6% (48.5–51.5 Hz). If the frequency exceeds the limits, then the current limit value (6 or 16 A) is set. The three droops are showed in Fig. 2 by the dashed lines.

In order to comply with the aforementioned [13] and [14] standards, the calculated current values need to be rounded. This results in step functions, showed by the solid lines in Fig. 2. To assure room to increase and decrease the charging level equally (±5 A), the EVs' initial current set-point is 11 A, the central point.

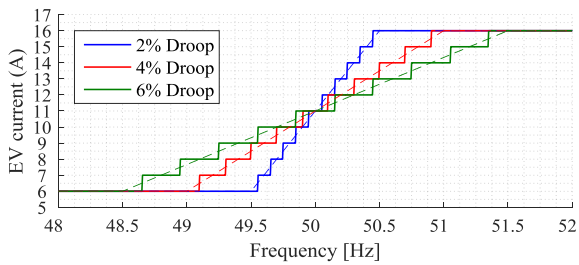

Fig. 2. 2%, 4% and 6% f-I droops: ideal and step functions.

Technically, EVs are largely capable of satisfying the requirements in terms of activation time for participating in the Danish market for primary frequency reserve in both the synchronous regions DK1 and DK2 [12]. In fact, DK1 requires the supply of the first half of the activated reserve within 15 s and the rest within 30 s, while DK2 requires the activation of the full reserve within 150 s. In practice, the participation in the Danish market is hindered by the minimum bid of 0.3 MW. This would correspond to a minimum number of EVs of about 260, considering a ±5 A flexibility per vehicle. Therefore, it is clear that an aggregator is needed to manage such a large number of units.

In this context, with the aim of reproducing a realistic scenario in which more EVs are managed by one single aggregator, the charging process of the three EVs is here managed by the same controller, which relies on a unique frequency measurement device. So, the EVs' inverters receive the same current set-point signal. It is clear that, in an ideal case of perfectly equal response time and inverter performance, the cars would charge exactly in the same way.

The controller's block diagram is shown in Fig 3-a. Basically, it is composed by three main blocks: the frequency measurement device, the control algorithm and the EV model. As explained, the control algorithm in Fig. 3-b receives the frequency measurement and provides the EV current set-point according to a particular f-I droop. To comply with the standards, the 'Round' block rounds the calculated current value. To represent the digital time delay due to measurement and communication, a time delay block is inserted inside the control algorithm block (T_{mc} = 0.5 s). The rounded current signal is sent to the EV model, which is composed by:

- A time constant block to imitate the EV battery dynamics.
- A time delay block to represent the delay due to internal EV communication and activation of the inverter (T_{EV} = 1.5 s).
- A block that converts the current to a power signal, as for RMS simulations in PowerFactory loads need power inputs.
- A load block, i.e., the EV unit in the modelled grid.

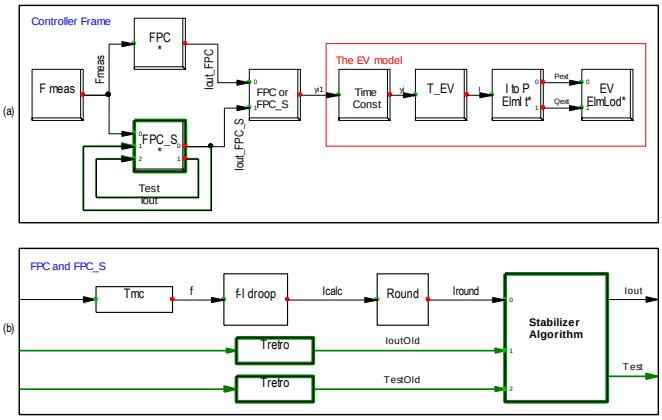

Fig. 3. Controller block diagram. The highlights show the parts added for FPC_S. (a) shows the measurement block, the control algorithm (FPC or FPC_S) and the EV model. (b) shows the control algorithm block diagram.

B. *Current oscillations*

In occasion of recent frequency regulation experimental and simulation activities in a microgrid using FPC by EVs, the authors have experienced some frequency oscillations [12]. The oscillations are due mainly to the technical requirement of 1-Amp granularity for the setting of the changing current. In fact, the rounding provided by the 'Round' block can cause 1-Amp oscillations, especially in presence of steep droops, low-inertia grid, large response times and high share of EVs power employed as reserve. The reason is the calculated current, which, in case it falls near the exact middle of two consecutive set-points, will be continuously rounded up and down.

For example, if the calculated current is 7.51 A, then the set-point will be 8 A. The same set-point signal is sent to an aggregated number of EVs. The difference between the 7.51 A and the 8 A in all the EVs would cause a significant change in the power flow in terms of total absorbed active power. This will affect the frequency, resulting in a new calculated current of 7.49 A, rounded down to 7 A. This process will turn in a loop that determines the 1-Amp oscillations.

C. *Addition of a Stabilizer Algorithm: FPC_S controller*

With the aim to avoid the mentioned 1-Amp current oscillations, an innovative controller called FPC_S is implemented. The proposed controller prevents 1-Amp current oscillations, while allows larger and highly less-probable 2-Amp or higher ones. This will reduce the overall probability of current oscillations.

To build the FPC_S controller, in addition to the presented FPC controller, the 'Stabilizer Algorithm' block is inserted. It, as the retroaction arrows, is highlighted in the block diagrams in Fig. 3. Basically, the Stabilizer Algorithm freezes the current set-point if a 1-Amp oscillation is detected. The Stabilizer Algorithm's flow-chart is presented in Fig 4. The controller calculates the current set-point (*Iout*) based on an algorithm which evaluates two conditions: the current set-point and an internal parameter (*Test*). The first condition is obtained by comparing the new calculated set-point (*Iround*) with the one from the previous time step (*IoutOld*). The second condition is evaluated through a consideration of a memory status (*TestOld*), which is the *Test* from the previous time step. *Test* indicates whether or not, and how, the current set-point is going to change compared to the value of the

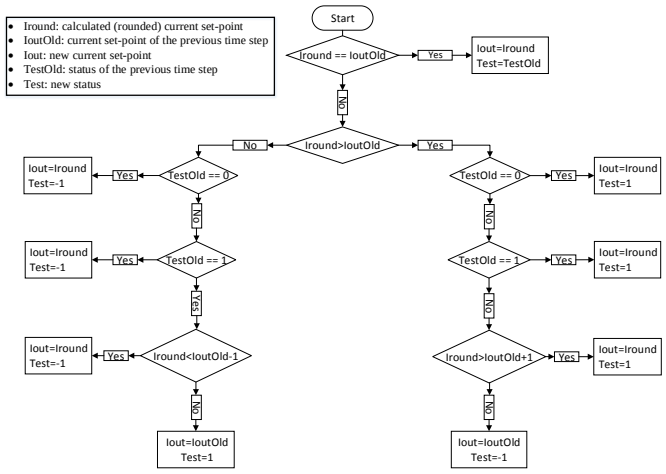

Fig. 4. Stabilizer Algorithm Flow-Chart of the FPC_S.

previous time step. It will take the values of -1, 0 or 1: the -1 indicates that in the previous time step the current set-point has been reduced, the 1 that it has been increased, while 0 is utilized for the initialization of the controller.

Since the aim of the controller is to avoid 1-Amp oscillations, the algorithm prevents 1-Amp steps from one time step to the next one under certain conditions. To do this, the algorithm compares *Iround* with *IoutOld* taking into account the value of *TestOld*. For instance, in case *Iround* is greater than *IoutOld* by 1-A difference, and *TestOld* is -1 then Iout will be kept as *IoutOld*. On the other hand, *Iout* will be changed only when the difference is at least 2 A.

To give a practical example, if *Iround* is 9 A, *IoutOld* is 8 A and *TestOld* is -1 then the controller prevents the current change. In fact *Iout* will take the same value of *Ioutold* and *Test* will be kept as *TestOld*. In case *Iround* will increase to 10 A, then the current change will be allowed: *Iout* will be 10 A and *Test* will be 1.

IV. SIMULATIONS: SCENARIOS' DEFINITION AND RESULTS

In order to evaluate the controller's effectiveness under different operating conditions, three scenarios have been considered and straightaway introduced. The purpose of the first scenario is to provide a general evaluation of the innovative FPC_S controller in case of contingencies taking place during stationary situations. On the other hand, the other two scenarios are characterized by continuous fluctuations of generation from the wind turbine, which now has been considered connected. This made it possible to evaluate the effectiveness of the controllers in a more realistic case, i.e., when continuous actions of the controllers are needed to follow continuous frequency deviations.

For Scenario #1, in the initial situation, the diesel power generation amounts to 19.5 kW, which corresponds to 12 kW of the resistive load (i.e., 4 kW per phase) plus 7.5 kW of the three EVs (i.e., 2.5 kW each, which corresponds to the mentioned initial condition of 11 A). For Scenarios #2 and #3, both load and EVs are kept as in #1, while, instead, the wind turbine is now considered connected.

A. *Scenario #1*

The first scenario aims at evaluating the FPC_S controller, by monitoring the frequency trends in case of balanced load events. The events have been used to destabilize the microgrid frequency, whose deviations will be contained by the FPC_S. The simulations have been carried out for a time slot of 20 minutes, during which, with intervals of 5 minutes, the events took place, as in Table I. The events' size amounts to ±3 kW, which corresponds to ±15.4% of the total generated power and to ±5 % of the rated power of the diesel generator.

TABLE I
LOAD EVENTS FOR DESTABILIZING THE FREQUENCY

Time	Load event
10 s	+ 3 kW
310 s	- 3 kW
610 s	- 3 kW
910 s	+ 3 kW

Comparisons of results with and without the Stabilizer Algorithm have been repeated for each one of the three droops presented in Section III-A, namely 2%, 4% and 6%. In this way, the effectiveness of the proposed controllers in case of different frequency limitations and slopes of the proportional controller has been tested.

Results from Fig. 5 show that, in case of 2% droop, the first and third load events led to undesired frequency fluctuations, due to the mentioned 1-Amp oscillations. It is possible to notice that they are substantially reduced by the FPC_S controller, which drastically reduces the number of switches from one set-point to the other (Fig. 6-a and Table II). An enlargement of the frequency deviations appears since it imposes to wait until the frequency change is big enough to make the set-point change by 2 A at the time. Similar effects are noticeable after the first event in case of 6% droop, with the difference that now not any larger fluctuation is caused.

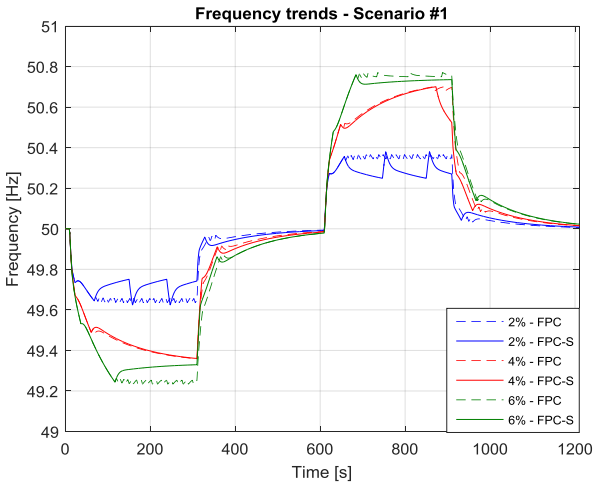

Fig. 5. Frequency trends employing FPC and FPC_S in Scenario #1.

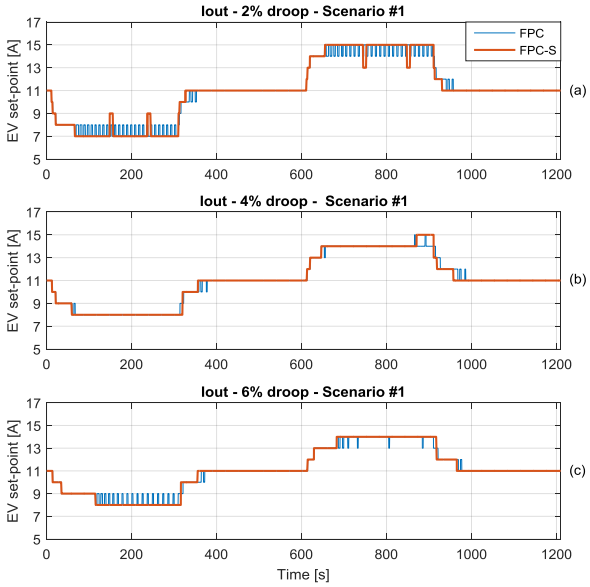

Fig. 6. EV current set-point signals employing FPC and FPC_S in Scenario #1. For 2% droop (a), for 4% droop (b), for 6% droop (c).

As general result for the three cases, it can be concluded that the primary frequency regulation effects are basically the same and potential oscillation conditions are avoided, with an absolute minor number of EV current set-point switching, as deducible from Fig. 6 and Table II.

TABLE II
RESULTS' OVERVIEW FOR SCENARIO #1

Droop	FPC				FPC_S			
	Nr. switchings	f_{max}	f_{min}	f_{mean}	Nr. switchings	f_{max}	f_{min}	f_{mean}
2%	128	50.37	49.64	50.00	22	50.38	49.63	50.00
4%	28	50.70	49.36	50.02	12	50.70	49.36	50.01
6%	62	50.77	49.23	50.01	10	50.76	49.24	50.02

B. *Scenario #2*

Scenario #2 considers a 30-minute wind production profile, in terms of active and reactive power, reported in Fig. 7. This allows an evaluation of the controllers in case of a realistic case, i.e., when continuous actions of the controllers are needed to follow continuous frequency variations.

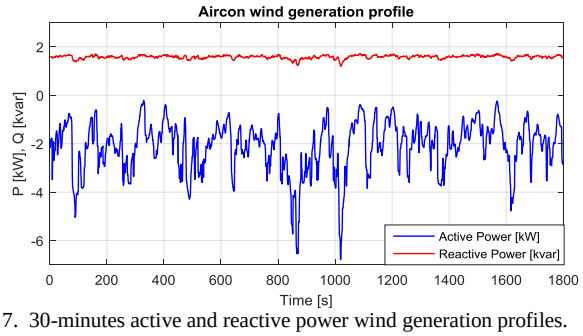

Fig. 7. 30-minutes active and reactive power wind generation profiles.

Fig. 8 shows that, as it was for Scenario #1, for all the considered droops the overall primary frequency containment benefits are not so influenced by the use of the additional Stabilizer Algorithm. A confirmation of this is provided by the numerical results in Table III, in terms of maximum, minimum and mean frequency values. Table III reports also frequency information in case of totally uncontrolled situation, the case presented by the black line in Fig. 11.

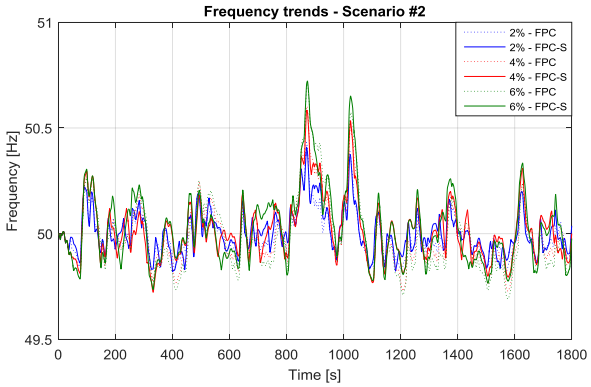

Fig. 8. Frequency trends employing FPC and FPC_S in Scenario #2.

On the other hand, the FPC_S controller provides absolute benefits in terms of EV current set-point adjustments number, as deducible from Fig. 9. In fact, as reported in Table III, for the 2%, 4% and 6% droops, the switch operations have been

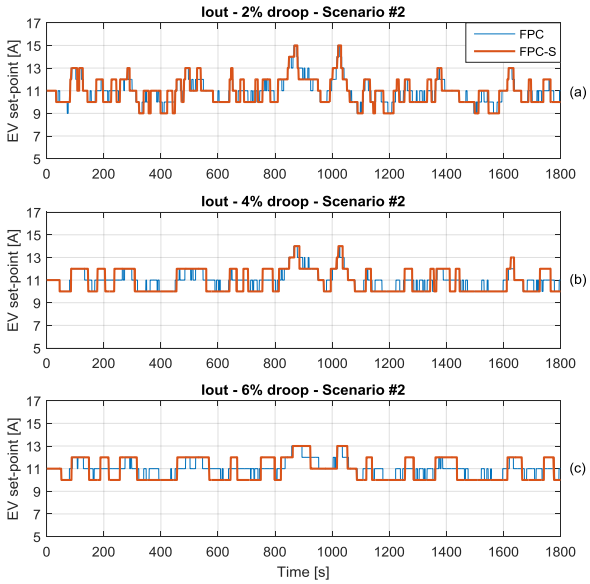

Fig. 9. EV current set-point signals employing FPC and FPC_S in Scenario #2. For 2% droop (a), for 4% droop (b), for 6% droop (c).

reduced by 48% (from 166 to 87), 59% (from 106 to 43) and 67% (from 88 to 29), respectively.

This result is very significant, especially if considered in a future scenario with EVs providing frequency regulation for the whole duration of the charging process. In fact, the FPC_S solution, allows significantly less degradation of the EV battery, assuring same performances in terms of frequency regulation.

Also the phase-neutral voltages at the EVs' connection point are monitored. It has been verified that the FPC_S controller does not influence them significantly.

TABLE III
RESULTS' OVERVIEW FOR SCENARIO #2

Droop	FPC				FPC_S			
	Nr. switchings	f_{max}	f_{min}	f_{mean}	Nr. switchings	f_{max}	f_{min}	f_{mean}
2%	166	50.43	49.82	49.99	87	50.41	49.82	50.00
4%	106	50.60	49.73	49.99	43	50.58	49.72	50.02
6%	88	50.71	49.69	49.99	29	50.72	49.74	50.03
No Contr.	-	51.11	49.34	49.99	-	-	-	-

C. *Scenario #3*

The main purpose of Scenario #3 is analyzing a situation characterized by different response times of the three EVs. In this way it is possible to reproduce the real different behaviors that EVs may have, although simultaneously receiving the same signal. As EVs are connected to different phases, controllers are tested in case of random unbalanced conditions, caused by the unsynchronized set-point variations.

Scenario #3 considers the same 30-minute wind production profile utilized for Scenario #2. However, only the 4% droop is considered. With the purpose of obtaining different EV response times, with reference to the block scheme representation of the EV model (in Fig. 3-a), it has been decided to modify the digital delay-time T_{EV}. For each time-

step of the RMS simulation, T_{EV} has been randomly changed for each EV, with values of 1.5 s, 2 s, 2.5 s or 3 s.

Fig. 10 reports a zoom-in capture of the switching events of the three EVs. It is possible to notice how the three EV set-points are changed in a non-synchronous way. The trends for the whole 30-minutes simulation is not reported, since it appears exactly as in Fig. 9-b (orange line).

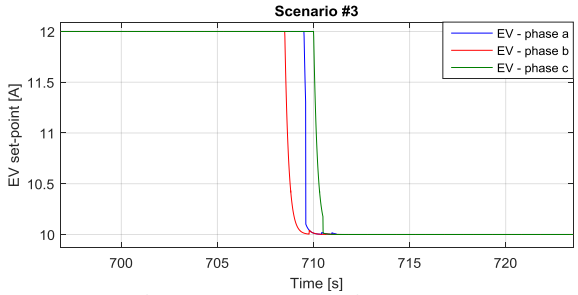

Fig. 10. Zoom-in of one set-point variation for the three EVs in Scenario #3.

As deducible from Fig. 11, the microgrid frequency is not subject to any kind of oscillations. This leads to the conclusion that, although the frequency is regulated by units with different response times that introduce unbalance conditions to the system, the proposed FPC_S controller does not cause any kind of system instability. Results also show that the Voltage Unbalance Factor ($VUF_{\%}$, defined in [15]) is contained below 0.18%. It would increase up to 0.3% in case the diesel generator would have only half of its apparent power or one tenth of its inertia. In any case, the unbalance introduced by the EVs in the microgrid is rather small, considering that the maximum acceptable limit is 2%.

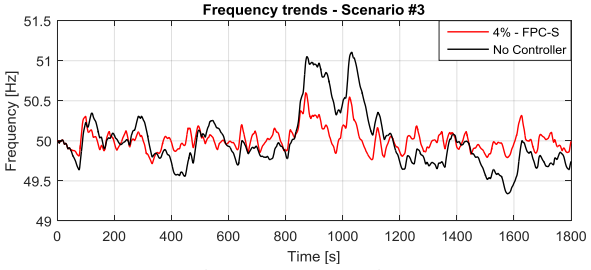

Fig. 11. Frequency trends for Scenario #3 and for uncontrolled case.

V. Conclusions and Future Works

This work presented modeling and analysis of frequency regulation provided by single-phase EVs connected to an islanded LV microgrid. By exploiting the high ramping times and precision that EVs can assure, the analyzed grid service was named Fast Primary Frequency Control (FPC).

The paper proposed an original solution to reduce the number of EV current set-point adjustment actions, which in a microgrid might become extremely high in case of standard droop-based primary frequency regulators. Specifically, the implemented logic prevented the undesired 1-Amp oscillations that the authors had experienced in occasion of previous frequency regulation experimental and simulation activities in a microgrid using FPC by EVs. Therefore, the paper presented a practical solution to the problem that appeared due to the 1-Amp granularity foreseen by the IEC 61851 and SAE J1772 technical standards.

Results showed that the addition of a Stabilizer Algorithm to the controller (now called FPC_S) certainly provided benefits in terms of EV current set-point switchings number, assuring same performances in terms of primary frequency regulation. The FPC_S controller has been further validated: it assured system stability in case of unbalances induced by the unsynchronized responses of the 3 single-phase EVs.

As future works, the innovative controller will be implemented in a real EV charging station at the experimental facility SYSLAB-PowerLabDK. The FPC_S controller will be validated in the same microgrid that has been utilized for the here-presented simulation studies.

References

[1] K. Knezović, M. Marinelli, P. Codani, and Y. Perez, "Distribution Grid Services and Flexibility Provision by Electric Vehicles: a Review of Options," *Proceedings of the 50th International Universities Power Engineering Conference (UPEC) IEEE*. Staffordshire, England, pp. 1–6, 2015.

[2] K. Clement-Nyns, E. Haesen, and J. Driesen, "The impact of vehicle-to-grid on the distribution grid," *Electric Power Systems Research*, vol. 81, no. 1, pp. 185–192, 2011.

[3] N. S. Pearre, W. Kempton, R. L. Guensler, and V. V Elango, "Electric vehicles : How much range is required for a day ' s driving?," *Transportation Research Part C*, vol. 19, no. 6, pp. 1171–1184, 2011.

[4] M. Esmaili and M. Rajabi, "Optimal charging of plug-in electric vehicles observing power grid constraints," *IET Generation, Transmission & Distribution*, vol. 8, no. 4, pp. 583–590, 2014.

[5] C. Gouveia, C. L. Moreira, J. Abel, P. Lopes, and D. Varajão, "Microgrid Service Restoration," *IEEE Industrial Electronics Magazine*, vol. 7, no. 4, pp. 26–41, 2013.

[6] J. Hu, S. Member, S. You, M. Lind, J. Østergaard, and S. Member, "Coordinated Charging of Electric Vehicles for Congestion Prevention in the Distribution Grid," *IEEE Transactions on Smart Grid*, vol. 5, no. 2, pp. 703–711, 2014.

[7] K. Knezović, M. Marinelli, R. J. Møller, P. B. Andersen, C. Træholt, and F. Sossan, "Analysis of Voltage Support by Electric Vehicles and Photovoltaic in a Real Danish Low Voltage Network," *Proceedings of the 49th International Universities Power Engineering Conference (UPEC) IEEE*. Cluj-Napoca, Romania, pp. 1–6, 2014.

[8] A. S. Masoum, S. Deilami, P. S. Moses, M. A. S. Masoum, and A. Abu-Siada, "Smart load management of plug-in electric vehicles in distribution and residential networks with charging stations for peak shaving and loss minimisation considering voltage regulation," *IET Generation, Transmission & Distribution*, vol. 5, no. 8, pp. 877–888, 2011.

[9] P. M. R. Almeida, F. J. Soares, and J. A. P. Lopes, "Electric vehicles contribution for frequency control with inertial emulation," *Electric Power Systems Research*, vol. 127, pp. 141–150, 2015.

[10] S. Izadkhast, P. Garcia-Gonzalez, and P. Frias, "An Aggregate Model of Plug-In Electric Vehicles for Primary Frequency Control," *IEEE Transactions on Power Systems*, vol. 30, no. 3, pp. 1475–1482, 2015.

[11] J. Meng, Y. Mu, H. Jia, J. Wu, X. Yu, and B. Qu, "Dynamic frequency response from electric vehicles considering travelling behavior in the Great Britain power system," *Applied Energy*, vol. 162, pp. 966–979, 2016.

[12] M. Marinelli, S. Martinenas, K. Knezović, and P. B. Andersen, "Validating a centralized approach to primary frequency control with series-produced electric vehicles," *Journal of Energy Storage*, vol. 7, pp. 63-73, 2016.

[13] IEC 61851-1:2010, "Electric vehicle conductive charging system – Part 1: General requirements." 2010.

[14] SAE J1772:2010, "Electric vehicle and plug in hybrid electric vehicle conductive charge coupler." 2010.

[15] P. Pillay and M. Manyage, "Definitions of voltage unbalance," *IEEE Power Engineering Review*, vol. 22, no. 11, pp. 49–50, 2002.

Paper C

Title:

Comparison Between Synthetic Inertia and Fast Frequency Containment Control Based on Single Phase EVs in a Microgrid

Authors:

Michel Rezkalla, Antonio Zecchino, Sergejus Martinenas, Alexander M. Prostejovsky and Mattia Marinelli

Published in:

Applied Energy (2018)
DOI: doi.org/10.1016/j.apenergy.2017.06.051

Comparison between Synthetic Inertia and Fast Frequency Containment Control Based on Single Phase EVs in a Microgrid

Michel Rezkalla[a], Antonio Zecchino[a], Sergejus Martinenas[a], Alexander M. Prostejovsky[a], Mattia Marinelli[a,*]

[a] *Center for Electric Power and Energy, Department of Electrical Engineering, Technical University of Denmark*

Abstract

The increasing share of distributed and inertia-less resources entails an upsurge in balancing and system stabilisation services. In particular, the displacement of conventional generation reduces the available rotational inertia in the power system, leading to high interest in synthetic inertia solutions. The objective of this paper is twofold: first, it aims to implement and validate fast frequency control and synthetic (virtual) inertia control, employing single phase electric vehicles as flexibility resources. Second, it proposes a trade-off analysis between the two controllers. The interdependency between frequency containment and synthetic inertia control on the transient frequency variation is shown analytically. The capabilities and limits of series produced EVs in providing such services are investigated, first on a simulation based approach and subsequently by using real hardware. The results show that fast frequency control can improve the transient frequency behaviour. However, both on the simulation and on the experimental level, the implementation of synthetic inertia control is more challenging. In fact, due its derivative nature and the system dynamics, its performance is limited. Furthermore, the crucial importance of the the EVs' response time for both controllers is highlighted.

Keywords: electric vehicles, experimental validation, frequency containment control, frequency stability, synthetic inertia.

*Corresponding author
Email address: matm@elektro.dtu.dk (Mattia Marinelli)

Nomenclature

$\bar{T}_D$	Frequency dependent loads
$\bar{T}_{FCC}$	Electric torque of devices participating in FCC
$\bar{T}_{SIC}$	Electric torque of devices participating in SIC
δ	Electrical rotor angle
δ_0	Rotor angle at t=0
ω_e	Angular velocity of the electrical rotor
ω_m	angular velocity
ω_{0m}	Rated angular velocity
f	Frequency
H	Kinetic energy in Watt-per-seconds at rated speed
I	EV absorbed Current
J	Moment of inertia
K_D	Load damping factor
K_{FCC}	FCC proportional control coefficient
K_{SIC}	SIC proportional control coefficient
P	EV absorbed active power
p	Number of pole pairs
S_b	Generator's rated power

t	time
T_a	Acceleration or deceleration torque
T_e	Electrical torque
T_m	Mechanical torque

1. Introduction

The rising share of inverter-coupled distributed energy resources (DER) raises new challenges in maintaining stable grid operation. One of the main issues is the reduction of the system inertia due to the replacement of rotating generators by converter-connected resources, as well as the expansion of high-voltage direct current (HVDC) connections, which decouples the inertial response between the interconnected areas [1]. Thus, the system's ability to withstand frequency changes by releasing or absorbing the energy stored in the rotating masses is notably reduced, leading to faster frequency dynamics [2]. Moreover, the high volatility of renewable energy sources (RES) contributes to the frequency stability issue by changing the grid inertia over time and increasing the need for better planning due to higher uncertainty.

Inertia is the parameter that represents the capability of rotating machines (including loads, when applicable) to store and inject their kinetic energy into the system [3]. The amount of inertia influences the frequency gradient, which is generally addressed as the rate of change of frequency (RoCoF) and the transient frequency values during a system incident. The RoCoF and the transient frequency values have a fundamental role in maintaining and operating the power system in a secure state. A large RoCoF and/or transient frequency deviations can lead to the automatic tripping of conventional generators and DER units [4] because they are connected to the grid by means of RoCoF or frequency relays [3]. The RoCoF relay limit is established by the grid code, which varies among countries.

Several transmission system operators (TSOs) have started to address this challenge, recognising the potential value of the inertial response of wind power plants, synchronous condensers, and synthetic inertia [5, 6]. One of the main concerns of TSOs is the RoCoF, which might lead to a cascade tripping of conventional and DER units connected by means of RoCoF relays [4, 7]. According to [8], an RoCoF relay has a typical delay in the range of 50 ms to 500 ms.

Further, the growing number of electric vehicles (EVs) has concerned distribution system operators (DSOs). The uncertainty of EV driving patterns, high penetration levels and charging in the distribution network could result in new system peaks and negative distribution system impacts, exceeding the load capacities of distribution lines and transformers [9, 10].

The effects of EVs on future power systems are investigated in several studies, such as in [11, 12]. In [11], the negative effects of uncoordinated charging of EVs on the power system was addressed. The authors presented the impacts that EV charging can have in an actual working wholesale electricity market. In [12] it was analysed how a large scale implementation of plug-in hybrid electric vehicles and full electric vehicles would influence the power system. This study shows that smart management of EVs bidirectional charging can alleviate peak power demand.

On the other hand, unscheduled high penetration of EVs may have detrimental effects on power system performance. Reliability and stability are the aspects of the grid that face the most challenges when EVs are used widely. Consequently, there is an exigent need to predict the EVs' customers in order to avoid irreparable effects, especially for the distribution network. Several studies have investigated these challenges, such as as in [13, 14]. In [13] the authors propose a simultaneous approach for allocation of EV parking lots and DRRs in a power distribution network to achieve a more reliable supply of the load demand. A probabilistic modelling of EVs' charging demand is presented in [14].

A noticeable amount of research has focused on the transition from the traditional system, where frequency is controlled by a small set of large generating units, to the future where it is controlled by a vast amount of small distributed resources [15, 16].

Given that EVs are essentially battery storages with a seconds-range response time, the TSO can greatly benefit from EV participation in frequency service provision. As analysed in [17], EV participation in the ancillary service market appears to be one of the most promising applications because it can offer substantial earnings to EV aggregators and EV owners. Ref. [18] concluded that although V2G capable EVs can provide great benefits to the ancillary service market, battery degradation may represent a challenge for their viability [19, 20].

EVs are able to provide fast regulating power bidirectionally using Vehicle-to-Grid or just by modulating the charging power unidirectionally [21, 22]. In this context, EVs can play a fundamental role in the future ancillary service market. Although the potential benefits of exploiting the V2G capability for ancillary services was introduced in [23], this study did not investigate uni-direction EVs charging in providing such services.

Due to the reduced system inertia, various studies have shown the techno-economic benefits and challenges of primary frequency provision from EVs, such as in [24–26]. In [24] the authors present the impact of declining system inertia on the primary frequency control (PFC) and future requirements. It also presents the impact of PFC provision from EVs on the system frequency performance. In [25] the authors present the general ability of EV fleets to utilize fluctuating renewable energy sources for charging and their effects on the power system. The authors in [26] summarise the challenges to control a system with low inertia. In this study, unlike in [11, 12, 23], EVs have been controlled by only modulating the charging current between 6 and 16A with steps of 1 A to comply with the technical constraints imposed by the IEC 61851 standard [27, 28].

Simultaneously, very few studies have investigated the EV's ability in providing synthetic inertia services. In [29] the authors presented a single-phase virtual synchronous machine (VSM) and its possible application for providing V2G services from an EV's batteries, this work was supported by an experimental setup that is based on the Opal-RT platform. In contrast, this paper presents a different approach in providing synthetic inertia services supported by an experimental investigation using series produced EVs.

The scope of this study is twofold: First, the EV's capabilities as flexibility resources are

investigated. In particular, this study looks at synthetic inertia control (SIC) and frequency containment control (FCC) as exemplary services. Second, it analyses and evaluates the pros and cons of SIC and FCC on the frequency dynamics (e.g. RoCoF and frequency nadir and zenith). The general objective is to determine if SIC and FCC delivered by converter connected resources, which are relatively fast compared to conventional units, can replace or at least reduce the need for a conventional inertial response.

Ultimately, the research question that this study addresses is: *given the trend of decreasing system inertia, can fast frequency containment compensate or replace the need for synthetic inertia?*

The method and the results presented in this study are part of the EU-funded project ELECTRA IRP, which proposes novel frequency and voltage control concepts to maintain and operate the power system in a secure state [30]. It considers the grid inertia (i.e. the synchronous and synthetic inertia) to be an active part of the frequency control process and it is addressed by inertia response power control (IRPC). In this study, the synthetic inertia is considered to be an active part of the IRPC process.

This paper is divided into the following five sections: Section 2 presents the frequency control in Europe and the analytical interdependency between frequency containment and synthetic inertia. Section 3 presents the frequency containment and the synthetic inertia controllers, along with the experimental layout. The simulations and experimental results are shown and discussed in section 4. Lastly, section 5 presents the conclusions and it outlines future research points.

2. Frequency Control in Europe and Analytical Formulation

This section presents a summary of the current framework for frequency control in Europe and it gives an overview of synthetic inertia and frequency assessment.

2.1. Framework for Frequency Control in Europe

Based on the network code that was defined by the European Network of Transmission System Operators for Electricity (ENTSO-E), frequency control is divided into the following

three phases: (i) Primary frequency control, (ii) Secondary power-frequency control, and (iii) Tertiary control. ENTSO-E refers to the reserves for frequency control as operating reserves, and it specifically indicates the previously mentioned controls, respectively, as: (i) Frequency Containment Reserves (FCR), (ii) Frequency Restoration Reserves (FRR), and (iii) Replacement Reserves (RR).

The frequency containment stabilises the frequency, after a disturbance, at a steady-state value within the permissible maximum steady-state frequency deviation. This is done by a joint action of FCR within the synchronous area [31]. The frequency restoration process controls the frequency towards its set-point value by activation of FRR and it replaces the activated FCR. The reserve replacement process replaces the activated FRR and/or supports the FRR activation by activation of RR. One can notice that the inertial response is considered to be a natural characteristic of the power system.

2.2. Analytical Interdependency Between Frequency Containment and Synthetic Inertia

According to IEEE/CIGRE task force, frequency stability is the ability of the power system to maintain steady state frequency following a severe system upset, resulting in a significant imbalance between generation and load [32]. Frequency stability depends on the system's ability to restore the equilibrium between generation and load demand.

During any disturbance that causes an imbalance between the torques acting on the rotor (i.e. active power imbalance between generation and consumption), the net torque causing acceleration or deceleration is $T_a = T_m - T_e$, where T_m is the mechanical torque applied on the rotor, T_e is the electrical torque on the rotor. The simplest model of electro-mechanical swings in a power system is based on the so called swing equation:

$$T_a = T_m - T_e = J\frac{d\omega_m}{dt} \tag{1}$$

where J is the combined moment of inertia of the generator and the turbine (kgm^2), and ω_m is the angular velocity of the rotor (rad/s).

Following an imbalance between the torques (i.e. imbalance between generation and demand), the kinetic energy stored in the rotating masses of the generator and the prime

mover is released. The kinetic energy at rated speed is expressed as $E_{kin} = \frac{1}{2}J\omega_{0m}^2$, where ω_{0m} is the rated angular velocity [33]. By normalising the previous equation in terms of the rated power of the generator S_b, the inertia constant H can be defined as the kinetic energy in Watt-per-seconds at rated speed:

$$H = \frac{J\omega_{0m}^2}{2S_b} \qquad \Longrightarrow \qquad J = \frac{2HS_b}{\omega_{0m}^2} \tag{2}$$

Equation (1) can be reformulated as:

$$\frac{T_m - T_e}{S_b/\omega_{0m}} = 2H\frac{\mathrm{d}}{\mathrm{d}t}(\frac{\omega_m}{\omega_{0m}}) \tag{3}$$

Since S_B/ω_{0m} is the base torque T_{base}, the (3) can be expressed in p.u. as:

$$\bar{T}_m - \bar{T}_e = 2H\frac{\mathrm{d}\bar{\omega}_r}{\mathrm{d}t} \tag{4}$$

$$\bar{\omega}_r = \frac{\omega_m}{\omega_{0m}} = \frac{\omega_e/p}{\omega_0/p} = \frac{\omega_e}{\omega_0} \tag{5}$$

where ω_e is the angular velocity of the electrical rotor, ω_0 is the rated one and p is the number of pole pairs.

The previous equations can be reformulated in terms of the electrical rotor angle. Assuming δ as the electrical rotor angle with respect to a synchronously rotating reference and δ_0 is the rotor angle at t=0, δ can be formulated as:

$$\delta = \omega_e t - \omega_0 t + \delta_0 \tag{6}$$

Therefore, the first and second derivatives of (6) are:

$$\frac{\mathrm{d}\delta}{\mathrm{d}t} = \omega_e - \omega_0 = \Delta\omega_e \tag{7}$$

$$\frac{\mathrm{d}^2\delta}{\mathrm{d}t^2} = \frac{\mathrm{d}\omega_e}{\mathrm{d}t} = \omega_0\frac{\mathrm{d}\bar{\omega}_r}{\mathrm{d}t} \tag{8}$$

Equation(1) can be reformulated in terms of the rotor angle:

$$\bar{T}_m - \bar{T}_e = \frac{2H}{\omega_0}\frac{\mathrm{d}^2\delta}{\mathrm{d}t^2} \tag{9}$$

Reformulating (9) in terms of $\bar{\omega}_e$:

$$\bar{T}_m - \bar{T}_e = 2H\frac{\mathrm{d}\bar{\omega}_e}{\mathrm{d}t} \tag{10}$$

Assuming that $\bar{T}_m$ is constant and that the frequency regulation is only from the load side, then one can assume that $\bar{T}_e$ is composed by: the frequency dependent loads ($\bar{T}_D$), devices participating in FCC ($\bar{T}_{FCC}$) and devices participating in SIC ($\bar{T}_{SIC}$):

$$\bar{T}_e = \bar{T}_D + \bar{T}_{FCC} + \bar{T}_{SIC} \tag{11}$$

where each is composed by a base value and frequency dependent value:

$$\bar{T}_D = \bar{T}_{D_0} + K_D\Delta\bar{\omega}_e \tag{12}$$

$$\bar{T}_{FCC} = \bar{T}_{FCC_0} + K_{FCC}\Delta\bar{\omega}_e \tag{13}$$

$$\bar{T}_{SIC} = \bar{T}_{SIC_0} + K_{SIC}\frac{\mathrm{d}\bar{\omega}_e}{\mathrm{d}t} \tag{14}$$

$\bar{T}_{D_0}$, $\bar{T}_{FCC_0}$ and $\bar{T}_{SIC_0}$ represent the base electric torques in steady state and is addressed further as $\bar{T}_{e_0} = \bar{T}_{D_0} + \bar{T}_{FCC_0} + \bar{T}_{SIC_0}$. K_D is a damping factor in pu, which considers the electrical loads which change the active power consumption due to frequency changes. $K_{FCC} = K_{FCC}(t - t0)$ is the FCC proportional control coefficient. $K_{SIC} = K_{SIC}(t - t0)$ is the SIC proportional control coefficient. K_{FCC} and K_{SIC} are represented in function of the time to represent the time required from those devices to get activated (i.e. time delay). Therefore, the swing equation can be formulated as:

$$\bar{T}_m - \bar{T}_{e_0} = (2H + K_{SIC})\frac{\mathrm{d}\bar{\omega}_e}{\mathrm{d}t} + (K_D + K_{FCC})\Delta\bar{\omega}_e \tag{15}$$

Equation (15) can be expressed as a function of $\frac{\mathrm{d}\bar{\omega}_e}{\mathrm{d}t}$ and $\Delta\bar{\omega}_e$:

$$\frac{\mathrm{d}\bar{\omega}_e}{\mathrm{d}t} = \frac{\bar{T}_m - \bar{T}_{e_0} - (K_D + K_{FCC})\Delta\bar{\omega}_e}{2H + K_{SIC}} \tag{16}$$

$$\Delta\bar{\omega}_e = \frac{\bar{T}_m - \bar{T}_{e_0} - (2H + K_{SIC})\frac{\mathrm{d}\bar{\omega}_e}{\mathrm{d}t}}{K_D + K_{FCC}} \tag{17}$$

From (16), one can notice that FCC and SIC can affect the RoCoF variation during a transient. Meanwhile, (17) shows that the frequency deviation from steady state can be

affected by introducing SIC and FCC. In this regard, the following investigation aims to assess the effects of the two controllers on frequency and RoCoF, by means of simulations and experimental validation.

3. Methodology

In this section, the mathematical formulation and characteristic of the implemented controllers as well as the experimental layout is presented.

3.1. Frequency Containment Control

Frequency containment control (FCC) is achieved by a joint action of FCC providing units within the whole synchronous area with respect to the frequency deviation. Generally, it is achieved using droop controllers, so that governors operating in parallel can share the load variation according to their rated power. The droop of the generator represents the ratio of frequency deviation to change in power output. The frequency variation, Δf, referred to the nominal frequency of the system and is given as a function of the relative power change ΔP or current change ΔI reported to the nominal machine power or current, respectively.

$$\text{a)}\frac{1}{K_{FCC}} = \frac{\Delta f/f_{nom}}{\Delta P/P_{nom}}; \qquad \text{b)}\frac{1}{K_{FCC}} = \frac{\Delta f/f_{nom}}{\Delta I/I_{nom}} \tag{18}$$

For example, a 5% droop ($\frac{1}{K_{FCC}}$) means that a 5% frequency deviation causes 100% change in valve position or power output.

In this study, EVs are used to provide frequency support in terms of FCC by modulating the EV's charging current. Defining a droop value for loads may not be straightforward because the nominal power may not always be determined unequivocally. To comply with the IEC 61851 standard, the EV's charging current can be modulated with a granularity of 1 A, and in this case between 6 and 16 A. This available range of regulating current of 10 A has been assumed as the EV's I_{nom} [34]. EV charging is controlled by charging controller with a 8% frequency-current droop with frequency limits of $48 - 52$ Hz.

The droop is presented in Figure 1-a, where the dash line represents the ideal droop and the solid line represents the real droop with 1 A granularity. To have an up and down

regulation capability of ±5 A, the EV's initial current set-point is set at 11 A. Due to the 1 A granularity and the established operating point, the EV's current set-point oscillated between 11 and 12 A. To avoid this oscillation, the droop characteristic was shifted; so that the frequency limits became $48.2 - 52.2$ Hz. The control diagram for the FCC is presented in Figure 2-a. Following various experiments, it was noticed that the EV's current was under-shooting. To compensate for this phenomena, we have used the ceil function for the different controllers instead of the rounding.

3.2. Synthetic Inertia Control

Although no direct coupling from converter connected generators to the grid is made, a large amount of kinetic energy is stored in these units (e.g. kinetic energy stored in a wind turbine's blades and gearbox). Together with different forms of energy storage in other units, this can be used to deliver synthetic inertia. This means that these units could mimic synchronous generators by delivering an active power response that is proportional to the RoCoF [35, 36].

A synthetic inertia controller (SIC) is implemented in this study, the control diagram is presented in Figure 2-b. The RoCoF is measured over 200 ms. This unit controls the EV's charging current as a function of a RoCoF-current droop characteristic. The droop is shown in Figure 1-b, the dashed line represents the ideal droop and the solid line represents the 1 A granularity. The droop is implemented by defining the RoCoF's low and high limits, with zero RoCoF corresponding to 11 A. The deadband of ±0.8 Hz/s was introduced during the tuning phase where smaller deadband values have led to frequency oscillation. Therefore, it results in a very limited contribution from the EVs.

3.3. EV dynamic model

To successfully integrate EVs into power systems, it is necessary to correctly understand and characterise their dynamic behavior. A detailed model is, therefore, derived considering the EV users' driving requirements, the battery charging and discharging characteristics, the battery dynamics (e.g. time response, ramping time, etc..) and the control/communication delays.

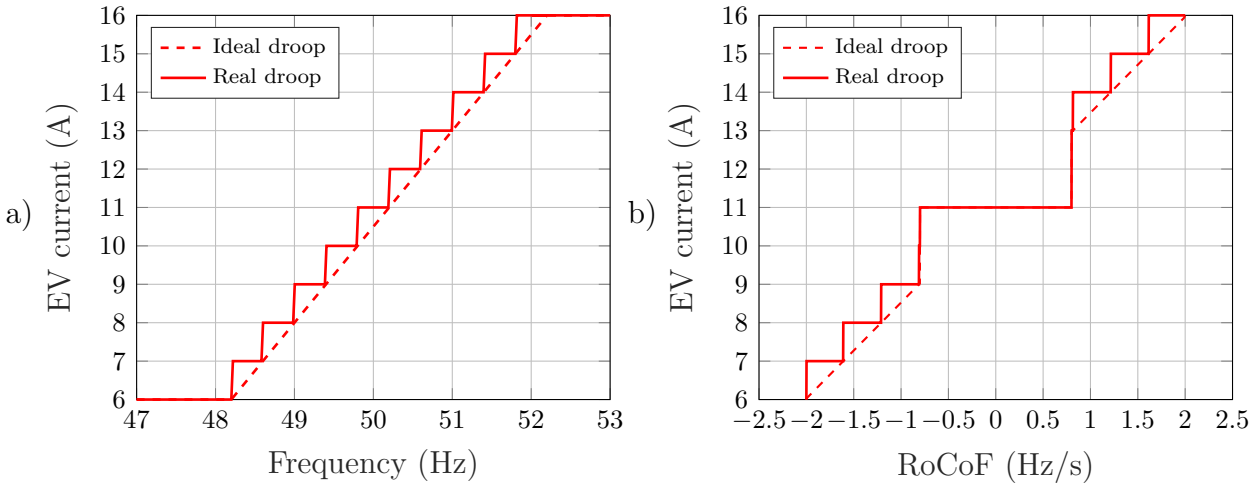

Figure 1: a)FCC droop characteristic, b) SIC droop characteristic

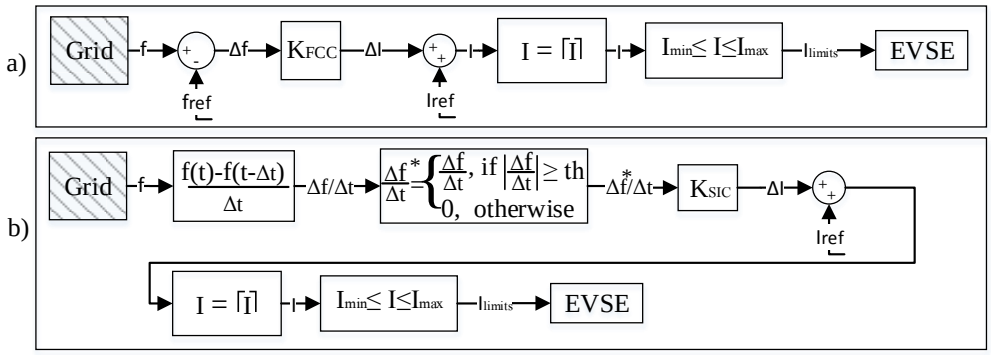

Figure 2: a) FCC control diagram, b) SIC control diagram

Since this study aims to investigate the EV's capabilities and limits in providing fast primary control and synthetic inertia control, the battery charge state was neglected. The EV model is presented in Figure 3. From the dynamic point of view, it is possible to identify two main latencies between the set and the actual current: specifically, a communication delay and the EV activation delay, the sum of which varies between 150ms and 2s. The communication delay depends mainly on latencies in the IT infrastructure, which is in the range of tens of milliseconds. The EV activation delay varies among brands and heavily depends on the embedded power electronics. The most recent models show a faster response time. In any case, the current standard IEC61850 solely requires the car to respond within

3s. The total delay observed in the experimental trials ranges between 200 and 400ms. Therefore, in the simulation study the total delay is considered to be 250ms. As a final note with respect to the voltage dependency, the EVs are modelled as constant current loads.

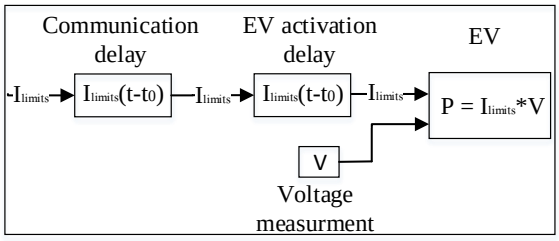

Figure 3: EV dynamic model

3.4. Experimental Layout and Power Components

The experiments are executed in the experimental infrastructure SYSLAB, which is part of the PowerLabDK platform. SYSLAB represents a small scale low voltage power system. It consists of a number of real power components that are interconnected by a three-phase 400 V AC power grid, which is distributed over the Risø campus of the Technical University of Denmark [28]. SYSLAB is also characterised by its communication and control nodes, which allow a strong controllability over the grid. The system may be connected to the utility or it can be islanded if desired. The experimental layout is shown in Figure 4.

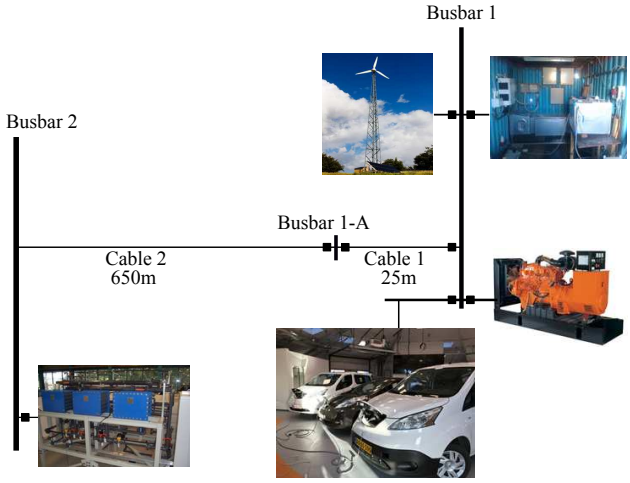

Figure 4: Experimental layout

The experimental setup is composed by two busbars that are connected by 675 m underground cable. The VRB is connected to busbar 2 and installed in building 2 where the busbar is located. The rest of the components are connected to busbar 1 and they are installed in the same building as the busbar. The Aircon wind turbine is installed around 10 m from building 1. The VRB, the Aircon and the Dump load are controlled through a Matlab/Java interface, while the EVs are controlled through a Python interface. Given that all of the components are 3-phase except the EVs, it has been necessary to create an intermediate phase splitter. Each EV is supplied on a different phase via a standard Mennekes (IEC 62196 Type 2) connector. The three Mennekes plugs are controlled separately by three different pieces of electric vehicle supply equipment (EVSE).

The experiments are executed in an islanded configuration where the diesel generator-set acts as the grid forming unit and is the only synchronous inertia device. It also compensates for the small amount of reactive power drawn by each EV, corresponding to 200 VAr each. The different components used during the experiment are listed in Table 1 where $P0$ is the base operating point. SC1 and SC2 refer to Study Case 1 and Study Case 2, respectively.

Table 1: Properties of the devices used in the experiments

Device	Capability	P0 (kW) SC1	P0 (kW) SC2	Description
Diesel	0 - 48 kW -20 - 30 kVAr	24	24	IVECO genset S = 60 kVA, 2 pole pairs
Aircon	10 kW @ 11ms	-	∼4	Wind turbine type 4
Battery	±15 kW ±12 kVA	9	-	Vanadium redox battery, 120 kWh
Dumpload	0 - 78 kW	7	21	Resistor load bank
EV1	6 - 16 A (1.4 - 3.7 kW)	2.5	2.5	Nissan leaf 2016, 30 kWh lithium battery
EV2	6 - 16 A (1.4 - 3.7 kW)	2.5	2.5	Nissan e-NV200 2014, 24 kWh lithium battery
EV3	6 - 16 A (1.4 - 3.7 kW)	2.5	2.5	Nissan e-NV200 2015, 24 kWh lithium battery

3.5. EV Charging Controller and Communication Architecture

Each of the 3 single phase EVs is connected to a different phase of the grid by means of three EVSE. The control and communication setup is shown in Figure 5.

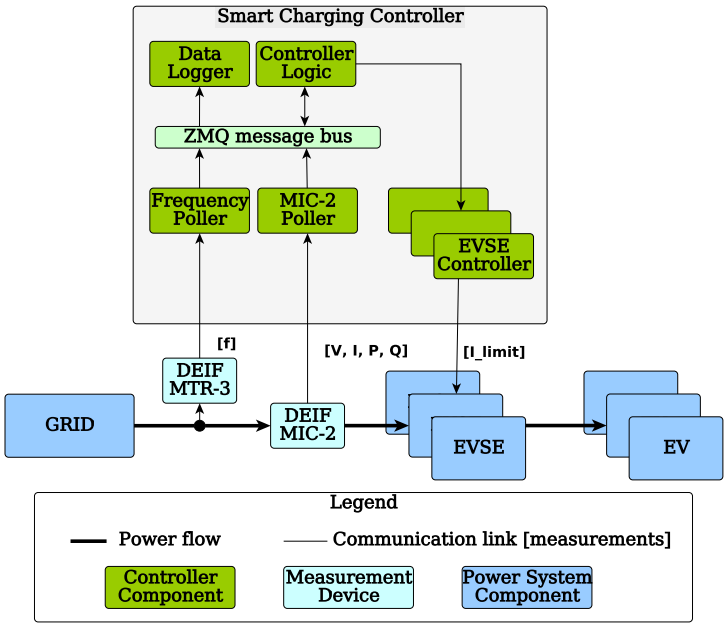

Figure 5: The communication architecture for the implemented smart charging controller

This consists of the following components:

- The smart charging controller − receives the measurements from the multi-instrument, it calculates the response and it sends control signals to the EVSE.
- DEIF MIC-2 − is a multi-instrument measurement device that shows the voltage, current and power measurements with 0.5% accuracy. The device is only used for data logging.
- DEIF MTR-3 − is a multi-instrument measurement device that is used here for fast frequency measurements, which are polled every 200ms.
- EVSE − is rated for 16A
- EV − is the three tested electric vehicles.

- Grid − is the grid connection at the SYSLAB experimental facility.

The smart charging controller consists of many sub-components, as follows:

- Controller logic − reads the latest frequency measurements from the message bus and calculates the $\Delta f/\Delta t$ and the Δf. Calculated set-points are directly sent to the EVSE controller.
- EVSE controller − acts as an interface between the physical EVSE and the controller logic.
- Frequency poller − acts as an interface to the frequency measurement device. In this case DEIF MTR-3 instrument used for frequency sampling every 0.2 seconds with accuracy of 10 mHz.
- MIC-2 poller − multi instrument device interface.
- Data logger − monitors the data exchange on the message bus and logs it to the database.
- ZMQ message bus − is the message bus that is used to represent the data exchange between the previously mentioned controller components.

The timing of the response is crucial for the provision of synthetic inertia. Therefore, the timing of each component in the control loop is important: frequency and RoCoF are measured every 200 ms, the controllers' response is almost instantaneous and communication delay (10-20 ms) to each EV/EVSE pair is optimised by controlling them independently. It uses multi-threading and each EVSE only receives a new control signal if the set-point has changed. Finally, the EV's reaction time is approximately 200–300 ms and, therefore, the whole control and actuator chain has an overall latency equal to 400–500 ms. According to this number, it is expected that the device could positively influence the whole frequency dynamic.

4. Results and Discussion

This section is composed by two subsections, in which the simulations and experimental validation are presented. Two study cases are analysed. In the first study case (SC1), the system is studied involving a set of load steps. An alternate load-increase and load-decrease are applied, so that both over and under frequency dynamics can be analysed. In the second study case (SC2), wind power generation is added to the system. It adds random power fluctuations over the tested period and it allows the possibility of investigating the behaviour of the two controllers and the EVs in a more realistic and challenging situation.

The two study cases are each composed of three scenarios: in the first scenario, the EVs are treated as a constant load; that is, constant current set-point equal to 11 A (Base scenario). In the second scenario, the EVs participate with a synthetic inertia response; that is, SIC. In the third scenario, the EVs participate with a fast frequency response; that is, FCC. An overview of the different scenarios is given in Table 2. During the simulation, only SC1 was analysed.

Table 2: Study cases overview

	Study Case 1	Study Case 2
Scenario 1	Base case	Base case + Wind
Scenario 2	SIC	SIC + Wind
Scenario 3	FCC	FCC + Wind

4.1. Simulations

In this section a simulation study in DigSilent PowerFactory is carried out. It aims to investigate the effects of synthetic inertia control and frequency containment control, and it aims to achieve preliminary results before experimentally validating the controllers. To explore the effects of the 1 A granularity that is imposed by the standard, a sensitivity analysis of different granularity values is conducted.

The same components and grid configuration that are presented in Figure 4 have been modelled, with the operating conditions of SC1, as shown in Table 1.

To make this study as realistic as possible, an oscillatory frequency has been induced in the system by means of a fictitious zero-mean variable load by means of fluctuating active power absorbed by the three-phase resistive load. In this way, it has been possible to emulate the realistic frequency oscillation that the real diesel synchronous generator would generate in such an islanded grid configuration.

First, a load event with amplitude of 2 kW (8.7% of the total consumption) was applied at $t = 10$ s and three scenarios were analysed. The first scenario is considered as a base case where the EVs are treated as a constant load; that is, constant current set-point equal to 11 A. In the second scenario, the EVs participate with a SIC. In the third scenario, the EVs are equipped with the FCC controller. Both the SIC and FCC controllers are implemented according to the control diagrams in Figure 2, thus applying integer EV current set-points to assure standard-compliance. Figure 6 shows the grid frequency, the RoCoF and the EVs' current set-point.

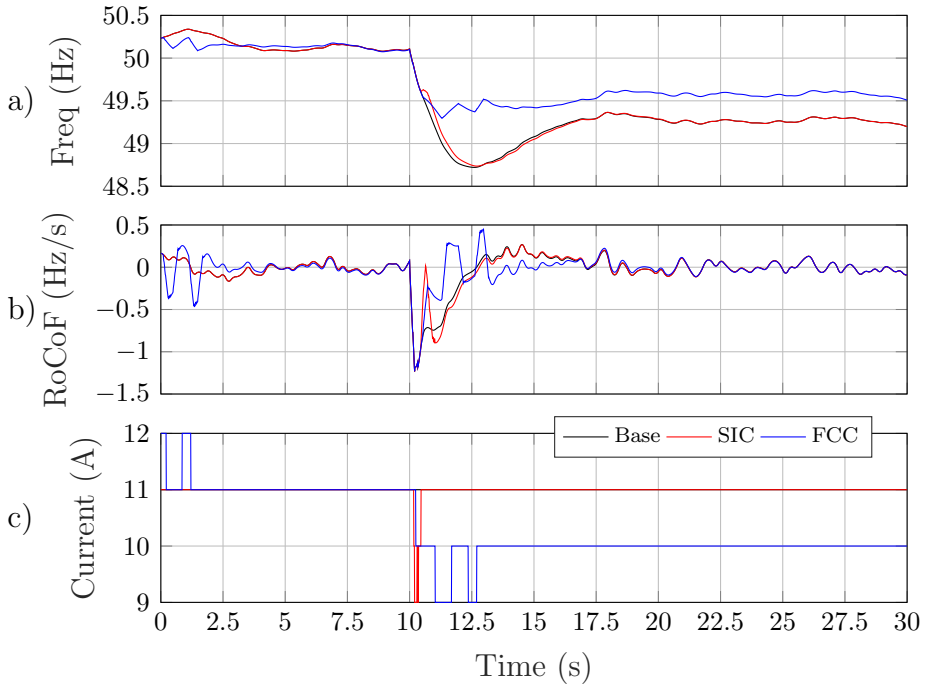

Figure 6: Simulation results obtained by applying ±0.8 Hz/s deadband for SIC: a) frequency, b) RoCoF and c) EV current set-points for the three analysed scenarios, in case of granularity of 1 A.

As expected, Figure 6-a shows that FCC improves the frequency behaviour in terms of frequency nadir and steady state value. It also shows that SIC ameliorates the frequency slope, which is a typical behaviour of introducing more synchronous and/or synthetic inertia into the system. On the other hand, unexpectedly, Figure 6-b shows that FCC has a better performance in terms of RoCoF compared to SIC.

However, a steeper droop and/or smaller deadband for SIC would have led to better performance regarding the RoCoF and the frequency slope. To demonstrate this point, the same simulations were executed changing the deadband of SIC to ±0.5 Hz instead of ±0.8 Hz. The results are presented in Figure 7.

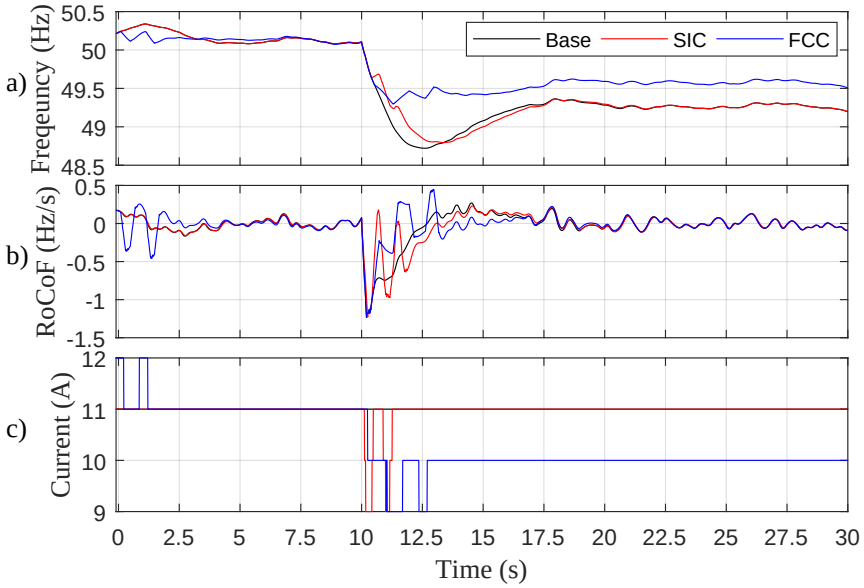

Figure 7: Simulation results by obtained applying ±0.5 Hz/s deadband for SIC: a) frequency, b) RoCoF and c) EV current set-points for the three analysed scenarios, in case of granularity of 1 A.

Figure 7-a shows an improvement regarding the frequency slope compared to the previous case. On the other hand, Figure 7-b shows a marginal improvement regarding the RoCoF. Compared to the previous scenario, Figure 7-c shows that the EVs were participating more by changing the current set-point.

A sensitivity analysis was performed to better understand the effects of the 1 A granularity imposed by the standard IEC 61851 [27] on the performance of the two controllers.

A series of simulations were carried out employing different load steps and different granularities. Frequency drops have been obtained by increasing the active power absorbed by the VRB by 20%, 40%, and 60%. They represent a load event of 8.7%, 15.7% and 23.5% of the total consumption, respectively. For the evaluation of the influence of the granularity, the following values of granularity have been applied, which are expressed as fraction of the actual granularity of 1 A: $\frac{1}{4}$, $\frac{1}{2}$ and 1. Moreover, for the sake of completeness, the case of continuous regulation (no granularity) and the uncontrolled case have also been included in the analysis.

Figure 8 reports 3D bar plots of the results for all of the performed simulations. The results are reported by means of standard deviations (SD) for both Frequency and RoCoF for FCC and SIC.

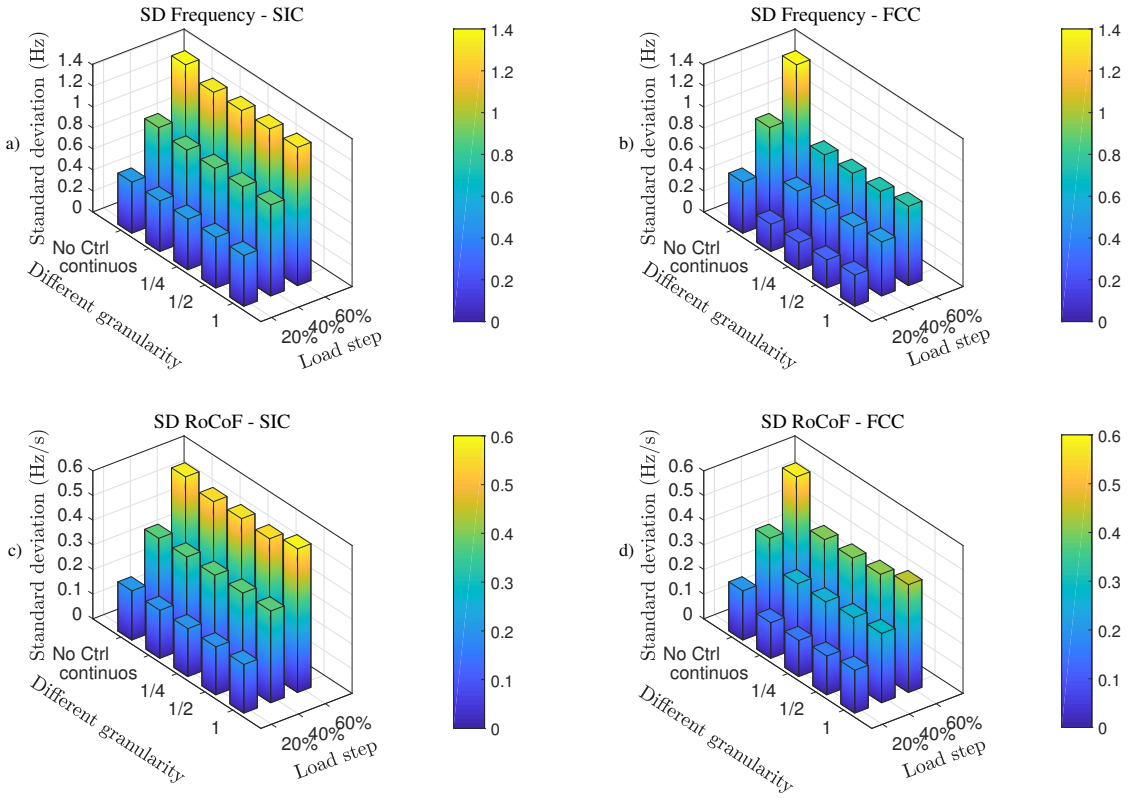

Figure 8: a)SD of the frequency applying SIC and b)SD of the frequency applying FCC, c)SD of the RoCoF applying SIC, d) SD of the RoCoF applying FCC

As expected, Figure 8 shows that in all of the cases the standard deviations depend

on the size of the load step. On one hand, they are mostly constant for the different considered granularity, on the other hand higher values are found in the uncontrolled cases. Moreover, it is noticeable that beneficial effects on the frequency are found in case of FCC. As presented in Figure 6, the EVs' effect makes the frequency rise to a higher steady-state value. Meanwhile, the SIC controller has an embedded reset logic, which makes the EV set-point go back to 11 A right after the event. It is of interest to highlight that the FCC shows an unexpected better contribution to the RoCoF limitation in comparison to the SIC. This is due to the limited number of control actions that took place in case of SIC, which is due to the implemented RoCoF deadband (Figure 1-b). Instead, when providing primary regulation via FCC, no deadband is applied, which activates the controller more often, thus contributing more to the RoCoF containment.

This sensitivity analysis shows that, in this islanded microgrid, the granularity does not influence the results. However, one should note that under a certain combination of system attributes (system inertia and stiffness of the power system) and control units (amount of power involved in the regulation, droop, response/ramp time and granularity of the control actions), the granularity might lead to system instability or oscillation between two consequent set-points, as was experienced during the validation phase.

4.2. Experimental Validation

Following the results obtained during the simulations, the authors will investigate the EVs capability to provide synthetic inertia and frequency containment control in an islanded grid in real circumstances. The experiments are executed in the islanded configuration that is shown in Figure 4, where the diesel is the grid forming unit.

4.3. Study Case 1

In the first study case, the frequency variation is triggered by several load steps. A set of load events from the VRB of the same amplitude is applied ($\approx \pm 2$ kW), namely, 8.7% of the initial installed load. To better investigate the controllers as well as the frequency dynamics, an additional set of load events with a different amplitude is applied, specifically

($\approx \pm 4$ kW), 17% of the initial installed load. The grid units as well as the initial conditions are reported in Table 1.

The three scenarios are characterised by the same initial conditions and load steps. The first scenario (S1) is a base case, in which the EVs receive a constant current set-point; that is, 11 A absorbing around 2.5 kW. In the second scenario (S2), the EVs are controlled by the synthetic inertia controller, which modulates the charging level between 6 and 16 A with steps of 1 A in function of the RoCoF-current droop characteristic presented in Figure 1-b. In the third scenario (S3), the EVs are controlled by the frequency containment controller. The controller modulates the EVs' charging level between 6 and 16 A with steps of 1 A in function of the frequency-current droop characteristic presented in Figure 1-a.

The results of the experiments are presented in Figure 9. Figure 9-a shows the system frequency for the three scenarios. Figure 9-b shows the RoCoF measured over 200 ms in grey and the filtered signal after applying the deadband in red (± 0.8 Hz/s deadband is considered). In Figure 9-c the controllers' current setpoint is plotted versus the EVs' absorbed current. Since the three EVs act similarly, only the current of EV1 is presented.

Figure 9-c shows that the EVs change the absorbed current as desired by the different controllers. However, due to the 1 A granularity, the implemented droop and the operating point, the 2 kW load event implies the FCC to oscillate between 12 and 13 A, and between 9 and 10 A. A 6 kW load event is only introduced for Scenario 3, at which a stable operating point was found. In fact, Figure 9-c shows that the EV's current did not oscillate for this load event (around t=450s). However, this oscillation can be reduced by implementing a hysteresis function.

Figure 9-a shows that FCC limits the maximum frequency deviation compared to the base case, while the SIC does not have an effect on it. On the other hand, due to the oscillation between the different set-points in case of FCC, Figure 9-b shows that the RoCoF was outside the deadband more frequently when compared to scenario 1 and 2.

Due to the response delay of the EVs and the dynamics of the diesel, which led to a continuous frequency oscillation, it is difficult to perceive a valuable improvement in terms of the RoCoF from SIC.

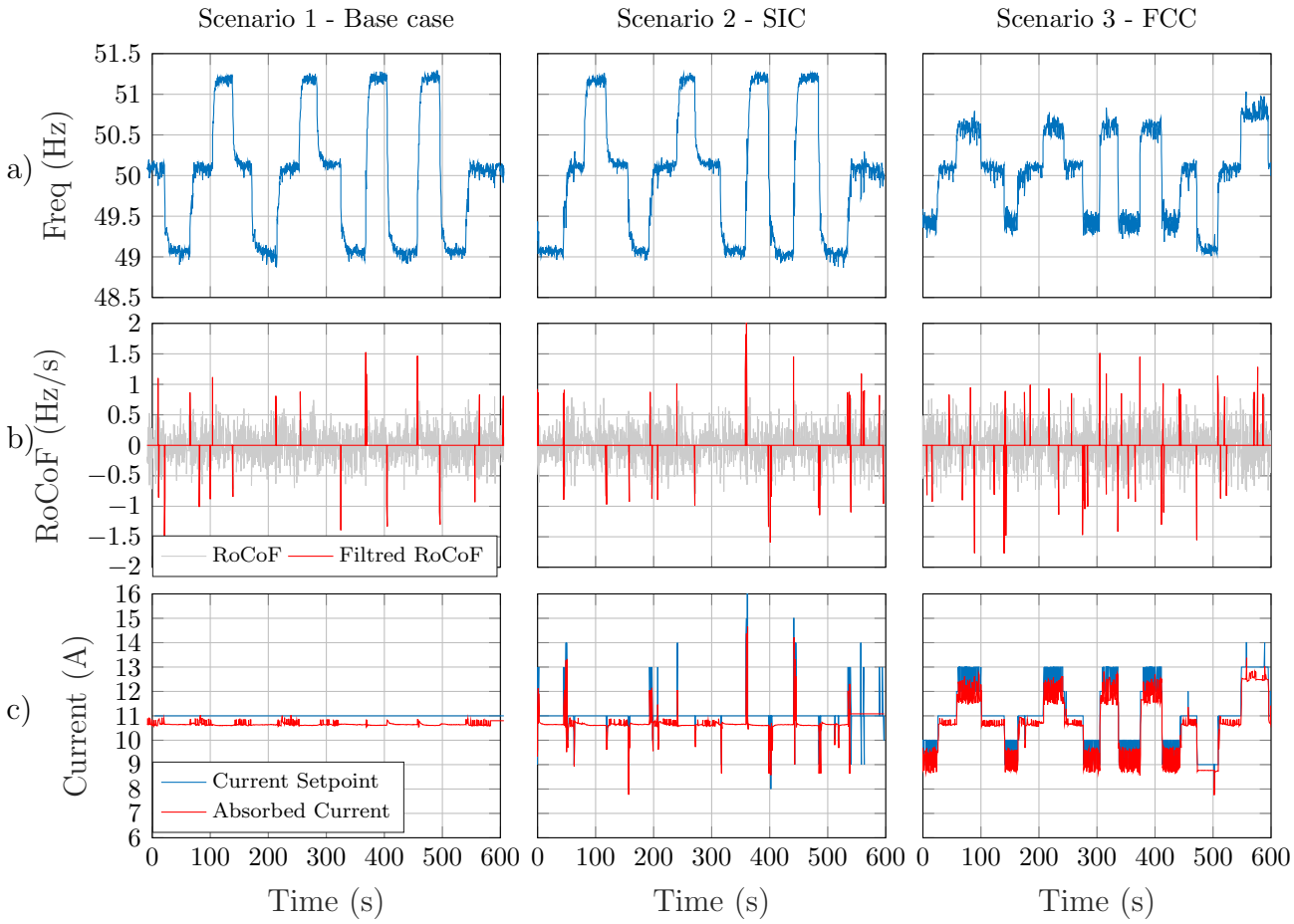

Figure 9: a)The grid frequency, b) the RoCoF, C) EV1's set-point vs absorbed current

To better compare the performance of the two controllers in terms of RoCoF and frequency, the standard deviation and the energy contained in the signal (also addressed as normalised energy) is calculated and presented in Table 3. For a discrete signal $x(n)$, the normalised energy is calculated as $\frac{1}{N}\sum_{n=1}^{N} x(n)^2$, where N is the number of samples taken for computation. It shows that the two controllers do not improve the RoCoF when compared to the base case.

To understand the effects of the SIC on the frequency compared to the base case, Figure 10 shows a zoom of the frequency, the RoCoF and the EV's absorbed current for the three scenarios. In Figure 10-a, one can notice that the SIC has improved the frequency slope as expected and as experienced during the simulations.

Table 3: SC1—Standard deviation and normalised energy

	RoCoF		Frequency
	SD	Normalised Energy	SD
Base	0.29	0.083	0.77
SIC	0.31	0.093	0.79
FCC	0.33	0.11	0.48

Due to the embedded deadband, the SIC contribution is very limited. However, since the three EVs are characterised by the same delay and granularity (i.e. acting simultaneously with steps), one can observe the sharp change in frequency, which will lead to worse RoCoF compared to the base case as shown in Figure 10-b. To overcome this issue, it might be of interest to study different delays and droops among the EVs. This might induce a more smooth frequency change and, therefore, a better RoCoF. It is of interest to notice from Table 3, where the SD is reported, and Figure 10-b that the FCC has worsened the RoCoF when compared to the SIC and the base case.

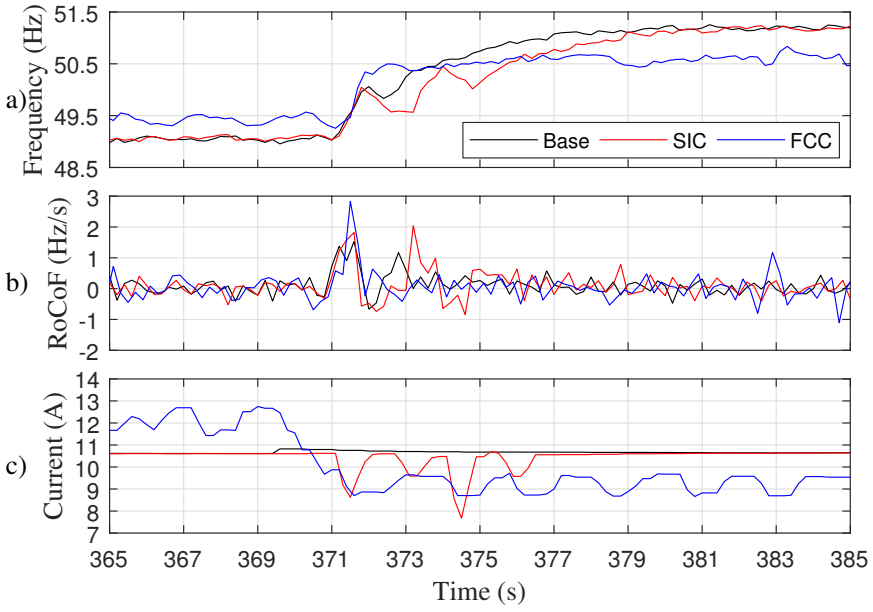

Figure 10: a) The grid frequency, b) the RoCoF, C) EV1's absorbed current

4.4. Study Case 2

In the second study case, the two controllers are analysed during wind power production. The VRB set-point is set to zero during this study case. The same scenarios and droop characteristic as the previous study case are applied. Due to the random stochasticity of the wind generation and the diesel dynamics, the initial and boundary conditions are not exactly identical. Nevertheless, this study case aims to investigate the performance of each controller and the EVs in a more challenging and realistic configuration rather than comparing the different scenarios. The results for SC2 are presented in Figure 11.

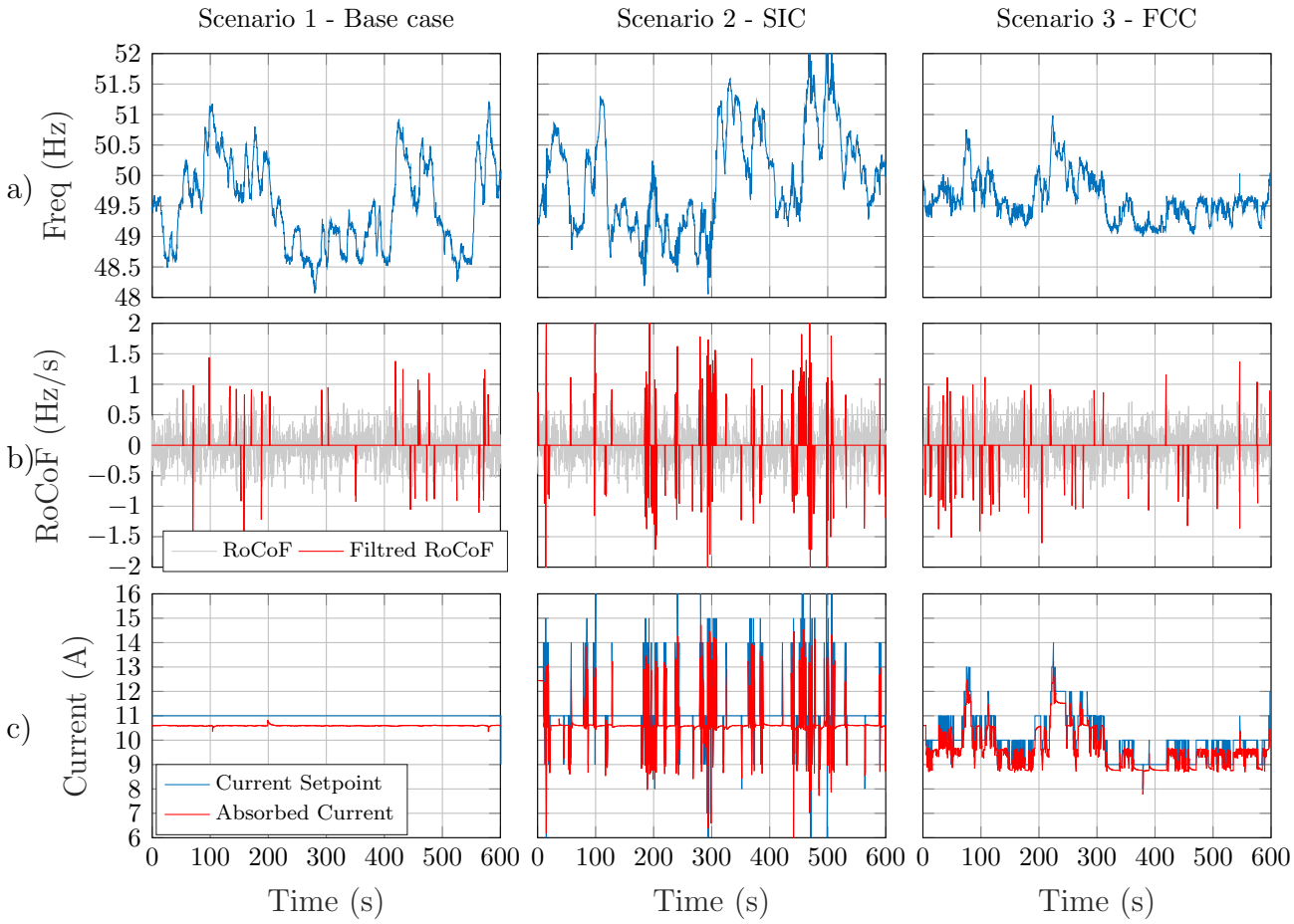

Figure 11: a)The grid frequency, b) the RoCoF, C)EV1's set-point vs absorbed current

Figure 11-a shows the grid frequency for the three scenarios. Figure 11-b shows the RoCoF measured over 200 ms in grey and the filtered signal after applying the deadband

in red. In Figure 11-c the controllers' current set-point is plotted versus the EVs' absorbed current. Since the three EVs are acting similarly, only the current of EV1 is presented.

The three scenarios were executed over a total time of 30 minutes. The average wind production did not differ so much among the three scenarios: so that the different scenarios are still comparable. Figure 11-a shows that the FCC does have a remarkable effect in limiting the maximum frequency deviation. Figure 11-b shows that by applying the SIC, the RoCoF is outside the deadband more frequently.

To better compare the three scenarios, mean value and standard deviation of the wind production together with the standard deviation of the frequency and the RoCoF are calculated and presented in Table 4.

Table 4: SC2—Standard deviation and normalised energy

	Wind Generation		RoCoF		Frequency
	Mean	SD	SD	Normalised Energy	SD
Base	3.5 kW	1.4	0.31	0.098	0.71
SIC	4.6 kW	1.68	0.45	0.2	0.83
FCC	3.1 kW	1.28	0.34	0.11	0.36

As mentioned previously, due to the random wind production and the non-replicability of the same conditions, the comparison is not perfect, especially in terms of RoCoF due to the continuous variation of the wind profile.
However, the mean value of the wind production among the three scenarios does not differ excessively, which allows us to compare the standard deviation of the frequency. Table 4 and Figure 11-a show the remarkable positive effect of FCC on the frequency.

5. Conclusion and Future Work

We started from the research question: given the trend of decreasing system inertia, can fast frequency containment compensate or replace the need for synthetic inertia? First, this work analytically showed the interdependence between frequency containment and synthetic inertia control on the transient frequency variation and the RoCoF. Second, on the simu-

lation level, it presented the ability of fast frequency control in improving the frequency in terms of nadir, steady state value and RoCoF. It also presented the ability of synthetic inertia control to improve the frequency nadir and slope following an event. While it was acknowledged that EVs could quickly and almost precisely respond to fast changing current set-points, some technical limitations in employing EVs for such services were found. Finally, an experimental validation was conducted, presenting the capabilities and limitations of the two controllers under two different circumstances: following load events in both directions and exogenous wind generation profiles.

Employing the FCC, the simulations results showed a remarkable improvement of the frequency nadir and steady state value. It showed also a very limited improvement in terms of RoCoF. The controller did not limit the maximum RoCoF following the event but it did improve the overall behaviour compared to the base case. Similarly, the experiments showed the ability of FCC in limiting the maximum frequency deviation, both following a series of load events or considering a wind power generation. Although in simulation the sensitivity analysis showed a very limited effect of the granularity, in the experimental phase, due the 1A granularity, the FCC controller caused the EV absorbed current to oscillate between two consecutive set points, worsening the calculated RoCoF. It should be noted that this oscillation was due the combination of 1A granularity, the implemented droop and the operating point. However, this effect can be limited by employing an hysteresis-based algorithm.

By applying the SIC, the simulations presented limited frequency improvements in terms of frequency nadir and frequency slope. They also showed that employing a smaller deadband allowed a better contribution, slightly improving frequency nadir and slope. On the other hand, the smaller deadband worsened the RoCoF trend when compared to the base case. However, in both cases, the controller did not limit the maximum RoCoF value. As mentioned, the SIC slightly improved the frequency slope but worsened the RoCoF. During our interpretation of this unexpected phenomena, it has been found that this might be due to the fact of using the same RoCoF signal for both control and examination purposes. In other words, the RoCoF used for control purpose should be calculated over a smaller time

window to the one used by the RoCoF relay to detect the variations. Nevertheless, considering the derivative characteristic of the SIC, its implementation might easily lead to frequency oscillation and this limits the ability to exploit the resource (e.g. large deadband). For the SIC, the experiments were conducted for two cases: first, following load events; and second, considering wind power generation. In terms of frequency, the SIC effects were negligible for both cases. For the first case, even if the EVs were able to follow the desired set points, the SIC did not show a noticeable improvement in terms of RoCoF. On the other hand, considering wind power generation, the SIC had very remarkable negative effects in terms of RoCoF. It should be noted that this effect might have been limited by employing less steep droop parameters; on the other hand, this would have limited the EVs participation (i.e. flexibility margin).

In general, employing faster response devices will allow us to better exploit the resource's capabilities. For example, this was shown in case of SIC where the smaller time response permitted the use of a narrower deadband. It can be concluded that the actual series produced EVs are able to provide ancillary services in terms of fast frequency response and synthetic inertia by solely relying on unidirectional charging. On the other hand, the experiments show that with the actual EV's response time, a large deadband was needed for the SIC and this limited its contribution. To achieve better performance, new requirements in terms of the EV's response time need to be set. In future work, the authors recognise the importance of extending the analytical formulation of the interdependence of the two controllers on the system frequency. Moreover, it is of interest to expand the analysis over a larger number of flexible units by employing different control attributes.

Acknowledgments

The work in this paper has been partly supported by the European Commission, under the FP7 project ELECTRA (grant no: 609687) and partly by the Danish research projects Parker (ForskEL kontrakt nr. 2016-1-12410) and Electra Top-up (grant: 3594756936313). The authors are also grateful to Nissan Denmark for providing the two Leafs that were used in the experiments.

References

[1] A. Adrees, P. N. Papadopoulos, J. V. Milanovi, A Framework to Assess the Effect of Reduction in Inertia on System Frequency Response, Power and Energy Society General Meeting (2016) 1–5doi:10.1109/PESGM.2016.7741695.

[2] A. Ulbig, T. Borsche, G. Andersson, Impact of Low Rotational Inertia on Power System Stability and Operation, in: The 19th World Congress ofthe International Federation of Automatic Control (IFAC14, 2014, pp. 1–12. arXiv:arXiv:1312.6435v2, doi:10.3182/20140824-6-ZA-1003.02615.

[3] ENTSO-E, Frequency Stability Evaluation Criteria for the Synchronous Zone of Continental Europe, Tech. rep., ENTSOE (2016).

[4] The Commission for Energy Regulation, Rate of change of frequency modification to the grid code, Tech. rep., CER (2014).

[5] E. Muljadi, V. Gevorgian, M. Singh, S. Santoso, Understanding inertial and frequency response of wind power plants, 2012 IEEE Power Electronics and Machines in Wind Applications (2012) 1–8doi:10.1109/PEMWA.2012.6316361.

[6] S. Sharma, S. H. Huang, N. D. R. Sarma, System inertial frequency response estimation and impact of renewable resources in ERCOT interconnection, IEEE Power and Energy Society General Meeting (2011) 1–6doi:10.1109/PES.2011.6038993.

[7] R. A. Walling, N. W. Miller, Distributed Generation Islanding Implications on Power System Dynamic Performance, in: Power Engineering Society Summer Meeting,, Chicago, 2002, pp. 92–96. doi:10.1109/PESS.2002.1043183.

[8] C. Ten, P. Crossley, Evaluation of ROCOF relay performances on networks with distributed generation, IET 9th International Conference on Developments in Power Systems Protection (DPSP 2008) 2008 (2008) 522–527. doi:10.1049/cp:20080092.

[9] Y. Mu, J. Wu, N. Jenkins, H. Jia, C. Wang, A Spatial-Temporal model for grid impact analysis of plug-in electric vehicles, Applied Energy 114 (February) (2014) 456–465. doi:10.1016/j.apenergy.2013.10.006.

[10] J. R. Pillai, B. Bak-Jensen, Impacts of electric vehicle loads on power distribution systems, IEEE Vehicle Power and Propulsion Conference, VPPC (2010) 6–11doi:10.1109/VPPC.2010.5729191.

[11] A. Foley, B. Tyther, P. Calnan, B. Ó. Gallachóir, Impacts of Electric Vehicle charging under electricity market operations, Applied Energy 101 (2013) 93–102. doi:10.1016/j.apenergy.2012.06.052.

[12] K. Hedegaard, H. Ravn, N. Juul, P. Meibom, Effects of electric vehicles on power systems in Northern Europe, Energy 48 (1) (2012) 356–368. doi:10.1016/j.energy.2012.06.012.

[13] M. H. Amini, M. Parsa, O. Karabasoglu, Simultaneous allocation of electric vehicles ' parking lots and distributed renewable resources in smart power distribution networks, Sustainable Cities and Society

28 (2017) 332–342. doi:10.1016/j.scs.2016.10.006.

[14] M. H. Amini, M. P. Moghaddam, Probabilistic Modelling of Electric Vehicles ' Parking Lots Charging Demand, in: Electrical Engineering (ICEE), 2013 21st Iranian Conference, 2013, pp. 3–6. doi:10.1109/IranianCEE.2013.6599716.

[15] A. Molina-garcía, F. Bouffard, D. S. Kirschen, Decentralized Demand-Side Contribution to Primary Frequency Control, IEEE Transactions on Power Systems 26 (1) (2011) 411–419. doi:10.1109/TPWRS.2010.2048223.

[16] M. R. V. Moghadam, S. Member, R. T. B. Ma, Distributed Frequency Control in Smart Grids via Randomized Demand Response, IEEE Transactions on Smart Grid 5 (6) (2014) 2798–2809.

[17] W. Kempton, J. Tomić, Vehicle-to-grid power implementation: From stabilizing the grid to supporting large-scale renewable energy, Journal of Power Sources 144 (1) (2005) 280–294. doi:10.1016/j.jpowsour.2004.12.022.

[18] E. Sortomme, M. A. El-sharkawi, Optimal Scheduling of Vehicle-to-Grid Energy and Ancillary Services, IEEE TRANSACTIONS ON SMART GRID 3 (1) (2012) 351–359. doi:10.1109/TSG.2011.2164099.

[19] D. Wang, J. Coignard, T. Zeng, C. Zhang, S. Saxena, Quantifying electric vehicle battery degradation from driving vs . vehicle-to-grid services, Journal of Power Sources 332 (2016) 193–203. doi:10.1016/j.jpowsour.2016.09.116.

[20] K. Knezović, C. Træholt, M. Marinelli, P. B. Andersen, Katarina Knezović Active integration of electric vehicles in the distribution network theory , modelling and practice, Phd thesis, Technical University of Denmark (2017).
URL http://orbit.dtu.dk/files/131995291/Knezovic{_}PhDthesis{_}final.pdf

[21] Y. Mu, J. Wu, J. Ekanayake, N. Jenkins, H. Jia, Primary frequency response from electric vehicles in the Great Britain power system, IEEE Transactions on Smart Grid 4 (2) (2013) 1142–1150. doi:10.1109/TSG.2012.2220867.

[22] K. Knezović, S. Martinenas, P. B. Andersen, A. Zecchino, M. Marinelli, Enhancing the Role of Electric Vehicles in the Power Grid: Field Validation of Multiple Ancillary Services, IEEE Transactions on Transportation Electrification 7782 (c) (2016) 1–1. doi:10.1109/TTE.2016.2616864.

[23] W. Kempton, J. Tomic, Vehicle-to-grid power implementation: From stabilizing the grid to supporting large-scale renewable energy, Journal of Power Sources, J. Power Sources, J Power Sou, J Power Sources 144 (1) (2005) 280–294. doi:10.1016/j.jpowsour.2004.12.022.

[24] F. Teng, Y. Mu, H. Jia, J. Wu, P. Zeng, G. Strbac, Challenges on primary frequency control and potential solution from EVs in the future GB electricity system, Applied Energy 194 (2016) 353–362. doi:10.1016/j.apenergy.2016.05.123.

[25] A. Schuller, C. M. Flath, S. Gottwalt, Quantifying load flexibility of electric vehicles for renewable

energy integration, Applied Energy 151 (2015) 335–344. doi:10.1016/j.apenergy.2015.04.004.

[26] P. Tielens, D. V. Hertem, The relevance of inertia in power systems, Renewable and Sustainable Energy Reviews 55 (2016) 999–1009. doi:10.1016/j.rser.2015.11.016.

[27] IEC 61851-1:2010, Electric vehicle conductive charging system Part 1: General requirements (2010).

[28] M. Marinelli, S. Martinenas, K. Knezović, P. B. Andersen, Validating a centralized approach to primary frequency control with series-produced electric vehicles, Advances in Life Course Research 7 (2016) 63–73. doi:10.1016/j.est.2016.05.008.

[29] J. A. Suul, S. D. Arco, G. Guidi, Virtual Synchronous Machine-Based Control of a Single-Phase Bi-Directional Battery Charger for Providing Vehicle-to-Grid Services, IEEE Transactions on Industry Applications 52 (4) (2016) 3234–3244. doi:10.1109/TIA.2016.2550588.

[30] L. Martini, A. Morch, L. Radaelli, C. Caerts, C. Tornelli, S. Hänninen, H. Brunner, Electra IRP approch to voltage and frequency control for future power systems with high DER penetration, in: 23rd International Conference on Electricity Distribution CIRED, 2015, pp. 1–5.

[31] ENTSO-E, ENTSO-E, Continental Europe Operation Handbook, Tech. Rep. Cc, ENTSOE (2009).

[32] P. Kundur, J. Paserba, V. Ajjarapu, G. Andersson, A. Bose, C. Canizares, N. Hatziargyriou, D. Hill, A. Stankovic, C. Taylor, T. Van Cutsem, V. Vittal, Definition and Classification of Power System Stability, IEEE Transactions on Power Systems 21 (3) (2004) 1387–1401. doi:10.1109/TPWRS.2004.825981.

[33] P. Kundur, Power System Stability and Control, McGraw-Hill, 1994.

[34] A. Zecchino, M. Rezkalla, M. Marinelli, Grid Support by Single-Phase Connected Electric Vehicles without V2G Capability : Fast Primary Frequency Control, in: International Universities' Power Engineering Conference - UPEC, Coimbra, 2016, p. 6.

[35] M. Rezkalla, S. Martinenas, A. Zecchino, M. Marinelli, Implementation and Validation of Synthetic Inertia Support Employing Series Produced Electric Vehicles, in: International Conference on Electricity Distribution - CIRED, 2017, pp. 12–15, accepted for publication.

[36] M. Rezkalla, M. Marinelli, M. Pertl, K. Heussen, Trade-off analysis of virtual inertia and fast primary frequency control during frequency transients in a converter dominated network, in: 2016 IEEE Innovative Smart Grid Technologies - Asia (ISGT-Asia), 2016, pp. 890–895. doi:10.1109/ISGT-Asia.2016.7796503.

Paper D

Title:

Enhanced Primary Frequency Control from EVs: a Fleet Management Strategy to Mitigate Effects of Response Discreteness

Authors:

Antonio Zecchino, Salvatore D'Arco, Atsede G. Endegnanew, Magnus Korpås and Mattia Marinelli

Published in:

IET Smart Grid (under review)

Enhanced Primary Frequency Control from EVs: a Fleet Management Strategy to Mitigate Effects of Response Discreteness

Antonio Zecchino [1], Salvatore D'Arco [2*], Atsede G. Endegnanew[2], Magnus Korpås[3], Mattia Marinelli[1]

[1] Department of Electrical Engineering, Technical University of Denmark, 4000 Roskilde, Denmark
[2] Department of Energy Systems, SINTEF Energy Research, 7465 Trondheim, Norway
[3] Department of Electric Power Engineering, Norwegian University of Science and Technology, 7465 Trondheim, Norway
[*] salvatore.darco@sintef.no

Abstract: This paper addresses the effects on power systems of control discreteness in aggregated electric vehicles (EVs) providing frequency regulation. The EV chargers are controlled according to the system frequency deviation by implementing a standard-compliant fast primary frequency controller (PFC). The possible consequences of relying on a discrete response are identified both in large power systems and in microgrids, in terms of reserve provision error and induced system frequency oscillations. Related challenges are first identified by a theoretical analysis and then an EV fleet management solution relying on droop shift strategies for the individual EVs within a fleet is proposed. Further, the PFC controller is implemented in a microgrid with a power-hardware-in-the-loop approach, to complement the investigation with an experimental validation. Both the analytical and the experimental results demonstrate how the controller performance is influenced by the response granularity and that related oscillations are prevented either by reducing the amplitude of such discrete responses or by applying appropriate shifts on the droops for individual EVs.

1. Introduction

Frequency stability has been traditionally assured relying on ancillary services provided by conventional large power plants that nowadays are being partly replaced by power electronics interfaced and variable renewable energy sources. This leads to the need of providing grid services relying more and more on small aggregated units connected to distribution grids. Beside small generating units such as photovoltaics and wind turbines, demand-side management is seen as a relevant prospective source of frequency regulation services, such a primary frequency control (PFC) [1]–[3]. However, as the primary function of distributed energy resources differs from the provision of grid services, many technical challenges arise when it comes to aggregate and control them. For example, although electric vehicles (EVs) are commonly considered flexible resources that can improve the system operation, technical barriers may emerge. In fact, the response times of both single EVs as well as aggregated EV fleets is one of the most challenging aspects in enabling EVs participation in the reserve provision. Furthermore, the compliance of each EV/EV charger with technical standard IEC 61851 for AC charging [4] and IEC 15118 for DC charging possibly with vehicle-to-grid (V2G) [5], along with the limitations in commercial standard-compliant hardware for EV charging [6], [7], require a given granularity when setting the charging rate.

In this paper the effects of EVs performing grid frequency regulation are investigated. An EV standard-compliant PFC controller is proposed, whose performance is assessed under different power system conditions, by analysing the responsiveness of the regulating EVs when relying on discrete responses. Furthermore, an analytical analysis of the possible consequences of the required discreteness in the EV response is presented, along with an EV fleet management solution to overcome such issues. The EV controller was tuned in a safe operation working point and tested in a microgrid modelled to replicate the experimental layout of previous related laboratory activities [8], [9]. Finally, results from laboratory experimental activities complement the granularity analysis with the employment of real hardware. The tests were carried out in a power-hardware-in-the-loop (P-HiL) experimental environment [10], [11], where two 3-phase 60 kVA power converters enabled the reproduction of the behaviour of an EV fleet, connected to a 200 kVA power amplifier, acting as a grid emulator.

The paper is structured as follows. Section 2 provides a literature survey with regards to the state-of-the-art of aggregation of EVs for system service provision and presents the novelty of the work. Section 3 outlines the proposed standard-compliant EV controller. Section 4 presents an analytical formulation to assess the effects of a discrete EV response, and proposes an EV fleet management strategy. In Section 5 the P-HiL experimental validation is reported, and results are discussed. Conclusions are in Section 6.

2. EVs as PFC Providers: Literature Survey

The aggregation of EVs as possible source of power system frequency regulation services with both uni- and bi-directional charging has been investigated in many works. A number of studies show the potential capability of EV fleets in performing power system services. In particular, [12] shows that evident improvements in islanded power system dynamics can be achieved relying on EV droop controllers. [13] demonstrates how large scale utilization of EVs utilized

as a demand response resource can promote the development of the wind generation in the Great Britain power system, also taking into account the EV users' travelling behaviour in the problem formulation. Similar results are found in other studies [14]–[17], which confirm the positive impact of EV charging control strategies at a system level with high penetration level of generation from renewable energy sources.

Possible aggregate EV models and control strategy approaches are also of interest. In [18] a discretised regulation dispatch approach is utilized, which aims at meeting the desired calculated total power signal by turning certain EVs on or off according to a priority index. In this way, the control architecture is merely centralized, since the aggregator sends on/off signals as results of its centralized dispatch algorithm. This kind of centralized approaches requires bidirectional real-time communication capabilities, as signals from the charging stations are supposed to be sent back to aggregators. In [19], [20] the communication complexity is drastically reduced by relying on a decentralized approach. In particular, in [20] the decision to change charging set-point is taken locally by the single EV, while a remote centralized frequency measurement is performed by the aggregator, who will dispatch the same correspondent signal to each EV. Nevertheless, despite the potential positive effects, the aggregate response can induce problems to the power system when the share of EV providing regulation is high and all the units respond to the same frequency signals. In this regard, accurate aggregated EVs models need to be implemented, which include proper overall response behaviour. Thus, [21] proposes a distributed frequency control that randomly assigns delays to each EV of the fleet. Additionally, [22] presents a novel methodology to design EV droop controller in a way to ensure the same stability margin with and without EVs during the primary frequency control.

The above-presented works mostly focus on simulations, whereas experimental validation is rarely carried out. In fact technical limitations due to standard requirements are neglected, and ideal response in terms of EV power exchange is considered. Testing activities have been performed by Lehfuss et al. [23], investigating the performance of a real charging EV at a charging post complying with the IEC 61851. In [24] the authors test a price signal-based charging algorithm on commercial EVs, although without providing any ancillary services. By contrast, experimental activities validating how series-produced EVs can provide grid services have been carried out both on an experimental testbed [8] and on a real field test [25]. These practical validation papers deal, among others, with the issue of charging-related controllability limitation due to technical standards requirements and real commercially-available hardware, commonly neglected in most of the literature.

Given the presented state-of-the-art on aggregation of EVs for power system service provision, this paper extends the existing literature by investigating implementation challenges in a microgrid and in large power systems given limitations due to components' design and charging-related technical standards requirements, and a control strategy approach is outlined. So, the novelty of the work is threefold:

i) After developing a standard-compliant EV fast frequency controller, an analytical investigation on the consequences of relying on a discrete EV response is presented, both in a large-size power system and in a microgrid;

ii) An EV fleet management solution to overcome related issues on an aggregated level is proposed;

iii) Results from a P-HiL experimental validation of the effectiveness of the EV controller are presented to complement the investigation.

3. Proposed Standard-Compliant EV Controller

This section presents the design and implementation of the proposed EV standard-compliant controller. Fast primary frequency control (PFC) is achieved by a joint action of PFC providing units within the whole synchronous area with respect to the frequency deviation. This is typically achieved via droop controllers, meaning that governors operating in parallel share the load variation according to their rated power [26]. The droop constant K_{PFC_pow} in [W/Hz] represents the change in power output ΔP for a given frequency deviation Δf:

$$\Delta P = K_{PFC\_pow} \cdot \Delta f \tag{1}$$

In this study frequency regulation is provided via single-phase EVs by modulating their power consumption. As the technical standards IEC 61851 [4] and IEC 15118 [5] require the charging process to be modulated by setting the charging current, (1) can be rewritten as in (2), where ΔI_{PFC_id} is the ideal current variation that the EV would assure in case of a given Δf, and K_{PFC} is the f-i droop constant in [A/Hz].

$$\Delta I_{PFC\_id} = K_{PFC} \cdot \Delta f \tag{2}$$

In practice, the real current variation applied to the EV ΔI_{PFC} differs from ΔI_{PFC_id} mainly for three reasons. First, an upper limitation of the set-point is determined by the size of the breaker in the EV charger circuit, e.g., for the single-phase Mode2 charging it can be 16 A. Second, EV technical standards impose constraints in the set-point granularity, which is typically handled by aggregators and hardware manufactures with 1 A discreteness [6], [7]. Third, lower current limits are imposed by the standards for some charging modes, e.g., IEC 61851 requires a minimum current set-point of 6 A for Mode2 charging. Given these considerations, Fig. 1 shows the regulation curve in case of K_{PFC}=2.5 A/Hz (K_{PFC_pow}=575 W/Hz). The dashed line represents the ideal current variation ΔI_{PFC_id} while the solid one shows the real current variation ΔI_{PFC} with 1 A granularity.

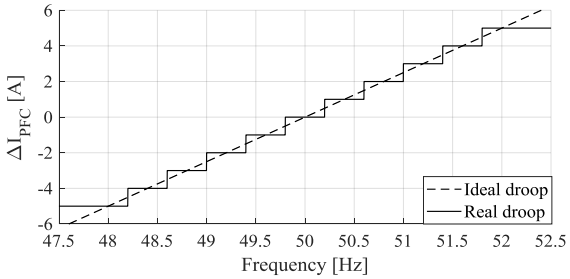

Fig. 1. *PFC ideal and discrete regulation curves.*

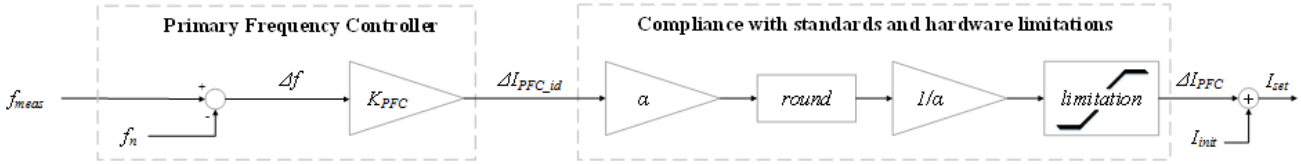

Fig. 2. *Block scheme for the implementation of the standard-compliant PFC. The implemented logics along with adjustments for the compliance with standards and employed hardware give the reference current signal to be set on the EV charger.*

Given the required EV set-point limitations I_{lim} of 6 and 16 A, to have a symmetrical up/down regulation capability I_{reg} of ±5 A, the EV's initial current set-point I_{init} is set at 11 A, which corresponds to a stable system load condition at 50 Hz. The current set-point I_{set} set by the controller on the EV charger is calculated as in (3), where the regulating contribution of the controller ΔI_{PFC} is positive or negative in case of over- or under-frequency, respectively.

$$I_{set} = I_{init} + \Delta I_{PFC} \tag{3}$$

Fig. 2 depicts the block diagram of the EV control loop, which can be divided into 2 sub-groups. The first one concerns the implementation of Equation (2), to calculate the frequency deviation Δf and provides as output ΔI_{FPC_id}. This is the input of the second group, which serves at implementing the appropriate discreteness as well as setting up/down current limitations. The output ΔI_{FPC} is then added to the initial current set-point I_{init} according to (3). In order to implement a proper granularity in the EV response, the index α is introduced, which indicates the size of the steps when controlling the EV charging; $\alpha = \{1, 2, 4, \infty\}$ corresponds to the cases of granularity of 1 A, 0.5 A, 0.25 A and 0 A (which is the ideal continuous case), respectively. Bearing in mind that when controlling an EV charger the EV set-points represents the RMS values of the current waveform, and that in our study EVs are single-phase units charging in an uni-directional fashion according to charging Mode2.

It is of interest to highlight that the proposed controller can be implemented also for bi-directional V2G applications, i.e., when the battery power flow can have both directions. In such case, the initial current I_{init} is set to 0 A, and positive or negative current values will then be set to charge or discharge the EV battery, respectively. Moreover, appropriate up/down limits will be set according to the type of charger. For example, in occasion of experimental tests on IEC 15118-compliant V2G-capable hardware using the CHAdeMO protocol the limits of ±25 A were used for the charger's size of ±10 kW. The characterization tests of such commercial hardware (operating in on-field projects) also confirmed the presence of similar 1 A current discreteness when setting the EV current set-point [27].

4. Effects of Granularity when Providing PFC

The EV set-point granularity is now investigated in order to assess potential implications on power system primary frequency control via aggregated EVs. As first step of the analysis, the case of ideal EV response, with no granularity when fixing the current set-point is proposed. So, to stabilize the frequency to a new steady-state value, a total power equal to the size of contingency ΔP_{load} that caused the imbalance will be provided by the conventional synchronous generators ΔP_{gen_id} and the EVs ΔP_{EV_id}, with shares given by their droops as in (4). For the sake of simplicity, the following formulation considers only one synchronous unit, whose governor droop is K_{gen}.

$$\begin{cases} \Delta P_{gen\_id} = \Delta P_{load} \cdot \dfrac{K_{gen}}{K_{PFC\_pow}+K_{gen}} \\ \Delta P_{EV\_id} = \Delta P_{load} \cdot \dfrac{K_{PFC\_pow}}{K_{PFC\_pow}+K_{gen}} = V_n \Delta I_{PFC\_id} \end{cases} \tag{4}$$

The after-contingency ideal steady-state frequency value f_{eq_id} will be

$$f_{eq\_id} = \frac{\Delta P_{load}}{K_{PFC\_pow}+K_{gen}} + f_n \tag{5}$$

The EV contribution in terms of current ΔI_{PFC_id} is calculated using (2) and a linear droop, while the correspondent power is ΔP_{EV_id}, assuming nominal phase-to-neutral voltage conditions V_n. In the realistic case of a given discreteness in the current set-point, a correspondent step function as the solid curve in Fig. 1 is utilized. To do this, the index α to indicate the size of the steps when controlling the EV charging is recalled. So, for a given measured frequency the correspondent ideal current set-point would be rounded up/down to the closest i-th value of the step function. The index i represents the i-th current set-point for a given granularity. The set current ΔI_{PFCi} is then calculated as:

$$\Delta I_{PFCi} = \alpha^{-1} \boldsymbol{round}(\alpha K_{PFC} \Delta f) \tag{6}$$

So, the current ΔI_{PFCi} will be set if the following condition is respected:

$$\Delta I_{PFC} = \Delta I_{PFCi}\,, if\ \ \Delta I_{PFC\_id} \in \{\Delta I_{PFCi\_min};\ \Delta I_{PFCi\_max}\}$$

$$with \begin{cases} \Delta I_{PFCi\_min} = \Delta I_{PFCi} - 0.5\alpha^{-1} \\ \Delta I_{PFCi\_max} = \Delta I_{PFCi} + 0.5\alpha^{-1} \end{cases} \tag{7}$$

Such condition determines which set-point will be set on the EV, given the calculated ideal value and the implemented granularity α. It is now investigated which consequences this may induce to the operation, both on a large power system and on a small one, i.e., on a microgrid level.

4.1. *Consequences in a Large Power System*

The main consequence related to a discreteness in the response for primary frequency regulation is the inaccuracy in the primary reserve provision. This is identified as the difference between the requested (or expected) power to be exchanged with the grid P_{req} and the actual provided power P_{prov}, and is defined as ε_P:

$$\varepsilon_P = \left| P_{req} - P_{prov} \right| \tag{8}$$

The presence of such difference, thus of the error in the reserve provision, is due to the granularity of the set-points. In fact, the expected power is calculated with the ideal current set-point, derived by the linear ideal droop curve, whereas the actual delivered power is the result of the rounding. As the source of such error is merely the granularity in the current that is added to the initial current set-point, (8) can be re-written in terms of current error:

$$\varepsilon_I = \left| I_{req} - I_{prov} \right| \tag{9}$$

where I_{req} is the requested current calculated using the expected ideal change in the current ΔI_{PFC_id} in Equation (3), whereas I_{prov} is the actual current exchanged with the grid, obtained using ΔI_{PFC} in (3).

With reference to Equation (7), one can note that for each *i*-th set-point the maximum error is given by the extreme values ΔI_{PFCi_max} and ΔI_{PFCi_min}. This means that the maximum error ε_{I_max} is defined as in (10):

$$\varepsilon_{I\_max} = 0.5\alpha^{-1} \tag{10}$$

It is clear that higher discreteness (smaller α) in the response reflects to larger reserve provision errors when providing PFC control. Fig. 3 reports a visual representation of the trend of the reserve provision error as a function of the requested current, for a number of granularity cases. It can be noticed that a granularity of 1 A (α = 1) implies a maximum error of 0.5 A, which represents 5% of the available regulating window I_{reg} of 10 A, i.e., the available reserve. For finer granularities the maximum error decreases proportionally: for α = 2 it is 0. 25 A (2.5% of I_{reg}), and for α = 4 it is 0. 125 A (1.25% of I_{reg}).

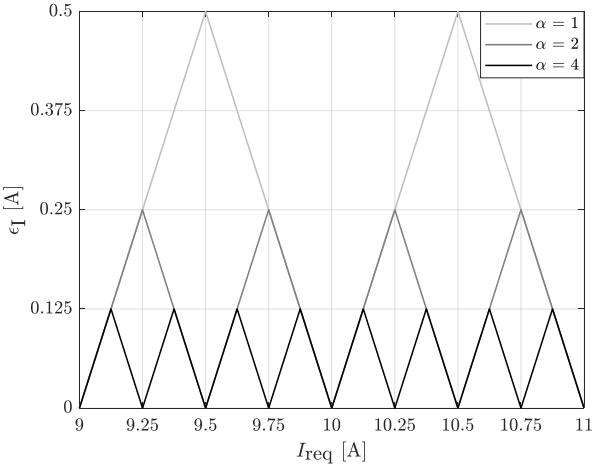

Fig. 3. *Response error as a function of the requested current, for different granularities.*

4.2. *Consequences in a Microgrid*

In low-inertia systems, e.g., in a microgrid, the discreteness in the response may cause different consequences related to the impossibility of reaching a stable steady-state frequency, f_{eq_id} in (5). This can lead to continuous oscillations between two consecutive current set-points, which will influence the frequency consequently. To better investigate such phenomena, the condition of setting a given set-point ΔI_{PFCi} reported in (7) can be re-written in terms of frequency limits, as in (11):

$$\Delta I_{PFC} = \Delta I_{PFCi}\,, \qquad if\ f_{meas} \in \{f_{i\_min};\ f_{i\_max}\}$$

$$with \begin{cases} f_{i\_min} = f_n - \frac{\Delta I_{PFCi\_min}}{K_{PFC}} \\ f_{i\_max} = f_n - \frac{\Delta I_{PFCi\_max}}{K_{PFC}} \end{cases} \tag{11}$$

Between two consecutive frequency intervals, a threshold value $f_{threshold(i;\, i-\alpha^{-1})}$ is defined, which is equal to the minimum frequency value of the *i*-th step's interval f_{i_min} and the maximum value of the previous step $f_{(i-\alpha^{-1})\_max}$. In case of current oscillations, two different steady-state values calculated for the two consecutive current set-points would be below and above the threshold $f_{threshold(i;\, i-\alpha^{-1})}$, meaning that:

$$f_{i\_eq} < f_{threshold(i;\, i-\alpha^{-1})} < f_{(i-\alpha^{-1})\_eq} \tag{12}$$

where

$$\begin{cases} f_{i\_eq} = f_n - \frac{\Delta P_{load} - V_n \Delta I_{PFCi}}{K_{gen}} \\ f_{threshold(i;\, i-\alpha^{-1})} = f_n - \frac{\Delta I_{PFCi} + 0.5\alpha^{-1}}{K_{PFC}} = f_n - \frac{V_n(\Delta I_{PFCi} + 0.5\alpha^{-1})}{K_{PFC\_pow}} \\ f_{(i-\alpha^{-1})\_eq} = f_n - \frac{\Delta P_{load} - V_n \Delta I_{PFC(i-\alpha^{-1})}}{K_{gen}} \end{cases} \tag{13}$$

The condition for current set-point oscillations between ΔI_{PFCi} and $\Delta I_{PFC(i-\alpha^{-1})}$ can be expressed as in (14):

$$f_{i\_eq} < f_{eq\_id} < f_{(i-\alpha^{-1})\_eq} \tag{14}$$

The condition in (14) is true whenever the steady-state frequency for any given current set-point differs from the ideal steady-state frequency value f_{eq_id} defined in (7). Thus, for any *i*-th set-point, the condition for two consecutive current set-point oscillations can be expressed as in (15) and in (16):

$$\forall\, i\,, f_{i\_eq} \neq f_{eq\_id} \tag{15}$$

which means

$$V_n \alpha^{-1} \boldsymbol{round}(\alpha K_{PFC} \Delta f) \neq \Delta P_{load} \left(1 - \frac{K_{gen}}{K_{gen} + K_{PFC\_pow}}\right) \tag{16}$$

It can be noticed that the evaluation of these conditions depends on the tuning of the regulating units (K_{gen}, K_{PFC}, α), the size of the contingency (ΔP_{load}), and on ΔI_{PFCi}, which in turn depends on α, K_{PFC} and the measured frequency variation Δf. Unlike all the other parameters, the measured system frequency cannot be known a priori, but can be estimated using Eq. (20) introduced in the next section, which includes parameters of the overall power system such as the total system inertia as well as the total apparent power of the rotating machines. To counteract the presented negative

consequences of discrete responses, a smart fleet management strategy is reported in the following.

4.3. *A Smart Fleet Management Strategy*

A smart fleet management strategy is presented to tackle the two identified possible consequences of a discrete response. Even though the best solution would be to operate with a linear droop (ideal case of $\alpha = \infty$, which reflects to the cases of no provision error nor oscillations), this may not be achievable due to hardware and/or communication limitations. However, an aggregated smoother response can be achieved if the EV fleet is properly managed, albeit each EV would be controlled using larger discrete steps. So, the proposed EV fleet management logic enables the achievement of a more accurate fleet response, still relying on larger granularities for each individual EV. In particular, the proposed solution is based on the shift of the droop characteristic for each EV. So, for a given individual EV granularity $\alpha_{individual}$ it is possible to obtain an aggregated granularity α_{aggr} for certain number of EVs n_{EV}, calculated as:

$$n_{EV} = \frac{\alpha_{aggr}}{\alpha_{individual}} \tag{17}$$

The shift of the discrete real droop f_{shift} is calculated as a translation along the x-axis in terms of frequency, of the employed frequency-current droop curve, thus depends on the droop constant K_{PFC}. The shifts for each EV are calculated as in (18):

$$f_{shift} = (2n_i + 1) \cdot \left(\pm \frac{0.5}{\alpha_{aggr} \cdot K_{PFC}}\right) \tag{18}$$

where

$$n_i \in A, A = \{n \in N \mid n \leq (n_{EV}/2 - 1)\} \tag{19}$$

As an example, for the case of droop constant K_{PFC} = 2.5 A/Hz as in Fig. 1, from $\alpha_{individual}$ = 1 to α_{aggr} = 4 the number of needed EVs n_{EV} is 4 and the frequency shifts are ±0.05 and ±0.15 Hz. Fig. 4 shows the combination of the 4 shifted droops, along with the aggregated equivalent droop, which allows the EV aggregator to reduce the reserve provision error from 5% to 1.25%, which in terms of currents is from 0.5 to 0.125 A. For the sake of completeness, Tables 1-3 show the parameters for the implementation of the proposed smart fleet management strategy for the example cases of individual EV granularity of 1 A, 0.5 A and 0.25 A, respectively.

Table 1 Parameters in case of $\alpha_{individual}$ = 1

α_{aggr}	n_{EV}	n	f_{shift} [Hz]
2	2	0	±0.1
4	4	0; 1	±0.05; ±0.015
8	8	0; 1; 2; 3	±0.025; ±0.075; ±0.0125; ±0.175
16	16	0; 1; 2; 3; 4; 5; 6; 7	±0.0125; ±0.0375; ±0.0625; ±0.0875; ±0.1125; ±0.1375; ±0.1625; ±0.1875

Table 2 Parameters in case of $\alpha_{individual}$ = 2

α_{aggr}	n_{EV}	n	f_{shift} [Hz]
4	2	0	±0.05
8	4	0; 1	±0.025; ±0.075
16	8	0; 1; 2; 3	±0.0125; ±0.0375; ±0.0625; ±0.0875

Table 3 Parameters in case of $\alpha_{individual}$ = 4

α_{aggr}	n_{EV}	n	f_{shift} [Hz]
8	2	0	±0.025
16	4	0; 1	±0.0125; ±0.0375

In general, in a microgrid such solution may not guarantee the prevention of induced oscillations, as it is not guaranteed that the ideal current value ΔI_{PFC_id} would be reached. However, this solution can drastically reduce the size of such oscillations, which can then be damped in a faster and easier way. The next sections present the experimental test-bed where the proposed standard compliant EV controller is implemented to complement the investigation study on the oscillations related to the EV set-point granularity in a real microgrid.

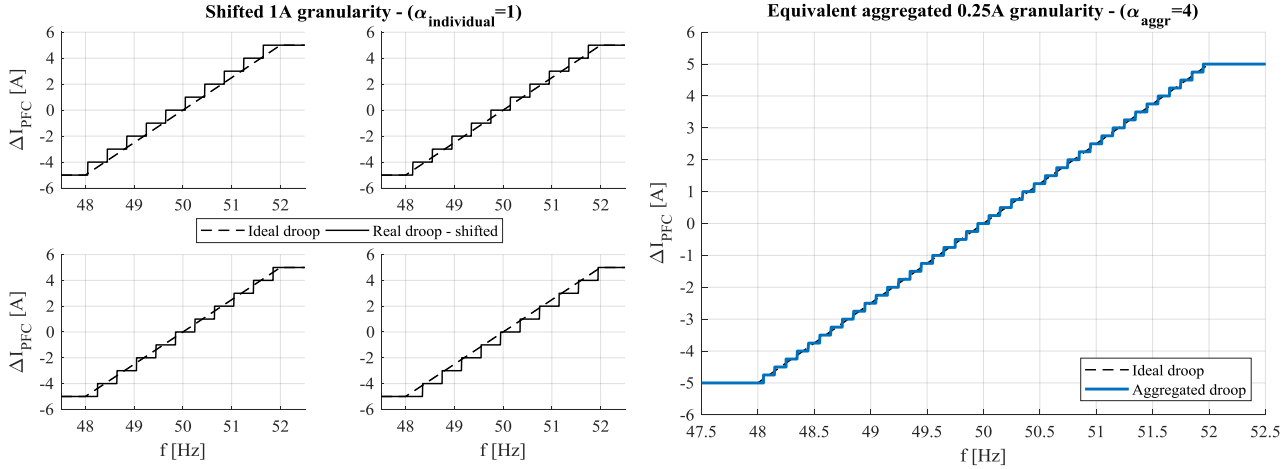

Fig. 4. *Proposed EV fleet management solution: with proper shifting of the droops of 4 EVs with $\alpha_{individual}$=1, the aggregated response is equivalent to the case α_{aggr}=4. This assures a reduction by a factor 4 of the maximum reserve provision error.*

5. Assessment of EV Response Granularity in a P-HiL Experimental Environment

The main purpose of the proposed experimental investigation is to sensitively assess the consequences on the system dynamics of a set of EVs performing simultaneous regulation with discrete responses. Specifically, different granularities when setting the EV charging current are studied, and results are compared with the ones expected from the investigations in Section 4. In this section, the experimental test-bed is presented along with its implementation within a P-HiL laboratory test environment. Then, the tested scenarios are defined, and relevant results are presented and discussed.

5.1. *Microgrid Layout and P-HiL Experimental Setup*

The tested microgrid aims at representing one of the possible islanded configurations of the experimental LV flexible grid SYSLAB previously utilized in other works [8]. The only unit that provides rotating inertia to the system is a diesel-set synchronous generator with 2 pole pairs p, rated apparent power S_{gen} = 60 kVA (nominal active power P_{gen} = 48 kW), and inertia constant $2H$ = 2 s. Thus, a change in the difference between mechanical power P_m and electrical power P_e would be reflected in a change in the system frequency as described by (20):

$$P_m - P_e = \frac{2H \cdot S_{gen} \frac{d\omega}{dt}}{\omega_n} \tag{20}$$

where ω is the angular velocity of the rotor [rad/s] and ω_n is its nominal value, obtained as in (21)

$$\omega_n = \frac{2\pi \cdot f_n}{p} \tag{21}$$

The governor of the diesel turbine operates with a droop K_{gen} of 2 kW/Hz. A static load P_{load} of 15 kW is constantly connected to the gen-set, and is increased/decreased to obtain frequency dynamics according to (21) that will be enhanced by the implemented EV controllers. A number of EVs are connected to the same busbar, with the option of activating the proposed PFC controller in case of contingency. A schematic representation of the described microgrid is shown in Fig. 5.

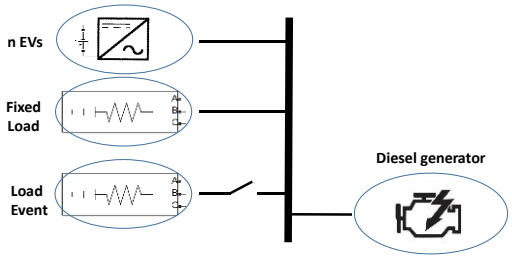

Fig. 5. *Microgrid layout.*

P-HiL experimental activities have been carried out at the Norwegian National Smart Grid Laboratory (NSGL), located in Trondheim at the campus of the Norwegian University of Science and Technology (NTNU) and jointly operated by SINTEF and NTNU [28]. The P-HiL hardware equipment utilized for the tests consists of the six-leg 200 kVA 5kHz Egston *power amplifier*, the real time simulator OPAL-RT OP5600 unit with I/O devices OP4520 (representing the *digital simulation system*), and three 60 kW two-level three-phase converters. In particular, either one or two of the converters (depending on the tested scenario) was the *hardware under test (HuT)*, i.e., the physical hardware under examination within a P-HiL test activity. In our case, the converters could reproduce the aggregated behavior of up to twelve single-phase EVs charging simultaneously according to Mode2 operation mode. The EV batteries were considered to be connected to the DC link, whose voltage was kept constant at 680 V by the third converter that was constantly operating as constant DC voltage source. The P-HiL experimental setup is depicted in Fig. 6, where the three main parts of the typical P-HiL setup are highlighted, namely the *digital simulation system*, the interface with *power amplifier*, and the *HuT* [10], [29], [30].

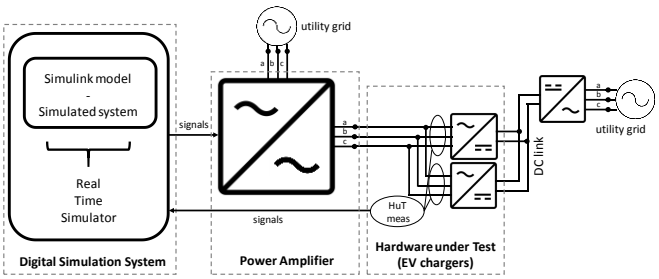

Fig. 6. *P-HiL experimental setup.*

As for the generation of the voltage signals that the power amplifier sets at its output channels, the block diagram in Fig. 7 has been implemented in the digital simulation system. It needs an RMS phase-to-neutral voltage reference value V_{ref} manually set constantly equal to 230 V, and it considers the active power measurements at the AC side of the two converters under study, namely P_{EVs} in Fig. 7. So, considering a given electrical load (with eventual steps) and the emulated power system parameters mentioned in the previous subsection, the implementation of (20) enabled the calculation of the rate of change of the angular velocity $d\omega/dt$ that, integrated twice, gives the reference angle θ for the generation of the voltage signals to create the AC microgrid for the tests.

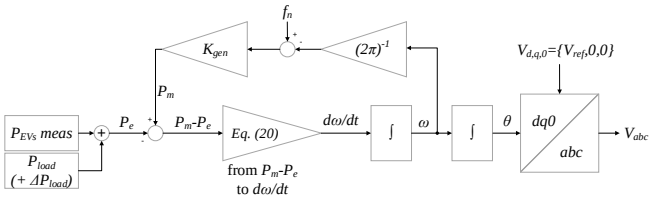

Fig. 7. *Generation of the three-phase voltage reference signals as output of the power amplifier.*

The EV current set-points to be set on the physical converters are computed as described in Section 3. With reference to the block diagram in Fig. 2, one has to note that multiple EV set-points can be computed independently, in order to emulate the case of more EVs with different time responsiveness, droops or granularities. In fact, before aggregating them, each EV can receive the same or a different

set-point for instance according to eventual droop shifts in case of the implementation of the proposed droop shift-based fleet management logic.

5.2. Definition of Scenarios

The investigation is carried out by monitoring the system frequency dynamics after a contingency. Each study case is tested with a given load step taking place on a stable operating condition with f = 50 Hz. With reference to the microgrid layout presented in Fig. 5, the resistive load is set to 15 kW, while 3 single-phase EVs are considered within the fleet, each one charging with RMS current I_{init} = 11 A, which corresponds to an aggregated EV fleet power P_{init} of 7.59 kW. Therefore, the total load that the emulated synchronous generator supplies at the initial equilibrium condition amounts to 22.59 kW, which corresponds to a loading factor of almost 50%, being the active power generation capability of the gen-set unit P_{gen} is 48 kW. The grid contingency is obtained with a load increment ΔP_{load} of 2 kW, which causes under-frequency conditions.

The PFC controller parameters are set considering a safe operating condition, as the one utilized in previous experimental activities [8], [9]. The parameters of the implemented PFC controller are reported in Table 4.

Table 4 PFC controller parameters

PFC controller parameter	Values set for the experimental validation
I_{reg}	10 A (±5 A)
I_{lim}	6-16 A
I_{init}	11 A
K_{PFC}	2.5 A/Hz
K_{PFC_pow}	575 W/Hz
K_{PFC_pow} *(for 3 EVs)*	1725 W/Hz
α	{1, 2, 4, ∞}
	{1, 0.5, 0.25, 0}A

One has to note that the initial absorbed power P_{init} ($=3I_{init}V_n$=7.59 kW) corresponds to 15.8% of the microgrid generation capacity P_{gen}. This percentage can appear as a very high share, but in reality is of roughly the same order of magnitude as a future scenario in the Nordic synchronous area. In fact, from the *Nordic EV Outlook 2018* report [31], the number of EVs in the Nordics is forecasted to be of 4 million, whereas the Nordic generation capacity is 103 GW, as stated in the *Nordic Market Report* [32]. In the worst-case scenario of all the EVs charging simultaneously, the correspondent initial absorbed power amounts to about 10 GW, which represents a share of about 10% of the installed Nordic generation capacity.

The implemented diesel gen-set droop K_{gen} (=2 kW/Hz) correspond to 48% droop on system base. 48% droop represents a high value when compared to hydro and gas power plants, however if seen from a system point of view it can represent a realistic case given the increasing penetration of uncontrolled small wind and solar plants that contribute to increase the total generation capacity without increasing the system absolute droop K_{gen}. High values mean that the conventional generator reacts smoothly, leaving space for regulation to other non-conventional units, such as EV fleets. These conditions may appear in islanded power systems or microgrids, where frequency regulation from small distributed energy resources will be crucial when increasing the penetration of renewables.

5.3. Results of Experimental Assessment

Firstly the same islanded configuration tested in previous experimental works [8] and presented in Section 5-1 is re-proposed. In this case a granularity of 1 A was implemented (α = 1). Fig. 8 shows results from the uncontrolled EV case and the case of EV performing PFC control. One can note that due to the discrete EV response, in case of PFC the current absorbed by one EV oscillates between two consecutive set-points, as none of them can allow a steady-state frequency to be reached without passing the threshold that triggers the consecutive set-point. This aspect is of outmost importance and therefore is tackled herein below by means of P-HiL experiments.

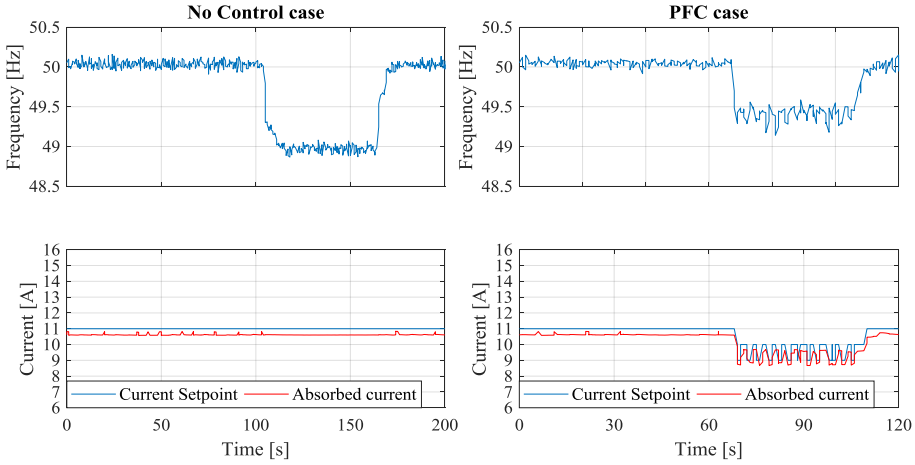

Fig. 8. *Experimental results with 3 EVs obtained in previous experimental works [6]. A granularity of 1 A is implemented (α=1).*

The first P-HiL test results are reported in Fig. 9, which shows the uncontrolled EV case. It can be seen that the P-HiL tests match the ones reported in Fig. 8, with an after-contingency steady-state frequency of 49 Hz. This value is motivated by the fact that the PFC controller is deactivated, and after the 2 kW contingency, frequency regulation is provided only by the diesel gen-set, whose governor acts with a droop K_{gen} of 2 kW/Hz.

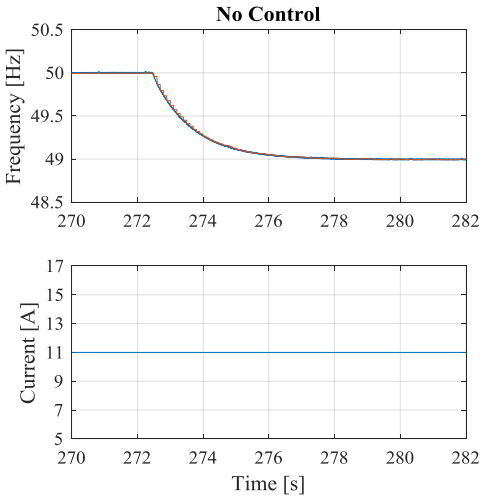

Fig. 9. *P-HiL experimental results: Frequency and EV current set-points for the uncontrolled EV case. The new steady-state frequency is 49 Hz, as the contingency is a 2 kW load increase, and frequency regulation is provided only by the diesel gen-set acting with a droop K_{gen} of 2 kW/Hz.*

To complement the analytical formulation proposed in Section 4, Fig. 10 reports results from experimental P-HiL tests with PFC implemented as described in Section 3 for four different granularity cases: $\alpha = \{1, 2, 4, \infty\}$, which correspond to the cases of granularity of 1 A, 0.5 A, 0.25 A and 0 A, respectively. Firstly, one can note that the controller is tuned in a safe operation zone since system instabilities do not occur. Secondly, it can be noticed that the 1-A oscillations found in the previous experimental work in Fig. 8 are replicated. Thanks to the elasticity of the employed P-HiL test setup, a deeper and more exhaustive investigation is possible. In particular, the cases of finer granularities are studied, and the experimental results are evaluated against the analytical formulations described in Section 4. From Fig. 10, one can note that oscillations take place even for the 0.5 A and 0.25 A discreteness cases, as none of the considered granularities lead to the ideal steady-state frequency value f_{eq_id} which is 49.463 Hz. Such value of f_{eq_id} is calculated using Equation (8) and confirmed from the P-HiL results of case $\alpha = \infty$. For the three discrete response cases, current set-point oscillations appear because the condition in Equation (14) is matched, and the threshold $f_{threshold(i;\, i-\alpha^{-1})}$ between two consecutive set-points is crossed. However, the case $\alpha = 4$ shows very limited frequency oscillations, that can be achieved either via such a very fine granularity or by smartly controlling the individual EV set-point as proposed smart EV fleet strategy. An analogue response could have been obtained if 4 EVs would have been controlled with shifted 1-A step functions. This is the case of applying horizontal shifts to the f-i step droop functions by f_{shift} of ±0.05 and ±0.15 Hz, obtaining α_{aggr} = 4 (0.25 A granularity) relying on implementation of 1-A step functions for each individual EV ($\alpha_{individual}$ = 1).

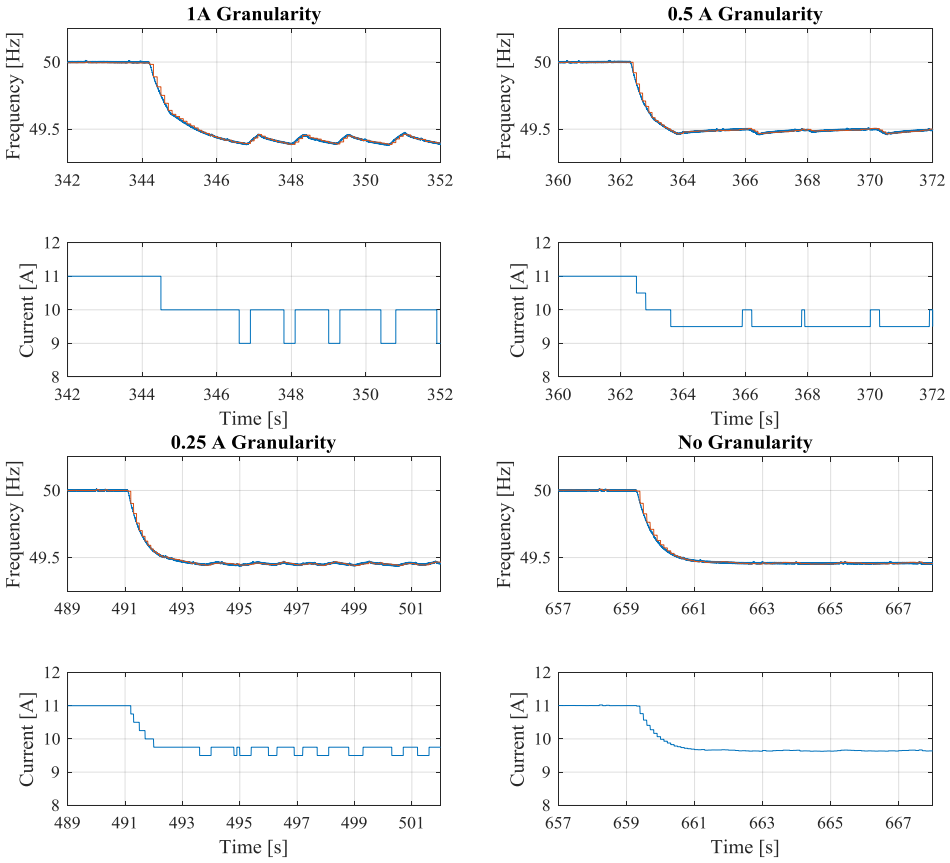

Fig. 10. *P-HiL experimental results: Frequency and current set-points for the EV response granularity sensitivity analysis.*

Table 5 reports steady-state frequency values for the consecutive set-points where the oscillations take place for different granularity cases, which confirm that the above-presented oscillation conditions are respected. In fact the numerical results calculated as explained in Section 4 match the P-HiL experimental results reported in Fig. 10. For $\alpha = 1$ the current set-point oscillates between 10 and 9 A, for $\alpha = 2$ between 10 and 9.5 A, and for $\alpha = 4$ between 9.75 and 9.5 A

Table 5 Results from experimental PFC activities

	$\alpha = 1$	$\alpha = 2$	$\alpha = 4$
ΔI_{PFCi}	-1 A	-1 A	-1.25 A
$\Delta I_{PFC(i-\alpha^{-1})}$	-2 A	-1.5 A	-1.5 A
f_{i_eq}	49.345 Hz	49.345 Hz	49.431 Hz
$f_{(i-\alpha^{-1})\_eq}$	49.690 Hz	49.518 Hz	49.518 Hz
$f_{threshold(i;\, i-\alpha^{-1})}$	49.400 Hz	49.500 Hz	49.450 Hz
f_{eq_id} $(\alpha = \infty)$	49.463 Hz	49.463 Hz	49.463 Hz
ΔI_{PFC_id} $(\alpha = \infty)$	-1.3425 A	-1.3425 A	-1.3425 A

6. Conclusions

This work investigated the implications of discrete responses of aggregated electric vehicles providing primary frequency regulation. An EV droop-based primary frequency controller was implemented, considering EV standard and commercial hardware limitations. The crucial role played by the EV current set-point granularity was analytically investigated assessing the consequences in applications in microgrids and large-scale power systems, and a smart EV fleet management strategy to overcome related issues was proposed. The analysis was complemented with real time P-HiL experimental tests in a microgrid. The microgrid was modelled within the P-HiL setup, and the EV PFC controller was tuned to operate in a safe operating zone.

Results from the experimental activities show the expected frequency oscillations due to the controller's discrete nature when setting the current set-points. Frequency oscillations are experimentally decreased by gradually reducing the amplitude of the required EV charging rate granularity, and the experimental results matched the numerical results obtained via the analytical formulation proposed in the paper. To prevent any possible frequency oscillations, the authors recognize that a continuous regulation may be necessary for microgrid applications, but this is not easily achievable due to standards and hardware limitations. Nevertheless, with the proposed EV fleet management method it is possible to achieve an aggregated response with an equivalent granularity lower than the one implemented on each individual EV. This is realized by shifting the control frequency-current droops, so that overall smaller oscillations are obtained, along with reduced primary reserve provision mismatches, which were identified as the major consequence of discrete regulation from the EV aggregator's perspective.

To conclude, one has to note that also in larger power systems such oscillations phenomena may take place when a considerable number of EVs respond simultaneously to the same discrete charging/discharging signal. Thus, the authors recognize that also on large scale applications, a smooth overall response may be needed to prevent system issues. This can be achieved either by making the regulation continuous, or by introducing additional requirements on the whole aggregated EV fleet response, for instance by means of overall ramping rate or fleet time response. These aspects are being investigated within future works.

7. Acknowledgments

The work in this paper was supported by the European Commission, under the FP7 project ELECTRA (Grant No.: 609687). More information at www.electrairp.eu

8. References

[1] D. S. Callaway and I. A. Hiskens, "Achieving Controllability of Electric Loads," *Proceedings of the IEEE*, vol. 99, no. 1, pp. 184–199, Jan. 2011.

[2] E. Vrettos, C. Ziras, and G. Andersson, "Fast and Reliable Primary Frequency Reserves from Refrigerators with Decentralized Stochastic Control," *IEEE Transactions on Power Systems*, vol. 32, no. 4, pp. 2924–2941, 2017.

[3] C. Gouveia, C. L. Moreira, J. Abel, P. Lopes, and D. Varajão, "Microgrid Service Restoration," *IEEE Industrial Electronics Magazine*, vol. 7, no. 4, pp. 26–41, 2013.

[4] IEC 61851-1:2010, "Electric vehicle conductive charging system – Part 1: General requirements." 2010.

[5] IEC/ISO 15118-1:2013, "Road vehicles — Vehicle to grid communication interface — Part 1: General information and use-case definition." 2013.

[6] "Nissan, enel and nuvve operate world's first fully commercial vehicle-to-grid hub in denmark," 2016. [Online]. Available: http://www.nissan-helsingor.dk/index.php/om-os/nyheder/show/news/id/4. [Accessed: 19-Oct-2018].

[7] Phoenix Contact, "EV Charge Control: Standard-compliant control of the Control Pilot and Proximity Plug interfaces between the electric vehicle and charging station. (User manual)." 2015.

[8] M. Rezkalla, A. Zecchino, S. Martinenas, A. M. Prostejovsky, and M. Marinelli, "Comparison between synthetic inertia and fast frequency containment control based on single phase EVs in a microgrid," *Applied Energy*, 2017.

[9] M. Marinelli, S. Martinenas, K. Knezović, and P. B. Andersen, "Validating a centralized approach to primary frequency control with series-produced electric vehicles," *Journal of Energy Storage*, vol. 7, pp. 63–73, 2016.

[10] E. De Jong, R. De Graff, P. Vaessen, P. Crolla, A. Roscoe, F. Lehfuss, G. Lauss, P. Kotsampopoulos, and F. Gafaro, "European White Book on Real-Time Powerhardware-in-the-Loop testing," Arnhem, Netherlands, 2011.

[11] O. Mo, S. DArco, and J. A. Suul, "Evaluation of Virtual Synchronous Machines With Dynamic or Quasi-Stationary Machine Models," *IEEE Transactions on Industrial Electronics*, vol. 64, no. 7, pp. 5952–5962, 2017.

[12] P. M. R. Almeida, F. J. Soares, and J. A. P. Lopes, "Electric vehicles contribution for frequency control with inertial emulation," *Electric Power Systems Research*, vol. 127, pp. 141–150, 2015.

[13] J. Meng, Y. Mu, H. Jia, J. Wu, X. Yu, and B. Qu, "Dynamic frequency response from electric vehicles considering travelling behavior in the Great Britain power system," *Applied Energy*, vol. 162, pp. 966–979, 2016.

[14] X. Luo, S. Xia, and K. W. Chan, "A decentralized charging control strategy for plug-in electric vehicles to mitigate wind farm intermittency and enhance frequency regulation," *Journal of Power Sources*, vol. 248, pp. 604–614, Feb. 2014.

[15] S. Izadkhast, P. Garcia-Gonzalez, and P. Frías, "An Aggregate Model of Plug-In Electric Vehicles for Primary Frequency Control," *IEEE Transactions on Power Systems*, vol. 30, no.

3, pp. 1475–1482, 2015.
[16] H. Liu, Z. Hu, Y. Song, and J. Lin, “Decentralized Vehicle-to-Grid Control for Primary Frequency Regulation Considering Charging Demands,” *IEEE Transactions on Power Systems*, vol. 28, no. 3, pp. 3480–3489, Aug. 2013.
[17] H. N. T. Nguyen, C. Zhang, and J. Zhang, “Dynamic Demand Control of Electric Vehicles to Support Power Grid With High Penetration Level of Renewable Energy,” *IEEE Transactions on Transportation Electrification*, vol. 2, no. 1, pp. 66–75, 2016.
[18] E. Sortomme and K. W. Cheung, “Intelligent Dispatch of Electric Vehicles Performing Vehicle-to-Grid Regulation,” in *2012 IEEE International Electric Vehicle Conference*, 2012, pp. 1–6.
[19] A. Molina-garcía, F. Bouffard, and D. S. Kirschen, “Decentralized Demand-Side Contribution to Primary Frequency Control,” *IEEE Transactions on Power Systems*, vol. 26, no. 1, pp. 411–419, 2011.
[20] M. González Vayá and G. Andersson, “Combined Smart-Charging and Frequency Regulation for Fleets of Plug-in Electric Vehicles,” in *2013 IEEE Power & Energy Society General Meeting*, 2013, pp. 1–5.
[21] M. R. V. Moghadam, R. Zhang, and R. T. B. Ma, “Distributed Frequency Control via Randomized Response of Electric Vehicles in Power Grid,” *IEEE Transactions on Sustainable Energy*, vol. 7, no. 1, pp. 312–324, 2016.
[22] S. Izadkhast, P. Garcia-Gonzalez, P. Frìas, L. Ramìrez-Elizondo, and P. Bauer, “An Aggregate Model of Plug-in Electric Vehicles Including Distribution Network Characteristics for Primary Frequency Control,” *IEEE Transactions on Power Systems*, vol. 31, no. 4, pp. 2987–2998, 2016.
[23] F. Lehfuss, M. Nöhrer, M. Faschang, S. Ledinger, and F. Kupzog, “Comprehensive Infrastrusture for Electric Vehicle Charging Interoperability and Grid Compliance Testing,” *International Journal of Distributed Energy Resources and Smart Grids*, pp. 29–42, 2015.
[24] R. Abousleiman and R. Scholer, “Smart charging: System design and implementation for interaction between plug-in electric vehicles and the power grid,” *IEEE Transactions on Transportation Electrification*, vol. 1, no. 1, pp. 18–25, 2015.
[25] K. Knezović, S. Martinenas, P. B. Andersen, A. Zecchino, and M. Marinelli, “Enhancing the Role of Electric Vehicles in the Power Grid : Field Validation of Multiple Ancillary Services,” *IEEE Transactions on Transportation Electrification*, vol. 3, no. 1, pp. 201–209, 2016.
[26] ENTSO-E, “Frequency Stability Evaluation Criteria for the Synchronous Zone of Continental Europe - Requirements and impacting factors,” Brussels, Belgium, 2016.
[27] A. Zecchino, A. Thingvad, P. B. Andersen, and M. Marinelli, “Suitability of Commercial V2G CHAdeMO Chargers for Grid Services,” in *EVS 31 & EVTeC 2018*, 2018, pp. 1–7.
[28] “National Smart Grid Laboratory.” [Online]. Available: https://www.sintef.no/en/all-laboratories/smartgridlaboratory/. [Accessed: 31-Jul-2017].
[29] C. Seitl, J. Kathan, G. Lauss, and F. Lehfuss, “Power hardware-in-The-loop implementation and verification of a real time capable battery model,” in *IEEE International Symposium on Industrial Electronics*, 2014, pp. 2285–2290.
[30] Q. Hong, I. Abdulhadi, A. Roscoe, and C. Booth, “Application of a MW-Scale Motor-Generator Set to Establish Power-Hardware-in-the-Loop Capability,” in *presented at IEEE International Conference on Innovative Smart Grid Technologies IEEE ISGT Europe 2017*, 2017, pp. 1–6.
[31] IEA International Energy Agency, “Nordic EV Outlook 2018,” 2018.
[32] Nordic Energy Regulators NordREG, “Nordic Market Report,” 2014.

Paper E

Title:

Suitability of Commercial V2G CHAdeMO Chargers for Grid Services

Authors:

Antonio Zecchino, Andreas Thingvad, Peter Bach Andersen and Mattia Marinelli

Published in:

31st International Electric Vehicles Symposium and Exhibition & International Electric Vehicle Technology Conference (EVS 31 & EVTeC - 2018)

Suitability of Commercial V2G CHAdeMO Chargers for Grid Services

V2G hardware tests with local and remote control setup: assessing the performance for quality grid services

Antonio Zecchino, Andreas Thingvad, Peter Bach Andersen, Mattia Marinelli

Center for Electric Power and Energy, Department of Electrical Engineering, Technical University of Denmark

Frederiksborgvej 399, Building 776, 4000 Roskilde, Denmark – e-mail: {antozec, athing, pba, matm}@elektro.dtu.dk

Presented at EVS 31 & EVTeC 2018, Kobe, Japan, October 1 - 3, 2018

ABSTRACT: Aggregation and control of electric vehicles (EVs) via vehicle-to-grid (V2G) technologies is seen as a valid option for providing ancillary power system services. This work presents results from V2G-ready equipment tests. The technical capabilities of an EV connected to a commercial V2G charger are investigated when controlled either locally or remotely. The charger is characterized in terms of efficiency characteristics, activation time, response granularity, ramping-up/down time, accuracy and precision. Results show the performance for different operating conditions, highlighting the importance of a good calibration and knowledge of the employed hardware when providing standard-compliant grid regulation services via V2G technology.

KEY WORDS: CHAdeMO, commercial EV chargers, electric vehicles, vehicle-to-grid

1. INTRODUCTION

Vehicle grid integration (VGI) research aims to support a seamless electrification of the transportation sector, proactively dealing with both challenges and opportunities which may arise. The term grid integrated vehicle (GIV) describes an electric vehicle (EV) purposely designed to limit its self-induced adverse effects in the power system, while also supporting the system by being able to provide a number of power and energy services. Such services may be aimed at achiving energy autonomy, supporting the local grid infrastructure or providing regional power and energy balancing [1], [2].

One class of system services EVs may provide is frequency containment reserves (FCR), which is required in the Nordic synchronous region. In order to provide such service, the EV charging or discharging would be controlled to support the system frequency. This service is interesting for two reasons. Firstly, the service is enumerated based on the available power [kW], not on the actual energy exchanged with the grid. Since the EV battery is an exhaustable resource in terms of energy but is capable of providing high instantaneous power, this represents a good technical match. Secondly, some markets already allow EV aggregators to participate in FCR provision. However, FCR is also one of the most technically demanding services with high requirements to a fast and reliable response and where access to vehcile-to-grid (V2G) strengthens the vehicles ability to provide the service considerably [3], [4].

Bidirectional V2G is presently only accessible through DC chargers using the CHAdeMO protocol. While DC chargers typically are associated with public fast-charging stations, reduction in size and price may ultimately allow for domestic use as well. A number of contemperary EV integration projects focused on V2G explore the use of early V2G-enabled DC chargers [5]–[8]. These chargers represent a key technology, enabling V2G across a broad number of EV models. It then becomes important to investigate the performance of these chargers on parameters specific to the provision of V2G based services – going beyond traditional one-way charging. This is the focus of this work, investigating the technical capabilities of V2G equipment when controlled either locally or remotely. This study presents an operational characterization of a commercial ±10 kW V2G DC charger [9] aimed at efficiency and active power control. Such characterization describes the extend to which DC chargers may be used to critical and demanding smart grid services such as FCR.

2. THE NEED FOR HARDWARE PERFORMANCE ASSESSMENT WHEN CONTROLLING EVS

In order to correctly procure the amount of reserve needed for ancillary services, it is necessary to define the most important attributes characteristing the unit response. The flexibility product can be defined as *the power adjustment sustained from a particular moment for a certain duration at a specific location* [10]. Given the nature of the service provided, the flexibility product can be either active or reactive power adjustment. However, as in this work reactive power exchange was not supported by the employed hardware, we always refer to active power.

In order to make the EV flexibility product a tradable asset, appropriate regulations and requirements should be introduced. Establishing standardized tests for evaluating the charger and EV performance are needed to categorize the supplied EV flexibility product. So, a deep knowledge of the controlled hardware performance is needed, including the EV charger efficiency for different set-points (presented in Section 3), to assess the accumulated losses during a V2G session. Such insights into the charger's efficiency can guarantee to the charger operator an accurate estimation of the real amount of energy flowing in/out of the battery. This is a necessary information for a safe and effective fleet operation, provided that low efficiencies may challenge the business case due to additional energy costs. Beside the necessity of a charging/discharging efficiency test, it is of utmost importance also to define the relevant charachteristics of the flexible EV when controlled for providing a power system service as FCR [3], to validate the fulfilment of the required performance. In this respect, we list seven attributes that have been experimentally assessed on V2G real hardware, the results of which are reported in Section 5:

(i) Direction: The information if an EV can provide only unidirectional or bidirectional (V2G) power flow.

(ii) Set-point linearity: The discreteness of the charging/discharging power set-point.

(iii) Starting time and maximum activation time: The period between receiving the set-point and activating the flexibility.

(iv-v) Ramp-up/ramp-down time: The up/downwards time between activation time and full service provision, and vice versa.

(vi) Accuracy: The difference between the required and the delivered response, e.g., the acceptable response band.

(vii) Precision: The variation of the delivered response for a given set-point.

Fig. 1 shows attributes *(iii)-(vii)* for an EV flexibility product, highlighting the difference between requested and provided power when controlling a flexible EV.

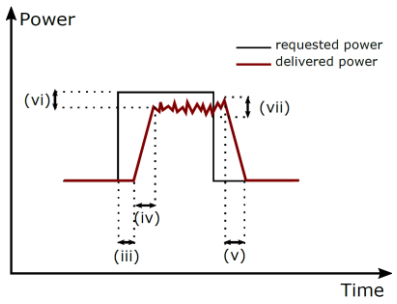

Fig. 1. Attributes *(iii)-(vii)* for an EV flexibility product.

3. LOCALLY AND REMOTELY CONTROLLED EVS PERFORMANCE TESTS

The first tests we present aim at assessing the efficiency of the V2G charger for a number of set-points. This is done in a local fashion, i.e., the set-points have been manually and locally set on the hardware, enabling us to derive the activation time of only the employed hardware. In order to evaluate the influence on the total activation time of additional communication latencies, the second tests were performed in a remote control fashion. The remote control test setup includes the communication and control infrastructure utilized by an actual EV aggregator, operating in on-field projects such as the Danish-funded projects ACES [5] and Parker [6]. Fig. 2 as a whole shows the test configuration for the centralized control architecture, enabling us to derive the total activation time including communication latencies. In this case the EVSE receives a power set-point remotely computed, and responds accordingly setting appropriate power flows in/out of the battery. With this design the aggregator calculates in a centralized way the appropriate V2G control signals to dispatch to its EVs, e.g., according to system frequency measurement in case of FCR. In case of the first local tests, the EV fleet operator platform is not utilized, whereas the set-points are directly set on the EVSE computer embedded in the charger.

In the proposed test activities two different active power test patterns were sent to the V2G-capable EVSE/EV. The first one is

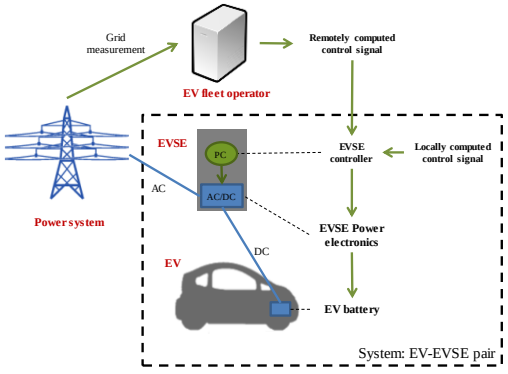

Fig. 2. Test configuration for the local and the remote control tests.

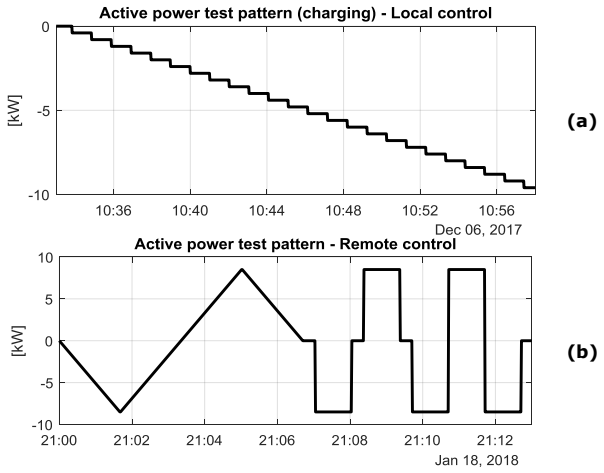

Fig. 3. Active power test patterns.

outlined in Fig. 3-a and represents different charging/discharging setpoints modulation from -10kW to +10kW with steps of 400 W. This test pattern allows the operational characterization of the V2G charger in terms of efficiency mapping. For the remote control test (Fig. 3-b), the pattern is designed in a way to allow an estimation of the seven flexibility service attributes defined in Section 2. Firstly, it enables us to validate the bidirectional capability and to assess total response time when controlling EVs in a remote fashion, including both communication latencies and charger and EV response time. This information is of utmost importance when assessing the capabilities on the provision of time-critical power system services from aggregated small distributed energy resources. Secondly, the remote test pattern consists first of a continuous and then of a step-wise variation of the charging/discharging power set-points. Such a cycle allows the measurement of the other five identified flexibility service attributes: the continuous part of the pattern allows the estimation of the step size granularity, whereas the step-wise part allows the estimation of the ramping times, the accuracy and the precision. Fig. 3-b shows the test cycle, which in practice was identically repeated 4 times, in order to have a more reliable measurement dataset for a more exhaustive and precise performance evaluation. Although the charger's size is ±10 kW, The extreme power set-points are ±8.5 kW due to an internal limitation set on the internal charger software

4. OUTCOME OF LOCAL CONTROL TESTS

The local control test intends to quantify the charger efficiency at all possible charging and discharging levels at different SOC. The tests where performed with a 30 kWh Nissan LEAF parked in a laboratory with 20°C for more than 24 hours. The AC side is measured with a DEIF MIC-2 power meter with 0.2 % accuracy and the DC side is measured with the internal DC voltage and current probe of the V2G charger, each with 1 s sample rate. The full range of the SOC is necessary to quantify the effect of changes in the internal battery voltage. This is achieved by repetively stepping through the possible charging/discharging setpoints with 1 A steps at the DC side, i.e., 400 W in case of 400 V DC – note that the actual DC power will depend on the DC voltage. For each power set-point, the efficiency is calculated and plotted in Fig. 4 with one line for each cycle, with the average SOC during the cycle, to assess the SOC influence on the efficiency. The discharge cycle is repeated until the Battery Management System (BMS), disconnects the EV as it reaches its internal discharge limit of 35%.

4.1. Calculation of efficiency map

In a first attempt we calculated the efficiency during a FCR provision session, and it resulted in a large variance of efficiency values for each power set point due to the large time constant of the charger, and the constantly changing set-point [11]. To avoid this problem, we decided to change the power setpoint only with one minute intervals, giving each charge/discharge cycle a 25 minute duration. The efficiency calculated for each DC power setpoint value is the average during the whole minute, giving a granularity of 25 values for each SOC level.

The results reported in Fig. 4 show that the large difference in the SOC has a negligible influence on the efficiency. The tests were performed only in the SOC range where the voltage changes linearly, so eventual difference in the results when operating in the extreme regions are not considered. However, it is not relevant considering the BMS limits in the useable range of the battery.

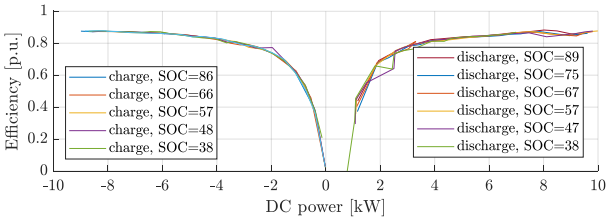

Fig. 4. V2G charger efficiency map for charging/discharging DC setpoints from -10kW to +10kW with steps of 400 W.

4.2. Calculation of activation time

The set-point control signal and the AC power provided on the grid side are shown in Fig. 5-a, which is a zoom-in of a part of the AC power measured during the charging test of Fig. 3-b. The time shift represents the activation time given the employed local control setup, thus it includes only the actual hardware response without any additional latencies due to control communications. Fig. 5-b shows the correlation of the two signals when applying different time shifts to one of them for the whole duration of the test. The maximum is found for a shift of 4 s, which is then considered as the activation time of the tested V2G equipment.

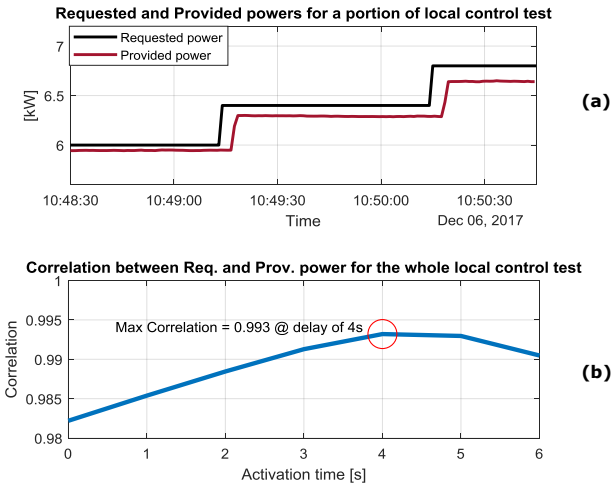

Fig. 5. The correlation between requested and provided power for local control shows a maximum for a delay of 4 s, which can then be considerd as the actual hardware response time.

5. OUTCOME OF REMOTE CONTROL TESTS

This Section presents the results of the performace test with the remote control setup. Note that the hardware under test and the laboratory environment conditions are the same as for the local control test.

Fig. 6 shows the required and the provided power of one cycle of the active power test pattern. In general, a time shift can be noticed, which here represents the total activation time given the employed remote control setup. Then, one can note the non-perfect linearity in the response to the signal in the continuous portion due to the set-point granularity imposed by protocols and the power electronics in the V2G charger. Finally, the time needed to reach the set-point is utilized for the calculation of the ramping rates, while the measured power at the stable set-point levels allows the calculation of accuracy and precision.

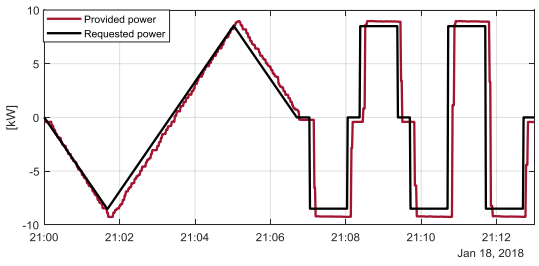

Fig. 6. 1 cycle of the performed remote performance assessment test.

5.1. Calculation of set-point linearity

The linearity in the response is studied in the continuous portion of the tested cycles, when a continuous linear setpoint is sent to the unit. The amplitude of the granular response is calculated as the difference of the measured provided power calculated at two consecutive time stamps. Hence a number of set-point granularities are calculated, which are then analysed.

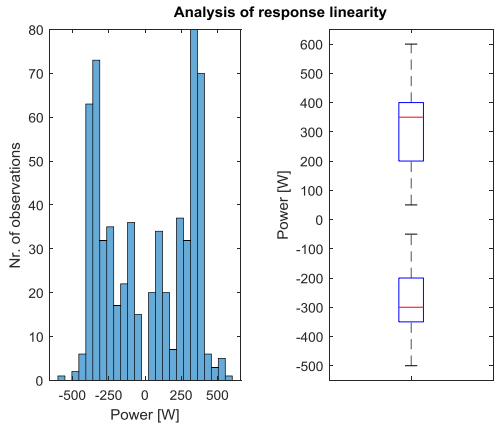

Fig. 7. Distribution of the observed granularities in terms of absolute and percentage observations. For the boxplots, the blue boxes indicate 50% of the observations, whereas the median is in red. Upper and lower quartiles (25% of the data) are located within the vertical black lines.

In this response linearity analysis we have excluded two sources of probable errors: the unavoidable noise in the measurements, and the response precision when setting a given set-point value. So, the calculation of the response linearity is done after applying a manual discreteness of 50 W on the measured data, given the average precision in the response calculated in subsection 5.4.

Results are reported in Fig. 7. The barplot shows the distribution of the observed granularities for different positive or negative sizes. First, the symmetrical distribution for charging (<0) and discharging (>0) can be noticed. Then the 2 bars with more observations (~50%) cover the range ±{300 400}W, whereas only in few cases (less than 5%) the absolute value of the granularity is > 400 W. The same results are reported in the boxplots, which show the median values -300 W and +350 W.

In general, one can conclude that in very few cases the EV responds with a discreteness larger than 400 W when controlled with a linear signal. 400 W in AC can thus be considered as the finest response granularity for the hardware under test. In this case, neglecting conversion losses, 400 W in DC means a granularity of 1 A, being the DC link voltage equal to 400 V, according to the technical CHAdeMO protocol.

5.2. Calculation of total activation time

The time shift shown in Fig. 6 represents the total activation time given the employed remote control setup, which includes both the 4 s delay of the actual hardware response time found in Section 4, and the additional latencies due to the centralized control architecture. Fig. 8 shows the correlation of the two signals of Fig. 6 when applying different time shifts to one of them. The maximum is found for a shift of 7 s, which is then considered as the total activation time when the tested V2G equipment is controlled via the centralized remote control setup.

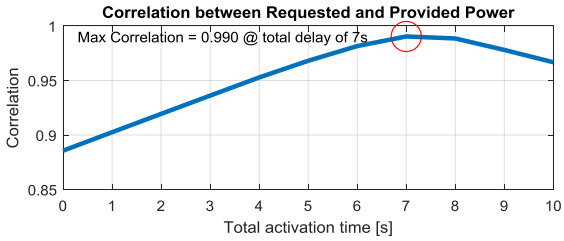

Fig. 8. The correlation between requested and provided power for remote control shows a maximum for a delay of 7 s, which can then be considerd the total activation time when the tested V2G equipment is controlled via the centralized remote control setup.

By comparing this analysis with the similar one proposed in Section 4 for local control, an assessment of the influence on the overall response time only due to a centralized control architecture can be derived. This validation can then provide a valuable information on the actual total activation time capabilities given either a local or a remote control. Such information is of utmost importance when assessing the capabilities on the provision of time-critical power system services from aggregated small distributed energy resources, so when evaluating whether to implement a centralized or a decentralized control strategy.

5.3. Calculation of ramping up/down

The ramping up/down capabilities are studied in the step-wise portion of the tested cycles, where 4 events up and 4 events down are performed as shown in Fig. 9. The charging power is changed from the zero set-point to the minimum and maximum values, back to zero. Also the largest possible steps are analysed, i.e., when setting the maximum power starting from the minimum set-point, and vice versa.

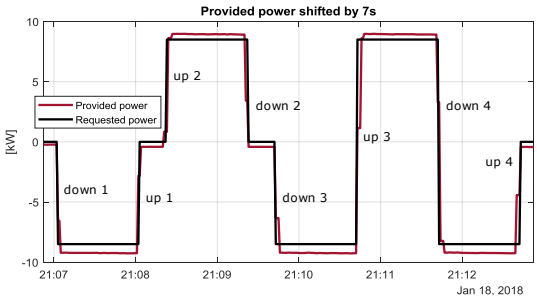

Fig. 9. For each cycle of the performed performance assessment test 4 events up and 4 events down are performed to calculate the ramping rate capability. For the step-wise portion, 4 cycles have been repeated.

Table 1 Measured ramping rates up/down.

	Cycle 1	Cycle 2	Cycle 3	Cycle 4
up 1	8.84kW in 3s	8.84kW in 4s	8.82kW in 3s	8.84kW in 4s
up 2	9.03kW in 4s	9.04kW in 4s	9.03kW in 4s	9.04kW in 5s
up 3	17.87kW in 6s	17.85kW in 6s	17.88kW in 4s	17.86kW in 6s
up 4	8.84kW in 4s	8.84kW in 1s	8.83kW in 4s	8.84kW in 3s
Ramp-up AVG	**3.35 kW/s**			
down 1	8.99kW in 3s	8.79kW in 4s	8.79kW in 4s	8.99kW in 3s
down 2	9.33kW in 3s	9.16kW in 1s	9.17kW in 1s	9.16kW in 4s
down 3	8.79kW in 4s	8.98kW in 3s	8.97kW in 4s	8.99kW in 4s
down 4	18.12kW in 6s	18.14kW in 7s	18.13kW in 7s	18.14kW in7s
Ramp-down AVG	**3.31 kW/s**			

Table 1 reports numerical results of the calculated up/down ramping rates. The average up and down rates almost coincide, and are equal to about 3.3 kW/s when expressed in the general unit of measurement [kW/s], i.e., related to 1 s time window. Nevertheless, the minimum calculated up and down rates are 1.8 kW/s (up2-cycle4) and 2.2 kW/s (down1-cycle2,3 and down3-cycle1) respectively, which is way lower than the average. This means that the unit on averege responds with 3.3 kW/s, but may respond slower.

This outcome is very important, as it can be valuable information for grid operators when performing grid regulation studies, assessing the impacts of grid regulation services provided by such units. Moreover, it can be useful also when defining requirements for grid connected V2G technologies, provided the knowledge of the technology under exam.

5.4. Calculation of set-point accuracy

The calculation of the set-point accuracy is done during the constant set-point levels of the step-wise portion of the tested cycles, as highlighted in Fig. 10. The accuracy is calculated as the difference between the requested and the provided power over the appropriate time windows.

It was found that for charging operations (power<0) the power drawn from the grid is larger than the requested power. The same happens in case of zero set-point, where the power consumption is justified as the own consumption of the power electronics on stand-by mode. During the discharge operations, the power injected into the AC grid is higher than expected. This is probably due to a wrong calibration of the internal EV charger power electronics, which should be tuned to avoid higher injection of power higher than the requested value, as it could compromise the safe operation.

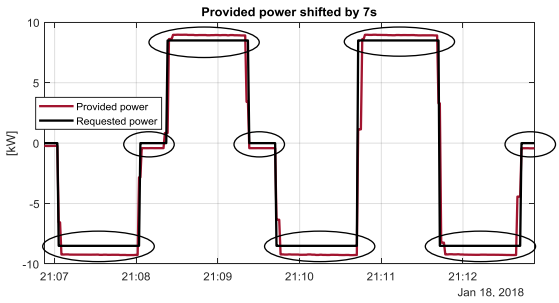

Fig. 10. For both accuracy and precision the calculation is done during the constant set-point levels of the step-wise portion of the tested cycles. This means at zero set-point at the maximum charging (-8.5 kW) and discharging power (+8.5 kW).

At zero set-point the charger drawns from the grid on average 420 W, which can then be considered as the unit's stand-by loss. In case of full charging operation (requested power = 8.5 kW), the calculated accuracy is 740 W, which represents the 8.7% of the power set-point. Such accuracy is higher than the stand-by losses, probably due to a non-optimal calibration of the unit. Finally, during the full discharging operation (requested power = -8.5 kW) an unexpected power value higher than the requested one was measured. Results show that the average power provided is higher than the requested by 440W, which is the 5.2% of the power set-point.

5.5. Calculation of set-point precision

As done for the accuracy, the precision is calculated during the constant set-point levels of the step-wise portion of the test cycles. The accuracy is calculated as the difference between the maximum and the minimum values of the provided power over the whole length of the time windows with stable extreme set-points. This means that the precision calculated with this test cycle can be considered as the worst case as for the extreme charging and discharging set-points.

It is found that the precision is about 50 W for both the extreme charging and discharging operation. This value justifies the choice of 50 W as manual discretization factor that has been utilized in the analysis of the granularity presented in subsection 5.1. In case of zero-setpoint the precision was much higher, since the difference between maximum and minimum of the measured power was about 6 W.

5. DISCUSSION AND CONCLUSIONS

In this paper the technical capabilities of a commercial V2G CHAdeMO charger have been identified to assess the suitability of such technology for grid service provision. Specifically, the importance of the knowledge of the efficiency for all the possible operating conditions has been highlighted, along with the seven attributes of a flexibility product to be traded in the market. Moreover, two different test setups were utilized to investigate how the total activation time would change in case of local or remote control. This provided crucially valuable information when assessing the capabilities on the provision of time-critical power system services from aggregated small distributed energy resources.

Table 2 shows the summary outcome of the performance tests results for each identified flexibility product attribute, with the respective performance target defined by current technical standards. In particular, the requirements have been adapted from the Danish technical standard for FCR provision [3] and the newly released Danish technical regulation for grid connected battery plants, which applies also for a number of aggregated EV chargers providing V2G services [12]. Such requirements are then considered as benchmarks when evaluating the eligibility of EVs in FCR service provision.

Table 2 Evaluation test results.

Attribute	**Short description**	**Unit**	**Target for Primary Reserve [3], [10]**	**Test result**
(i) Direction	Support of bidirectional power flow	+/-/±	±	± i.e. V2G capable
(ii) Set-point linearity	Supported setpoint throughout the power range	[W]	Linear at 1%	< 400 W (4%) (1 A @ 400V DC)
(iii) Starting time and maximum activation time	Time between setpoint request and change in active power	[s]	< 15 s	Local control: 4 s Remote control: 7 s
(iv) Ramp-up time	Supported rate of change in power (increase)	[kW/s]	For the aggregate: 10-300 kW/s	AVG = 3.35 kW/s Max = 8.84 kW/s min = 1.81 kW/s
(v) Ramp-down time	Supported rate of change in power (decrease)	[kW/s]	For the aggregate: 10-300 kW/s	AVG = 3.31 kW/s Max = 9.17 kW/s min = 1.98 kW/s
(vi) Accuracy	Difference between required and delivered response	[W]	±5% of setpoint & ±0.5% of rated pow.	Negative setpoint: 740W (+8.7% of setpoint) (+7.4% of rated pow.) Positive setpoint: -440W (-5.2% of setpoint) (-4.4% of rated pow.) 420 W @ zero setpoint (4.2% of rated pow.)
(vii) Precision	Variation of the delivered response	[W]	±5% of setpoint & ±0.5% of rated pow.	≈ 50 W (0.6% of setpoint) (0.5% of rated pow.) 6 W @ zero setpoint (0.06% of rated pow.)

Going through the seven attributes, firstly it can be seen that the symmetric power reserve bid requested by [3] applies to a bidirectional power flow capability, which is available due to the V2G technology. As for the set-point linearity, generally a linearity of 1% of the rated power is requested. It is found that the finest response has a granularity of 400 W, which represents the 4% of the rated power, thus not fulfilling the requirement. However, as this is the linearity for only one single unit, when managing an EV fleet the fleet operator should then apply smart logics, e.g., based on stochastic logics aimed at reaching – as proposed in [13] – the required target on an aggregated level. As for the activation time, the latencies due to remote control communication amount to about 3 s, while the mere hardware is

characterized by an activation time of 4 s. Ref. [3] requires the activation of half of the full capacity within 15 s, which is then respected considering an instantaneous response. In reality, the response has an up-down ramping rate, which amounts to an average value of 3.3 kW/s. For the tested charger, this means that the total activation time for half of the reserve (5 kW) would be about 8.6 s, which is lower than the requested 15 s. Ref. [12] requires a ramping rate capability for the aggregated fleet within the range of 10-300 kW/s, which is out of the range of capabilities of the single units. This means that, considering again the everage value of 3.3 kW/s, the minimum and maximum number of EVs to be employed for matching the required 10-300 kW/s ramping range will be 3 and 91, respectively. Finally for accuracy and precision, [12] requires a response within ±5% of the set-point and ±0.5% of the rated power. The requirement on the precision is respected, wheres for the accuracy, the limits at the two maximum charging and discharging levels are overcome. This issue may be dealt with proper calibration of the internal power electronics that should be tuned to avoid such inaccurancies. Furthermore, as the requirements refer to the overall battery plant, smart fleet management solutions could be implemented, to reduce the reserve provision error via appropriate individual control of the single EVs, e.g., as proposed in [13].

To conclude, in order to make the EV flexibility product a tradable asset, relevant regulations and requirements should be respected, and standardized tests for evaluating charger's and EV's performance should be established. In fact, a deep knowledge of the controllable hardware is needed to categorize the supplied EV flexibility product. On the one hand, insights into the charger's efficiency for different set-points allow the calculation of the accumulated losses during a V2G session, which is a crucial information for the estimation of the actual state of charge of the controlled EV. On the other hand, the proposed investigation of the identified charachteristics of the V2G unit provides valuable information for grid operators when performing grid regulation studies, assessing the impacts of FCR provided by such units with realistic models to emulate their behavior. Furthermore, it can be useful also when defining new requirements for grid connected V2G technologies, provided an orientative knowledge of the employed technology's capabilities. Ultimately, the proposed investigation results provide insights also for the EV fleet operators in terms of actions needed for smart fleet management aimed at respecting the grid code restrictions.

ACKNOWLEDGMENTS

The authors would like to acknowledge the support of the EUDP project ACES - Across Continent Electric Vehicle Services (grant EUDP17-I-12499, website: www.aces-bornholm.eu) and the Danish research Parker project under ForskEL contract no. 2016-1-12410, http://parker-project.com.

REFERENCES

[1] M. N. B. Arias, S. Hashemi, P. B. Andersen, C. Træholt, and R. Romero, "V2G Enabled EVs Providing Frequency Containment Reserves: Field Results," in *2018 IEEE International Conference on Industrial Technology (ICIT 2018)*, 2018, pp. 1–6.

[2] K. Knezović, S. Martinenas, P. B. Andersen, A. Zecchino, and M. Marinelli, "Enhancing the Role of Electric Vehicles in the Power Grid : Field Validation of Multiple Ancillary Services," *IEEE Transactions on Transportation Electrification*, vol. 3, no. 1, pp. 201–209, 2016.

[3] Energinet.dk, "Danish Technical Standard: ancillary services to be delivered in Denmark - tender conditions," *https://en.energinet.dk/-/media/Energinet/El-RGD/Dokumenter/Ancillary-services-to-be-delivered-in-Denmark.pdf*, 2017. .

[4] A. Thingvad, S. Martinenas, P. B. Andersen, M. Marinelli, C. Bjørn E, and O. J. Olesen, "Economic Comparison of Electric Vehicles Performing Unidirectional and Bidirectional Frequency Control in Denmark with Practical Validation," in *2016 Proceedings of the 51st International Universities Power Engineering Conference*, 2016, pp. 1–6.

[5] "ACES project - across continents electric vehicle services," *http://aces-bornholm.eu*, 2017. .

[6] "The Parker project," *http://parker-project.com*, 2016. .

[7] "INVENT project - Intelligent Electric Vehicle Integration," *https://rmp.ucsd.edu/_files/sei/INVENT-Flyer.pdf*, 2017. .

[8] "GridMotion project - reducing electric vehicle usage cost thanks to smartcharging process," *https://www.enel.com/content/dam/enel-common/press/en/1667129-2_PDF-1.pdf*, 2017. .

[9] NISSAN, "Nissan, enel and nuvve operate world's first fully commercial vehicle-to-grid hub in denmark," *http://www.nissan-helsingor.dk/index.php/om-os/nyheder/show/news/id/4*, 2016. .

[10] K. Knezović, M. Marinelli, A. Zecchino, P. B. Andersen, and C. Træholt, "Supporting involvement of electric vehicles in distribution grids: Lowering the barriers for a proactive integration," *Energy*, 2017.

[11] A. Thingvad, C. Ziras, J. Hu, and M. Marinelli, "Assessing the Energy Content of System Frequency and Electric Vehicle Charging Efficiency for Ancillary Service Provision," in *Proceedings of the 52nd International Universities' Power Engineering Conference*, 2017, pp. 1–6.

[12] "Danish Technical regulation 3.3.1 for battery plants." 2017.

[13] C. Ziras, A. Zecchino, and M. Marinelli, "Response Accuracy and Tracking Errors with Decentralized Control of Commercial V2G Chargers," in *20th Power Systems Computation Conference (PSCC 2018)*, 2018, pp. 1–7.

Paper F

Title:

Response Accuracy and Tracking Errors with Decentralized Control of Commercial V2G Chargers

Authors:

Charalampos Ziras, Antonio Zecchino and Mattia Marinelli

Published in:

20th Power Systems Computation Conference (PSCC - 2018)
DOI: 10.23919/PSCC.2018.8442488

Response Accuracy and Tracking Errors with Decentralized Control of Commercial V2G Chargers

Charalampos Ziras, Antonio Zecchino, Mattia Marinelli
Center for Electric Power and Energy - Department of Electrical Engineering
DTU - Technical University of Denmark
Risø Campus, Roskilde, Denmark
{chazi, antozec, matm}@elektro.dtu.dk

***Abstract*—There is a growing interest in using the flexibility of electric vehicles (EVs) to provide power system services, such as fast frequency regulation. Decentralized control is advocated due to its reliability and much lower communication requirements. A commonly used linear droop characteristic results in low average efficiencies, whereas controllers with 3 modes (idle, fully charging, fully discharging) result in large reserve errors when the aggregation size is small. To address these issues, we propose a stochastic, decentralized controller with tunable response granularity which minimizes switching actions. The EV fleet operator can optimize the chargers' performance according to the fleet size, the service error requirements, the average switching rate and the average efficiency. We use real efficiency characteristics from EVs and chargers providing fast frequency regulation and we show that the proposed controller can significantly reduce reserve errors and increase efficiency for a given fleet size, while at the same time minimizing the switching actions.**

***Index Terms*—Decentralized control, electric vehicles, primary frequency control, stochastic control, V2G chargers.**

I. Introduction

Electric vehicles (EVs) are recognized as an important source of load flexibility and as a potential provider of power systems services in the context of vehicle to grid (V2G) technologies. A suitable service for EVs is primary frequency control (PFC), due to the chargers' high power capacity and very fast response, as well as the relatively low energy requirements of this service. EVs' technical capabilities in providing different ancillary services including PFC have been experimentally proven both at a microgrid level and on a real distribution network [1], [2]. Even though a single EV's capacity is not particularly large compared to generators, if a large number of EVs is controlled by an aggregator, it is possible to offer significant amounts of reserve capacity. The literature proposes aggregate models and control schemes for both centralized [3], [4] and decentralized [5]–[8] solutions for the optimal management of EV fleets performing frequency control.

A centralized controller was proposed in [4] for offering secondary frequency control, where a discretized regulation logic is utilized, aiming at meeting the desired calculated total power signal by turning certain EVs on or off according to a priority index. More advanced control strategies have also been proposed to track reference signals with EVs, considering uncertainties and charging efficiencies [9]. However, as the control architecture is centralized, real-time communication is required, which may result in high infrastructure costs, as well as in loss of controllability in case of an outage of the communication system. Due to the critical nature of PFC to a power system's stability and stricter requirements than secondary control, very high reliability and very low latencies are required.

Such risks are highly reduced in the case of decentralized EV control, as decentralized PFC offers higher reliability and significantly reduces the communication requirements compared to real-time centralized control. A decentralized stochastic control component is proposed in [3], where the decision to change the charging set-point is taken locally by the EVs, even though with a remote centralized frequency measurement performed by the aggregator, who will dispatch the same correspondent signal to the EVs of the portfolio. In [6] it is shown how demand can respond to frequency deviations in a manner similar to the generators in a purely decentralized way, making it a significant and reliable asset as contribution to PFC. In [5] optimal EV droop curves are designed to improve system stability and in [10] adaptive droops are proposed for EVs offering PFC, to take state of charge (SOC) requirements into account. Finally, [7] proposes a distributed frequency control method, which randomly assigns delays to each EV of the fleet, aiming at avoiding problems to the power system in case of high shares of EVs providing regulation and simultaneous response of all units to the same frequency signals.

However, all the mentioned works do not consider the implications of using droop curves with regards to reserve errors, average charging efficiency, average equipment switching rates and aggregation size when offering PFC in a decentralized way. The commonly used droop-curve characteristic that EVs must follow to provide PFC results in a low average efficiency because of the low loadings of the inverters in most cases. Additionally, as we show in Section IV, a deterministic response always results in reserve errors due to the ISO 15118, ICE 61851 standard requirement of 1 A granularity when setting the charging rate of the inverter [11]. A stochastic controller (where EVs alternate between idle and full response stochastically and do not respond linearly to the frequency deviation) can significantly increase the efficiency, albeit the resulting errors depend on the aggregation size.

The main contribution of this paper is the investigation of the trade-off between service accuracy and efficiency under stochastic decentralized control. More specifically, we propose a stochastic controller with a varying number of states, as a trade-off between accuracy and efficiency, which the aggregator can tune depending on the size of the fleet and the service requirements. We show the dependency of the reserve error on the aggregation size and the controller's tuning and we determine the minimum amount of EVs to guarantee a service provision error. Additionally, we calculate the efficiencies achieved with each controller tuning, using real data of V2G chargers from ENEL, which are currently installed in Denmark and offer fast frequency control grid services [12].

The proposed method allows an EV aggregator to maximize efficiency for a specified number of EVs, by respecting the average reserve error requirements of the provided service. Additionally, we propose a modified version of the control algorithm which decreases the switching rate of the inverters, a modification which can potentially reduce the wear of the components. We show via simulations that our controller significantly increases the service accuracy of the droop-based control, under the 1 A granularity limitation, even for very small aggregation sizes, and that much higher average efficiencies can be achieved for smaller aggregation sizes, when a 3 mode response (idle, full charge, full discharge) results in large reserve errors.

The remainder of the paper is structured as follows. Section II introduces the principles of the frequency-controlled normal operation reserve service and frequency control with EVs. Section III presents an efficiency characteristic from operational V2G chargers. In Section IV we present the proposed discretized, stochastic decentralized controller. In Section V simulation results are presented and discussed. Conclusions are reported in Section VI.

II. Frequency control with EVs

Fast frequency control, i.e. PFC, can take different forms depending on the implementation of each Transmission System Operator (TSO). In the Regional Group Nordic (RG-N) synchronous area, PFC consists of two separate services, namely frequency-controlled normal operation reserve (FNR), which is activated linearly for all system frequency deviations up to ± 100 mHz and frequency-controlled disturbance reserve (FDR), activated only when system frequency drops below 49.9 Hz. We are focusing on FNR, since the revenue potential is higher and this service is currently being provided by commercial V2G chargers in Denmark within a pilot project [12].

In the case of a frequency deviation, the purpose of FNR is to react quickly and try to contain the frequency deviation. The TSOs in RG-N are jointly responsible for procuring 600 MW of FNR reserves, which are divided proportionally to each TSO. FNR is a symmetrical service, which means that the provider must offer the same upwards and downwards reserve capacity. Frequency reserve is provided linearly, with full activation for deviations of ± 100 mHz. According to the service requirements, response has to be provided linearly and deployed within 150 seconds [13]. These requirements are designed for slower-acting conventional power plants; instead, we consider instant reserve activation reserve in the case of V2G chargers, because this can significantly improve system performance.

For a frequency value f_t at time t, the normalised requested load $P_{\text{req},t}$ is calculated as

$$P_{\text{req},t} = \begin{cases} -1 & \text{if } f_t < 49.9 \text{ Hz} \\ (f_t - 50)/0.1 & \text{if } 49.9 \text{ Hz} \leq f_t \leq 50.1 \text{ Hz} \\ 1 & \text{if } f_t > 50.1 \text{ Hz} \end{cases} \quad (1)$$

By normalized response we refer to the reserve capacity, P_{res}, of a service provider. As already explained, there are two ways that an aggregation of EVs can modulate its load to provide FNR. In a centralized control scheme the aggregator will calculate the required change in the aggregate load of the EVs and send signals to the individual EVs when it is required. These signals may correspond to deterministic commands, i.e. explicit set-points, or signals containing switching probabilities. In the latter case, the EV will draw a random number and decide to change its set-point or not [5]. However, in these approaches very advanced and reliable real-time communication is required.

In a decentralized control scheme, each EV measures frequency locally and changes its set-point based on a control logic and the individual reserve capacity assigned to it. Other control layers can periodically modify each EV's reserve capacity or target set-point, i.e. the operating set-point when no reserve is offered, on longer time scales based on various parameters. This control structure, which adjusts each EV's reserve capacity and target set-point on a longer time scale (e.g. 15 minutes), while each EV responds based on local measurements, can reduce the communication requirements significantly and retain the robustness of reserve provision. The decentralized nature of reserve provision is thus maintained and EVs respond by only measuring local frequency, whereas the upper control layer can make adjustments on the reserve capacity and target set-point. In this paper we focus on the lower, decentralized control layer assuming that the target set-point is equal to zero and P_{res} is symmetrical and equal to the maximum capability of each EV. In our future work we will generalize our method by considering arbitrary target set-points and non-symmetrical assigned reserve capacities. The most standardized, simple and common control method is for a charger to respond linearly to frequency deviations based on a droop curve, as shown in Fig. 1 [14] for a charger with a capacity of ± 25 A.

Due to the 1 A response granularity, some reserve errors will occur because the requested response $P_{\text{req},t}$ is rounded to the nearest corresponding power value. This is an inherent limitation of the response granularity (the implemented droop curve cannot match the ideal one), but these errors can be significantly reduced if a stochastic controller is introduced, as explained in Section IV. At this point we must introduce

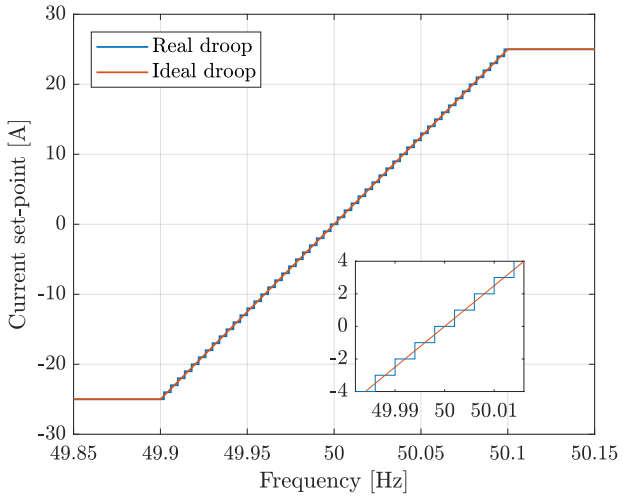

Figure 1: Real and ideal droop curves with 1 A granularity.

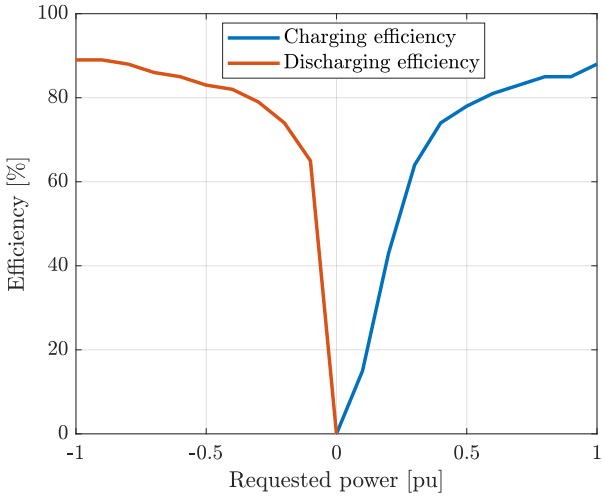

Figure 2: Efficiency characteristics based on real data.

a metric to assess the accuracy of the various controllers. Without loss of generality, we consider the case where all EVs (with i being the index of N EVs) offer the same reserve capacity and we denote by y_t^i the actual, normalized load of EV i at step t. A deterministic controller will then result to the same error for all EVs, assuming that the measured f_t is the same for the whole aggregation, which is a realistic assumption as long as the aggregated set of chargers is not too geographically dispersed. If each EV is offering a different reserve capacity, then their contributions must be weighted appropriately. For simplicity we use normalized variables, i.e. on the maximum charger capacity which is equal to 10 kW, and for a period of t_{tot} the mean average percentage error (MAPE) will be equal to

$$MAPE[\%] = \frac{\sum_{i=1}^{\text{N}} \sum_{t=1}^{t_{\text{tot}}} |y_t^i - P_{\text{req},t}^i|}{\text{N}\ t_{\text{tot}}} \cdot 100\% \qquad (2)$$

III. V2G Charger Efficiency Characteristic

An EV performing FNR in a decentralized manner is expected to continuously alternate between charging and discharging modes to follow the frequency deviations and provide reserve power. Apart from the battery degradation that this may cause (and the associated costs), efficiency losses may significantly affect the economic performance of an aggregator performing this service. As we will show next, the way EVs perform FNR has a considerable impact on the efficiency losses during reserve provision. In Fig. 2 a V2G charger efficiency characteristic is presented, which was derived by real data from EVs performing FNR [14].

One can notice that efficiency is considerably lower for small loadings because the inverter is designed to operate more efficiently closer to the maximum loading values. In Fig. 3 a histogram of 10 days of frequency values for 2016 is presented, where it is evident that most frequency samples lie within a narrow band around 50 Hz. The frequency data corresponds to real frequency measurements of RG-N area from the Norwegian TSO [15]. Approximately 85% of the samples are between 49.95 Hz and 50.05 Hz, which means that a droop curve like the one in Fig. 1 would result in normalized loads below 0.5 for most of the time and consequently low average efficiencies, according to Fig. 2.

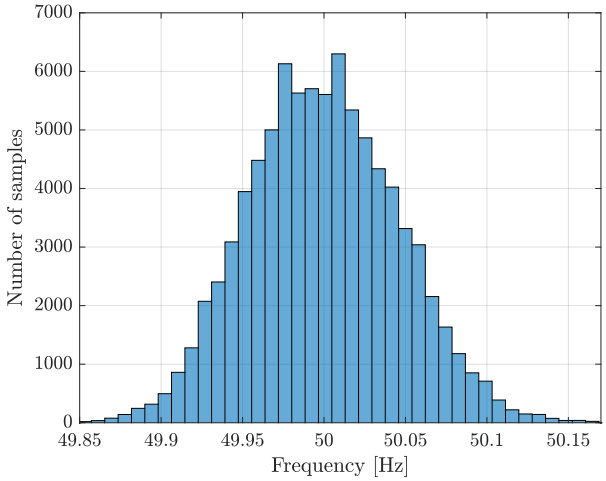

Figure 3: Histogram of frequency values for 10 days.

Other inverters may have significantly higher efficiencies in lower operating points, if they are designed accordingly. Even if in that case a droop-based response with 1 A steps will not result in very low average efficiency, still the proposed controller can optimize the aggregation's average efficiency under a decentralized control scheme. However, we consider the presented efficiencies as a more realistic case, because they are obtained from actual V2G chargers performing FNR.

IV. Discretized Decentralized Control

A. Basic algorithm

As shown in the following example, a deterministic droop controller with a non-continuous response will always result in a response error, except for the cases where the requested response coincides with a discrete step of the charger's output.

Consider the case of a 1 A granularity, which corresponds to 0.4 kW steps for a DC voltage equal to 400 V. If the power response is rounded to its closest value, the response error as a function of the requested power will be as shown in Fig. 4.

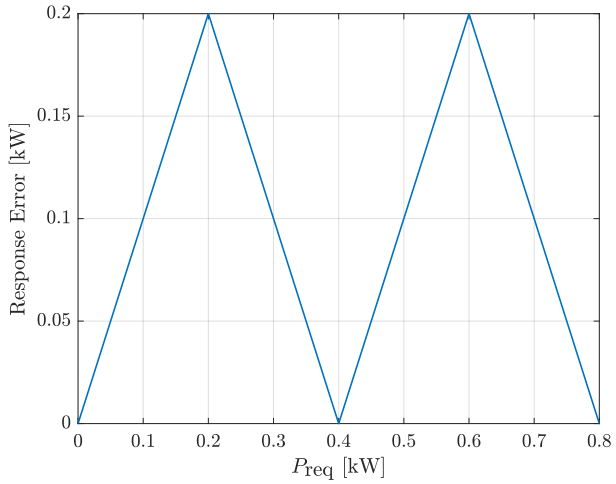

Figure 4: Response error (absolute value) as a function of the requested power.

As already shown, frequency is normally distributed around 50 Hz. If the frequency distribution is discretized in so many steps as in our case, i.e. 25 steps, the resulting probability distributions for each bin can be very well approximated by uniform distributions. Considering a uniform distribution of the frequency within each bin, the distribution of the response errors will retain the triangular shape shown in Fig. 4. It is trivial to show that this results in an average error of 0.1 kW, which for a reserve capacity of 10 kW is equivalent to a MAPE of 1%. This error is of course independent of the number of EVs and is relatively small; however, it can be drastically reduced by employing a simple stochastic strategy as explained later. The main drawback of this method is that it results in very low efficiencies, since the EVs operate at low loadings most of the time.

We propose a decentralized stochastic controller whose tuning objective is to compromise efficiency and reserve errors, taking into account the size of the EVs aggregation. Stochastic controllers based on random number generations which force loads to operate either at full capacity or to be idle have been proposed in the literature, such as [3], [16]. Our approach differs because it employs an arbitrary discretization of the response to address efficiency and aggregation size. A very fine discretization results in small errors but poor efficiencies. On the other hand, 3 states (idle, fully charging or discharging) will result in high efficiencies but high errors, unless the aggregation is large.

First, the response of each EV is discretized in bins represented by a vector $\mathbf{v}$ in ascending order and normalized per reserve capacity. We define the mapping $\mathbf{g} : \mathbb{R} \rightarrow \mathbb{R}^2$, which maps a value $P_{\text{req},t}$ to bins i and j of the vector $\mathbf{v}$ so that $\mathbf{v}(i) \leq P_{\text{req},t} \leq \mathbf{v}(j)$. Depending on the calculated $P_{\text{req},t}$, the controller identifies the 2 bins its response must lie within, calculates a switching probability p and draws a random number. This simple Bernoulli trial, denoted by $h(p)$ and its outcome b, will determine the state s of the EV. The control algorithm is illustrated in Algorithm 1.

Algorithm 1 Stochastic switching algorithm

```
calculate P_req,t
i, j ← g(P_req,t)
d = v(j) − v(i)
if P_req,t ≥ 0 then
    p ← (P_req,t − v(i))/d
    b ← h(p)
    if b = 0 then
        s ← v(i)
    else
        s ← v(j)
    end if
else
    p ← (v(j) − P_req,t)/d
    b ← h(p)
    if b = 0 then
        s ← v(j)
    else
        s ← v(i)
    end if
end if
```

B. Switching minimization

We presented the basic version of the control algorithm. It is possible to minimize the switching actions of the inverters by modifying the algorithm for the cases where the requested power lies within the same 2 bins in two consecutive time steps. We illustrate the algorithm's modification with an example instead of an algorithm diagram, due to space limitations. Consider the case of two time steps t_1, t_2 where $P_{\text{req},t_1} = 0.2$ and $P_{\text{req},t_2} = 0.3$ and $\mathbf{v} = [-1, -0.5, 0, 0.5, 1]$. At t_1, approximately 60% of the chargers' outputs will be equal to 0 and 40% equal to 50%. Instead of all the EVs drawing random numbers at t_2, only a portion of the loads with power equal to 0 have to switch to the next bin; more specifically, these loads will apply the stochastic process with $p = 0.1/(0.5 * 0.6) = 33.3\%$. Similarly, if $P_{\text{req},t_2} = 0.1$, then only only a portion of the loads with power equal to 50% will apply the stochastic process with $p = 0.1/(0.5 * 0.4) = 50\%$. Following similar arguments, the chargers can minimize their switching in the cases of negative $P_{\text{req},t}$. Note that this algorithm is also decentralized and no coordination is required. Each load will apply this algorithm considering the expected state of the population and not the exact number of EVs in each state, whereas only the change $P_{\text{req},t_2} - P_{\text{req},t_1}$ determines which loads will apply the stochastic process. These modifications in the algorithm can drastically reduce the number of switchings without noticeable increases in the MAPEs, as shown in the following section.

V. Results

We used a real 4 hour frequency sample to assess the performance of the different control strategies. We assume that all EVs are available during reserve provision, as is the case in [12], and provide the maximum reserve capacity, equal to ± 10 kW. The chosen frequency sample satisfies two conditions: (a) frequency does not have a significant bias, so that charging and discharging are almost equally represented, and (b) frequency presents a relatively large variance around 50 Hz so that small frequency deviations are not over-represented. Frequency samples with small variance are expected to yield worse efficiencies when a droop curve is used and our purpose is to make a fair comparison with our proposed controller. The normalized requested power corresponding to the frequency sample is shown in Fig. 5 and the time step used for all simulations is 1 s.

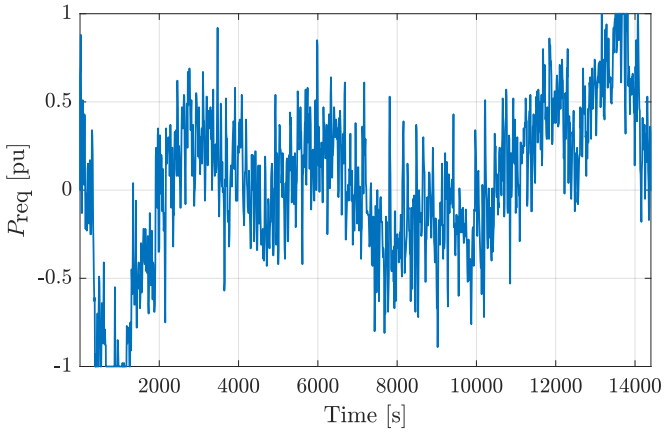

Figure 5: Normalized requested power for a 4 h frequency sample.

A. Effect of aggregation size and controller granularity on MAPE

We first analyzed the performance of a deterministic controller with a 4% granularity (corresponding to the 1 A steps) which simply rounds the requested power to the closest possible power output; we found that it results in a MAPE equal to 1%, as theoretically calculated in Section IV. Due to the deterministic nature of the controller, the error does not depend on the aggregation size.

We then examined the effect of the discretization step on the average reserve error. We used the modified controller which minimizes the switching rate in our simulations. As already explained, a discretization with very small steps is expected to produce very small reserve errors, since any inaccurate number draws have a small impact on the error. On the other hand, large steps are expected to result in larger MAPEs because inaccurate number draws produce relatively large errors. However, as the number of EVs increases, the results of the random-number generations are closer to the expected values and the errors decrease. The reserve MAPEs as a function of the EVs number for 6 different discretization steps are shown in Fig. 6.

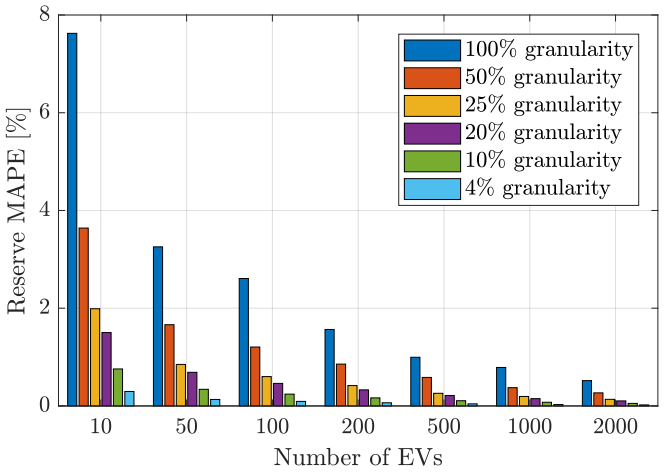

Figure 6: Reserve MAPEs as a function of the EVs number for different granularities of the response.

It is evident that for small aggregations a large granularity results in significant MAPEs. The advantage of using a stochastic controller even for the case of the 4% granularity is evident by the fact that MAPE decreases from 1% (deterministic case) to 0.4% for 10 EVs and 0.17% for 50 EVs. A MAPE of 1% requires more than 500 EVs for a granularity of 100% and as few as 50 EVs for a granularity of 25%.

Next, we calculated the MAPEs when the modification for minizing the switchings was not used. A continuous switching is expected to produce smaller MAPEs because at each time step all EVs will draw a random number and respond; when the switching minimization is applied, the EVs switch based on the expected distribution of the EVs between two bins. For smaller aggregation sizes the actual and expected distributions may not be the same (for larger sizes the difference is negligible) and thus the calculated probability may not reflect the ideal probability. However, simulations showed that the exclusion of the modification in the controller results in very small differences in the MAPE and for a size larger than 100 EVs the errors are almost the same. For 10 EVs and 100% granularity, the modification increases the MAPE from 7.6% to 7.9% and for 50 EVs from 3.36% to 3.4%.

B. Effect of controller granularity on the average efficiency

To calculate the effect of the controller's granularity on the average efficiency we used the modified algorithm because it significantly reduces the switching actions and it has a minimal effect on the MAPEs. We calculated the average charging and discharging efficiencies for the entire reserve provision duration for each granularity; the results are shown in Fig. 7. We observed that the efficiencies do not depend on the number of the EVs because the stochastic process itself is the same for all loads and on average it doesn't affect efficiency. As already discussed, most frequency samples are distributed close to 50 Hz, which would force the EVs to operate on low loadings if they use a typical droop curve with small steps. This is reflected in the simulation results, where the

average efficiencies increase significantly as the steps become larger. This can be explained by the fact that when large steps are used, e.g. 50% or 100%, the EVs will be either idle or charging/discharging at much higher capacities even for small requested powers.

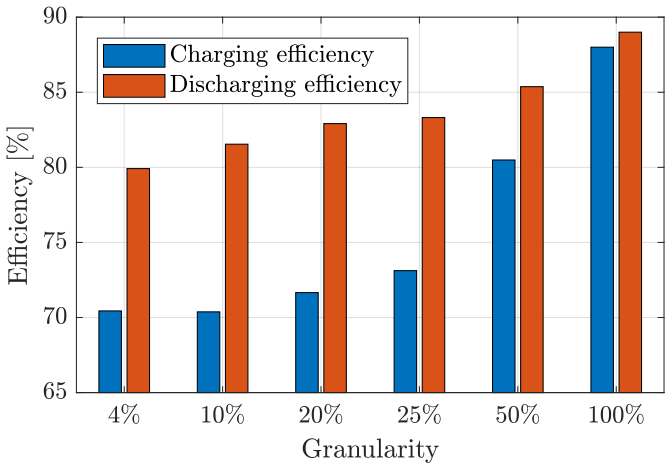

Figure 7: Average charging and discharging efficiencies for the different controller granularities.

To illustrate the effect of such differences on the average EVs SOC when they are offering FNR, we simulated their SOC for 4 different discretizations and for the case without any losses. The average SOC is expressed in pu of P_{res}, i.e. for $P_{\text{res}} = 10$ kW a SOC value of 1 corresponds to 10 kWh. We show the change of SOC, denoted by ΔSOC, compared to an initial zero value for the different cases in Fig. 8.

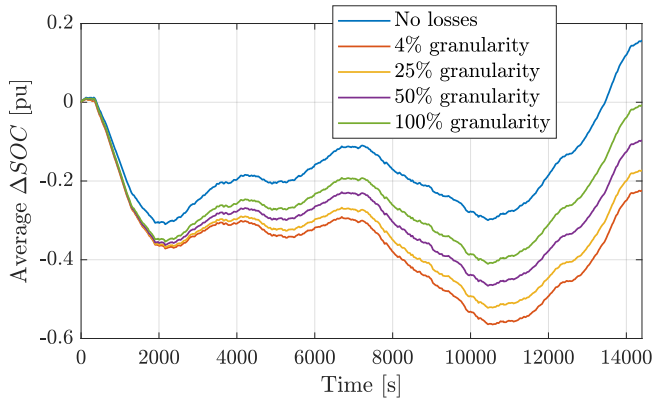

Figure 8: Evolution of the average ΔSOC for different controller discretizations, compared to a lossless operation.

Notice the effect the different controllers have on the average SOC over a period of 4 hours providing FNR. If no losses occurred, then the average SOC at the end of the period is equal to 0.15 pu, or 1.5 kWh for a $P_{\text{res}} = 10$ kW. Instead of charging with this amount, the EVs would discharge by more than 2 kWh using a droop curve of 1 A steps, whereas with 3 modes the average SOC would be equal to zero. Notice also the variance in the evolution of the SOC; the larger it is throughout the reserve provision period, the harder it is for the EVs to offer reserves. In other words, the aggregator needs to be more conservative in the amount of offered reserve capacity, so as not to reach the upper or lower battery limits while providing reserves.

C. Average switching actions

A potential disadvantage of using a discretized decentralized controller is the frequent switching of the inverters. Usually inverters are designed to handle frequent changes in their output but the impact on the inverters and EV batteries should also be considered when designing the controller. Recognizing the potential wear on the equipment, we proposed a modification of the controller in Section IV to minimize the switching actions. We simulated both control approaches and we present the average switching rates for each granularity in Fig. 9. Note that the average switching rate is presented as a percentage of the time steps, i.e. a rate of 1% means that an inverter will change state 144 times over 4 hours.

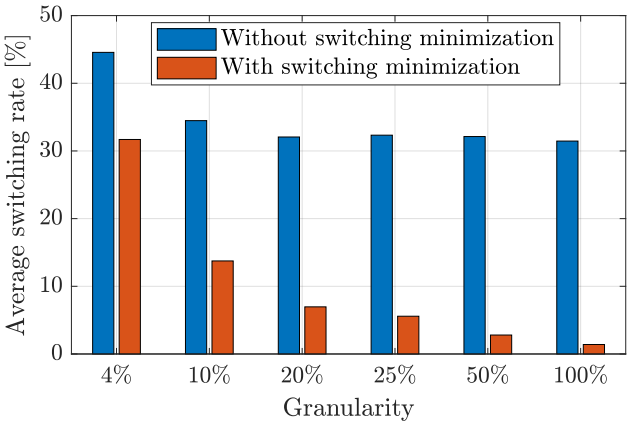

Figure 9: Average switching rates with and without switching minimization.

It is interesting to note that without switching minimization the average switching rate is almost constant and very high (more than 30%); this means for the control time step of 1 s, then on average an inverter will switch every 3 s, which is a very high rate. If we modify the controller, as explained in Section IV, the switching rates are reduced dramatically, reaching an average value of 1.4% (or less than 1 switching per minute) if only 3 modes are used. More complicated control approaches may further reduce the switching rates.

D. Optimizing the controller's discretization steps

With the proposed decentralized control approach it is possible to define different discretizations, without necessarily having equal distances between two consecutive bins. For example, it is reasonable to design a controller with a finer granularity in higher loadings, which at the same time avoids operating at loadings below 50%. In this regard, in Fig. 10 the MAPEs and the average efficiencies for 3 different strategies are shown. It is interesting to note the different performance of the controllers for the used discretizations. By taking the $[-100 \quad -50 \quad 0 \quad 50 \quad 100]\%$ discretization as the benchmark, the addition of an intermediate upper state

equal to 75% of the capacity has a minimal effect on the average efficiencies but reduces the errors. Additionally, a discretization of $[-100 \ -60 \ 0 \ 60 \ 100]\%$ of the response results in slightly larger errors compared to the previous case but increases the average efficiencies.

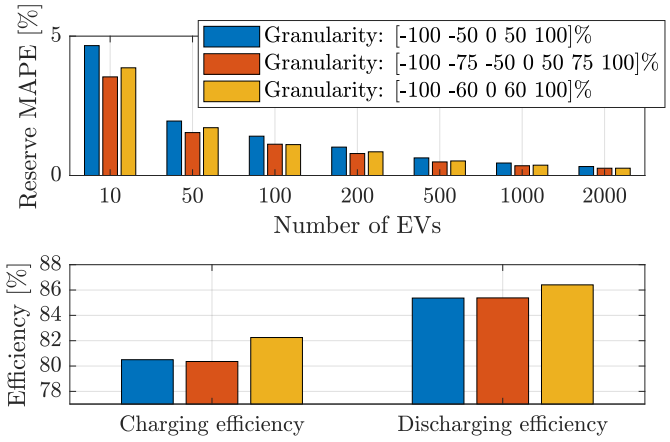

Figure 10: MAPEs and average efficiencies for 3 different discretizations of the controller.

Our purpose is not to present the best discretization for the efficiency values we use in this study, but to show that there are various trade-offs when designing the controllers. In particular, we showed that the efficiency curves, the allowed reserve errors based on the service requirements, the allowed switching rates and the number of EVs must be all taken into account to find the optimal discretization for a given EV fleet offering FNR.

VI. Conclusion

We proposed a stochastic, decentralized controller which relies only on local frequency measurements and whose discretized response can be optimized according to a set of criteria. We showed that a droop-curve response with a 1 A granularity results in low efficiencies and high average switching rates, albeit in low reserve errors. On the other hand, a response with only 3 states results in high efficiencies but unacceptable reserve errors for small EV fleets. The proposed controller, which is also designed to minimize the switching actions of the chargers, can compromise efficiency, average switching rates and reserve errors for a given EV fleet size.

Thus, if the fleet size does not allow the EVs operator to choose the most efficient response discretization (which is fully charging, idle or fully discharging), it can optimize the discretization based on an efficiency, reserve error and average switching rate trade off. It is interesting to note that since the chargers' efficiency characteristics are highly non-linear, the ideal response discretization which maximizes efficiency and guarantees a maximum reserve error is not trivial to be found and may also depend on the frequency signal characteristics. It is thus necessary to take all the aforementioned factors into account and their effect on performance when optimizing the proposed controller. In our future work we will generalize the controller by considering arbitrary target set-points and non-symmetrical assigned reserve capacities and we will perform a validation on the proposed controller on real V2G chargers performing FNR under realistic conditions.

VII. Acknowledgments

The authors would like to acknowledge the support of the EUDP projects ACES - Across Continents Electric Vehicle Services (grant EUDP17-I-12499, website: www.aces-bornholm.eu) and Ecogrid 2.0 (grant 64015-0082, website: www.ecogrid.dk)

References

[1] M. Rezkalla, A. Zecchino, S. Martinenas, A. M. Prostejovsky, and M. Marinelli, "Comparison between synthetic inertia and fast frequency containment control based on single phase evs in a microgrid," *Applied Energy*, vol. 210, pp. 764 – 775, 2018. [Online]. Available: http://www.sciencedirect.com/science/article/pii/S0306261917308024

[2] K. Knezović, S. Martinenas, P. B. Andersen, A. Zecchino, and M. Marinelli, "Enhancing the role of electric vehicles in the power grid: Field validation of multiple ancillary services," *IEEE Transactions on Transportation Electrification*, vol. 3, no. 1, pp. 201–209, March 2017.

[3] M. G. Vayá and G. Andersson, "Combined smart-charging and frequency regulation for fleets of plug-in electric vehicles," in *2013 IEEE Power Energy Society General Meeting*, July 2013, pp. 1–5.

[4] E. Sortomme and K. W. Cheung, "Intelligent dispatch of electric vehicles performing vehicle-to-grid regulation," in *2012 IEEE International Electric Vehicle Conference*, March 2012, pp. 1–6.

[5] S. Izadkhast, P. Garcia-Gonzalez, P. Frias, and P. Bauer, "Design of Plug-in Electric Vehicle's Frequency-Droop Controller for Primary Frequency Control and Performance Assessment," *IEEE Transactions on Power Systems*, vol. PP, no. 99, pp. 1–1, 2017.

[6] A. Molina-Garcia, F. Bouffard, and D. S. Kirschen, "Decentralized demand-side contribution to primary frequency control," *IEEE Transactions on Power Systems*, vol. 26, no. 1, pp. 411–419, Feb 2011.

[7] M. R. V. Moghadam, R. Zhang, and R. T. B. Ma, "Distributed frequency control via randomized response of electric vehicles in power grid," *IEEE Transactions on Sustainable Energy*, vol. 7, no. 1, pp. 312–324, Jan 2016.

[8] S. Izadkhast, P. Garcia-Gonzalez, and P. Frías, "An aggregate model of plug-in electric vehicles for primary frequency control," *IEEE Transactions on Power Systems*, vol. 30, no. 3, pp. 1475–1482, May 2015.

[9] G. Wenzel, M. Negrete-Pincetic, D. E. Olivares, J. MacDonald, and D. S. Callaway, "Real-time charging strategies for an electric vehicle aggregator to provide ancillary services," *IEEE Transactions on Smart Grid*, vol. PP, no. 99, pp. 1–1, 2017.

[10] H. Liu, Z. Hu, Y. Song, and J. Lin, "Decentralized vehicle-to-grid control for primary frequency regulation considering charging demands," *IEEE Transactions on Power Systems*, vol. 28, no. 3, pp. 3480–3489, 2013.

[11] "Road vehicles — vehicle to grid communication interface — part 1: General information and use-case definition," https://www.iso.org/obp/ui/#iso:std:iso:15118:-1:ed-1:v2:en, 2013.

[12] ENEL, "Nissan, enel and nuvve operate world's first fully commercial vehicle-to-grid hub in denmark," https://www.enel.com, 2016.

[13] Energinet.dk, "Ancillary services to be delivered in denmark - tender conditions." https://en.energinet.dk/-/media/Energinet/El-RGD/Dokumenter/Ancillary-services-to-be-delivered-in-Denmark.pdf, 2017.

[14] A. Thingvad, C. Ziras, J. Hu, and M. Marinelli, "Assessing the energy content of system frequency and electric vehicle charging efficiency for ancillary service provision," *2017 Proceedings of the 52nd International Universities Power Engineering Conference*, 2017.

[15] http://www.statnett.no.

[16] E. Vrettos, C. Ziras, and G. Andersson, "Fast and Reliable Primary Frequency Reserves From Refrigerators with Decentralized Stochastic Control," *IEEE Transactions on Power Systems*, vol. 32, no. 4, pp. 2924–2941, 2017.

Paper G

Title:

Large-scale Provision of Frequency Control via V2G: the Bornholm Power System Case

Authors:

Antonio Zecchino, Alexander M. Prostejovsky, Charalampos Ziras and Mattia Marinelli

Published in:

Electric Power Systems Research (under 2nd round of review).

Large-scale Provision of Frequency Control via V2G: the Bornholm Power System Case

Antonio Zecchino, Alexander M. Prostejovsky*, Charalampos Ziras, Mattia Marinelli

Center for Electric Power and Energy, Technical University of Denmark,
DTU Risø Campus, Frederiksborgvej 399, 4000 Roskilde, Denmark

Abstract **–** This paper assesses the impact of electric vehicles (EVs) providing primary frequency regulation via vehicle-to-grid (V2G) technology. The aim of the work is to define a set of recommendations in order to guarantee a stable large-scale deployment of EV fleets as primary reserve providers. A realistic fleet model is proposed, which emulates the aggregated response of a number of EVs characterized by V2G hardware response times derived in laboratory tests. The effects of primary frequency control via EV fleets replacing conventional generating units are assessed with a sensitivity study in a single-bus power system with growing fleet sizes and response times. Two recommendations are derived to guarantee safe and stable operation: *Recommendation 1* requires the share of EVs providing primary reserve to be smaller than the reserve from conventional units; *Recommendation 2* requires response times below a given limit value, calculated as a function of the following power system parameters: the system inertia, the total primary reserve over the rotating generation capacity, and the employed droop gain. The full 60 kV power system of the Danish island of Bornholm is then employed to evaluate the validity of the proposed requirements on a real system with complex dynamics, non-linearities and voltage dependencies.

Index Terms **–** electric vehicles; electric vehicles aggregation; frequency control; frequency stability.

---

*Corresponding author: tel: 0045 93511216, e-mail: alepros@elektro.dtu.dk

1. Introduction

Electric vehicles (EVs) are considered promising sources of power system services, provided that their individual responses are properly aggregated in order to enable a safe and stable replacement of conventional sources. By modulating their battery charging/discharging process, EVs can perform vehicle-to-grid (V2G) services such as primary frequency control (PFC). The research emphasis in the field is put, among others, on EV fleet modelling for V2G services [1]–[3], combined smart charging and frequency regulation [4]–[6], and impact on the distribution level [7]–[9]. Studies on improvements in islanded power systems dynamics with high shares of renewable generations are also found in the literature [10]–[16]. For example in [12], [13], the frequency control actions implemented in EV controllers include an innovative inertial emulation logic, to counteract the reduction of system inertia due to large-scale generation from renewable energy resources. However, most of the contemporary literature rarely considers some technical hardware aspects are when modelling EVs for demand response purposes. As the primary function of an EV is transportation, their components are not designed to offer power system services, and thus many technological barriers need to be overcome when they are aggregated and controlled [17]. Critical response times of the aggregated EV fleet, as well as the need for each EV to comply with the ISO 15118 technical standard requirement of charging/discharging rate granularity, play an important role when dynamically assessing the response characteristics [18]. In fact, relatively large discrete step responses may trigger frequency stability problems, as presented in the literature within the domain of demand response [19]–[23], and also experienced in an experimental microgrid with smart-charging EVs [24], [25]. The stability of the power system may be jeopardized by V2G EV fleets in case of simultaneous and high ramping-rate responses, especially under large response delays. The state-of-the-art is lacking of exhaustive contributions on this topic: investigations are proposed only in [22] and in [23]. In Ref. [22] the authors propose a decentralized control scheme to assign randomized delay times on each individual EV, which reacts by setting one of the three possible states (full charging, idle or full discharging) instead of considering a linear control modulation. In [23] EV droop

controllers are designed for a centralized control scheme in a way to ensure the same stability margin with and without EVs performing PFC control. However, the typical delay accounting for the EV activation is not implemented.

In the present manuscript we aim at assessing the potential impact of aggregated ±10 kW off-board EV chargers performing PFC on a real power system, relying on centralized control schemes already operating in field trial applications [26]. The choice of the 10 kW size is motivated by the outcome of the Danish founded demonstration projects Parker and ACES [27], [28], where the suitability of such chargers for the provision of grid services is recognized by the involved stakeholders. In particular, the development of commercial applications employing commercial fleets within companies or municipalities is of high interest, which enables high availability for reserve capacity during the evening time. Firstly, the employed EV fleet model is presented and characterized with realistic parameters obtained from commercial V2G hardware tests [29]. Secondly, the stability margin of the model is investigated, and the need for dedicated recommendations for grid operators is presented in terms of PFC from EVs replacing PFC provided by conventional generation units (CGUs).

The main contribution of this paper is the definition of two recommendations that EV fleet operators performing PFC need to fulfill in order to participate in the regulating market. In particular, limit values are found in terms of safe EV response times and overall primary reserve share from V2G units. This is obtained by carrying out a stability assessment, implementing accurate aggregated EV models and a representative single-bus power system testbed. The investigation is then extended to a real system with complex dynamics, non-linearities and voltage dependencies of the units, allowing the validation of the identified recommendations as well as the confirmation of the need for proper safety factors and simultaneous fulfilment of the two recommendations. The analysis is performed on the Danish island of Bornholm once it is disconnected from the mainland and therefore lacking of large synchronizing torques. The grid is therefore considered an excellent test case for investigating stability issues already arising with a limited number of

chargers in case of slow time responses. The grid is implemented at 60 and 10 kV levels with charging stations aggregated at the 10 kV busbars. Frequency and voltage stability are investigated by means of RMS simulations in DIgSILENT PowerFactory software environment under different EV penetration scenarios as well as fleet response characteristics. The findings of this investigation will support system operators facing the future challenges due to frequency service procurement by EVs.

The paper is structured as follows. Section 2 presents the current framework for frequency control in the Nordic synchronous region and characterizes the power system of Bornholm Island. Section 3 describes the employed fleet model characterized with realistic parameters. Section 4 presents a single-bus case investigation, defining a set of recommendations in terms of critical activation times, and share of PFC from EVs for a given power system. In Section 5 the real power system of Bornholm is implemented in detail and realistic scenarios are investigated, and results are discussed. Conclusions are in Section 6.

2. Conventional System Frequency Control

This section first presents a summary of the current framework for frequency control in the Nordic synchronous region, and then it describes in detail the power system of the Danish island of Bornholm, which belongs to the Nordic area. The aim is to investigate barriers and opportunities for the provision of power system services via aggregated electric vehicles within the context of the Nordic frequency control framework, exploiting a testbed that can be operated also in islanded mode, i.e., when frequency control becomes more challenging due to less synchronous rotating mass.

2.1. Framework for Frequency Control in the Nordic Area

In general, frequency control is achieved in three subsequent phases, namely: (i) Primary frequency control, (ii) Secondary power-frequency control and (iii) Tertiary control [30]. The Regional Group Nordic (RGN) synchronous area is composed by the interconnected power systems of Norway, Sweden, Finland, and Eastern Denmark (DK2). In the RGN synchronous area, primary frequency control is achieved via two separate services: frequency-controlled normal operation reserve (FNR), activated linearly with no dead band

for all frequency deviations within ±100 mHz, and frequency-controlled disturbance reserve (FDR), activated in addition to FNR only when system frequency drops below 49.9 Hz. In the current framework there is no automatic secondary frequency control in the RGN power system, whereas tertiary reserve is in place [31].

FNR is a symmetrical service, meaning that the same upwards and downwards reserve capacity must be provided. According to the service requirements, the reserve has to be provided within 150 seconds [31]. The minimum size of total FNR reserve that has always to be procured in the RGN is 600 MW, divided proportionally among transmission system operators (TSOs). FDR is a non-symmetrical service, as the involved units respond with only frequency up-regulation by linearly injecting power into the system when the measured frequency is below 49.9 Hz, with full reserve activation at 49.5 Hz. The 50% of the response has to take place within 5 s, whereas the remaining 50% within an additional 25 s.

The listed requirements set the basis for benchmarking the performance of the simulation activities performed on the real power system of the Danish island Bornholm, which is described in the following.

2.2. Description of the Bornholm power system

Bornholm is a Danish island in the Baltic Sea, located in the east of Denmark and the south of Sweden. The Bornholm electric power system is composed of distribution networks at three voltage levels: 60 kV, 10 kV and 0.4 kV [32], [33]. A 43.5 km long sea cable at 60 kV with 60 MVA capacity connects the island to the Swedish system, which means that the Bornholm system is electrically coupled with the Nordic power system [34]. As from an electricity market and regulatory framework point of view the system belongs to the RGN, frequency control is performed as indicated in the previous subsection. Occasionally, the sea cable connection to Sweden is disrupted due to maintenance or incidents, forcing the Bornholm power system to run into islanding mode. During these periods, system frequency control is performed by the local distribution system operator (DSO) Bornholm Energi & Forsyning (BEOF) relying on a set of units that provide conventional reserve, while at the same time shutting down most of the wind generators. As the goal

of the proposed investigation is to replace conventional generation units employed for reserve with EV fleet providing frequency control via V2G, the islanded operation mode is studied.

The grid is modelled at the 60 kV medium voltage (MV) level with real models of all the 60 kV lines along with the 60/10 kV substations. Aggregated loads, conventional generation units, renewable energy plants (wind turbines and photovoltaics (PV)) and EV fleet models are connected at the 10 kV buses, and the detailed 10 kV lines are not modelled since the 10 kV system is not presenting any potential overloading issues. Since the aim of the analysis is the assessment of large-scale V2G employment on a system level, the complete 60 kV grid is considered sufficient. The 60 kV grid is shown in Fig. 1, with names and locations of the nodes with 60/10 kV substations. The 60 kV network has 16 60/10 kV substations, 23 60/10 kV transformers with On-Load Tap Changers, and 22 cables and overhead lines of a total length of 131 km. The peak load in Bornholm is 63 MW, whereas the minimum load is 13 MW. The complete generation set updated in May 2018 includes:

- 16 MW biomass combined heat and power plant (CHP) with steam turbine, named **Blok 6**. It has an inertia time constant $2H$=6.4 s and apparent power S=46.8 MVA. It is equipped with primary frequency droop control at 2%, and automatic voltage regulator. The unit responds with a ramping rate of 0.2 MW/min (1.25% P_{nom}/min). As a side note, if it runs with coal/oil it can be boosted to 24/36 MW, respectively.
- 2·1 MW biogas CHP gas turbine, each with inertia $2H$=5.6 s and apparent power S=1 MVA. These units are not equipped with primary frequency droop control.
- 37 MW wind (24 machines <100kW; 16 machines between 100 and 1000 kW; 17 machines> 1000 kW. The largest machines are three Siemens 2.3 MW wind turbines at the 60/10 kV substation in Hasle and three Vestas 2 MW units at Aakirkeby).
- 23 MW PV (8 MW distributed on rooftops at 0.4 kV; 2 newly-installed 7.5 MW PV plants at 10 kV at the secondary sides of the 60/10 kV substations in Aakirkeby and Bodilsker).

On top of the above listed generating units, there are other conventional units utilized only during islanded operation, for a total amount of 58 MW of reserve. One of these conventional fossil fuel units utilized only for primary frequency reserve provision will then be replaced with a number of EV fleets in the following simulation studies. As of today, the total primary reserve portfolio includes:

- 25 MW oil-powered steam turbine, named **Blok 5**. It has an inertia $2H$=8.6 s and an apparent power S=29.4 MVA. It is equipped with primary frequency droop control at 2%, and an automatic voltage regulator. The unit responds with a ramping rate of 0.25 MW/min (=1% P_{nom}/min). It is important to note that the droop control of Blok 5 is generally not used in conjunction with Blok 6 due to hunting issues.
- 4·4.5 MW diesel generators, each equipped with 2% frequency droop control and voltage control. Each unit has inertia $2H$=8s, whereas two units have S=5.8 MVA and the others S=6.3 MVA.
- 10·1.5 MW diesel generators, named **Blok 7**. Each unit has an inertia $2H$=1.1 s and an apparent power S=2 MVA. They are not equipped with primary frequency droop nor voltage control. Each unit responds with a ramping rate of 1 MW/min (66% P_{nom}/min).

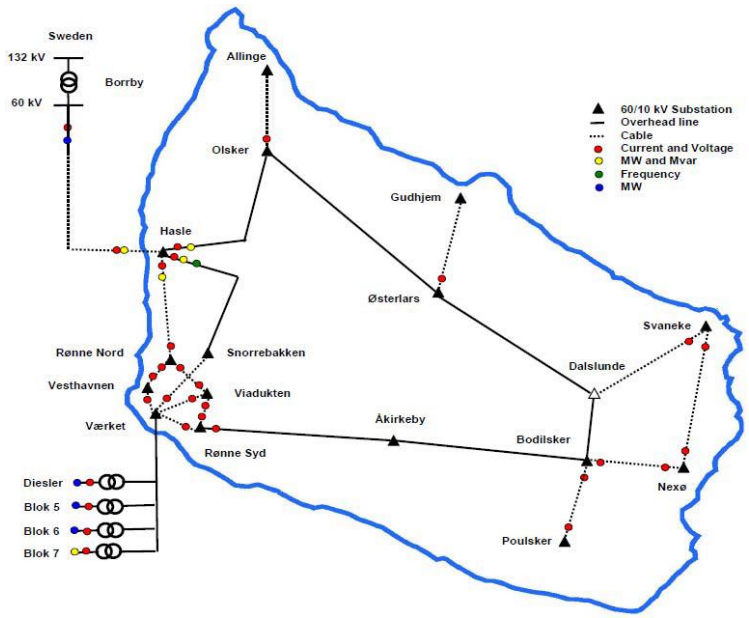

Fig. 1. Bornholm Island 60 kV grid with major generation units and nodes with 60/10 kV substations.

Today on the island of the Bornholm there are more than 17000 internal combustion engine cars. The share of EVs will increase dramatically in the coming years, according to the *Nordic EV Outlook 2018* report [35]. As it is expected that a number of EVs will constantly be available for V2G services, realistic models of controlled EV fleets need to be developed when assessing the major impacts on the power system. Already today, 21 10-kW chargers with bidirectional capability are employed to provide frequency regulation. In the next section we propose the novel EV fleet model utilized for power system studies.

3. Aggregated EV fleet modelling

In this section we present the adopted EV aggregation model, which is commonly utilized for power system studies. The fleet model is then characterized with real V2G hardware test results.

3.1. Adopted EV Fleet Aggregation Model

Given a population of N EV chargers indexed by i, the most common representation of their response to a change in their power output is via a transfer function of the following form:

$$H_i(s) = \frac{k_{EV,i}}{1+T_{EV,i}s} e^{-\tau_i s} \tag{1}$$

where $k_{EV,i}$ is the controller's gain, $T_{EV,i}$ the first-order time constant, and τ_i the response delay.

The adopted aggregation model is a model where average values for the three sets of parameters are used, along with a gain N, representing the fleet size. A good approximation of the actual response of N EV chargers is given by the transfer function $R_{EV}(s)$:

$$R_{EV}(s) = \frac{N\overline{k_{EV}}}{s+\overline{T_{EV}}s^2} e^{-\overline{\tau}s} \ . \tag{2}$$

The symbol $\overline{(\cdot)}$ denotes the average value of the three parameters in Eq. (1) (gains, first-order time constants and response delays) for the N considered EVs. This model is named *average model* in the rest of the paper.

3.2. Characterization with Real EV Response Times from Lab and Field Tests

The presented *average model* is characterized with parameters derived from test results, and is adopted for the stability investigation when large-scale provision of frequency control is achieved via V2G technology.

In this subsection, we present the main outcome of tests on real ±10 kW V2G chargers responding to charging/discharging control signals, setting power set-points both in a local and in a remote fashion, meaning that the control signal has been computed locally and remotely, respectively. This enabled us to derive the activation time of only the employed hardware, and to assess the additional communication latencies on the total activation time when an aggregator acts remotely. It is worth mentioning that the remote

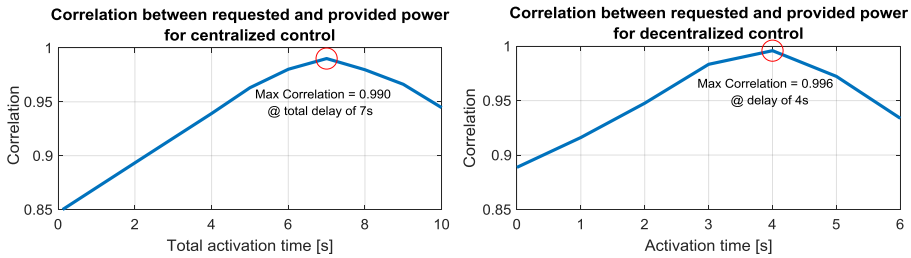

Fig. 2. Correlation between requested and provided power for remote and local control, which enabled us to derive the EV delays.

control test setup includes the communication and control infrastructure utilized by an actual EV aggregator, operating in on-field projects such as the Danish-funded projects ACES [28] and Parker [27]. Appropriate test patterns with all the possible charging/discharging set-points were sent to the V2G chargers, as presented in the dynamic characterization tests presented in Ref. [29], allowing the calculation of the most probable response times of real commercial V2G-capable hardware.

The main test results are shown in Fig. 2, which reports the correlation between the requested and provided power when applying different time shifts to one of them for the whole duration of the test. This allows the estimation of the most probable activation time for both test setups, which resulted to be 7.0 s and 4.0 s for the remote and local control case, respectively.

One has to note that these results were obtained for one type of V2G chargers and one type of control and communication infrastructure in case of remote control. Thus, slightly different results can be obtained in case of faster or slower hardware and/or communications. However, such results provide a valuable asset for the characterization of the proposed EV fleet model, as well as for the analysis of power system stability aspects related to frequency regulations via such resources.

4. Effects of Primary Frequency Control via EVs Replacing CGUs

The purpose of this section is to provide general insights on the effects of large-scale PFC provision via aggregated EVs, and to outline safety recommendations to prevent system instability. Firstly, the dynamic performance of the aggregation models introduced in Section 3 is evaluated by investigating the frequency response of the models' transfer functions by their own as well as in a simulated simplified power system. Secondly, a set of simulations is carried out with increasing EV penetration share, for different activation times. The analysis proposes a method for defining critical activation times and V2G primary frequency regulation shares over the total primary reserve from conventional units. However, the numeric outcome of this investigation is not meant to be safely applicable in the real operation of any possible power system, but it should rather be considered as a benchmark for further grid analysis in more complete and complex simulation environments. In this context, we will implement the outlined recommendations in the detailed model of the Bornholm power system to evaluate their effectiveness in a real low-inertia system.

4.1. Simplified Power System Layout and Modelling

The first analysis is carried out by implementing the simplified power system in Fig. 3, with the single-bus layout proposed by [36] extended with the EV fleet models. The conventional generators are modelled with the transfer functions representation proposed in the literature, equipped with a proportional droop for primary frequency regulation. The system parameters are chosen in accordance with one possible islanded configuration of the Bornholm power system, and are listed in Table 1.

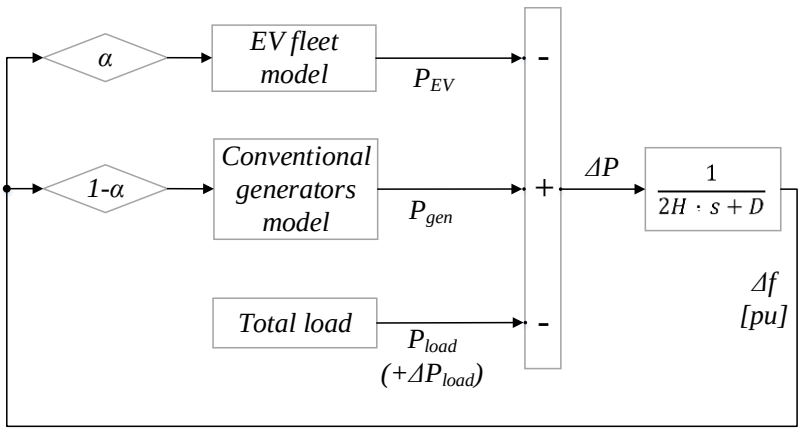

Fig. 3. Simplified power system with the classical single-bus layout.

TABLE 1. SYSTEM PARAMETERS

Parameter	Symbol	Value	Unit
Base Frequency	ω_0	314	rad/s
Inertia constant	H	3.6	s
Rated power	S_{rated}	108.2	MVA
Damping factor	D	0	%
Total load	P_{load}	60	MW
Load step	ΔP_{load}	2	MW
Primary reserve	$P_{reserve}$	10	MW
Primary frequency control normalized droop gain	*droop*	2	%

The EV fleet is modelled as described in Section 3, acting with the same relative droop of the replaced CGU and with different participation factor α and activation times, which for the first set of simulation are considered to have an average value of 7 s. The combined response of 100 individually simulated EVs with normally distributed delays and standard deviation of 0.1 s serves as the reference.

Frequency dynamics are modelled using the linearized swing equation $J\omega_0\dot{\omega} + D\omega = \Delta P_{load}$ and the inertia constant $H = \frac{J{\omega_s}^2}{2S_{rated}}$ according to [36]. No damping (D = 0) is considered as conservative assumption for the stability analysis. The Laplace-transformed representation of the grid is therefore

$$G_{grid}(s) = \frac{f_0}{2HS_{rated}s} \quad . \tag{3}$$

Despite the typical variety of types of rotating CGUs within the portfolio of an operating power system, in this preliminary study we consider only one type of CGU, i.e., diesel generator sets. In fact at this stage the aim is not a detailed power system analysis, but rather the provision of general insights on technical barriers of EV fleets management on a system level. The detailed power system with complete generation portfolio, real line and load models and voltage dependencies will be implemented later on, in order to validate the outcome of this first part of the study. The standard diesel model given in [37] is implemented, equipped with an electric control box:

$$R_{CGU}(s) = \frac{1}{1+T_g s}\frac{1+T_3 s}{1+T_1 s+T_1 T_2 s^2}\frac{k_{CGU}}{1+T_4 s} \, . \tag{4}$$

The implemented EV aggregation model is the *average model* described by Equation (2), which guarantees a finer representation of a large-scale EV fleet with EV delays compared to the commonly used

averaging models. The resulting dynamic system in open- and closed-looped form is so described by *L(s)* and *T(s)*

$$L(s) = G_{grid}(s)(R_{CGU}(s) + R_{EV}(s)) \ , \qquad T(s) = \frac{G_{grid}(s)}{1+L(s)} \tag{5}$$

where $R_{EV}(s)$ is the average EV aggregation model. The share of EVs and conventional resources is expressed over the factor α as in

$$k_{EV} = \alpha k \ , \quad k_{CGU} = (1-\alpha)k \ , \qquad k = \frac{P_{reserve}}{f_0}\frac{1}{droop} \tag{6}$$

where k is the absolute primary droop gain, and $P_{reserve}$ the total power allocated for primary reserve.

4.2. Model Dynamics

Fig. 4-a shows the Bode magnitude plot of the real EV fleet (used as reference) and the *average model*, where the input is the frequency deviation $\Delta f = f - f_0$ and the output is the power delivered by the EVs. As can be observed, magnitude and phase of the *average model* match well with the real EV fleet in the frequency range below 1 Hz. At 1 Hz the deviation amounts to about 1 dB, whereas a deviation of 3 dB is found for a frequency of 1.5 Hz.

Within the given Bornholm power system context, we expect similar behavior of the models due to the smoothing effect of the grid's inertia and the 50 % conventional resources, being α = 0.5 for this first simulation. This is confirmed in Fig. 4-b on the open-loop *L(s)* of (5), where the characteristic system behaviors happen in frequency ranges a full magnitude below those seen in Fig. 4-a. Here, load power is the input signal and requested EV power the output. The results of the full EV fleet and the aggregation model

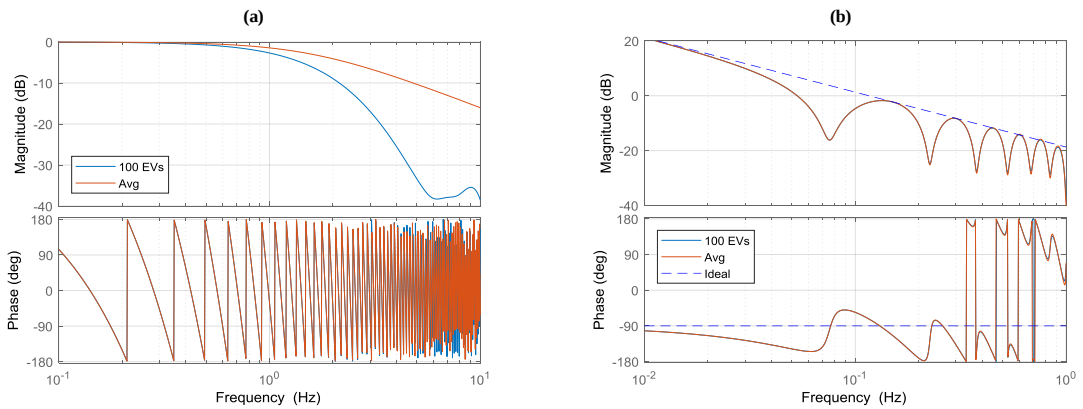

Fig. 4. Bode plot of the EV fleet and the corresponding aggregated *average model* in its open-loop form (a) and within a simulated one-bus system (b). Input is the frequency deviation Δf, output the delivered EV power normalized to their nominal droop gain. The phase is wrapped between ±180 degrees.

are furthermore compared to the response of ideal conventional primary resources with no dynamics of their own, shown by the dotted line in Fig. 4-b. The *average model* performs almost identical to the simulated fleet, rendering it valid for subsequent investigations.

4.3. Stability Investigation

In order to make more generalized statements on stability of primary support using EVs, the impact of the EV share α to the total primary reserve is now investigated. The linearized dynamic system can be written as

$$\dot{x}(t) = A_0 x(t) + A_1 x(t-\tau) \ , \quad \tau \geq 0 \tag{7}$$

with the n states $x \in \mathbb{R}^{n\times 1}$, the system matrices $A_0,\ A_1 \in \mathbb{R}^{n\times n}$ on which the normal and delayed states act, and the delay time τ. Rearranging the strictly proper transfer functions (2)-(4) into the monic form $G(s) = \frac{b_0+b_1 s+\cdots+b_{n-1}s^{n-1}+b_n s^n}{a_0+a_1 s+\cdots+a_{n-1}s^{n-1}+a_n s^n}$ allows their transformation into the canonical state-space observer representation $A_{grid} = 0$, $\boldsymbol{b}_{grid} = b_{grid}$, $A_{CGU} \in \mathbb{R}^{4\times 4}$, $\boldsymbol{b}_{CGU} \in \mathbb{R}^{4\times 1}$ and $A_{EV} = a_{EV}$, $\boldsymbol{b}_{EV} = b_{EV}$. By choosing the state vector $x = \left[\Delta f \ \ \Delta\ddot{P}_{CGU} \ \ \Delta\ddot{P}_{CGU} \ \ \Delta\dot{P}_{CGU} \ \ \Delta P_{CGU} \ \ \Delta P_{EV}\right]^T$, the system matrices of (7) result in

$$A_0 = \begin{bmatrix} 0 & \begin{bmatrix}\mathbf{0} & \mathbf{0} & \mathbf{0} & -b_{grid}\end{bmatrix} & -b_{grid} \\ \boldsymbol{b}_{CGU} & A_{CGU} & \mathbf{0} \\ \mathbf{0} & \mathbf{0} & -a_{EV} \end{bmatrix}, \ A_1 = \begin{bmatrix} \mathbf{0} & \mathbf{0} \\ -b_{EV} & \mathbf{0} \end{bmatrix} \tag{8}$$

Using these system matrices of the instantaneous and delayed states, a frequency sweeping test as described by Theorem 2.1 in [38] is utilized, which allows to find the maximum share of EVs for which the system remains stable independently of the delay. Independence of delay is imperative, as the response of real EVs is non-deterministic and subject to various uncertain factors (battery management, communication systems, charging station electronics, etc.). The three necessary and sufficient conditions of the test are:

1) A_0 is stable (for $\tau \to \infty$);

2) $A_0 + A_1$ is stable (for $\tau \to 0$);

3) $\rho((j\omega I - A_0)^{-1}A_1) < 1, \quad \forall\omega > 0$,

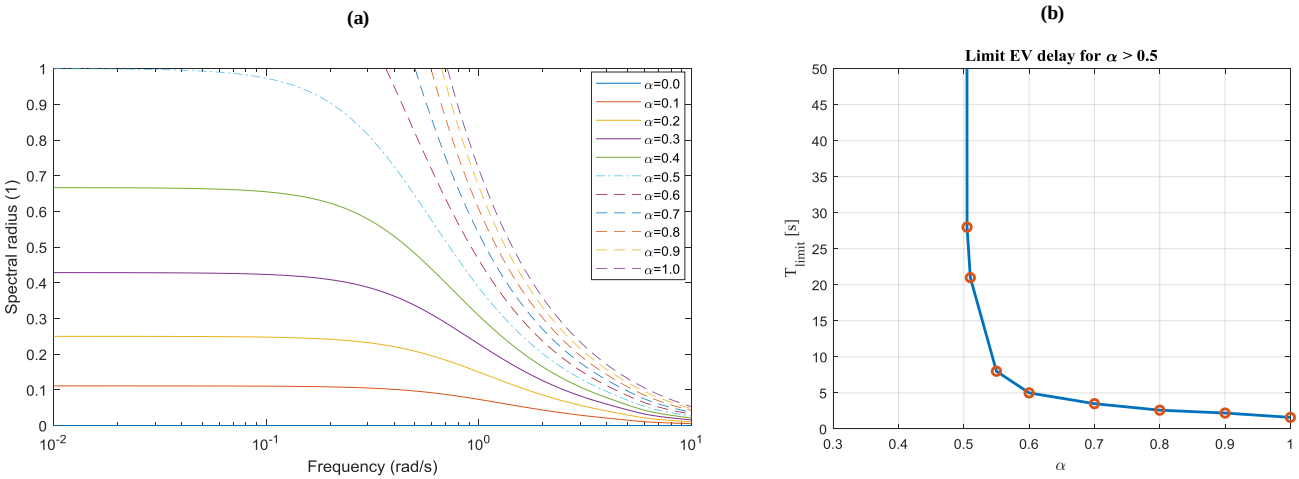

Fig. 5. Frequency sweep of the spectral radius as part of the frequency sweep test (a). (b) shows the Limit EV delay T_{limit} for $\alpha > 0.5$. A clear delay-independency of the stability is graphically confirmed for $\alpha < 0.5$.

with $\rho(\cdot)$ as the spectral radius of a matrix. Conditions 1 and 2 are fulfilled for the given system because the corresponding eigenvalues are in the left half of the complex plane. Condition 3 is evaluated in Fig. 5-a, where we find valid solutions for $\alpha < 0.5$. The system is stable independently of the delayed EV response for EV shares < 50%. It is noted that the results mark the fundamental stability limit of the linearized system. Non-linearities inherent to real systems as well as voltage-related dynamics will generally decrease the available margin. For practical applications with the given EV/Diesel primary reserve mix, it is therefore recommended that the share of EVs stays below 50% (***Recommendation 1***) in order to guarantee stable, EV delay-independent grid operation. For the sake of completeness, Fig. 5-b confirms that only for $\alpha > 0.5$ the stable operation is limited by the critical time delays, which are inversely proportional to the EV share.

In order to take into account the probable reduction of the α limit in case of non-linearities and voltage-dependencies related to more complex systems, a recommendation in terms of maximum time delay is also introduced. In this respect, we hereby propose results from a sensitivity study that allowed the definition of a set of first-order equations, to calculate the maximum acceptable EV delay. It is important to note that the time limits are calculated for a share that is larger than the limit ($\alpha = 0.55$), in order to have delay-dependency of the stability margin. The analysis has been performed for different system parameters that could influence the results: the system inertia *2H*, the primary reserve *droop*, and the index ξ, which

gives an idea of the amount of total primary reserve over the rotating energy $E_{rotating}$ for the n rotating CGUs with installed capacity $P_{n,i}$ that are connected to the system, as defined in Equation (9):

$$\xi = \frac{P_{reserve}}{E_{rotating}} \quad , \quad E_{rotating} = \sum_{i=1}^{n} P_{n,i} 2H_i \ . \tag{9}$$

The influence of the three parameters on the critical EV delay as been assessed for a set of values: $2H$ = {2.4, 3.6, **7.2**, 14.4}, *droop* = {**0.02**, 0.03, 0.04, 0.05, 0.06}, ξ = {0.01, 0.02, **0.03**, 0.04}. The dependency of the time limits on the three parameters is considered almost linear, as deducible also by the example in Fig. 6. The figure shows the dependency on the three parameters and the linear interpolation, performed to derive the three first order equations. So, the outcome of the proposed parametric study allows the identification of the coefficients a_i and b_i for the calculation of the time limit T_{limit}, given the considered system parameters.

$$T_{limit} = \begin{cases} a_k \cdot droop + b_k & with\ a_k, b_k\ function\ of\ (2H, \xi) \\ a_{iner} \cdot 2H + b_{iner} & with\ a_{iner}, b_{iner}\ function\ of\ (droop, \xi) \\ a_\xi \cdot \xi + b_\xi & with\ a_\xi, b_\xi\ function\ of\ (droop, 2H) \end{cases} \tag{10}$$

The resulting coefficients are reported in Tables 2-4, which allow the calculation of the maximum response time of the EVs in order to prevent system instability. Note that the bold values both in the text and in the tables relate to the realistic islanded operation mode of the Bornholm power system, which gives a delay limit of 8 s. So, we hereby deduct the second recommendation (***Recommendation 2***) for a safe and stable primary reserve provision from a fleet of EVs: $\boldsymbol{\tau < T_{limit}/2}$, i.e., operate with a delay smaller than the half of the calculated T_{limit}. 2 is a safety factor, introduced to prevent operating too close to the limit and to take into account possible imperfections in the calculation of T_{limit} given the extrapolation of the coefficients.

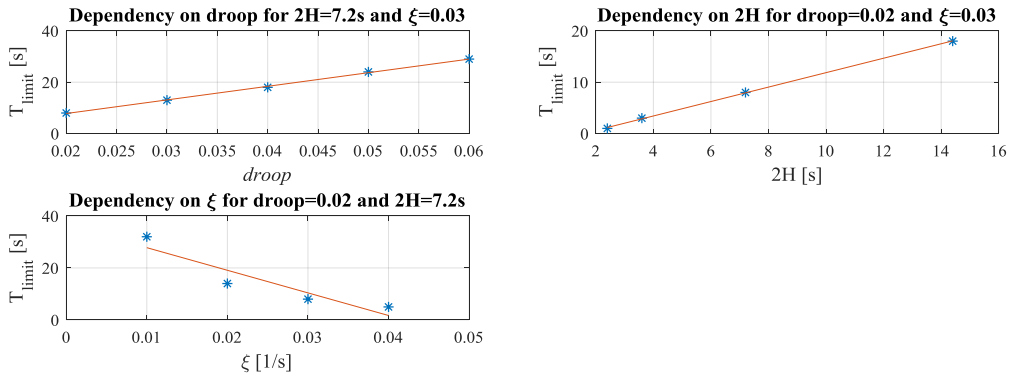

Fig. 6. Dependency of the limit time T_{limit} for different system parameters. It can be noticed that the approximation to a first-order equation for the dependency of the three parameters causes a relatively small error in the calculation of T_{limit}.

TABLE 2. COEFFICIENTS TO CALCULATE T_{LIMIT} AS FUNCTION OF *droop*

		2H [s]			
		2.4	3.6	7.2	14.4
ξ [s^{-1}]	0.01	a = 570 ; b = -2.2	a = 860 ; b = -2.2	a = 1720 ; b = -3	a = 3360 ; b = -2.4
	0.02	a = 270 ; b = -2.4	a = 400 ; b = -2	a = 800 ; b = -2	a = 1710 ; b = -5.4
	0.03	a = 170 ; b = -2.4	a = 250 ; b = -2.2	**a = 530 ; b = -2.8**	a = 1000 ; b = -2
	0.04	a = 111 ; b = -2.12	a = 164 ; b = -1.9	a = 360 ; b = -2.4	a = 720 ; b = -2.8

TABLE 3. COEFFICIENTS TO CALCULATE T_{LIMIT} AS FUNCTION OF THE SYSTEM INERTIA *2H*

		droop				
		0.02	0.03	0.04	0.05	0.06
ξ [s^{-1}]	0.01	a = 4.74 ; b = -2.20	a = 6.89 ; b = -1.29	a = 9.08 ; b = -0.66	a = 11.67 ; b = -1.55	a = 13.96 ; b = -0.81
	0.02	a = 2.24 ; b = -2.20	a = 3.25 ; b = -1.66	a = 4.48 ; b = -2.40	a = 5.74 ; b = -2.88	a = 7.01 ; b = -3.37
	0.03	**a = 1.41 ; b = -2.20**	a = 2.10 ; b = -2.26	a = 2.81 ; b = -2.40	a = 3.31 ; b = -2.23	a = 4.17 ; b = -1.77
	0.04	a = 0.98 ; b = -2.12	a = 1.39 ; b = -2.02	a = 1.98 ; b = -2.40	a = 2.59 ; b = -3.12	a = 2.94 ; b = -2.26

TABLE 4. COEFFICIENTS TO CALCULATE T_{LIMIT} AS FUNCTION OF ξ

		droop				
		0.02	0.03	0.04	0.05	0.06
2H [s]	2.4	a = -281 ; b = 10.35	a = -441 ; b = 17.35	a = -610 ; b = 24	a = -740 ; b = 30	a = 870 ; b = 36.5
	3.6	a = -441 ; b = 17.35	a = -680 ; b = 27.5	a = -870 ; b = 36.5	a = -1100 ; b = 46	a = -1350 ; b = 57
	7.2	**a = -870 ; b = 36.5**	a = -1290 ; b = 55	a = -1710 ; b = 74	a = -2180 ; b = 95	a = -2600 ; b = 113.5
	14.4	a = -1740 ; b = 75	a = -2570 ; b = 111.5	a = -3360 ; b = 148	a = -4280 ; b = 189	a = -5200 ; b = 229

5. Validation on the real Bornholm (DK) Power System

This section presents the validation study carried out on a simulation basis on the Bornholm system. The grid layout along with the load and generation portfolio during islanded operation is presented, and scenarios with a 2040 EV penetration are outlined. Aggregated EVs are modelled according to the *average model*, and the recommendations for preventing instabilities found in Section 4 are implemented. These analyses complete the study, assessing the applicability on a real and complex power system of the recommendations.

5.1. Definition of Scenarios

The investigation is carried out on an islanded configuration of the Bornholm power system, in a probable 2040 scenario with 50% EV penetration, meaning that out of the total 17000 cars on the island, 8500 will be EVs [39]. We consider an evening hour (e.g., between 18:00 and 19:00) when we can realistically assume that 40% of the EVs are charging at home on the 3.7 kW slow charging mode (Mode 2), leading to about 12 MW of total extra load. This is added to the rather high evening load condition assumed to be 48 MW, leading to a total load of 60 MW. Furthermore we assume that a portion of the remaining EVs not charging at home are connected to V2G chargers and are available for grid frequency regulation. Specifically, the V2G-ready EVs could be the 5% of the total EVs, i.e., 450 EVs: considering each vehicle interfaced with a 10 kW bidirectional charger, the total regulation capacity is equal to ±4.5 MW. To make the analysis more realistic the fleet is not considered connected to a single bus of the grid, instead the 450 EVs are connected to the four largest urban areas in the island with the following criteria: 225 EVs are in the capital city of Rønne (*EV fleet #1*), whereas the remaining 225 EVs are equally split over the cities of Hasle, Nexø, and Svaneke, leading to an amount of 75 EVs per city (*EV fleet #2, #3, #4*).

As for the generation portfolio, despite the today operation policy of disconnecting all renewable generation when the systems becomes islanded, we consider that a very high share of renewables is present. In particular, half of the generation (30 MW) coming from wind turbines, whereas no PV production due to the assumption of operating in evening time. The other half of the generation is coming from the two biogas plants (1 MW each), the CHP plant Blok 6 (operating at 8 MW - 50% of full power), and the oil-powered steam turbine Blok 5 (operating at 20 MW - 80% of full power). Furthermore one 4.5 MW diesel unit is considered connected but operating at zero set-point, ready to react in case of frequency disturbances as primary frequency regulator. As the framework of the proposed validation simulation study is the real operating condition during an islanded configuration, some of the CGUs today employed only as back-up units for primary reserve are included. In this configuration the system has a primary frequency control

reserve capacity of 5 MW over 200 mHz from the Blok 5, and additional 4.5 MW which are available either by a dedicated 4.5 MW diesel unit (operating at zero set-point but connected as mere frequency regulation unit upwards), or alternatively by the V2G-capable EV fleet. This means that for the proposed study case the share of EVs participating in the reserve is $\alpha = 0.45$, fulfilling ***Recommendation 1*** presented in the previous section. Both the synchronous units and the V2G EV fleet operate with a relative droop of 2%. In this islanded configuration the system inertia H will be 3.63 s if the diesel is connected, and 3.60 s in case it is not connected. The destabilizing contingency is the loss of a 2 MW wind turbine.

5.2. Results

Fig. 7 shows the effects of EVs replacing the diesel generator with $\alpha = 0.45$ (fulfilling ***Recommendation 1***) in case of different EV delays, with delays normally distributed around 1, 4, 7 and 10 s with standard deviation σ=0.1. In the Section 4 it was found that for this setup a response equal to or faster than 4 s is needed to fulfill ***Recommendation 2***. This is guaranteed in the cases of 1 s and 4 s delay. The 7 s case would fulfill the recommendation only if the safety factor 2 is not be included, whereas the 10 s case is above the requirement.

With a very fast EV response (e.g., 1 s) the fleet can perform well, as the frequency settles to the steady-state value $f_{steady\text{-}state} = 49.65$ Hz even faster than in the case of the diesel. In case of larger delays, frequency stability is compromised: with the EVs responding in 4 s and 7 s, damped oscillations appear, with settling time that increases dramatically in the case of 7 s, which is very close to the limit of 8 s found in Section 4. It can be noticed that the fulfilment of ***Recommendation 2*** including the safety factor 2 guarantees the frequency to settle much faster than in the case of 7 s, justifying the need for the inclusion of the safety factor for safer operations. In case of 10 s delay, the frequency is not damped and stability is lost. At this point it is relevant to highlight the fact that, despite in a simplified system the share $\alpha = 0.5$ would allow any possible EV delay without incurring in instabilities, here the complex dynamics that describe the real power system model's behavior are reducing the stability limits as instability conditions are found for $\alpha = 0.45$ for a 10 s delay. This is due to the fact the implemented Bornholm power system now includes the different dynamics of the CGUs of

the complete generation portfolio along with the models of lines, transformers and loads. This brings along correspondent non-linearities and voltage dependencies that could not be included in the preliminary analysis of Section 4, where a simplified single-bus power system was modelled. This shows the need for the additional requirement in terms of maximum EV time delay (***Recommendation 2***), as the limit of $\alpha = 0.5$ may not be sufficient to guarantee an EV delay-independent system stability in such large and complex systems. This confirms the considerations presented in the previous Section, when it comes to cautionary recommendations, and the inclusion of ***Recommendation 2***, which in addition to ***Recommendation 1*** allows the definition of safe operative conditions with large-scale frequency control via EV fleets replacing CGUs.

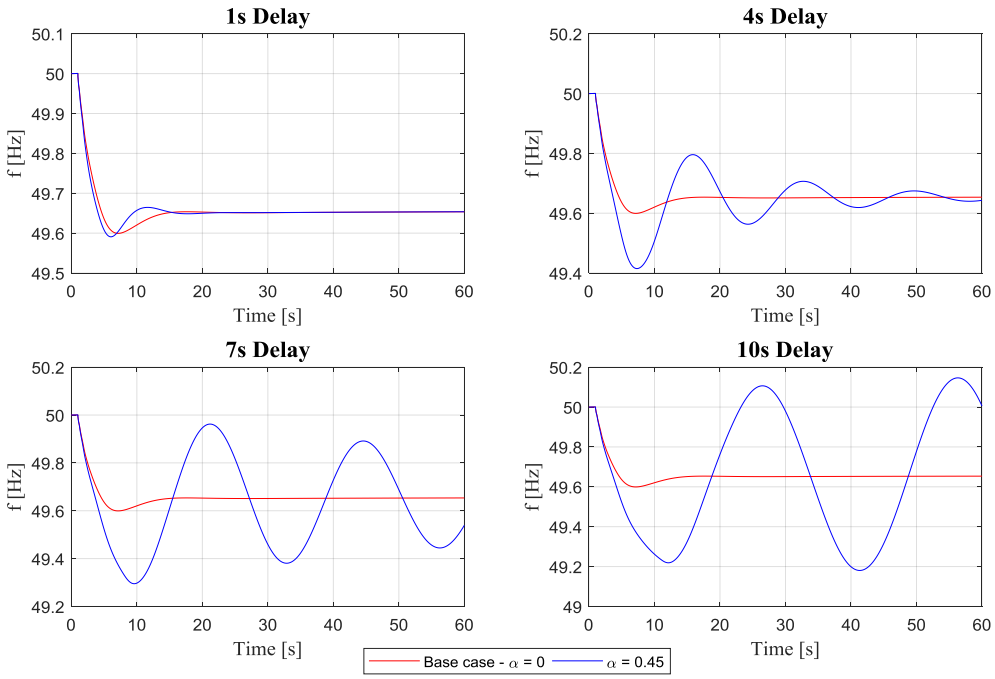

Fig. 7. Power system frequency behavior for $\alpha = 0$ and $\alpha = 0.45$ with increasing EV response times.

The voltage profiles at the connection buses for the different study cases as well as the power exchanges from EV fleets and diesel are reported in Fig. 8 and 9, respectively. It can be noticed that acceptable voltage levels are found at the 4 EV fleets connection buses, as the RMS values of the line-to-ground bus voltages do not exceed the 10% of deviation from the nominal value, as required by the European grid standard EN 50160. As for the provided power, for the $\alpha = 0.45$ cases at steady-state the sum of the powers from the EV fleets corresponds to the reserve that is provided by the diesel unit in the base case scenario with $\alpha = 0$. The power

provided from the EV fleets has negative sign, since they are modelled with the load convention. Moreover, as expected, it can be noticed that *fleet #1* provides triple the power of *fleets #2*, *#3* and *#4*, being the fleet sizes 225, 75, 75 and 75 EVs, respectively.

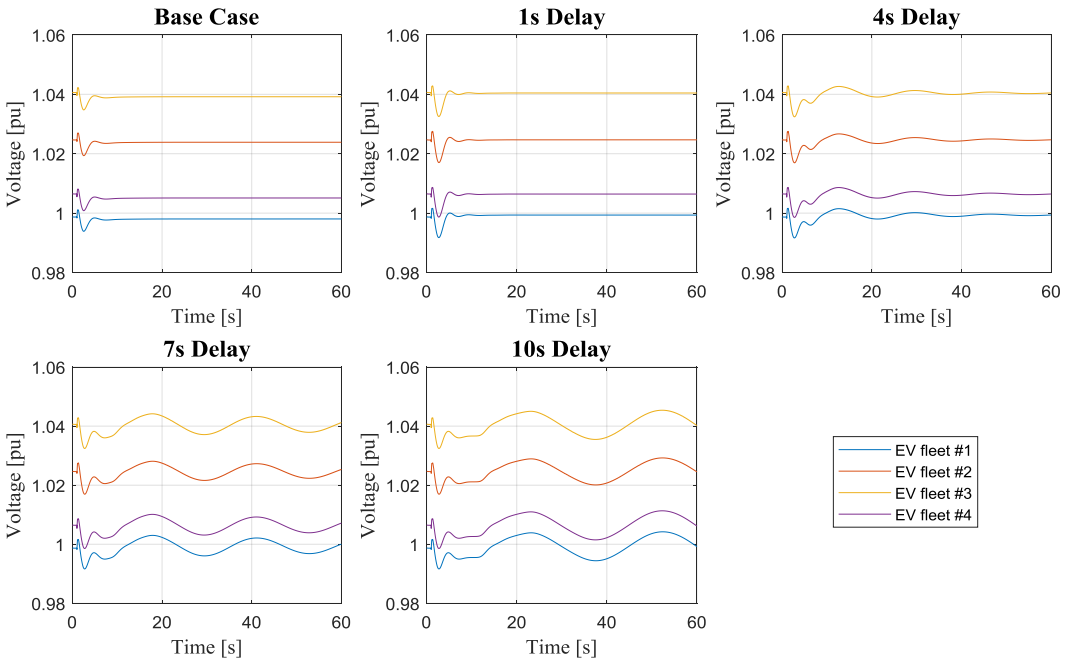

Fig. 8. Line-to-ground voltages at the EV fleet buses.

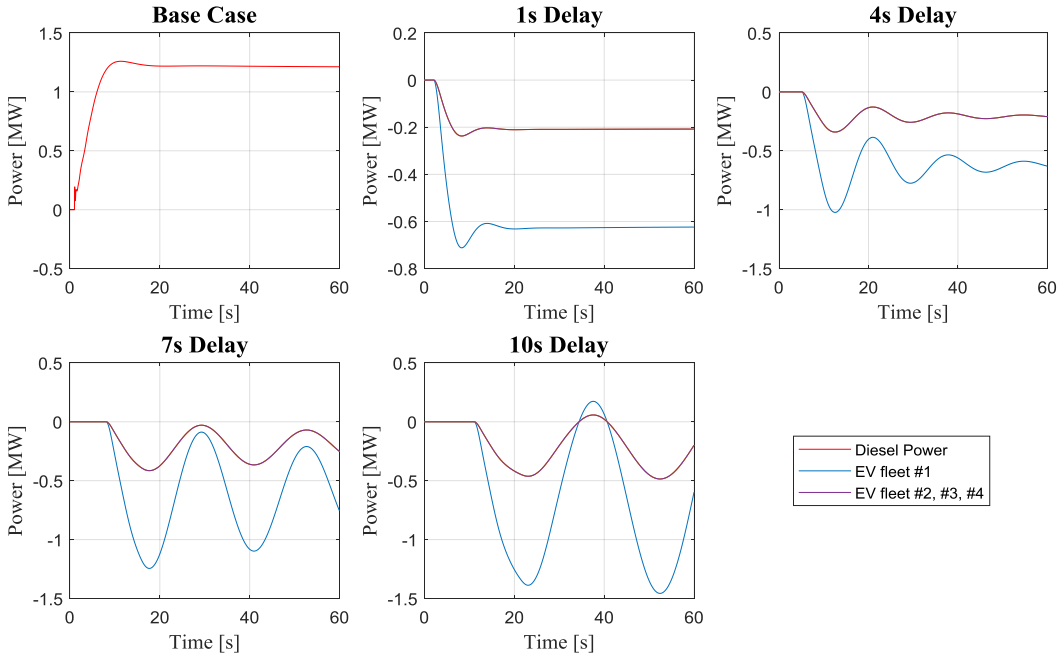

Fig. 9. Power profiles of the Diesel generator in case of $\alpha = 0$, and of the 4 EV fleets in the cases of $\alpha = 0.45$.

6. Discussion and Conclusions

This work investigated the impact of EV fleets providing primary frequency regulation via V2G technology as well as the importance of introducing requirements for large-scale applications. The aim of the paper was to assess the implications of large-scale employment of EV fleets as primary reserve providers given growing activation delays and shares of primary reserve acquired from non-conventional rotating units. An EV fleet model was proposed to emulate the aggregated response of a number of EVs reacting with realistic V2G hardware response times, obtained through laboratory tests. The stability limits when operating a representative power system are investigated to assess the effects of primary frequency control via V2G-capable EV fleets replacing conventional generation units.

The first part of the analysis aimed at defining general recommendations in terms of response time and size of the overall fleet, given the implemented simplified single-bus power system. Two recommendations with conservativeness considerations are derived to guarantee safe and stable operation. Specifically, ***Recommendation 1*** requires to operate with a share of primary reserve from EVs that would not exceed the reserve from conventional rotating units ($\alpha < 0.5$). ***Recommendation 2*** requires response times below the half of a limit value T_{limit} that can be calculated as function of the system inertia, of the total primary reserve over the rotating generation capacity, and of the employed droop gain.

The second part of the study proposes a set of simulations of an islanded configuration with 50% of renewables of the Bornholm power system, with the scope of evaluating the reliability of the proposed recommendations in a system with complex dynamics, non-linearities and voltage dependencies of the units. Results show that only one recommendation was not sufficient: for $\alpha = 0.45$ instability may occur for relatively large EV response times, despite the share below the 0.5 limit. In fact, although the 0.5 limit was valid in the single-bus power system, when non-linearities and detailed power components models come into play the time-independency of the stability for such share may not be valid. This confirmed the need for the inclusion of a recommendation on the EV response time (***Recommendation 2***). Results show that for EV

response times of 1 s and 4 s the stability was assured, whereas for 7 s (very close to the calculated T_{limit} = 8 s), slowly damped oscillations appeared before settling to the steady-state frequency value. On the one hand, this proved the need for the simultaneous fulfilment of the two proposed requirements when including EV fleets as primary reserve providers. On the other hand, these results confirmed that the proposed recommendations can be a valuable tool for defining benchmark limit values to be implemented for subsequent sets of simulation studies in exhaustively modelled power systems.

As a discussion topic, the authors would like to point out that in case relatively large EV share and too slow EV responses, the power system instability conditions may be prevented only if additional counteractions are taken. An example could be the inclusion of a rate limiter able to smooth the aggregated EV response. When implementing a rate limiter the system frequency could be recovered in a safe band around the steady-state value and uncontrolled growing oscillations could be prevented. Nonetheless, the nadir and the settling time would be dramatically influenced by the sensitiveness of the employed limiter, and new slowly damped oscillations around the steady-state frequency may appear. Rate limiters should then be properly tuned and all the eventual introduced effects should be taken into account.

To conclude, the proposed recommendations should be considered as a tool for power system studies to be utilized as a benchmark for further grid analysis in more complete and complex simulation environments. In fact, this was done in the second part of this paper with the detailed implementation of the Bornholm Island power system. However, it is worth mentioning that possible additional precautions could be deployed and included with the aim at assuring safe and reliable operation also for larger EV shares and/or delays. In fact, the authors recognize that in some cases a smooth overall response could be needed, achievable for instance by introducing additional requirements on the whole aggregated EV fleet response. These aspects are being investigated within future works.

Acknowledgements

The authors would like to thank the financial support of the Danish EUDP program for the project 'ACES – Across Continent Electric Vehicle Services'. (Grant EUDP17-I-12499, website: www.aces-bornholm.eu).'

References

[1] E. L. Karfopoulos, K. A. Panourgias, and N. D. Hatziargyriou, "Distributed Coordination of Electric Vehicles providing V2G Regulation Services," *IEEE Transactions on Power Systems*, vol. 31, no. 4, pp. 2834–2846, 2016.

[2] S. Izadkhast, P. Garcia-Gonzalez, and P. Frías, "An Aggregate Model of Plug-In Electric Vehicles for Primary Frequency Control," *IEEE Transactions on Power Systems*, vol. 30, no. 3, pp. 1475–1482, 2015.

[3] C. Ziras, J. Hu, S. You, and H. W. Bindner, "Modelling the aggregated dynamic response of electric vehicles," in *2017 IEEE PES Innovative Smart Grid Technologies Conference Europe (ISGT-Europe)*, 2017, pp. 1–6.

[4] E. Sortomme and K. W. Cheung, "Intelligent Dispatch of Electric Vehicles Performing Vehicle-to-Grid Regulation," in *2012 IEEE International Electric Vehicle Conference*, 2012, pp. 1–6.

[5] C. Peng, J. Zou, and L. Lian, "Dispatching strategies of electric vehicles participating in frequency regulation on power grid: A review," *Renewable and Sustainable Energy Reviews*, vol. 68, no. July 2015, pp. 147–152, 2017.

[6] M. González Vayá and G. Andersson, "Combined Smart-Charging and Frequency Regulation for Fleets of Plug-in Electric Vehicles," in *2013 IEEE Power & Energy Society General Meeting*, 2013, pp. 1–5.

[7] K. Clement-Nyns, E. Haesen, and J. Driesen, "The impact of vehicle-to-grid on the distribution grid," *Electric Power Systems Research*, vol. 81, no. 1, pp. 185–192, 2011.

[8] H. R. Galiveeti, A. K. Goswami, and N. B. Dev Choudhury, "Impact of plug-in electric vehicles and distributed generation on reliability of distribution systems," *Engineering Science and Technology, an International Journal*, vol. 21, no. 1, pp. 50–59, 2018.

[9] Y. Kongjeen and K. Bhumkittipich, "Impact of Plug-in Electric Vehicles Integrated into Power Distribution System Based on Voltage-Dependent Power Flow Analysis," *Energies*, vol. 11, no. 6, p. 1571, 2018.

[10] X. Luo, S. Xia, and K. W. Chan, "A decentralized charging control strategy for plug-in electric vehicles to mitigate wind farm intermittency and enhance frequency regulation," *Journal of Power Sources*, vol. 248, pp. 604–614, Feb. 2014.

[11] H. N. T. Nguyen, C. Zhang, and J. Zhang, "Dynamic Demand Control of Electric Vehicles to Support Power Grid With High Penetration Level of Renewable Energy," *IEEE Transactions on Transportation Electrification*, vol. 2, no. 1, pp. 66–75, 2016.

[12] J. C. Hernández, F. Sanchez-Sutil, P. G. Vidal, and C. Rus-Casas, "Primary frequency control and dynamic grid support for vehicle-to-grid in transmission systems," *International Journal of Electrical Power and Energy Systems*, vol. 100, no. July 2017, pp. 152–166, 2018.

[13] P. M. R. Almeida, F. J. Soares, and J. A. P. Lopes, "Electric vehicles contribution for frequency control with inertial emulation," *Electric Power Systems Research*, vol. 127, pp. 141–150, 2015.

[14] J. Meng, Y. Mu, H. Jia, J. Wu, X. Yu, and B. Qu, "Dynamic frequency response from electric vehicles considering travelling behavior in the Great Britain power system," *Applied Energy*, vol. 162, pp. 966–979, 2016.

[15] J. A. P. Lopes, P. M. R. Almeida, F. J. Soares, and C. L. Moreira, "Electric vehicles in isolated power systems: Conceptual framework and contributions to improve the grid resilience," *IFAC Proceedings Volumes*, vol. 1, no. PART 1, pp. 24–29, 2010.

[16] M. Vahedipour-Dahraie, H. Rashidizaheh-Kermani, H. Najafi, A. Anvari-Moghaddam, and J. Guerrero, "Coordination of EVs Participation for Load Frequency Control in Isolated Microgrids," *Applied Sciences*, vol. 7, no. 6, p. 539, 2017.

[17] K. Knezović, M. Marinelli, A. Zecchino, P. B. Andersen, and C. Træholt, "Supporting involvement of electric vehicles in distribution grids: Lowering the barriers for a proactive integration," *Energy*, 2017.

[18] C. Ziras, A. Zecchino, and M. Marinelli, "Response Accuracy and Tracking Errors with Decentralized Control of Commercial V2G Chargers," in *20th Power Systems Computation Conference (PSCC 2018)*, 2018, pp. 1–7.

[19] J. A. Short, D. G. Infield, and L. L. Freris, "Stabilization of grid frequency through dynamic demand control," *IEEE Transactions on Power Systems*, vol. 22, no. 3, pp. 1284–1293, 2007.

[20] C. Ziras, E. Vrettos, and S. You, "Controllability and stability of primary frequency control from thermostatic loads with delays," *Journal of Modern Power Systems and Clean Energy*, vol. 5, no. 1, pp. 43–54, 2017.

[21] M. R. Vedady Moghadam, R. T. B. Ma, and R. Zhang, "Distributed Frequency Control in Smart Grids via Randomized Demand Response," *IEEE Transactions on Smart Grid*, vol. 5, no. 6, pp. 2798–2809, 2014.

[22] M. R. V. Moghadam, R. Zhang, and R. T. B. Ma, "Distributed Frequency Control via Randomized Response of Electric Vehicles in Power Grid," *IEEE Transactions on Sustainable Energy*, vol. 7, no. 1, pp. 312–324, 2016.

[23] S. Izadkhast, S. Member, P. Garcia-gonzalez, and P. Fr, "Design of Plug-In Electric Vehicle ' s Frequency-Droop Controller for Primary Frequency Control and Performance Assessment," vol. 32, no. 6, pp. 4241–4254, 2017.

[24] M. Rezkalla, A. Zecchino, S. Martinenas, A. M. Prostejovky, and M. Marinelli, "Comparison between Synthetic Inertia and Fast Frequency Containment Control on Single Phase EVs in a Microgrid," *Applied Energy*, 2017.

[25] M. Marinelli, S. Martinenas, K. Knezović, and P. B. Andersen, "Validating a centralized approach to primary frequency control with series-produced electric vehicles," *Journal of Energy Storage*, vol. 7, pp. 63–73, 2016.

[26] "Nissan, enel and nuvve operate world's first fully commercial vehicle-to-grid hub in denmark," 2016. [Online]. Available: http://www.nissan-helsingor.dk/index.php/om-os/nyheder/show/news/id/4. [Accessed: 19-Oct-2018].

[27] "The Parker project," *http://parker-project.com*, 2016. .

[28] M. Marinelli, "The ACES Project - Large-scale Integration of Electric Vehicles into the Electric Power System," *Abstract from Sustain 2018, Denmark*, 2018.

[29] A. Zecchino, A. Thingvad, P. B. Andersen, and M. Marinelli, "Suitability of Commercial V2G CHAdeMO Chargers for Grid Services," in *EVS 31 & EVTeC 2018*, 2018, pp. 1–7.

[30] ENTSO-E, "ENTSO-E, Continental Europe Operation Handbook," 2009.

[31] Energinet.dk, "Danish Technical Standard: ancillary services to be delivered in Denmark - tender conditions," *https://en.energinet.dk/-/media/Energinet/El-RGD/Dokumenter/Ancillary-services-to-be-delivered-in-Denmark.pdf*, 2017. .

[32] J. Østergaard and J. Nielsen, "The Bornholm Power System An Overview," 2008.

[33] Y. Chen, Z. Xu, and J. Østergaard, "Frequency Analysis for Planned Islanding Operation in the Danish Distribution System - Bornholm," *Proceedings of the Universities Power Engineering Conference*, pp. 9–13, 2008.

[34] E. James-Smith and M. Togeby, "Security of Supply of Bornholm - Demand Side Options for System Reserves," 2007.

[35] IEA International Energy Agency, "Nordic EV Outlook 2018," 2018.

[36] P. Kundur, *Power system stability and control*. 1994.

[37] S. R. P. Malik and G. S. Hope, "An adaptive control scheme for speed control of diesel driven power-plants," *IEEE Transactions on Energy Conversion*, vol. 6, no. 4, pp. 605–611, 1991.

[38] K. Gu, J. Chen, and V. Kharitonov, *Stability of Time- Delay Systems*. Secaucus, NJ, USA: Birkhauser Boston, Inc., 2003.

[39] C. Hjalmar, "Danish National Travel Survey," 2017.

Paper H

Title:

Guidelines for Distribution System Operators on Reactive Power Provision by Electric Vehicles in Low Voltage Grids

Authors:

Antonio Zecchino, Mattia Marinelli, Magnus Korpås and Chresten Træholt

Published in:

CIRED - Open Access Proceedings Journal, presented at 24th International Conference on Electricity Distribution (2017)
DOI: 10.1049/oap-cired.2017.0377

GUIDELINES FOR DISTRIBUTION SYSTEM OPERATORS ON REACTIVE POWER PROVISION BY ELECTRIC VEHICLES IN LOW VOLTAGE GRIDS

Antonio ZECCHINO, Mattia MARINELLI,
Chresten TRÆHOLT
Technical University of Denmark – Denmark
{antozec, matm, ctr}@elektro.dtu.dk

Magnus KORPÅS
Norwegian University of Science and Technology – Norway
magnus.korpas@ntnu.no

ABSTRACT

The increasing success of electric vehicles is bringing new technical challenges to power system operators. This work intends to provide guidelines for distribution system operators in terms of reactive power requirements when evaluating and authorizing electric vehicles supply equipment with fast charging capability in existing low voltage distribution feeders. The aim is to prevent the voltage to exceed the permitted values when charging at high power, by exploiting the effect of the reactive power. The proposed guidelines for distribution system operators are reported in a matrix, which indicates the amount of reactive power that an individual electric vehicle is expected to provide when connected to a low voltage feeder, in order to benefit of the desired voltage rise effect in comparison to the case of unitary power factor.

INTRODUCTION

The growing penetration of electric vehicles (EVs) brings new challenges to power system operators. Great research effort is made in smart integration solutions of large amount of EVs in the power system, e.g., smart charging according to market price signals or relying on specific control logics with the aim of making EVs a reliable source of system-wide ancillary services [1], [2]. Within this context, to validate the feasibility of the proposed solutions, the technical capabilities of series-produced EVs in performing smart charging are of high interest [3].
One of the most challenging aspects of the integration of EVs in the power system is their impact on distribution grids [4]. In fact, when connected to electric vehicles supply equipment (EVSE), they behave as large concentrated loads, that may cause technical issues on the electrical infrastructure. Overloading conditions may arise both in distribution transformers and feeders and the power quality may drastically worsen, which is supposed to be assured at standard-compliant levels by distributor system operators (DSOs).
For this reason, many studies have been conducted with the aim to demonstrate the potentials of distributed control for EV charging to solve local voltage issues and allowing high EV penetration to be technically acceptable without the need of investment in additional units for grid reinforcement [4].
In general, voltage support by reactive power provision is seen as one of the most effective solutions to solve local voltage issues in distribution networks [5]. Similarly to the case of small distributed generation plants connected at low voltage levels [6], [7], it is expected that there might by a need for DSOs to require voltage support capability also to the new EVSEs [8], [9].
In this context, for installations of new commercial EVSEs with fast charging capability in existing low voltage (LV) distribution feeders, a certain amount of reactive power needs to be available in order to prevent undesired under-voltages. This work focuses on the potential of reactive power in distribution networks, and provides guidelines for DSOs in a matrix, which indicates the amount of reactive power that an individual EV must be able to provide when charging at high power connected at a LV level. Specifically, the proposed analysis demonstrates that both the MV/LV transformer and the MV grid (unless extremely weak) have marginal influence on the effects of reactive power on the voltage. Moreover, it is also found that the R/X ratio of the LV feeder does not significantly influence the results, whereas a meaningful comparison is instead the absolute values of R and X, i.e., the LV feeder length.
An analytical formulation is proposed and an analysis has been carried out by implementing the equations in MATLAB, The MathWorks, Inc. For a further validation, load flow calculations in the power system simulation tool DIgSILENT PowerFactory have been run.

ELECTRIC VEHICLES AS SUPPORT FOR DITRIBURION NETWORKS

In general, DSOs should be always able to operate their distribution networks assuring standard-compliant levels of power quality. The increasing penetration of small distributed energy resources is making the operation more challenging. For example, unless opting for expensive investments in grid reinforcement, a massive penetration of EVs in distribution networks will force DSOs relying on third party service solutions by smart EV charging.
One of the most straightforward ways of identifying distribution grid services is to associate them with the DSO's needs of optimally operating the grid. Accordingly, correspondent EV charging strategies should be defined depending on the objective set for a particular grid service. The EV charging objectives can

be either technical, economic or a combination of both.
Aiming at achieving technical objectives, the services can generally be divided in two groups depending on the targeted grid constraint, namely services for solving loading issues and services for solving voltage issues. The first group can be further divided into two sub-groups, i.e., congestion prevention and loss reduction. Voltage issues can be solved by regulating the voltage magnitude or by reducing phase-unbalances caused by single-phase connected units.
In this work, the voltage magnitude regulation is investigated. In particular, the use of reactive power for voltage support is analysed. Reactive power can be seen both as a traded flexibility service that the EV owner can offer to the DSO, or it can be seen as an implicit EV charging characteristic. In the latter case, it would be seen as a mere technical capability both for the EV and the EVSE. Within this context, this work highlights the effective contribution of reactive power to local voltage support by EVs connected to typical LV feeders.

REACTIVE POWER MANAGEMENT IN DISTRIBUTION NETWORKS

Local voltage support by reactive power provision is seen as one of the most effective solutions to solve local voltage issues in distribution networks. As low voltage distribution grids are typically characterized by average R/X ratio of 0.5-5, the reactive power has significant effects on the voltage [8], [9].
For residential photovoltaic installations connected to distribution grids voltage regulation by reactive power provision is already required in most of the European countries, where national grid codes require reactive power management. [6], [7]. Similarly, the EV charging process could be performed utilizing a capacitive power factor, i.e., injecting reactive power, with the aim at avoiding under-voltage conditions.
In distribution grids the transversal parameters conductance and susceptance are negligible for LV levels. All the grids with negligible transversal parameters can be represented by an R-L circuit as the one in Fig.1, which shows the single-phase equivalent circuit of a three-phase line, where R_l and X_l are the longitudinal parameters of the distribution line, $\overline{E_1}$ and $\overline{E_2}$ the phase-neutral voltages at the two terminals, and $\overline{\Delta E}$ the voltage drop along the line.
As it can be seen in the phasor diagram in Fig. 2-a, $\overline{E_2}$ is considered as reference, and therefore $\overline{E_1}$ and $\bar{I}$ are shifted by ε and φ, respectively. Note that the sign of the real component of the current I_r indicates whether the EV is

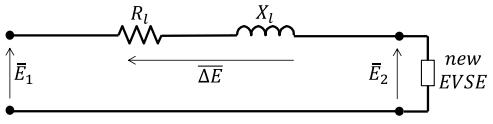

Fig. 1. Single-phase equivalent circuit of a three-phase LV line.

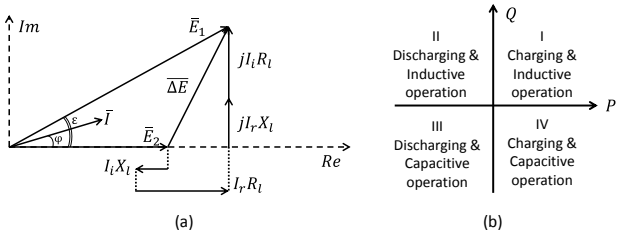

Fig. 2. a: vector diagram. b: 4-quadrant EVSE converter operating scheme.

charging or discharging, corresponding to the I/IV or II/III quadrants of the P-Q 4-quadrant EVSE converter operating scheme of Fig. 2-b. The phase angle φ and therefore the imaginary component I_i, shows if it is exchanging inductive or capacitive reactive power (I/II or III/IV quadrant).
As it can be deduced by the phasor diagram and by the general Eq. (1), by considering I_r and I_i, it is possible to notice how they influence the voltage magnitude $|\overline{E_2}|$, due to the impedance of the line (R_l+jX_l).

$$|\overline{E_2}| = \sqrt{|\overline{E_1}|^2 - |I_iR_l + I_rX_l|^2} - |I_rR_l| + |I_iX_l| \qquad (1)$$

It is clear that the voltage drop due to active current absorption $-I_rR_l$ is partially compensated by the voltage rise due to the reactive current $+I_iX_l$. Thus, in order to support the grid during EV charging, instead of reducing the active charging power and thereby impacting the user comfort, injecting capacitive reactive power can be seen as an attractive alternative, thus operating in the IV quadrant of the EVSE converter charging capabilities in Fig. 2-a.
The main purpose of the proposed analysis is to provide guidelines for DSOs in terms of reactive power provision requirement for new EVSEs installation. Therefore, the determination of the effect of reactive power on the voltage at the end of the line as function of the installed apparent power is of high importance. Eq. (1) has been re-formulated in Eq. (2), which highlights separately the active power P and the reactive power Q. In this way it is possible to calculate the voltage magnitude at the end terminal of a line $|\overline{E_2}|$, given the line parameters, the voltage at the source terminal, and the EV charging power, in terms of P and Q, i.e., in terms of P and power factor cos(φ).

$$|\overline{E_2}| = \sqrt{\frac{1}{2}\left[|\overline{E_1}|^2 + \frac{2}{3}(-PR_l + QX_l) + \sqrt{|\overline{E_1}|^4 + \frac{4}{3}|\overline{E_1}|^2(-PR_l + QX_l) - \frac{4}{9}(QR_l + PX_l)^2}\right]} \qquad (2)$$

METHODOLOGICAL APPROACH

The first part of the investigation aims at evaluating the influence of the MV grid, the MV/LV transformer, and the LV feeder on the effects of reactive power on voltage support. In order to do that, the single-line equivalent circuit in Fig. 3-a was considered, which has been schematized by considering the equivalent single-phase circuit with all the parameters referred to the 0.4 kV LV

level, reported in Fig. 3-b. In the proposed model no other loads are considered in the analysis. Specifically, if the voltage raises a constant-power load would draw less current, thus enhancing the voltage regulation effect determined by reactive power provision. On the other hand, a constant-impedance load would consume more, thus reducing the effectiveness.

Fig. 3-b shows the resistive and inductive components referred to the LV level of MV grid, MV/LV transformer, and LV feeder. These are termed R_{MVgrid} and X_{MVgrid}, R_{trafo} and X_{trafo}, and $R_{LVfeeder}$ and $X_{LVfeeder}$, respectively. Referring to the analysis in the previous Section, the series of the three resistive and inductive components correspond to R_l and X_l of Fig. 1 and Eq. (1) and (2).

Eq. (2) has been implemented, and $|\overline{E_1}|$ set to 1 p.u. as for an ideal voltage source. Anyway, the aim of the study is assessing the voltage difference, thus the findings are still applicable also in other situations (i.e., higher voltages such as 1.05 because of reverse flow, or lower voltages such as 0.95 because of loaded feeders).

Typically, the 10 kV MV grid's characteristics are represented by the short-circuit power S_{sc_MVgrid} and the $R/X_{\_MVgrid}$ ratio. Taking the MV equivalent network of European LV distribution network proposed by Cigrè [10], typical values are 10 MVA and 0.5, respectively. Through calculation of the short-circuit impedance, the resistive and inductive components referred to the LV level R_{MVgrid} and X_{MVgrid} amount to 0.00716 Ω and 0.01431 Ω, respectively.

A typical MV/LV distribution power transformer has been modelled [3]. It is characterized by nominal apparent power S_{n_trafo} of 0.4 MVA, short-circuit voltage $v_{sc\%\_trafo}$ of 4%, and $R/X_{\_trafo}$ ratio of 0.1. R_{trafo} and X_{trafo} amount to 0.00159 Ω and 0.0159 Ω, respectively.

As proposed by Cigrè [10], typical values of the cable resistance and reactance per km are 0.163 and 0.136 Ω/km, respectively ($R/X_{\_LVfeeder}$ ratio of 1.2). A length of 1 km has been chosen, as it is indicated as a typical length for LV feeders in [11]. Therefore, $R_{LVfeeder}$ and $X_{LVfeeder}$ amount to 0.163 Ω and 0.136 Ω, respectively.

Table 1 reports the considered typical values of power system components when modelling LV distribution grids. It also includes the related equivalent resistance and reactance referred to the LV level, with reference to the simplified single-phase equivalent circuit in Fig. 3-b.

Considering installation of new EVSEs with fast-charging capability up to 12 kW, it has been decided to assume a total EV active power demand of 50 kW, which represent a realistic case of 4 new EVSEs.

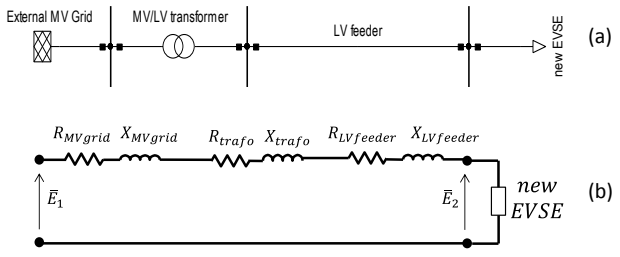

Fig. 3. Single-phase equivalent circuit of the three-phase power system under exam.

In order to evaluate the voltage rise due to reactive power, Eq. (2) has been implemented with power factor cos(φ) equal to 1 and then repeated with capacitive cos(φ) equal to 0.9, and the difference ΔE_2 was evaluated.

Table 1 – Standard parameters for distribution grids

	S_{sc_MVgrid} [MVA]	S_{n_trafo} [MVA]	$v_{sc\%\_trafo}$ [%]	R/X	R referred to LV level [Ω]	X referred to LV level [Ω]
MV grid	10	-	-	0.5	0.00716	0.01431
MV/LV trafo	-	0.4	4	0.1	0.00159	0.0159
LV feeder	-	-	-	1.2	0.163	0.136

Considering the calculated constant values of the series resistive and reactive components of the circuit in Fig. 3-b, a preliminary analysis of the influence of the three single components on the effects of reactive power is now presented. In case of unitary and capacitive power factor equal to 0.9, E_2 resulted in 0.9673 and 0.9415 p.u., respectively. It is clear that the difference ΔE_2 (0.0258 p.u.) represents the voltage rise due to the reactive power injected by the EVs at the ending terminal of the line. The resulting ΔE_2 is obtained from all the three modelled components. Specifically, the MV grid contributed 8.5%, the transformer 9.4%, while the LV feeder contributed 82.1%, as illustrated schematically in Fig. 4.

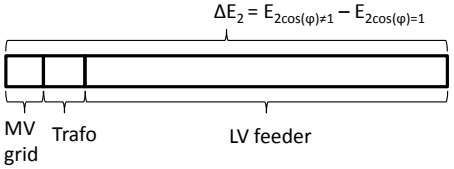

Fig. 4. Contribution to the reactive power effect on the voltage at the end of the line for each component.

It is therefore found that the effect of the reactive power on the local voltage depends mainly on the characteristics of the LV feeder. This result was obtained considering one possible combination of typical distribution network components. Thus, it is of interest to see how different values of these components may impact the result. In this regards, the next part of the investigation aims at evaluating the influence of the MV grid, the MV/LV transformer, and the LV feeder parameters on the effects of reactive power on the voltage.

Influence of the MV grid

The influence of the external MV grid was evaluated by calculating ΔE_2 first for different short-circuit powers S_{sc_MVgrid} (1-10 MVA) and then for different $R/X_{\_MVgrid}$ (0.05-0.5), keeping constant the typical parameters of transformer and LV feeder of Table 1.

Fig. 5-a shows that the trend of ΔE_2 is influenced by the stiffness of the external MV grid, keeping, as in [10], the constant value of 0.5 for $R/X_{\_MVgrid}$. In particular, it is found that for very weak grids, results differ from the

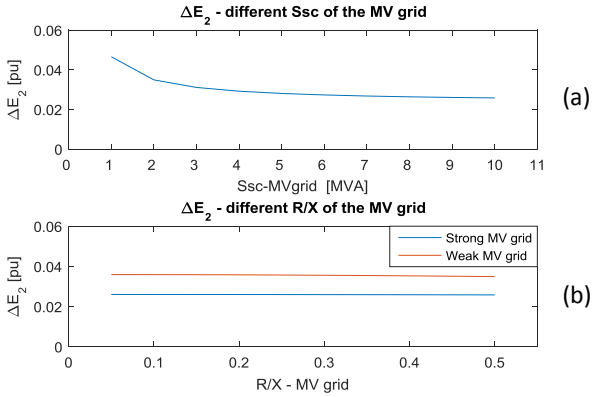

Fig. 5. Influence of MV grid.

case of strong ones. Therefore, it was decided to carry out all the studies hereafter by considering always the comparison of two kinds of MV grid: a weak grid (S_{sc_MVgrid}=2MVA) and a strong grid (S_{sc_MVgrid}=10MVA). Fig. 5-b shows that, for both the compared MV grids, the effect of reactive power on the ending terminal voltage is constant for all the considered $R/X_{\_MVgrid}$ ratios. For this reason, hereafter the constant value of 0.5 for $R/X_{\_MVgrid}$ was used.

Influence of the distribution MV/LV transformer

The influence of the distribution MV/LV transformer has been evaluated by calculating ΔE_2 for different nominal apparent powers S_{n_trafo} (0.1-1 MVA), keeping constant the typical parameters of $v_{sc\%\_trafo}$, $R/X_{\_trafo}$ and LV feeder reported in Table 1. As motivated before, the analysis is done both for weak and strong MV grid.

Fig. 6 shows that the influence of the distribution transformer on the effect of reactive power is marginal for $S_{n\_trafo} \geq 0.2$ MVA, while for very small sizes ($S_{n\_trafo} < 0.2$ MVA), the contribution becomes noticeable. As the grid model considers a LV feeder at the secondary side of the transformer, it is to be expected that in addition to the new EVSEs at the line end, distributed loads may be connected along the feeder. Thus, as in this study a realistic case of new EVSEs installation for a total of 50 kW is considered, a minimum size of 0.2 MVA is to be considered for the transformer.

For this reason, hereafter the typical values of the MV/LV transformer reported in Table 1 have been considered and kept constant, as its influence on the effect of the reactive power is considered marginal.

Influence of the LV feeder

The influence of the LV feeder has been evaluated by calculating ΔE_2 first for different $R/X_{\_LVfeeder}$ and then for

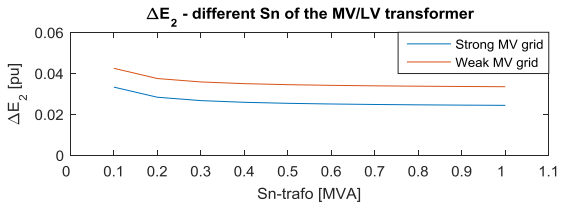

Fig. 6. Influence of the MV/LV transformer.

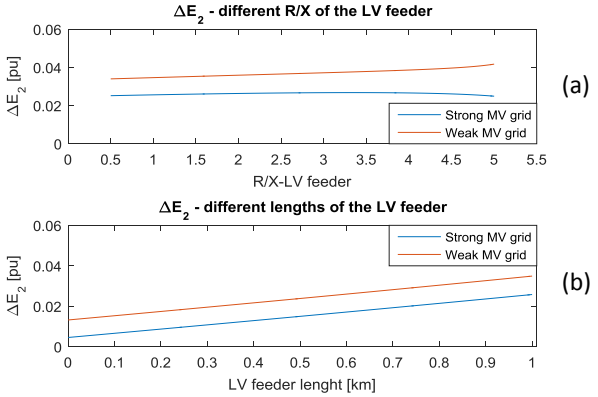

Fig. 7. Influence of the LV feeder

different lengths, considering both weak and strong MV grid, and the MV/LV transformer from Table 1.

Since it is known that the reactance per km is usually constant for different kinds of cables, for the first case different $R/X_{\_LVfeeder}$ have been obtained by varying the value of the resistive component (0.07-0.7 Ω/km), i.e., by considering different sections of the cable conductors, keeping the length equal to 1 km [11]. For the case of different lengths (0-1 km), the values per km reported in Table 1 were used and kept constant.

Fig. 7-a shows that for different $R/X_{\_LVfeeder}$, ΔE_2 results relatively constant, while from Fig. 7-b it is possible to deduce that the main influence is given by the absolute values of $R_{LVfeeder}$ and $X_{LVfeeder}$, i.e., by the length.

Voltage rise as function of cos(φ) and length

As demonstrated, the main influence on the voltage from reactive power provided by charging EVs is determined by the absolute values of the LV feeder impedance. Furthermore, it is clear that ΔE_2 depends on the amount of the capacitive reactive power provided by the EV, i.e., on the power factor cos(φ) set by the EVSE. For these reasons, with reference to Eq. (2), the last formulation proposed in this work considers ΔE_2 as function of the LV feeder length (varied again between 0 and 1 km) and the cos(φ), varied between 0.9 and 1.

Fig. 8 reports the results of the analysis by means of a 3D plot for the calculated ΔE_2 in case of both weak MV grid (top surface) and strong MV grid (bottom surface).

Table 2 presents numerical results for the case of the strong MV grid, i.e., the most common one.

Table 2 – ΔE_2 for different cos(φ)/length combinations

		cos(φ)					
		1	**0.98**	**0.96**	**0.94**	**0.92**	**0.9**
Length [km]	**0.2**	0	0.0037	0.0053	0.0066	0.0077	0.0087
	0.4	0	0.0055	0.0078	0.0097	0.0114	0.0129
	0.6	0	0.0073	0.0104	0.0129	0.0151	0.0171
	0.8	0	0.0092	0.0131	0.0162	0.0189	0.0214
	1.0	0	0.0111	0.0158	0.0195	0.0228	0.0258

As expected, the effectiveness of the reactive power on the voltage support is increasing with decreasing power factor, up to the maximum value of 0.0258 p.u. for standard LV feeder length of 1 km, for strong MV grid. Moreover, it is noticeable that for any given cos(φ)

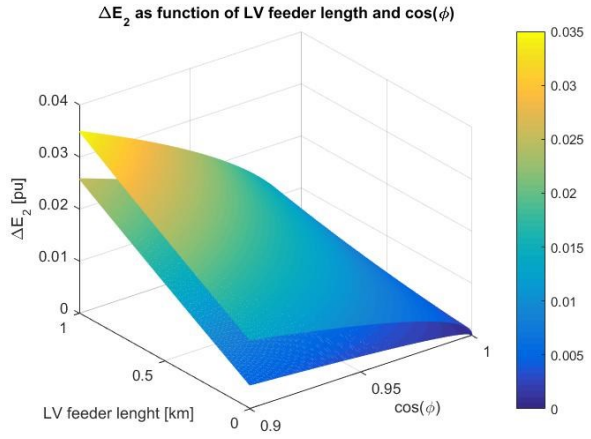

Fig. 8. Voltage rise effect of the reactive power provided by EVs as function of the LV feeder length.

provided by the EV charging, the effects are linearly dependent on the absolute value of the LV feeder impedance, as previously reported in Fig. 7-b for the case of cos(φ) of 0.9.

CONCLUSIONS AND FUTURE WORKS

Due to expected self-induced under-voltage conditions caused by the EV charging, new fast charging EVSEs may be reluctantly allowed by the local grid operator. In order to permit installation without the need of expensive grid reinforcement, capacitive reactive power is an effective mean to reduce under-voltages. The aim of the proposed work was to analyse the potentials of reactive power provision by EVs on voltage support, depending on the grid characteristics.

A simplified distribution grid layout was considered, composed by an external MV grid, a MV/LV distribution transformer, and a single radial LV feeder. Considering multiple values of the parameters of the modelled components, it was found that the effect of the capacitive reactive power is influenced only by the stiffness of the external MV grid and by the absolute values of the LV feeder impedance. Specifically, it was found that the R/X ratio of the LV feeder did not significantly influence the results, while its absolute impedance was crucial. Since the LV cable reactance per km is substantially constant for most cross sections, the variety of the absolute values was obtained by considering different cable lengths.

In conclusion, the main outcome of the paper is the numerical assessment of the voltage rise due to the application of a particular power factor by the fast charger while charging, given as input the EVSE installed power and the LV feeder length. In this way, DSOs can clearly evaluate the effect of the reactive power for any of their LV feeders when the power absorbed by EVs chargers would cause unacceptable under-voltages.

It is important to state that injecting reactive power might have different effects depending on the load distribution and its nature. In fact, in case of constant-power loads, raising the voltage means reducing the active part of the current, while in case of constant-impedance loads, the consumption would increase, with the risk of experiencing overloading conditions or of increased grid losses. For this reason, the authors recognize that, case by case, additional analyses are needed to evaluate the potential drawbacks of such a solution. The proposed method is to be seen as a preliminary measure for DSOs when evaluating new EVSE installations.

Future work should cover the complete analysis of the problem, modelling a realistic and more complex distribution grid. In fact the effect on cable/transformer loading and line losses of unbalanced loads along with their voltage dependency need to be investigated.

REFERENCES

[1] S. Izadkhast, P. Garcia-Gonzalez, and P. Frias, 2015, “An Aggregate Model of Plug-In Electric Vehicles for Primary Frequency Control,” *IEEE Transactions on Power Systems*, vol. 30, no. 3, 1475–1482.

[2] A. Zecchino, M. Rezkalla, and M. Marinelli, 2016, “Grid Frequency Support by Single-Phase Electric Vehicles : Fast Primary Control Enhanced by a Stabilizer Algorithm,” in *2016 Universities Power Engineering Conference (UPEC)*, 1–6.

[3] K. Knezović, S. Martinenas, P. B. Andersen, A. Zecchino, and M. Marinelli, “Enhancing the Role of Electric Vehicles in the Power Grid : Field Validation of Multiple Ancillary Services,” *IEEE Transactions on Transportation Electrification*, vol. 99, 1–9.

[4] K. Clement-Nyns, E. Haesen, and J. Driesen, 2011, “The impact of vehicle-to-grid on the distribution grid,” *Electric Power Systems Research*, vol. 81, no. 1, 185–192.

[5] A. Kechroud, P. F. Ribeiro, and W. L. Kling, 2014, “Distributed generation support for voltage regulation: An adaptive approach,” *Electric Power Systems Research*, vol. 107, 213–220.

[6] “Italian Technical Standard CEI 0-21”, 2012.

[7] “German Technical Standard VDE-AR-N 4105”, 2011.

[8] K. Knezović and M. Marinelli, 2016, “Phase-wise enhanced voltage support from electric vehicles in a Danish low-voltage distribution grid,” vol. 140, 274–283.

[9] N. Leemput, F. Geth, J. Van Roy, J. Büscher, and J. Driesen, 2015, “Reactive power support in residential LV distribution grids through electric vehicle charging,” *Sustainable Energy, Grids and Networks*, vol. 3, 24–35.

[10] K. Strunz, 2009 “CIGRE Task Force C6.04.02 - Benchmark Systems for Network Integration of Renewable and Distributed Energy Resources,”.

[11] L. Felix, K. Serdar, R. S. Raul, 2014, “COTEVOS-Specification of reference electricity networks,” .

Paper I

Title:

Analytical Assessment of Voltage Support via Reactive Power from new Electric Vehicles Supply Equipment in Radial Distribution Grids with Voltage-Dependent Loads

Authors:

Antonio Zecchino and Mattia Marinelli

Published in:

International Journal of Electrical Power & Energy Systems (2018)
DOI: doi.org/10.1016/j.ijepes.2017.10.034

Analytical Assessment of Voltage Support via Reactive Power from New Electric Vehicles Supply Equipment in Radial Distribution Grids with Voltage-Dependent Loads

Antonio Zecchino[a], Mattia Marinelli[*a]

[a]Center for Electric Power and Energy, Technical University of Denmark,
DTU Risø Campus, Frederiksborgvej 399, 4000 Roskilde, Denmark.

Abstract

Grid operators have to cope with secure electric vehicles integration in the power system, which may lead to violations of the allowed voltage band. This work intends to provide an analytical assessment and guidelines for distribution system operators when evaluating new electric vehicle supply equipment installations with fast charging capability in existing low voltage distribution feeders. The aim is to prevent the voltage to exceed the permitted values when charging at high power, by exploiting the effect of reactive power. The contribution of each power component in distribution grids is analyzed, including the loads' voltage-dependency, which influences the effectiveness of reactive power control. The proposed guidelines indicate the amount of capacitive reactive power that an individual electric vehicle supply equipment is expected to provide, in order to effectively manage the voltage rise. The proposed method is validated on the Cigrè benchmark low voltage distribution network as well as on a real Danish low voltage grid.

Keywords: Distribution Grid, Electric Vehicle, Electric Vehicle Supply Equipment, Reactive Power, Voltage Support.

*Corresponding author: Tel: 0045 20124369, Email: matm@elektro.dtu.dk

List of symbols

$\overline{\mathrm{E}_1}$	Phase-neutral voltage phasor at the starting terminal of the line
$\overline{\mathrm{E}_2}$	Phase-neutral voltage phasor at the ending terminal of the line
E_1	Phase-neutral voltage magnitude at the starting terminal of the line
E_2	Phase-neutral voltage magnitude at the ending terminal of the line
$\overline{\Delta E}$	Complex voltage drop along the generic distribution line
R_l	Resistance of the generic distribution line
X_l	Reactance of the generic distribution line
P	Total active power absorbed by the customer
Q	Total reactive power absorbed by the customer
$\overline{I}$	Phasor current flowing along the line
I_r	Real component of the current flowing along the line
I_i	Imaginary component of the current flowing along the line
$a_0,\ a_1,\ a_2,\ b_0,\ b_1,\ b_2$	Load voltage dependence modelling coefficients
P_{EV}	Electric vehicle active power
Q_{EV}	Electric vehicle reactive power
P_{load}	Load active power
Q_{load}	Load reactive power
P_{load_0}	Load active power at nominal voltage condition
Q_{load_0}	Load reactive power at nominal voltage condition
$\cos\varphi_{EV}$	Power factor of the charging electric vehicle
$\cos\varphi_{load}$	Power factor of the load
S_{sc_grid}	External grid short-circuit power
R_{grid}	External grid resistance referred to the low voltage level
X_{grid}	External grid reactance referred to the low voltage level

R/X_{grid}	Resistance over reactance ratio of the transformer
S_{n_trafo}	Transformer nominal power
S_{sc_trafo}	Transformer short-circuit power
Z_{sc_trafo}	Transformer short-circuit impedance
$v_{sc\%\_trafo}$	Transformer short-circuit voltage
R_{trafo}	Transformer resistance referred to the low voltage level
X_{trafo}	Transformer reactance referred to the low voltage level
R/X_{trafo}	Resistance over reactance ratio of the transformer
$R_{LVfeeder}$	Low voltage feeder resistance
$X_{LVfeeder}$	Low voltage feeder reactance
$R/X_{LVfeeder}$	Resistance over reactance ratio of the low voltage feeder

1. Introduction

The increasing success of electric vehicles (EVs) is bringing new challenges to power system operators. On the one hand, great research effort is made on smart integration solutions of large amount of EVs in the power system, such as aggregation strategies for smart EV charging aim at making EVs a reliable source of system-wide ancillary services [1–3]. On the other hand, to evaluate the practical feasibility of such solutions, the technical capabilities of series-produced EVs in performing smart charging are of high interest too [4,5]. However, since mostly connected at a low voltage (LV) level, one of the most challenging aspects of the integration of EVs in the power system is the impact on distribution grids [6,7].

Distribution system operators (DSOs) should be always able to operate their distribution networks assuring standard-compliant levels of power quality, according to the European technical standard EN 50160 [8]. When connected to electric vehicles supply equipment (EVSE), EVs behave as large concentrated loads. Thus, they may cause technical issues on the electrical infrastructure, such as overloading conditions both in distribution transformers and feeders and drastic power quality worsening. Unless opting for grid reinforcement solutions, a

massive penetration of EVs in distribution networks may force DSOs to rely on smart EV charging.

In general, reactive power provision can – to a certain extent – mitigate local voltage issues in distribution networks [9]. In case of small distributed generation plants connected at low voltage levels such as photovoltaics (PVs), grid technical standards require reactive power capability to the inverter-interfaced units [10–12]. Many studies have proved the effectiveness of such capabilities in voltage support in active distribution networks [13,14]. Similarly, it is expected that there might by a need for DSOs to require voltage support capability also to the new EVSEs.

Under a technical feasibility point of view, many studies propose new on-board chargers design and investigate the barriers within the power electronics in applying reactive power solutions [15–17]. Among others, [17] presents an analysis of the technical performance of a conventional unidirectional on-board charger during bidirectional four-quadrant operation, showing how reactive power exchange could be achieved without any considerable changes in the converter type and size. Furthermore, many other studies deal with the development of off-board chargers capable of reactive power operation, showing possible designs and layouts of such technologies [18,19]. Hence, given the mentioned concrete technical feasibility, it is of paramount interest to perform assessment studies upon the effective contribution of such reactive power voltage regulation strategies by charging EVs.

Among other possible control techniques, many reactive power control strategies based on solution of optimization problems are proposed in the literature, both with centralized and decentralized control structure. In general, centralized control approaches for this kind of voltage regulation at LV distribution level [20,21] may result in huge amount of data that need to be transported from smart meters to a centralized control room for the elaboration of the proper control signal to be dispatched back to the units. Therefore, in many volt-VAR optimization works it is preferred to rely on decentralized logics, avoiding the need for complex data management [22–25].

Independently on the control logic applied, many other studies have been conducted with the aim to demonstrate the potentials of distributed EV chargers control to solve local voltage issues and allowing high EV penetration to be technically acceptable, deferring the need for grid reinforcement [26–30]. In [26] and [27] the

positive effects of reactive power support by EVs applying voltage-dependent reactive power strategies is analyzed. An implementation of a bi-directional EVSE controller is developed in [28], which proposes a control logic able to regulate the bus voltage by exchanging reactive power, while maintaining a given DC-link voltage for the designed charging station. In [29] an example of the impact in the power grid is evaluated by implementing different reactive power control logics such as fixed power factor, power factor as function of either active power or local voltage, and an hysteresis control. An innovative reactive power capability curve as function of both active power and local voltage is proposed in [30], where EVs are considered to be single-phase connected, thus unbalance conditions are evaluated.

The above-listed works do present the positive effects on local voltage by reactive power provision from EVs; however, all these study cases are validated in single distribution grids. As the effectiveness of such controllers depends on the electrical characteristics of the power system, it is of high interest to evaluate their influence in different grid cases. In this respect, in [31] the effectiveness of reactive power control from PV inverters is evaluated with respect to different R/X grid characteristic, and it is shown how, depending on the grid characteristics, over-voltages can be reduced.

Similarly, it is expected that for installations of new commercial EVSEs with fast charging capability in existing LV distribution feeders, the reactive power needed to prevent undesired under-voltages depends on the grid characteristic. Within this context, in [32] we have investigated the influence of the single distribution grid components on the reactive power effect. Specifically, the proposed analysis demonstrates that both the MV/LV transformer and the MV grid (unless extremely weak) have marginal influence on the effects of reactive power on the voltage. Moreover, it is also found that the R/X ratio of the LV feeder does not significantly influence the results, whereas an important role is played by the absolute values of R and X, i.e., the LV feeder length. In this work we aim at extending and enhancing the investigation proposed in [32], by including the voltage-dependency of the loads in the analytical formulation, as well as carrying out a validation on different grids. The reactive power effects on the local voltage are evaluated in case of different load models in terms of inductive power factor as well as voltage-dependent behaviour.

So, the identified research questions we are trying to answer with these contributions are: *how much is it*

possible to exploit the potential flexibility of EV fast chargers in providing reactive power for voltage control in LV distribution grids? Which guidelines can be given to DSOs in terms of the amount of reactive power that an individual EV must be able to provide?

The novelty lies on the provision of such guidelines for DSOs, applicable to different types of customers, e.g., residential, commercial, and industrial. The proposed method is to be seen as an assessment criterion when DSOs have to evaluate requests for installation of new EV fast chargers in LV networks. The proposed analytical formulation has been validated by implementing equations in MATLAB. The further validation has been carried out by running load flow calculations in the power system simulation tool DIgSILENT PowerFactory on the LV Cigrè residential radial benchmark [33], as well as on a real Danish LV distribution network previously utilized for other EV integration-related studies [30].

The paper is structured as follows. Section 2 presents the analytical formulation for assessing reactive power effects in distribution grids. Section 3 outlines the methodology to evaluate the contribution of the single power system components. In Section 4 a detailed sensitivity analysis including the load models is presented. Section 5 reports the validation of the proposed methodology. Conclusions are reported in Section 6.

2. Voltage Drop Assessment in Distribution Grids

Although reactive power management for voltage support has major effects at HV/MV levels due to low R/X ratios (0.1-0.2), in LV distribution networks (average R/X ratio of 0.5-5) it is anyway seen as a feasible mean to maintain voltages within the allowed limits of ±10% of the nominal value [8]. In fact, the operation of modern distribution grids is challenged by the increasing penetration of renewable energy resources as well as new electrical loads, such as EVs [26,30]. For instance, in most of the European countries for residential PV installations connected to LV distribution grids, voltage regulation by reactive power provision is already required [10–12]. Similarly, the EV charging process could be performed by utilizing a capacitive power factor, i.e., injecting reactive power, to avoid under-voltages.

In distribution grids the transversal parameters conductance and susceptance are negligible for LV levels. All the grids with negligible transversal parameters can be represented by an R-L circuit as the one in Fig.1, which shows the single-phase equivalent circuit of a balanced three-phase line, where R_l and X_l are the longitudinal

parameters of the distribution line, $\overline{E_1}$ and $\overline{E_2}$ the phase-neutral voltages at the two terminals, and $\overline{\Delta E}$ the voltage drop along the line. The assumption of a balanced three-phase system is motivated by the fact that the new fast-charger has a three-phase connection, thus not introducing any additional unbalance components, such as the one utilized in the field trial mentioned in [34].

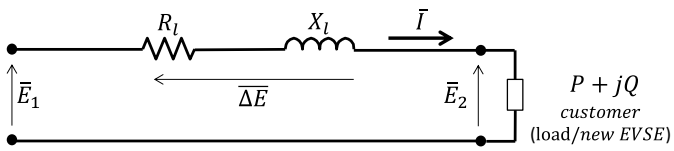

Fig. 1. Single-phase equivalent circuit of a three-phase LV line.

The apparent power absorbed by the customer at the end of the line $\overline{S}$, can be expressed as in Equation (1), where $\overline{I}^*$ is the conjugate of the drawn complex current.

$$\overline{S} = 3\overline{E_2} * \overline{I}^* = P + jQ \tag{1}$$

From (1) it is possible to obtain $\overline{I}$ as function of the voltage $\overline{E_2}$ (taken as reference), and of the real and imaginary components of $\overline{S}$, i.e., P and Q, respectively. This formulation is reported in Equation (2).

$$\overline{I} = \left(\frac{\overline{S}}{3\overline{E_2}}\right)^* = \frac{\overline{S}^*}{3\overline{E_2}^*} = \frac{(P+jQ)^*}{3E_2} = \frac{P-jQ}{3E_2} \tag{2}$$

Equation (3) reports the complex phasor $\overline{I}$, whose real and imaginary components I_r and I_i are made explicit in Equations (4) and (5).

$$\overline{I} = I_r + jI_i \tag{3}$$

$$I_r = \frac{P}{3E_2} \tag{4}$$

$$I_i = \frac{-Q}{3E_2} \tag{5}$$

Note that the sign of the real component of the current I_r indicates whether the customer is absorbing or injecting power. In case of an EV, this means it is charging or discharging, corresponding to the I/IV or II/III quadrants of the P-Q 4-quadrant EVSE converter operating scheme of Fig. 2. The phase angle φ and therefore the imaginary component I_i, shows if the customer is exchanging inductive (positive) or capacitive (negative)

reactive power, which corresponds to the I/II or the III/IV quadrant, respectively. As it can be seen in the phasor diagram in Fig. 3, $\overline{E_2}$ is considered as reference, and therefore $\overline{E_1}$ and $\bar{I}$ are shifted by ε and φ, respectively.

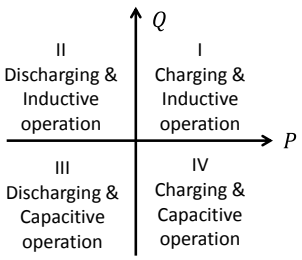

Fig. 2. 4-quadrant EVSE converter operating scheme (load convention).

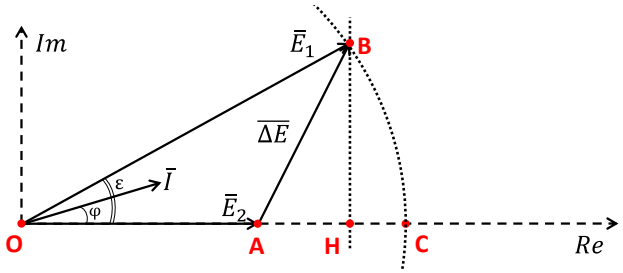

Fig. 3. Vector diagram.

The complex voltage at the starting terminal of the line $\overline{E_1}$ is equal to $\overline{E_2}$ with the addition of the complex voltage drop along the line $\overline{\Delta E}$, as in Equation (6). $\overline{\Delta E}$ is the complex product of current $\bar{I}$, which can be written as in (2), and the line impedance $\overline{Z_l}$, which can be written as $(R_l + jX_l)$.

$$\overline{E_1} = \overline{E_2} + \overline{\Delta E} = \overline{E_2} + \bar{I} * \overline{Z_l} = E_2 + \frac{P - jQ}{3E_2} * (R_l + jX_l) = \left(E_2 + \frac{PR_l + QX_l}{3E_2}\right) + j\left(\frac{PX_l - QR_l}{3E_2}\right) \quad (6)$$

From Equation (6), the voltage magnitude E_1 and angle ε at the starting bus can be derived as in Equations (7) and (8), respectively [35].

$$\left|\overline{E_1}\right| = E_1 = \left[\left(Re\left(\overline{E_1}\right)\right)^2 + \left(Im\left(\overline{E_1}\right)\right)^2\right]^{0.5} = \left[{E_2}^2 + \frac{2}{3}(PR_l + QX_l) + \frac{(P^2+Q^2)({R_l}^2+{X_l}^2)}{9{E_2}^2}\right]^{0.5} \quad (7)$$

$$\varepsilon = \tan^{-1}\left[\frac{Im\left(\overline{E_1}\right)}{Re\left(\overline{E_1}\right)}\right] \quad (8)$$

In the proposed analytical assessment the module of E_1 (i.e., the length *OB* of Fig. 3) is set to a particular value independently of its angle ε, which is thus not included in the final formulation. In fact, the proposed formulation enables us to estimate the actual magnitude of the voltage E_2 independently from its shift over E_1. In

comparison to the traditional way of simplifying the formulation by neglecting the imaginary part of (6) (thus considering only the projection of E_1 on the real axis, i.e., *OH*), this formulation takes into account the entire magnitude of the vector E_1, i.e., *OB*=*OC*. Although it still differs from the traditional exact complex estimation of the line voltage drop, crucial when assessing grid losses, still it represents a precise way for estimating the impact on the local voltage of new EVSEs installations.

By combining Equations (2) and (7), and with reference to the phasor diagram in Fig. 3, it is possible to express the magnitude of E_2 as in Equation (9), i.e., as function of E_1, the real and imaginary components of the current (I_r and I_i), and the line impedance ($R_l + jX_l$):

$$E_2 = \left[{E_1}^2 - (I_i R_l + I_r X_l)^2\right]^{0.5} - I_r R_l + I_i X_l \tag{9}$$

In case of capacitive reactive power (negative Q, which means positive I_i) the voltage drop due to active current absorption $-I_r R_l$ is partially compensated by the voltage rise due to the reactive current $+I_i X_l$. Thus, in order to support the grid during EV charging, instead of reducing the active charging power and thereby impacting the user comfort, injecting capacitive reactive power can be seen as an attractive alternative, thus operating in the IV quadrant of the EVSE converter charging capabilities in Fig. 2.

The main purpose of the proposed analysis is to provide guidelines for DSOs in terms of reactive power provision requirement for new EVSEs installation. Therefore, the determination of the effect of reactive power on the voltage at the end of the line as function of the installed apparent power is of high importance. For this reason, Equation (9) has been combined with (4) and (5), in order to highlight separately the active power P and the reactive power Q, giving as result the formulation reported in Equation (10) [32]. Note that (10) can be derived also directly from Equation (7), without making explicit the real and imaginary current components I_r and I_i.

$$E_2 = \left\{\frac{1}{2}\left[{E_1}^2 - \frac{2}{3}(PR_l + QX_l) + \left({E_1}^4 - \frac{4}{3}{E_1}^2(PR_l + QX_l) - \frac{4}{9}(PX_l + QR_l)^2\right)^{0.5}\right]\right\}^{0.5} \tag{10}$$

With (10) it is possible to calculate the voltage magnitude at the line ending terminal E_2, given the line parameters, the voltage at the source terminal, and the EV charging power in terms of P and Q.

Equation (10) provides the expected phase-neutral voltage for fixed values of P and Q, thus considering that the actual absorbed power does not depend in any way on the local voltage. The assumption of considering no

voltage-dependency, i.e., constant-power units, for new electrical installation is a common practice for grid operators when evaluating the grid impact of new eventual units (e.g., large loads, PVs, EVSEs). In fact, DSOs commonly consider the size of the new unit in terms of capacity, i.e., amount of power is going to be exchanged at the point of common coupling. For this reason, in this work the constant-power load model has been utilized for the new EV fast charger, whose size is indicated in terms of maximum charging power capacity.

By contrast, passive loads in power system are typically characterized by different voltage-dependency behaviours. According to the ZIP theory [36], each load can be modelled with reference to its nature: it can simply be a 'constant-power', a 'constant-voltage' or a 'constant-impedance' load, or it could be represented as a mix of the previous characteristics. A typical load representation is given by the polynomial model in Equations (11) and (12), which show voltage dependency of the actual absorbed active and reactive power P_{load} and Q_{load} according to the expected power values (P_{load_0} and Q_{load_0}) in case of nominal local voltage E_{2_0} of 230 V.

$$P_{load} = P_{load\_0}\left[a_0 + a_1\frac{E_2}{E_{2\_0}} + a_2\left(\frac{E_2}{E_{2\_0}}\right)^2\right] \tag{11}$$

$$Q_{load} = Q_{Load\_0}\left[b_0 + b_1\frac{E_2}{E_{2\_0}} + b_2\left(\frac{E_2}{E_{2\_0}}\right)^2\right] \tag{12}$$

Coefficients a_0, a_1, a_2 represent the shares of the constant-power, constant-current and constant-impedance contributions, respectively, and their sum is always equal to 1. The extreme cases of totally constant-power/current/impedance units are obtained by consider a_i= 1. Similar considerations are valid for coefficients b_0, b_1 and b_2, for the voltage-dependency of the reactive power. Typical ZIP coefficients for residential, industrial and commercial loads are reported in Section 5 [37].

The level of the investigation is now enhanced by considering the customer at the ending bus of Fig. 1 as a combination of certain load and the new EVSE. So, P and Q can be split in the two components relative to the EV (P_{EV} and Q_{EV}) and the load (P_{load} and Q_{load}), as shown in Equations (13) and (14).

$$P = P_{EV} + P_{load} \tag{13}$$

$$Q = Q_{EV} + Q_{load} \tag{14}$$

One can note that Equations (13) and (14) can be extended by including other types of units, such as inverter driven distributed energy resources. In this case, with reference to the ZIP modelling, the new P and Q power exchanged would be modelled as constant-power units.

If the voltage rises, on the one hand it is expected that a constant-power load would draw less current, thus enhancing the voltage regulation effect determined by reactive power provision. On the other hand, a constant-impedance load would consume more, thus reducing the effectiveness. Note that for the load the absorbed Q is typically inductive ($Q_{LOAD} > 0$), while for the charging EV it is generally capacitive ($Q_{EV} < 0$).

At this point, by combining Equation (10) with (11)-(14), it is possible to derive the fourth order equation, shown in Equation (15).

$$E_2{}^4 * \alpha + E_2{}^3 * \beta + E_2{}^2 * \gamma + E_2 * \delta + \xi = 0 \quad (15)$$

The coefficients $\{\alpha, \beta, \gamma, \delta, \xi\}$ are calculated as in Equations (16)-(20).

$$\alpha = 1 + \frac{2}{3E_{2_0}{}^2}(R_l P_{load_0} a_2 + X_l Q_{load\_0} b_2) + \frac{1}{9E_{2\_0}{}^4}(R_l{}^2 + X_l{}^2)\left[(P_{load\_0} a_2)^2 + \left(Q_{load\_0} b_2\right)^2\right] \quad (16)$$

$$\beta = \frac{2}{3E_{2_0}}(R_l P_{load_0} a_1 + X_l Q_{load\_0} b_1) + \frac{1}{9E_{2\_0}{}^3}(R_l{}^2 + X_l{}^2)\left(2P_{load\_0}{}^2 a_1 a_2 + 2Q_{load\_0}{}^2 b_1 b_2\right) \quad (17)$$

$$\gamma = -E_1{}^2 + \frac{2}{3}\left[R_l\left(P_{EV} + P_{load\_0} a_0\right) - X_l\left(Q_{EV} + Q_{load\_0} b_0\right)\right] + \frac{1}{9E_{2\_0}{}^2}\left\{\left(R_l{}^2 + X_l{}^2\right)\left[\left(P_{load\_0} a_1\right)^2 + 2P_{load\_0}{}^2 a_0 a_2 + 2P_{EV} P_{load\_0} a_2 + \left(Q_{load\_0} b_1\right)^2 + 2Q_{load\_0}{}^2 b_0 b_2 + 2Q_{EV} Q_{load\_0} b_2\right]\right\} \quad (18)$$

$$\delta = \frac{1}{9E_{2\_0}}(R_l{}^2 + X_l{}^2)\left(2P_{load\_0}{}^2 a_0 a_1 + 2P_{EV} P_{load\_0} a_1 + 2Q_{load\_0}{}^2 b_0 b_1 + 2Q_{EV} Q_{load\_0} b_1\right) \quad (19)$$

$$\xi = \frac{1}{9}(R_l{}^2 + X_l{}^2)\left[P_{EV}{}^2 + (P_{load\_0} a_0)^2 + Q_{EV}{}^2 + (Q_{load\_0} b_0)^2 + 2P_{EV} P_{load\_0} a_0 + 2Q_{EV} Q_{load\_0} b_0\right] \quad (20)$$

With (15), E_2 is calculated as function of the source voltage E_1, the line impedance, and the total active and reactive power, given a certain voltage-dependency of the load. With this formulation, the effect of the capacitive reactive power can be evaluated given a certain active power charging capacity P_{EV} of the new EVSE installation, by applying different Q_{EV}. In the proposed assessment analysis, the amount of reactive power Q_{EV} provided by the EVSE is determined by the power factor $\cos\varphi_{EV}$ set for the charging process, resulting in a fixed power factor operation mode, as commonly applied in small PV inverters. One can note that reactive power is provided only when the car is charging, i.e., when there is a need for a certain active power flow for the

analysed voltage support control. So, for a given charging behaviour influenced by stochastic factors, the reactive power is to be seen as a mean to reduce the potential self-induced voltage issues, by constantly raising the bus voltage via a fixed $\cos\varphi$ logic. The control is completely decentralized and based merely on the implemented constant power factor logic, thus not including any centralized remote grid monitoring. The logic of the proposed methodology can be therefore summarized with the block diagram reported in Fig. 4.

The proposed formulation is a possible explicit formulation analytically derived by fundamental electrotechnical laws that gives the exact direct calculation of the voltage magnitude at the considered bus, with no need for iterative calculations as for the case of power flows calculation. The solution of Equation (15) can be seen as a computationally simple and fast method able to provide a precise estimation of the voltage magnitude at the EVSE bus, with no need for iterative calculations.

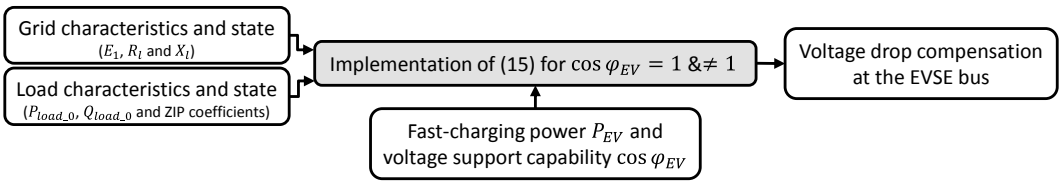

Fig. 4. Block diagram of the logic of the proposed method.

3. Grid and Components Equivalent Models

The first part of the investigation aims at evaluating the influence of the different power components (MV grid, MV/LV transformer, and LV cable) on the effectiveness of reactive power for voltage support, highlighting how much each component contributes to the total voltage drop. The single-line equivalent circuit in Fig. 5-a is considered. The representation seen from the LV side is illustrated by the equivalent single-phase circuit with all the parameters referred to the 0.4 kV LV level V_{n_LV}. At this stage, no other loads are considered, thus only the impact of charging EVs with/without reactive power support is investigated. Fig. 5-b shows the resistive and inductive components referred to the LV level of MV grid, MV/LV transformer, and LV feeder. These are termed R_{grid} and X_{grid}, R_{trafo} and X_{trafo}, and $R_{LVfeeder}$ and $X_{LVfeeder}$, respectively. With respect to the analysis in Section 2, the series of the three resistive and inductive components correspond to R_l and X_l of Fig. 1.

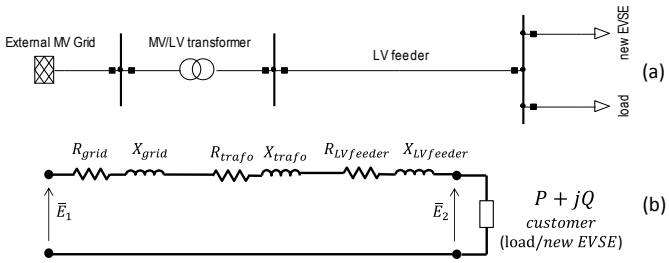

Fig. 5. Single-line (a) and single-phase equivalent circuit referred to the LV level (b) of a three-phase power system.

Typically, the V_{n_MV} 10 kV MV grid's characteristics can be represented by the short-circuit power S_{sc_grid} and the R/X_{grid} ratio: common values are 10 MVA and 0.5, respectively [33]. Through calculation of the short-circuit impedance Z_{MVgrid_MV} and its components R_{grid_MV} and X_{grid_MV} the resistive and inductive components referred to the LV level R_{grid} and X_{grid} amount to 0.00716 Ω and 0.01431 Ω, respectively. The calculation is done using Equations (21)-(23).

$$Z_{grid\_MV} = \frac{{V_{n\_MV}}^2}{S_{sc\_grid}} = \left({R_{grid\_MV}}^2 + {X_{grid\_MV}}^2\right)^{0.5} \tag{21}$$

$$R_{grid} = R_{grid\_MV}\left(\frac{V_{n\_MV}}{V_{n\_LV}}\right)^{-2} \tag{22}$$

$$X_{grid} = X_{grid\_MV}\left(\frac{V_{n\_MV}}{V_{n\_LV}}\right)^{-2} \tag{23}$$

A typical MV/LV distribution power transformer is modelled in [30]. It is characterized by nominal apparent power S_{n_trafo} of 0.4 MVA, short-circuit voltage $v_{sc\%\_trafo}$ of 4%, and R/X_{trafo} ratio of 0.1. Via calculation of short-circuit power S_{sc_trafo} and impedance Z_{sc_trafo} – Equations (24) and (25) – the resistive and inductive components referred to the LV level R_{trafo} and X_{trafo} amount respectively to 0.00159 Ω and 0.0159 Ω.

$$S_{sc\_trafo} = \frac{100 * S_{n\_trafo}}{v_{sc\%\_trafo}} \tag{24}$$

$$Z_{sc\_trafo} = \frac{{V_{n\_LV}}^2}{S_{sc\_trafo}} = \left({R_{trafo}}^2 + {X_{trafo}}^2\right)^{0.5} \tag{25}$$

This formulation does not include no-load current and no-load losses, which was found do not significantly impact the results. In particular, they only cause a minor off-set on the total voltage drop estimation of less than 0.1% of the nominal voltage.

Typical values of cable resistance and reactance per km are 0.163 and 0.136 Ω/km, respectively ($^{R}/_{X_{LVfeeder}}$ = 1.2, i.e., $^{X}/_{R_{LVfeeder}}$ = 0.8) [33]. The length of 1 km is chosen, as it can be considered as an upper limit of LV feeders length [38]. So, absolute $R_{LVfeeder}$ and $X_{LVfeeder}$ amount to 0.163 and 0.136 Ω, respectively.

Table 1. Standard parameters for distribution grids, adapted from [30] and [33].

	S_{sc_grid} [MVA]	S_{n_trafo} [MVA]	$v_{sc\%\_trafo}$ [%]	R/X	R referred to LV level [Ω]	X referred to LV level [Ω]
MV grid [33]	10	-	-	0.5	0.00716	0.01431
MV/LV trafo[30]	-	0.4	4	0.1	0.00159	0.0159
LV feeder [33]	-	-	-	1.2	0.163	0.136

Table 1 reports the considered typical values of power system components when modelling LV distribution grids. It also includes the related equivalent resistance and reactance referred to the LV level, with reference to the simplified single-phase equivalent circuit in Fig. 5-b.

Equation (10) has been implemented with E_1 set to 1 p.u. as for an ideal voltage source and P and Q equal to P_{EV} and Q_{EV}, respectively – only EVs as customer. Anyway, the aim of the study is assessing the voltage difference, thus the findings are still applicable also in other situations (i.e., higher voltages such as 1.05 because of reverse flow, or lower voltages such as 0.95 because of loaded feeders). One should also note that Equation (10) could be implemented considering that the starting terminal of the line does not necessarily need to be at the MV grid or transformer level. Instead, it could be at any node of the distribution network. In this case, the ending terminal could be at the end of one of the branches derived from that very node.

Considering installation of new EVSEs with fast-charging capability up to 12.5 kW, it has been decided to assume a total EV active power demand of 50 kW, which represent a realistic case of 4 new EVSEs. Equation (10) is implemented twice: with power factor $\cos\varphi_{EV}$ equal to 1 and then repeated with capacitive $\cos\varphi_{EV}$ equal to 0.9, and the difference ΔE_2 was evaluated as in Equation (26).

$$\Delta E_2 = E_{2\_\cos\varphi_{EV}\neq 1} - E_{2\_\cos\varphi_{EV}=1} \quad (26)$$

The choice of considering a limit value of $\cos\varphi_{EV}$ of 0.9, is motivated by the fact that also in case of reactive power provision by PV inverters, the maximum reactive power exchange is limited by a power factor of 0.9 [10–12]. This value was identified as the maximum power factor that can be applied to the converter without excessive over-sizing. For this reason, the same value has been set for the EVSE inverters under analysis.

Considering the calculated constant values of the series resistive and inductive components of the circuit in Fig. 4-b, a preliminary analysis of the influence of the three single components on the effects of reactive power is now presented. E_2 resulted in 0.9415 and 0.9673 p.u. for $\cos\varphi_{EV}$ equal to 1 and 0.9, respectively. It is clear that ΔE_2 (0.0258 p.u.) represents the voltage rise due to the reactive power injected by the EVs at the ending terminal of the line. The resulting ΔE_2 is obtained as effect of the three components. Specifically, the MV grid contributed 8.5%, the transformer 9.4%, while the LV feeder contributed 82.1%, as illustrated schematically in Fig. 6.

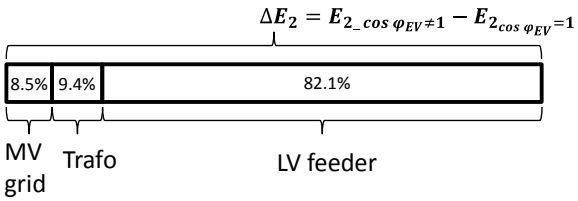

Fig. 6. Contribution to the reactive power effect on the voltage at the end of the line for each component.

It is therefore found that the effect of the reactive power on the local voltage depends mainly on the characteristics of the LV feeder. This result was obtained considering one possible combination of typical distribution network components. Thus, it is of interest to see how different values of these components may impact the results. In this regards, the next part of the investigation aims at evaluating the single influence of the MV grid, the MV/LV transformer, and the LV feeder parameters.

4. Sensitivity Analysis

4.1 Influence of the MV grid

The influence of the external MV grid is evaluated by calculating ΔE_2 first for different S_{sc_grid} (1-10 MVA) and then for different R/X_{grid} (0.05-0.5), keeping constant the typical parameters of transformer and LV feeder

of Table 1. Fig. 7-a shows that the trend of ΔE_2 is influenced by the stiffness of the external MV grid, keeping, as in [33], the constant value of 0.5 for R/X_{grid}. In particular, for very weak grids results differ from the case of strong ones. Thus, hereafter all the studies consider two kinds of MV grid: weak and strong grid (S_{sc_grid} = 2 and 10 MVA, respectively). Fig. 7-b shows that in both the cases the effect of reactive power on the ending terminal voltage is constant for all the considered R/X_{grid} ratios. Thus, hereafter the constant value of 0.5 for R/X_{grid} is used.

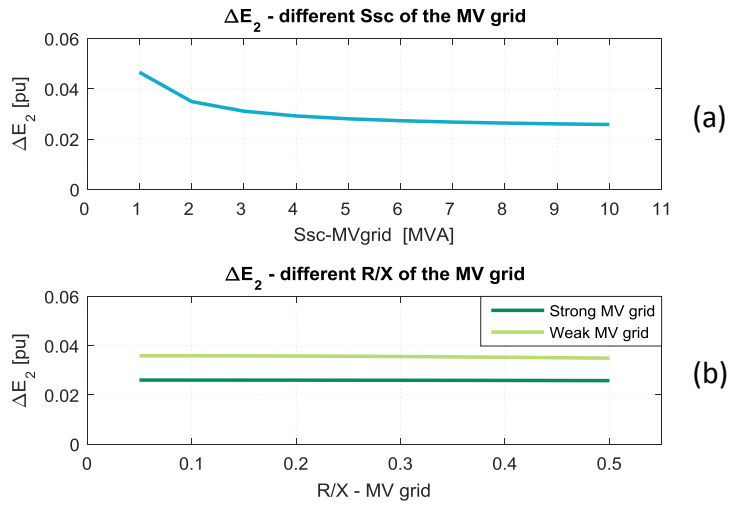

Fig. 7. Influence of MV grid for $\cos \varphi_{EV\neq 1}$ = 0.9.

4.2 Influence of the distribution MV/LV transformer

The influence of the distribution MV/LV transformer is evaluated by calculating ΔE_2 for different S_{n_trafo} (0.1-1 MVA), keeping constant the typical values of $v_{sc\%\_trafo}$, R/X_{trafo} and LV feeder, as in Table 1. The analysis is carried out for weak and strong MV grid. Fig. 8 shows that the influence of the transformer on the effect of reactive power is marginal for $S_{n\_trafo} \geq 0.2$ MVA, while for smaller sizes, the contribution becomes noticeable. As the grid model considers a LV feeder at the secondary side of the transformer, it is to be expected that in addition to the new EVSEs at the line end, distributed loads are connected along the feeder. Thus, as in this study a realistic case of new EVSEs installation for a total of 50 kW is considered, a minimum size of 0.2 MVA has to be considered for the transformer. For this reason, hereafter the typical values of the MV/LV transformer

reported in Table 1 are considered and kept constant, as its influence on the effect of the reactive power is considered marginal.

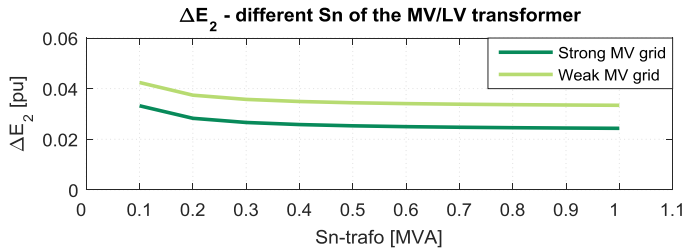

Fig. 8. Influence of the MV/LV transformer for $\cos \varphi_{EV \neq 1}$ = 0.9.

4.3 Influence of the LV feeder

The influence of the LV feeder is evaluated by calculating ΔE_2 first for different $R/X_{LVfeeder}$ and then for different lengths, considering both weak and strong MV grid, and the MV/LV transformer from Table 1. Since it is known that the reactance per km is usually constant for different kinds of cables, for the first case different $R/X_{LVfeeder}$ are obtained by varying the value of the resistive component (0.07-0.7 Ω/km), i.e., by considering different sections of the cable conductors, keeping the length equal to 1 km [38]. For the case of different lengths (0-1 km), the values per km reported in Table 1 are used and kept constant. Fig. 9-a shows that for different $R/X_{LVfeeder}$, ΔE_2 results relatively constant, while from Fig. 9-b it is possible to deduce that the main influence is given by the absolute values of $R_{LVfeeder}$ and $X_{LVfeeder}$, i.e., by the length.

It is found that the main influence of reactive power on the voltage support is determined by the absolute values of the LV feeder impedance, i.e., by the length, rather than by the $R/X_{LVfeeder}$ ratio.

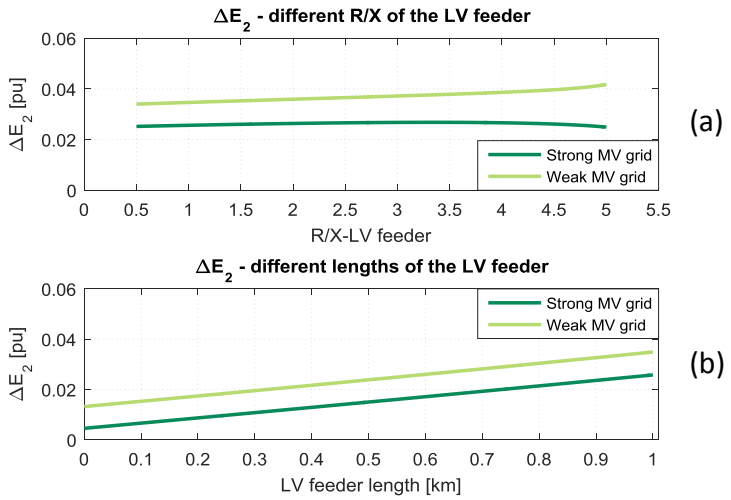

Fig. 9. Influence of the LV feeder for $\cos \varphi_{EV \neq 1} = 0.9$.

4.4 Voltage rise as function of cos(φ_{EV}) and length

It is clear that ΔE_2 depends on the amount of the capacitive reactive power provided by the EV, i.e., on the power factor $\cos \varphi_{EV}$ set by the EVSE. Therefore, the last formulation proposed in this Section considers ΔE_2 as function of the LV feeder length and $\cos \varphi_{EV}$, varied between 0.9 and 1.

Table 2 presents numerical results for the case of the strong MV grid, i.e., the most common one. As expected, the effectiveness of the reactive power on voltage support is increasing with decreasing power factor, up to the maximum value of 0.0258 p.u. for standard LV feeder length of 1 km, for strong MV grid. Moreover, it is noticeable that for any given $\cos \varphi_{EV}$, the effects are linearly dependent on the absolute value of the LV feeder impedance (thus the length), as previously demonstrated.

Table 2. ΔE_2 for different $\cos \varphi_{EV}$ – length combinations.

		$\cos \varphi_{EV}$					
		1	**0.98**	**0.96**	**0.94**	**0.92**	**0.9**
Length [km]	**0.2**	0	0.0037	0.0053	0.0066	0.0077	0.0087
	0.4	0	0.0055	0.0078	0.0097	0.0114	0.0129
	0.6	0	0.0073	0.0104	0.0129	0.0151	0.0171
	0.8	0	0.0092	0.0131	0.0162	0.0189	0.0214
	1.0	0	0.0111	0.0158	0.0195	0.0228	0.0258

4.5 Inclusion of voltage-dependent loads

The analysis presented so far has not considered any loading except for the new EVSE itself, in fact Equation (10) was implemented considering only EVs as customer. Now the investigation is enhanced through the implementation of (15), for different voltage-dependent loads in addition to the EVs. The nominal active power P_{load_0} is kept constantly equal to 50 kW, while different load types and different amount of inductive reactive power active power Q_{load_0} (i.e., different values of $\cos\varphi_{load}$) are considered.

Fig. 10 shows the effect of capacitive reactive power provided from EVs on the voltage at the ending terminal of the feeder for different load types (constant P, I or Z). In this case, the comparison is done for $\cos\varphi_{EV\neq1}$ = 0.9, considering constant $\cos\varphi_{load}$ = 0.9. It can be noticed that the load type influences the results for lines longer than 0.4 km, with more evident effects in case of no voltage-dependency (constant-P load) rather than for voltage-dependent load. Specifically, for a 1 km line, ΔE_2 amounts to 0.0319, 0.0277 and 0.0253 for constant-P, constant-I and constant-Z loads, respectively. Although an exhaustive sensitivity analysis would require load models with mixed coefficients, the results of the three analyzed load types represent the extreme cases. In fact, by using mixes of the coefficients, intermediate results would be obtained.

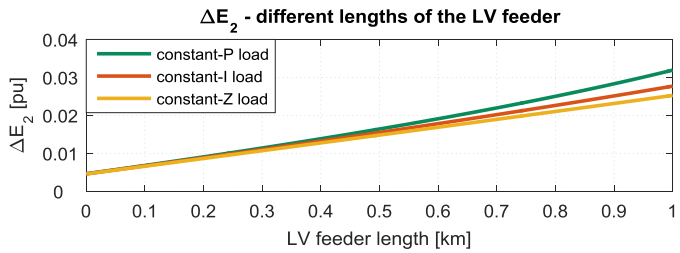

Fig. 10. Voltage rise effect of the reactive power provided by EVs for $\cos\varphi_{EV\neq1}$ = 0.9, as function of the LV feeder length for different voltage-dependency of loads, for strong MV grid.

Similarly to the analysis reported in Section 4.4, it is of interest to evaluate ΔE_2 as function of the LV feeder length and $\cos\varphi_{EV}$, varied between 0.9 and 1, for the three different load types.

Fig. 11 shows 3D bar plots of ΔE_2 for the three different load types and $\cos\varphi_{load}$ equal 0.85, 0.9, 0.95 and 1, in subfigures (a), (b), (c) and (d), respectively. Note that the three different widths of the bars indicate the load

type, in particular, the widest one is for constant-Z loads, the middle one for constant-I loads, while the tightest one for constant-P loads.

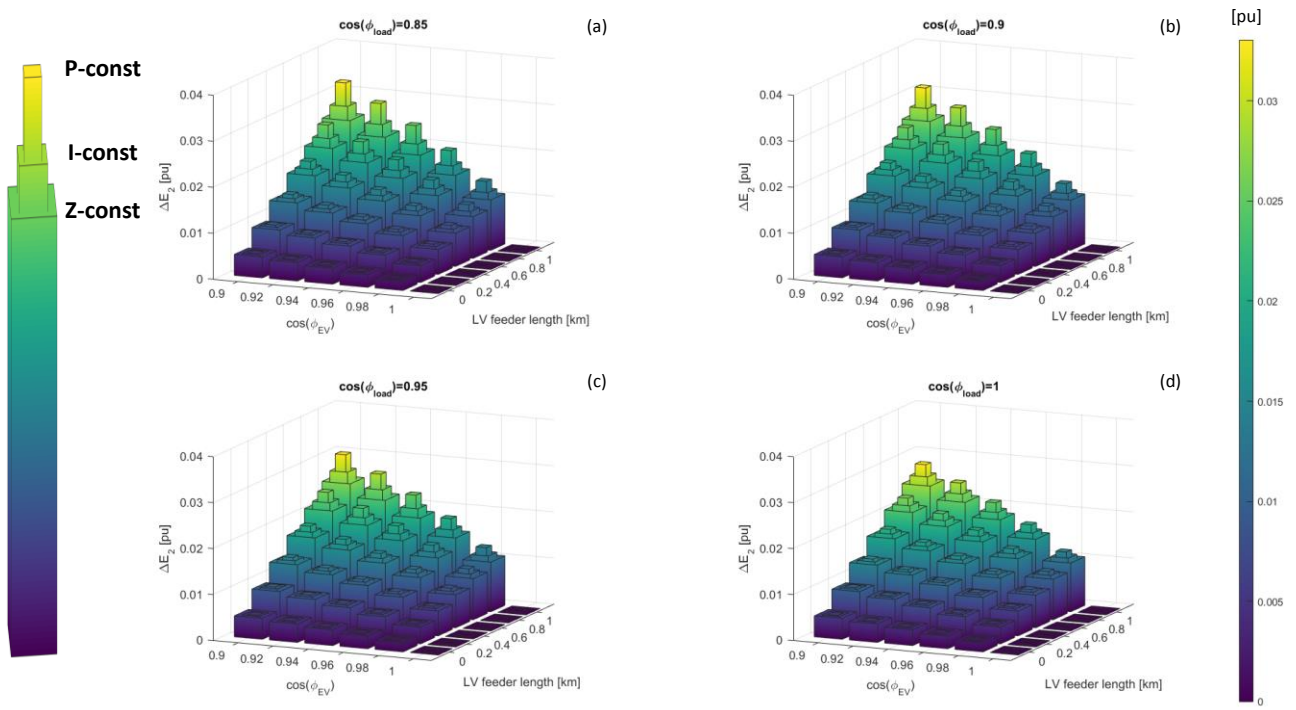

Fig. 11. Voltage rise effect of the reactive power provided by EVs as function of the LV feeder length and $\cos\varphi_{EV}$, for different voltage-dependent loads and for $\cos\varphi_{load}$=0.85, 09, 0.95, 1 in (a), (b), (c) and (d), respectively.

As expected, Fig. 11 shows that the more the load is voltage dependent, the smaller is the contribution of the capacitive reactive power in rising the voltage. In fact, as shown in Fig. 10 in case of constant-P load, ΔE_2 is higher than in the case of constant-I load, which is higher than in the case of constant-Z load. Furthermore, as demonstrated in Section 4.4, ΔE_2 is higher with decreasing amount of the capacitive reactive power provided by the EV, i.e., with decreasing $\cos\varphi_{EV}$.

Table 3 presents numerical results of the cases of highest reactive power contribution from EVs, i.e., the case of $\cos\varphi_{EV\neq1}$ = 0.9. Results confirm the linear trend with the LV feeder length, and show less voltage support effects in case of higher load power factors $\cos\varphi_{load}$.

Table 3. ΔE_2 for different lengths – load model combinations with $\cos\varphi_{EV\neq 1}$ = 0.9.

		Constant-P load	**Constant-I load**	**Constant-Z load**
		$\cos\varphi_{load} = 0.85$		
Length [km]	**0.2**	0.0091	0.0089	0.0087
	0.4	0.0140	0.0133	0.0128
	0.6	0.0194	0.0180	0.0169
	0.8	0.0256	0.0229	0.0212
	1.0	0.0330	0.0282	0.0254
		$\cos\varphi_{load} = 0.9$		
Length [km]	**0.2**	0.0091	0.0088	0.0086
	0.4	0.0138	0.0132	0.0127
	0.6	0.0191	0.0178	0.0169
	0.8	0.0250	0.0226	0.0210
	1.0	0.0319	0.0277	0.0253
		$\cos\varphi_{load} = 0.95$		
Length [km]	**0.2**	0.0090	0.0088	0.0086
	0.4	0.0137	0.0131	0.0127
	0.6	0.0187	0.0176	0.0168
	0.8	0.0243	0.0223	0.0209
	1.0	0.0308	0.0272	0.0250
		$\cos\varphi_{load} = 1$		
Length [km]	**0.2**	0.0089	0.0087	0.0086
	0.4	0.0133	0.0129	0.0126
	0.6	0.0180	0.0172	0.0166
	0.8	0.0231	0.0216	0.0206
	1.0	0.0286	0.0262	0.0246

5. Validation on typical LV distribution grids

This Section reports a validation of the proposed method on the reference Cigrè European LV distribution feeder [33] as well as on a real Danish LV distribution network previously utilized for other EV integration-related studies [30]. Simulations are carried out both applying the proposed formulation and by means of DIgSILENT PowerFactory load flows. For the implementation of Equations (11) and (12), the typical ZIP coefficients for residential load class have been utilized, which are reported in Table 4 along with industrial and commercial load classes.

Table 4. Standard parameters for distribution grids, adapted from [37].

	a_0	a_1	a_2	b_0	b_1	b_2
Residential	1.27	-1.12	0.85	8.77	-18.73	10.96
Industrial	1	0	0	1	0	0
Large commercial	1.06	-0.53	0.47	4.43	-8.73	5.30
Small commercial	0.63	-0.06	0.43	3.59	-6.65	4.06

5.1 Cigrè European LV reference grid

The residential reference Cigrè European LV distribution feeder is schematized in Fig. 12. Installation of four new 12.5 kW EVSEs (for a total of 50 kW) is considered at buses 2-6, which are, case by case, the ending terminal bus with respect to the formulation proposed in Section 3. The loading and the single-feeder characteristics (transformer-bus) are in Table 5.

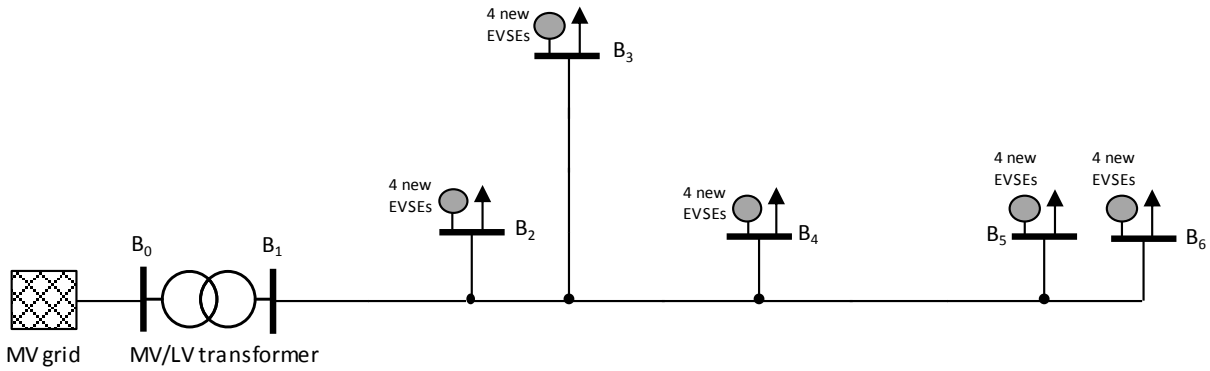

Fig. 12. Single-phase circuit of the modelled Cigrè distribution grid under study.

Table 5. Properties of the Cigrè transformer-bus feeder and loading at each bus.

Bus	**Total Length [m]**	$R/X_{LVfeeder}$	P_{load_0} **[kW]**	$\cos\varphi_{load}$
B2	95	3.67	5.13	0.9
B3	240	2.08	51.3	0.9
B4	205	1.57	22.5	0.9
B5	310	2.08	5.13	0.9
B6	345	1.74	22.5	0.9

Due to the limited length of the line, results are not expected to be dramatically influenced by the voltage dependency of the loads type. However, the typical ZIP coefficients for residential load class indicated in Table 4 are utilized. Results are reported in Table 6, which shows voltage E_2 for unitary $\cos\varphi_{EV}$, for $\cos\varphi_{EV}$ = 0.9, and the difference ΔE_2 in case of 50 kW of EVs charging at buses 2-6.

Table 6. Results from validation analyses on the Cigrè grid for 50 kW EVSE connected at the different buses.

Bus	Proposed Method			Power Flow in PowerFactory		
	E_2 [p.u.]		ΔE_2	E_2 [p.u.]		ΔE_2
	$\cos \varphi_{EV}$ =1	$\cos \varphi_{EV}$ =0.9		$\cos \varphi_{EV}$ =1	$\cos \varphi_{EV}$ =0.9	
B2	0.9760	0.9825	0.0065	0.9760	0.9825	0.0065
B3	0.9491	0.9587	0.0096	0.9491	0.9587	0.0096
B4	0.9711	0.9796	0.0085	0.9711	0.9796	0.0085
B5	0.9629	0.9738	0.0109	0.9629	0.9738	0.0109
B6	0.9508	0.9626	0.0118	0.9508	0.9626	0.0118

As deducible from Table 6, the results from the implementation of the proposed method respect very accurately the ones obtained carrying out iterative power flow simulations in DIgSILENT PowerFactory. This is true given a sufficiently small tolerance (equal to 0.1 kVA) when solving Newton-Rapson calculations. In this case the difference between the results from the two methods is smaller than 0.01%. In case of larger tolerance the convergence might still be obtained, though with minor differences in the results, as less iterations would be needed due to the less tight tolerance. Moreover, the expected trend of growing ΔE_2 with the line length independently from the $R/X_{LVfeeder}$ ratio demonstrated in Section 4 is confirmed.

5.2 Real Danish LV distribution grid

As for the validation on the real Danish LV grid, the schematic is shown in Fig. 13, and the installation of four new 12.5 kW EVSEs (for a total of 50 kW) is considered cyclically at each bus from 602 to 613. The voltage values of the EVSE bus is E_2 in the proposed formulation (Equation (15)), which corresponds to the ending terminal bus with reference to the diagram on Fig. 5. The loading and the single-feeder characteristics (transformer-bus) are in Table 7. It has been decided to simulate the worst case of maximum loading condition of a winter week, when high load demand is present due to heat pumps heating systems, while there is no PV production due to weather conditions.

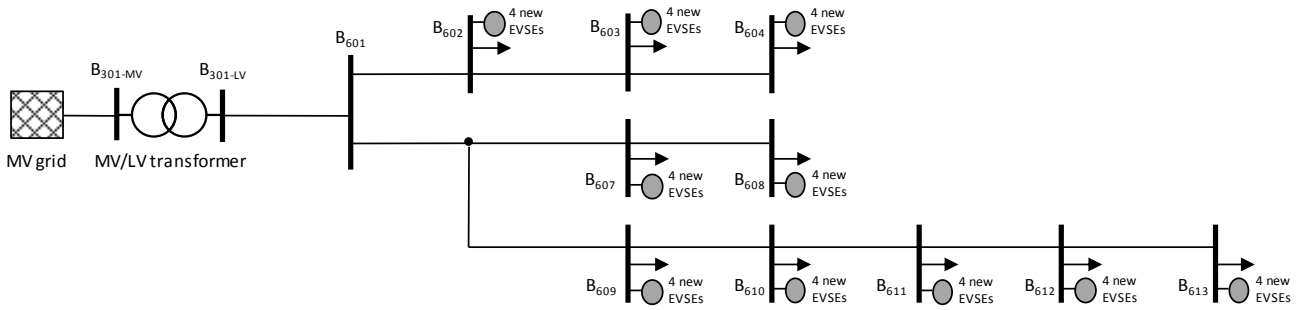

Fig. 13. Single-phase circuit of the modelled Danish distribution grid under study.

Table 7. Properties of the real Danish LV grid transformer-bus feeder and loading at each bus.

Bus	Total Length [m]	$R/X_{LVfeeder}$	P_{load_0} [kW]	$\cos\varphi_{load}$
B601	112	2.8	0	-
B602	161	2.8	8.21	0.95
B603	225	2.8	5.48	0.95
B604	312	2.8	11.88	0.95
B607	263	2.8	16.14	0.95
B608	300	2.8	11.19	0.95
B609	257	2.8	9.98	0.95
B610	292	2.8	13.71	0.95
B611	328	2.8	13.85	0.95
B612	363	2.8	14.18	0.95
B613	398	2.8	12.59	0.95

Again, the typical ZIP coefficients for residential load class in Table 4 are utilized. Results are reported in Table 8, which shows voltage E_2 for unitary $\cos\varphi_{EV}$, for $\cos\varphi_{EV}$ = 0.9, and the difference ΔE_2 in case of 50 kW of EVs charging at all the buses.

Table 8. Results from validation on the real Danish grid for 50 kW EVSE connected at the different buses.

Bus	Proposed Method			Power Flow in PowerFactory		
	E_2 [p.u.]		ΔE_2	E_2 [p.u.]		ΔE_2
	$\cos\varphi_{EV}$ =1	$\cos\varphi_{EV}$ =0.9		$\cos\varphi_{EV}$ =1	$\cos\varphi_{EV}$ =0.9	
B602	0.9866	0.9908	0.0042	0.9866	0.9908	0.0042
B603	0.9826	0.9875	0.0049	0.9826	0.9875	0.0049
B604	0.9728	0.9787	0.0059	0.9728	0.9787	0.0059
B607	0.9751	0.9805	0.0054	0.9751	0.9805	0.0054
B608	0.9741	0.9799	0.0058	0.9742	0.9800	0.0058
B609	0.9783	0.9836	0.0053	0.9783	0.9836	0.0053
B610	0.9736	0.9793	0.0057	0.9736	0.9793	0.0057
B611	0.9704	0.9765	0.0061	0.9704	0.9765	0.0062
B612	0.9670	0.9736	0.0066	0.9670	0.9735	0.0065
B613	0.9649	0.9718	0.0069	0.9649	0.9718	0.0069

The results obtained from the implementation of the proposed formulation respect very accurately the ones obtained carrying out power flow simulations in DIgSILENT PowerFactory. Again, the sufficiently small tolerance (equal to 0.1 kVA) utilized when solving power flow calculations enables the results to look identical, as difference smaller than 0.01% are obtained. As in this case the cable lines of the modelled network are all of the same type, they have the same $R/X_{LVfeeder}$ ratio. Nonetheless, the expected trend of growing ΔE_2 with the line length is confirmed.

6. Conclusions and Future Works

The aim of the work was to analyse the potentials of reactive power provision by EVSEs on voltage support, depending on grid's and load's characteristics. This is considered as a possible mean of evaluation for the DSO when assessing the grid impact of new fast charging EVSEs and the respective flexibility in terms of voltage control. An analytical formulation is proposed to calculate the expected voltage at the ending-terminal of a distribution line given as input the grid characteristic, the load and its voltage-dependency.

The considered simplified distribution grid is composed by an external MV grid, a MV/LV distribution transformer, and a single radial LV line, and all their impedances have been referred to the LV level. Considering multiple values of the parameters of all the components, it was found that the effect of the capacitive reactive power is influenced mostly by the stiffness of the external MV grid and by the absolute values of the LV feeder impedance. Specifically, it was found that the R/X ratio of the LV feeder did not significantly influence the results, while its absolute impedance was crucial. Since the LV cable reactance per km is substantially constant for most cross sections, the variety of the absolute values was obtained by considering different cable lengths.

It was found that results are influenced by the load voltage-dependency only for lines longer than 400 m. In particular, the more the load is voltage dependent, the smaller is the contribution of the capacitive reactive power in rising the voltage, and vice versa. In fact, in case of constant-power loads the studied EV voltage support is more effective than in case of constant-impedance-load.

With the proposed formulation the DSO is able to assess the voltage drop compensation due to the application of a particular power factor by the EV fast charger as function of the LV feeder length, given as input the EVSE

installed power and the load condition. In this way, DSOs can clearly evaluate the effect of the reactive power for any of their LV feeders when the power absorbed by EVs chargers would cause unacceptable under-voltages.

Results showed that for an autonomous decentralized reactive power provision control embedded in the new fast charging EVSE, the voltage support to the DSO is limited by the technical characteristics of the feeder. In particular, the proposed validation analysis on realistic LV feeders for the case of a fixed capacitive power factor of 0.9 proves that the voltage rise would amount to 0.012 p.u., in comparison to the case of EV charging with unitary power factor. The authors recognize that such voltage drop reductions can potentially avoid the violation of voltage thresholds, thus assuring compliance with grid technical standards on voltage levels. At any rate, this precaution may not be sufficient for massive penetration of EVSEs, since a combination with other smart charging strategies such as charging modulation and/or charging shifting may be essential for prevention of unacceptable under-voltage conditions. In conclusion, the authors believe that reactive power solutions is to be seen as a possible connection capability requirement, able to mitigate the self-induced negative effects of fast charging EVs in LV distribution grids, similarly to the current requirements for new PV system installation in many European countries. In this regard, reactive power capabilities are required by the newly released Danish technical standard for stationary storage systems including vehicle-to-grid EV charging station [39].

Future research works should cover the investigation of reactive power provision in unbalanced distribution grids. In this case, the approach to the problem would be slightly different, as the DSO analysis would not be aiming at evaluating permission for installation of new EVSE with fast-charging capability, instead the focus would be on the effects of unbalanced voltage support by capacitive reactive power provision by single-phase EVs.

Acknowledgments

The authors would like to acknowledge the support of the EUDP projects ACES - Across Continent Electric Vehicle Services (grant EUDP17-I-12499, website: www.aces-bornholm.eu).

References

[1] S. Izadkhast, P. Garcia-Gonzalez, P. Frías, An Aggregate Model of Plug-In Electric Vehicles for Primary Frequency Control, IEEE Transactions on Power Systems. 30 (2015) 1475–1482. doi:http://dx.doi.org/10.1109/TPWRS.2014.2337373.

[2] A. Zecchino, M. Rezkalla, M. Marinelli, Grid Frequency Support by Single-Phase Electric Vehicles : Fast Primary Control Enhanced by a Stabilizer Algorithm, in: 2016 Universities Power Engineering Conference (UPEC), Coimbra, Portugal, 2016: pp. 1–6.
[3] M. González Vayá, G. Andersson, Combined Smart-Charging and Frequency Regulation for Fleets of Plug-in Electric Vehicles, in: 2013 IEEE Power & Energy Society General Meeting, Vancouver, BC, 2013: pp. 1–5. doi:http://dx.doi.org/10.1109/PESMG.2013.6672852.
[4] K. Knezović, S. Martinenas, P.B. Andersen, A. Zecchino, M. Marinelli, Enhancing the Role of Electric Vehicles in the Power Grid : Field Validation of Multiple Ancillary Services, IEEE Transactions on Transportation Electrification. 3 (2016) 201–209. doi:http://dx.doi.org/10.1109/TTE.2016.2616864.
[5] S. Martinenas, K. Knezović, M. Marinelli, Management of Power Quality Issues in Low Voltage Networks using Electric Vehicles: Experimental Validation, IEEE Transactions on Power Delivery. 8977 (2016) 1–9. doi:10.1109/TPWRD.2016.2614582.
[6] K. Clement-Nyns, E. Haesen, J. Driesen, The impact of vehicle-to-grid on the distribution grid, Electric Power Systems Research. 81 (2011) 185–192. doi:http://dx.doi.org/10.1016/j.epsr.2010.08.007.
[7] A. Rodriguez-Calvo, R. Cossent, P. Frías, Integration of PV and EVs in unbalanced residential LV networks and implications for the smart grid and advanced metering infrastructure deployment, International Journal of Electrical Power and Energy Systems. 91 (2017) 121–134. doi:http://dx.doi.org/10.1016/j.ijepes.2017.03.008.
[8] European Technical Standard EN 50160, (2011).
[9] A. Kechroud, P.F. Ribeiro, W.L. Kling, Distributed generation support for voltage regulation: An adaptive approach, Electric Power Systems Research. 107 (2014) 213–220. doi:http://dx.doi.org/10.1016/j.epsr.2013.09.004.
[10] Italian Technical Standard CEI 0-21 Rules for the connection to the LV electrical utilities, (2012).
[11] German Technical Standard VDE-AR-N 4105 Power generation systems connected to the low-voltage distribution network, (2011).
[12] Energinet.dk, Danish Technical Regulation 3.2.2 for PV power plants with a power output above 11 kW, (2015).
[13] R. Caldon, M. Coppo, R. Turri, Distributed voltage control strategy for LV networks with inverter-interfaced generators, Electric Power Systems Research. 107 (2014) 85–92. doi:http://dx.doi.org/10.1016/j.epsr.2013.09.009.
[14] J. Hu, M. Marinelli, M. Coppo, A. Zecchino, H.W. Bindner, Coordinated voltage control of a decoupled three-phase on-load tap changer transformer and photovoltaic inverters for managing unbalanced networks, Electric Power Systems Research. 131 (2016) 264–274. doi:http://dx.doi.org/10.1016/j.epsr.2015.10.025.
[15] M.C. Kisacikoglu, M. Kesler, L.M. Tolbert, Single-Phase On-Board Bidirectional PEV Charger for V2G Reactive Power Operation, IEEE Transactions on Smart Grid. 6 (2015) 767–775.
[16] R.J. Ferreira, L.M. Miranda, R.E. Ara, A New Bi-Directional Charger for Vehicle-to-Grid Integration, in: Innovative Smart Grid Technologies (ISGT Europe), 2011 2nd IEEE PES International Conference and Exhibition O, Manchester, UK, 2011.
[17] M.C. Kisacikoglu, B. Ozpineci, L.M. Tolbert, Reactive Power Operation Analysis of a Single-Phase EV/PHEV Bidirectional Battery Charger, in: 8th International Conference on Power Electronics (ECCE), Jeju, Korea, 2011: pp. 585–592.
[18] M.C. Kisacikoglu, B. Ozpineci, L.M. Tolbert, Examination of a PHEV Bidirectional Charger System for V2G Reactive Power Compensation, in: Proc. IEEE APEC Exposition, Palm Springs, CA, USA, 2010: pp. 458–465.
[19] M. Kesler, M.C. Kisacikoglu, L.M. Tolbert, Vehicle-to-Grid Reactive Power Operation Using Plug-In Electric Vehicle Bidirectional Offboard Charger, IEEE TRANSACTIONS ON INDUSTRIAL ELECTRONICS. 61 (2014) 6778–6784.
[20] B.A. De Souza, A. Márcio, F. De Almeida, Multiobjective Optimization and Fuzzy Logic Applied to Planning of the Volt / Var Problem in Distributions Systems, IEEE Transactions on Power Systems. 25 (2010) 1274–1281.
[21] W. Huang, D. Gan, X. Xia, N. Kobayashi, X. Xu, Distributed Generation on Distribution System Voltage Regulation : An Optimization-based Approach, in: Power and Energy Society General Meeting, 2010 IEEE, Providence, RI, USA, 2010: pp. 1–7.
[22] M. Manbachi, H. Farhangi, A. Palizban, S. Arzanpour, A novel Volt-VAR Optimization engine for smart distribution networks utilizing Vehicle to Grid dispatch, International Journal of Electrical Power and Energy Systems. 74 (2016) 238–251. doi:10.1016/j.ijepes.2015.07.030.
[23] H. Fakham, A. Ahmidi, F. Colas, X. Guillaud, Multi-Agent System for Distributed Voltage Regulation of Wind Generators Connected to Distribution Network, in: Proc Innovative Smart Grid Technologies Conference Europe (ISGT Europe), IEEE PES, Gothenburg, Sweden, 2010: pp. 1–6.
[24] B. Morvaj, K. Knezović, R. Evins, M. Marinelli, Integrating multi-domain distributed energy systems with electric vehicle PQ flexibility : Optimal design and operation scheduling for sustainable low-voltage distribution grids, Sustainable Energy, Grids and Networks. 8 (2016) 51–61. doi:10.1016/j.segan.2016.10.001.

[25] J. García-Villalobos, I. Zamora, K. Knezović, M. Marinelli, Multi-objective optimization control of plug-in electric vehicles in low voltage distribution networks, Applied Energy. 180 (2016) 155–168. doi:10.1016/j.apenergy.2016.07.110.
[26] N. Leemput, F. Geth, J. Van Roy, J. Büscher, J. Driesen, Reactive power support in residential LV distribution grids through electric vehicle charging, Sustainable Energy, Grids and Networks. 3 (2015) 24–35. doi:http://dx.doi.org/10.1016/j.segan.2015.05.002.
[27] R. Kohrs, K. Dallmer-Zerbe, M. Mierau, C. Wittwer, Autonomous Reactive Power Control by Electric Vehicles, in: Innovative Smart Grid Technologies Conference Europe (ISGT-Europe), 2014 IEEE PES, Instanbul, Turkey, 2014: pp. 1–6. doi:http://dx.doi.org/10.1109/ISGTEurope.2014.7028771.
[28] J. Ying, V.K. Ramachandaramurthy, K. Miao, N. Mithulananthan, Bi-directional electric vehicle fast charging station with novel reactive power compensation for voltage regulation, International Journal of Electrical Power and Energy Systems. 64 (2015) 300–310. doi:http://dx.doi.org/10.1016/j.ijepes.2014.07.025.
[29] P. Krasselt, M.R. Suriyah, T. Leibfried, Reactive Power Support for Optimal Grid Integration of Fast-Charging Infrastructure in German Low-Voltage Networks, in: 23rd International Conference on Electricity Distribution (CIRED), Lyon, France, 2015: pp. 1–5.
[30] K. Knezović, M. Marinelli, Phase-wise enhanced voltage support from electric vehicles in a Danish low-voltage distribution grid, 140 (2016) 274–283. doi:http://dx.doi.org/10.1016/j.epsr.2016.06.015.
[31] C. Winter, R. Schwalbe, M. Heidl, W. Prüggler, Harnessing PV inverter controls for increased hosting capacities of smart low voltage grids Recent results from Austrian research and demonstration projects, in: 4th Interntaional Workshop on Integration of Solar Power into Power Systems, Berlin, Germany, 2014: pp. 1–6.
[32] A. Zecchino, M. Marinelli, M. Korpås, T. Chresten, Guidelines for Distribution System Operators on Reactive Power Provision by Electric Vehicles in Low Voltage Grids, in: 24th International Conference on Electricity Distribution (CIRED), In Press, 2017: pp. 1–5.
[33] K. Strunz, CIGRE Task Force C6.04.02 - Benchmark Systems for Network Integration of Renewable and Distributed Energy Resources, 2009.
[34] NISSAN, Nissan, enel and nuvve operate world's first fully commercial vehicle-to-grid hub in denmark, Http://www.nissan-Helsingor.dk/index.php/om-os/nyheder/show/news/id/4. (2016).
[35] M.H. Haque, Load flow solution of distribution systems with voltage dependent load models, Electric Power System Research. 36 (1996) 151–156. doi:http://dx.doi.org/10.1016/0378-7796(95)01025-4.
[36] W.W. Price, IEEE Task Force on Load Representation for Dynamic Performance, Load representation for dynamic performance analysis, IEEE Transactions on Power Systems. 8 (1993) 472–482.
[37] M. Diaz-Aguiló, J. Sandraz, R. Macwan, F. de León, S. Member, D. Czarkowski, C. Comack, D. Wang, S. Member, Field-Validated Load Model for the Analysis of CVR in Distribution Secondary Networks : Energy Conservation, IEEE Transactions on Power Delivery. 28 (2013) 2428–2436. doi:http://dx.doi.org/10.1109/TPWRD.2013.2271095.
[38] F. Lehfuss, S. Kadam, R. Rodriguez Sanchez, COTEVOS - Specification of reference electricity networks, 2014.
[39] Energinet.dk, Danish Technical regulation 3.3.1 for battery plants, (2017).

Center for Electric Power and Energy
DTU Electrical Engineering
Frederiksborgvej 399, Building 776
DK-4000 Roskilde
Denmark

www.cee.elektro.dtu.dk
Tel: (+45) 45 25 35 00
Fax: (+45) 45 88 61 11
E-mail: cee@elektro.dtu.dk